UNIVERSITÀ DEGLI STUDI DI TRIESTE

UNIVERSITÀ DEGLI STUDI DI UDINE

UNIVERSITÀ DEGLI STUDI DI TRIESTE

UNIVERSITÀ DEGLI STUDI DI UDINE

XXXV CICLO DEL DOTTORATO DI RICERCA IN AMBIENTE E VITA

PO FRIULI VENEZIA GIULIA - FONDO SOCIALE EUROPEO 2014/2020

MERCURY CYCLING AND TRANSFORMATIONS AT THE WATER-AIR AND SOIL-AIR INTERFACES IN A CONTAMINATED REGIONAL CONTEXT

Settore scientifico-disciplinare: **GEO/08 GEOCHIMICA E VULCANOLOGIA**

DOTTORANDO / A
FEDERICO FLOREANI

COORDINATORE
PROF. GIORGIO ALBERTI

SUPERVISORE DI TESI
PROF. STEFANO COVELLI

CO-SUPERVISORE DI TESI
PROF. JADRAN FAGANELI

ANNO ACCADEMICO 2021/2022

Table of contents

Plain Language Summary

Thanks to its high volatility, mercury can easily be released from soils and waterbodies into the atmosphere in its gaseous form, particularly in areas characterised by high mercury concentration due to natural local geology or anthropogenic contamination. The aim of this research was to study the gaseous exchanges of mercury between both water and soil surfaces and the atmosphere in selected contaminated sites within the Friuli Venezia Giulia Region (Northeastern Italy). This area has been subject to notable past supplies of mercury due to the transport by the Isonzo River of contaminated material from the Idrija mercury mining district (Slovenia) and, secondarily, the past uncontrolled wastewater discharges of a chlor-alkali plant in Torviscosa (Italy). Monitoring sites in different environmental contexts were selected as follows:

- Coastal marine environments: gaseous mercury fluxes were studied during the entire day-night cycle in a confined strongly contaminated fish farm of the Marano and Grado Lagoon (Val Noghera) and in a more dynamic and less contaminated open marine area, the Bay of Piran (Slovenia);
- Freshwater environments: to evaluate the effect of the type of mercury source on present-day fluxes, measurements were conducted during the diurnal period at sites impacted by mining (Solkan Reservoir, Slovenia) and industrial activity (Torviscosa Dockyard, Italy) and at a third site with no known mercury sources (Cavazzo Lake, Italy) selected as the natural background of this region;
- Terrestrial environments: gaseous mercury evasion during the diurnal period from soils with and without natural grass cover near the riverbanks of the Isonzo River were evaluated at six sites characterised by a different degree of soil contamination.

Fluxes were measured in field in different seasons by means of transparent flux chambers coupled with a portable real-time gaseous mercury analyser. Water and soil samples were collected to evaluate the total amounts and the forms of mercury occurring in the selected sites. The relation between mercury fluxes and the main meteorological (UV radiation and temperature) and physico-chemical parameters was also assessed.

Generally, gaseous mercury fluxes obtained in this study both in aquatic and in terrestrial environments were higher than those commonly reported for uncontaminated areas, confirming that mercury is still emitted in the atmosphere even decades after the closure of the main contamination source. Moreover, fluxes from soils were considerably higher than those from water surfaces likely due to the greater availability of mercury. The highest fluxes in all

contexts were observed in summer thanks to high insolation and temperatures, which may have favoured the reactions leading to the formation of the volatile form of mercury. However, gaseous mercury concentrations in the atmosphere recorded during sampling were relatively low thanks to atmospheric dilution.

Considering the water surfaces, conditions of scarce water movement and mixing likely limited gaseous exchanges at Val Noghera and Torviscosa, resulting in fluxes comparable to those recorded in the uncontaminated dynamic environments of Piran and Cavazzo despite the significantly higher mercury concentrations.

Gaseous mercury emissions from soils were strongly influenced by the concentration of this metal in the first centimeters of surface soil in summer and autumn, whereas fluxes resulted more homogeneous between sites in winter. This was likely due to low temperatures that may have limited the degradation of the predominant form of mercury in these soils (mercury sulphide: red cinnabar), which is particularly stable compared to the other forms of mercury, which were present in similar amounts in all analysed soils. Finally, living grass cover significantly limited mercury fluxes by reducing soil temperatures and light reaching the surface, acting as a natural mitigation mechanism for mercury emissions from contaminated soils.

Abstract

Mercury (Hg) can be easily released into the atmosphere from natural water and soil surfaces thanks to the high volatility of its elemental form (Hg^0). These emissions can be particularly high in areas characterised by notable Hg concentrations in the environment as a result of natural geological enrichment or anthropogenic releases of this metal related to mining or various industrial activities. As a result, these Hg-enriched or contaminated areas may represent a relevant secondary source of Hg^0 for the atmosphere. The study of dynamics of gaseous exchanges of Hg^0 in these contaminated sites is essential to fully understand the fate of this metal once released in the environment and to assess the potential risks for ecosystems and human health associated with its occurrence.

The aim of this research was therefore to study the processes and environmental factors that affect Hg^0 exchanges at water-air and soil-air interfaces in selected environments within the area between Friuli Venezia Giulia Region (Northeastern Italy) and Western Slovenia. The study area is characterised by a widespread Hg contamination related to the dispersion by the Isonzo River of Hg-enriched material generated by the historical cinnabar mining at Idrija (Slovenia) and, secondarily, by the past uncontrolled wastewater discharges of a chlor-alkali plant (CAP) in Torviscosa (Italy).

Taking into consideration the Hg^0 fluxes at the water-air interface, the research was divided into two parts. The first was devoted to study the dynamics of Hg^0 fluxes during complete 24 h cycles in coastal environments: in order to understand the influence of different degree of Hg contamination and hydrodynamic conditions, a strongly impacted confined fish farm (Val Noghera, Italy) and an open marine area (Bay of Piran, Slovenia) in a relatively pristine area of the Gulf of Trieste were selected. The second part of the research was focused on evaluating the effect of past Hg anthropogenic supplies from different types of sources on present-day Hg^0 fluxes during the diurnal period: measurements were conducted in freshwater environments impacted by mining (Solkan Reservoir, Slovenia) and industrial activity (Torviscosa Dockyard near the former CAP, Italy) and the results were compared with those obtained in a pristine site (Cavazzo Lake, Italy) with unknown Hg sources. Hg^0 fluxes were evaluated in field by means of a transparent floating chamber taking measures at regular time intervals. Dissolved gaseous mercury (DGM) concentrations in surface water layers were also determined as the volatile fraction available for volatilisation together with main meteorological and physico-chemical water parameters. Generally, higher Hg^0 fluxes were recorded in more impacted sites than in pristine areas for both coastal and freshwater environments. Fluxes were related to both UV

irradiation and water temperatures, which may have favoured Hg abiotic (photochemical) and possibly biotic reduction to DGM and its subsequent release to the atmosphere. However, particularly at the CAP (Torviscosa) and at the fish farm (Val Noghera), Hg^0 fluxes were comparable to those observed at the relative pristine areas of Cavazzo Lake and Piran Bay despite the significantly higher Hg concentrations in water: this may have been due to water thermo-aline stratification and scarce water turbulence, which probably limited vertical Hg diffusion and gaseous exchanges with the atmosphere.

Regarding the terrestrial environment, the Hg^0 fluxes at the soil-air interface were measured at six selected sites along the Isonzo River alluvial plain characterised by variable total Hg concentration in surface soils. Several replicate measurements were performed by a non-steady state transparent flux chamber on both bare and grass-covered soil plots in different periods of the year (summer, autumn, winter) during diurnal hours, in order to evaluate the temporal variability of the evasion and a potential effect of the presence of vegetation. Total Hg concentration and Hg speciation in topsoils were also assessed and the main meteorological parameters and soil physico-chemical characteristics were determined. Fluxes of Hg^0 recorded at the soil-air interface were higher than those found at the water-air interface and positively correlated with soil Hg content and both UV irradiation and temperature, similar to what was observed in aquatic environments. Only in winter, no correlation was found between soil Hg content and fluxes, likely due to scarce contribution of the predominant cinnabar fraction to Hg^0 formation at low temperatures. Soil shading by active vegetation significantly reduced Hg^0 emissions from soil surfaces in summer and autumn, whereas this effect was not observable in winter due to the scarce vegetation development.

The relatively high Hg^0 fluxes recorded in this study for both aquatic and terrestrial environments suggest that the studied areas can represent a secondary atmospheric Hg source even decades after the phase out of the main anthropogenic contamination sources. However, atmospheric Hg concentrations recorded during sampling days were on average well below threshold values for inhalation exposure, likely due to atmospheric dilution of emitted Hg^0.

1. Introduction

1.1 Preface

Mercury (Hg) is well recognised for its characteristics of mobility in the environment, toxicity, and bioaccumulation potential mostly of its organic form, methylmercury (MeHg). In addition to be the only liquid metal at room temperature, a peculiarity of this element is the relatively high volatility and vapour pressure (0.246 Pa at 25°C) of its elemental form (Hg^0) (Mason and Sheu, 2002; Schroeder and Munthe, 1998). Consequently, Hg^0 can easily be released into the atmosphere from both natural and anthropogenic sources and usually represents the most abundant fraction (>90%) of Hg in this compartment (Beckers and Rinklebe, 2017; Poissant et al., 2005) where it is usually indicated as GEM (Gaseous Elemental Mercury). Furthermore, thanks to its low reactivity and solubility, once emitted Hg^0 can persist in the atmosphere for a relatively long time estimated between 6 months and 2 years (Saiz-Lopez et al., 2018). Therefore, it can be subject to a long-range atmospheric transport before being converted into more soluble oxidised form (Hg^{2+}) more subject to adsorption on particulate matter and removal through dry and wet depositions (Amos et al., 2012). In this way, Hg can reach and impact also remote ecosystems far from the emission source (Hammerschmidt and Fitzgerald, 2006; Travnikov, 2005).

The spatial redistribution of Hg in the environment is further enhanced by the possible re-emission into the atmosphere after reduction to Hg^0 (Agnan et al., 2016). This prolongs its recycling in the environment before being sequestered through burial in deep-sea sediments, an extremely slow process (Selin, 2009). As a result, Hg has been recognised as a global contaminant, identified as one of the 10 chemicals of major public health concern by the World Health Organisation (WHO, 2020). Taking into consideration also the detrimental effects on ecosystems and biota and human health, mainly on the nervous system (Díez, 2009), the problem of Hg pollution has received a growing attention on a global scale which, especially in more recent years, has led to the emergence of several programs aimed at limiting its use and release into the environment (Pirrone et al., 2010). These efforts culminated in the Minamata Convention in October 2013, which was signed by 139 countries and entered into force in 2017 after the ratification by 50 nations. The main goal of this Convention is to protect human health and the environment from negative effects resulting from the use and dispersion of Hg through the adoption of policies to reduce its uses and emissions, while constantly monitoring the effectiveness of the approaches taken (Selin et al., 2018).

For the implementation of the Convention the parties must take actions to develop and improve methods for enforcing the knowledge and monitoring Hg emissions from all relevant sources and its dispersion in the environment, relating it to ecological and ecotoxicological effects (Bank et al., 2014; Cabassi et al., 2022; Selin et al., 2018). Due to the chemical inertness of Hg^0 once released in the atmosphere, all potential sources represent a concern (Custodio et al., 2020). According to recent model estimates, primary anthropogenic emissions of Hg related to several mining and industrial activities (UN Environment, 2019) currently accounts for roughly only one third of the global amount of Hg^0 annually released to the atmosphere. The remaining fraction is attributable to secondary emissions from natural surfaces of soils and waterbodies of Hg previously mobilised from lithospheric reservoirs by human activities (Driscoll et al., 2013).

A source of Hg^0 into the atmosphere frequently omitted by global inventories is represented by the releases from natural soil or water surfaces of contaminated sites. This is mainly related to a lack of direct measurements of this phenomenon in these sites, resulting in large uncertainties in the estimates of their contribution to global atmospheric Hg pool which is based on only a limited number of site-specific studies (Kocman et al., 2013; Osterwalder et al., 2019). However, this contribution is considered to account only for a small percentage of global Hg^0 emissions due to the limited spatial extension of these sites (Agnan et al., 2016; Kocman et al., 2013).

Risk assessment in Hg-contaminated sites is more frequently focused on the evaluation of methylation and bioaccumulation *in situ* or in downstream environments rather than on estimating the volatilisation of Hg^0 to the atmosphere (Eckley et al., 2020). Gaseous exchanges at the surface-atmosphere interfaces should be carefully considered at these sites as they can represent a long-term source of Hg for the local atmosphere (Gustin et al., 2003) even years after the phase out of the main contamination source (Eckley et al., 2015; Nacht et al., 2004). In this way, Hg^0 emissions can deeply influence the local atmospheric Hg concentrations (Eckley et al., 2013), sometimes resulting in values above the chronic inhalation criteria level (e.g. 300 ng m^{-3} established by the United States Environmental Protection Agency (U.S. EPA) or 1000 ng m^{-3} indicated by the WHO) (Acquavita et al., 2017; Fornasaro et al., 2022; Robins et al., 2012; Wang et al., 2019). These high atmospheric Hg levels are typically restricted to few hundred of meters around the emission area and are associated with the presence of former facilities or dumped Hg-contaminated materials (Esbri et al., 2020; Kocman et al., 2011; Vaselli et al., 2013). On the other hand, mostly in aquatic environments the evasion of Hg^0 at

the water-air interface can contribute to reduce the amount of Hg^{2+} in the water column available for methylation (Cossa et al., 2022; Feng et al., 2008; Horvat et al., 2003).
Generally, Hg^0 emissions from natural surfaces are $\leq$ 1 ng m^{-2} h^{-1} and can be overcome by atmospheric depositions, mostly in forested areas (Eckley et al., 2021), whereas in contaminated sites these releases can reach values up to thousands of ng m^{-2} h^{-1} (Agnan et al., 2016). These sites include, among others, areas near:

- former Hg mines (Conaway et al., 2003; Fantozzi et al., 2013a; Gustin et al., 2003; Kotnik et al., 2005; Wang et al., 2005);
- gold and silver mines were Hg was used for amalgamation or is present in the ore body (Dalziel and Tordon, 2014; García-Sánchez et al., 2006; Gustin et al., 2003; Miller et al., 2011);
- industrial facilities where Hg was used as a catalyst in the industrial process such as chlor-alkali plants (Bagnato et al., 2013; Huremović et al., 2017; Olofsson et al., 2005) or polymers (e.g. acetaldehyde, vinyl acetate, vinyl chloride) production (Marumoto and Imai, 2015; Osterwalder et al., 2019; Zhu et al., 2018)
- chemical factories for the production of Hg-containing products such as fungicides (Fu et al., 2012);
- metal smelters (Eckley et al., 2015);
- coal-fired power plants that emitted significant amounts of Hg in the atmosphere as a by-product and largely contaminated the surrounding areas (Eckley et al., 2013; Li et al., 2018).

Mercury concentration in the substrate is widely recognised as the primary driver of Hg^0 emission from natural terrestrial and aquatic surfaces of contaminated areas (Agnan et al., 2016; Conaway et al., 2003; Marumoto and Imai, 2015). This phenomenon can be influenced also by the Hg speciation in the substrate, which affects its availability for the conversion to Hg^0 and subsequent evasion (Gustin et al., 2002; O'Driscoll et al., 2018). Moreover, similarly as in pristine areas, Hg^0 fluxes depend on environmental parameters that naturally influence both the abiotic (photochemical) and biotic reduction of Hg^{2+} to Hg^0 and the gaseous exchanges at the interface with the atmosphere (Miller et al., 2011; Poissant et al., 2000). These factors include incident solar radiation (Fantozzi et al., 2013b; García-Sánchez et al., 2006), temperature (Chen et al., 2020; Kyllönen et al., 2012), organic matter concentration and speciation (Soerensen et al., 2013; Yuan et al., 2019b), wind speeds (Feng et al., 2004; Polyzou

et al., 2019), precipitation (Feng et al., 2008; MacSween and Edwards, 2021), water turbulence and currents (Sharif et al., 2013), surface shading e.g. by vegetation (Cizdziel et al., 2019; Tao et al., 2017).

The evaluation of Hg^0 exchanges between the atmosphere and natural surfaces in contaminated sites is therefore a key aspect in fully understanding the fate of Hg released into the environment as a result of anthropogenic activities and its potential impact on target ecosystems and human health. The aim of this research was therefore to investigate through direct *in situ* measurements the magnitude, dynamics and main drivers of atmospheric release of Hg in gaseous form from various environmental compartments (soils and waterbodies) in the Friuli Venezia Giulia region (North-eastern Italy). Mostly in its south-eastern part, this region has been subject to a widespread Hg contamination due to past anthropogenic releases of this metal related to two main sources (Fig. 1): the historic cinnabar (α-HgS) mining at the Idrija Hg mine (Slovenia) active for ~500 years until its closure in 1995 (Acquavita et al., 2022; Covelli et al., 2012) and, to a lesser extent, the wastewater discharges from a chlor-alkali plant (CAP) in Torviscosa (Italy) between 1949 and 1984 (Covelli et al., 2009; Piani et al., 2005).

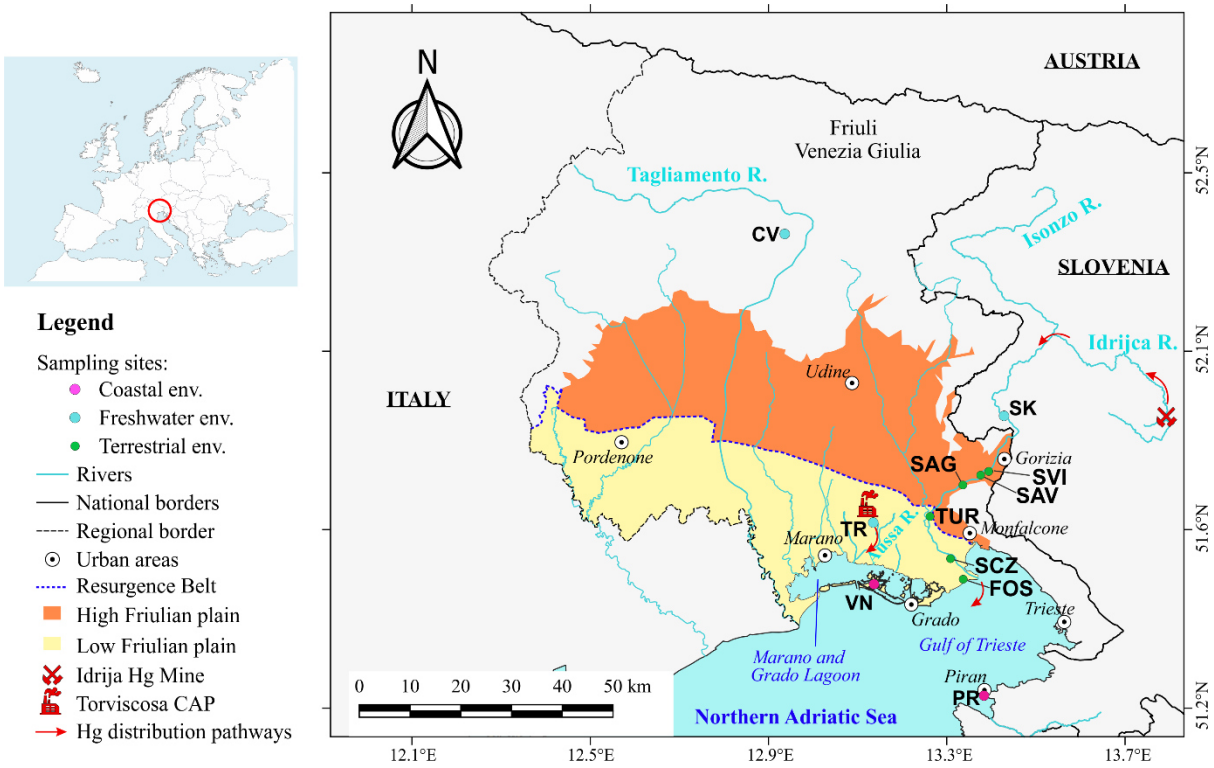

Figure 1: study area and location of selected sampling sites in coastal marine environments (VN: Val Noghera, PR: Bay of Piran), freshwater environments (SK: Solkan Reservoir, TR: Torviscosa Dockyard, CV: Cavazzo Lake), and terrestrial environments (SVI and SAV: Savogna d'Isonzo, SAG: Sagrado, TUR: Turriaco, SCZ: San Canzian d'Isonzo, FOS: Fossalon di Grado).

1.2 Study area and selection of sampling sites

The Idrija mining district is located in western Slovenia, about 60 km from the capital Ljubljana, in the narrow valley of the Idrijca River and its confluent Nikova River. Idrija was one of the most important Hg mining centres worldwide, second only to that of Almadén (Spain). During the mining period, around 5 million tonnes of rock were excavated from which through the roasting process approximately 105,000 t of metallic Hg were obtained. However, an estimated total amount of ~37,000 t of this metal was dispersed into the local environment during mining operations (Gosar et al., 1997; Gosar and Teršič, 2012; Mlakar, 1974).

The 1500 m long, 300-600 m wide and 450 m deep deposit formed in the Middle Triassic was exploited through more than 700 km of mining galleries, extending also below the town of Idrija. According to what reported by Kotnik et al. (2005), mining activity in the district began around 1490 with the excavation of carboniferous schists containing elemental Hg. This activity was replaced by smelting in simple earthen vessel at various locations after the discovery of α-HgS ore in 1508. The first "industrial" smelting plant was built in 1652 on the left bank of the Idrijca River and was characterised by a recovery of ~65%; it is estimated that during its activity around 13,000 t of Hg were lost into the environment, mostly to the atmosphere or through direct discharge of smelting residues into the river. Starting from 1868, with the construction of new smelting plants on the right bank of the river which remained active until the end of the Second World War, the recovery further improved (75%). This coincided with the most productive period of the mine, with a peak in 1913 (Mlakar, 1974). However, during this period ~20,000 tons of Hg were lost into the atmosphere and dispersed into surrounding soils (Dizdarevič, 2001), sank into the ground, or dumped as a by-product on riverbanks. After 1963, new modern rotatory furnaces were built and the recovery increased to 92%: this coincided with the period when worldwide Hg consumption and price peaked. Ecological catastrophes related to Hg releases in Japan (Kudo and Miyahara, 1991) and in Iraq (Bakir et al., 1973) drew attention on the hazards related to Hg use and its price dropped dramatically, leading to a crisis of the mine which permanently ceased operations in 1995 (Kotnik et al., 2005).

Releases related to mining and smelting caused a relevant contamination of all environmental compartments in the surroundings of Idrija. Indeed, Hg concentration in soils and sediments of the mining district can reach values up to thousands of mg kg^{-1}, progressively decreasing downstream the mining area (Gosar and Teršič, 2012 and reference therein). Contaminated

soils still represent a source of Hg^0 for the atmosphere together with mine ventilation shafts, mineralised rock dump sites and outcrops of ore deposit (Grönlund et al., 2005; Kocman et al., 2011; Kotnik et al., 2005). Moreover, particularly during heavy rain events, dumped residues and polluted soils and sediments represent a source of Hg for the Idrijca River due to erosion and leaching of Hg-enriched material. Mercury is then transported downstream by the current, mainly in particulate form, a process still active nowadays due to the high amount of this element still stored in local soils and sediments (Baptista-Salazar et al., 2017; Gosar and Teršič, 2012; Žibret and Gosar, 2006).

At Most na Soči, the Idrijca River flows into the Isonzo/Soča River, which runs for approximately 135 km from the Julian Alps in Slovenia to the Northern Adriatic Sea (near Monfalcone, Italy) and represents the main freshwater input for this marine area (Pavoni et al., 2020). After the confluence with the Idrijca River, Hg-enriched material is so transported to the Isonzo/Soča River mouth, where relatively high Hg concentrations in water are usually observed mostly during river plumes (Covelli et al., 2007, 2006). Even 25 years after the mine closure, after rain events the Isonzo/Soča River still carries relevant amounts of Hg-enriched material to downstream environments (Baptista-Salazar et al., 2017; Pavoni et al., 2021).

As a result of past and present high Hg loadings, bottom sediments of the most northern part of the Adriatic Sea, the Gulf of Trieste, are characterised by high Hg concentrations (up to ~30 mg kg^{-1}) particularly near the mouth of the Isonzo/Soča River (Covelli et al., 2001). As a result, this coastal marine area is considered one of the most impacted by Hg over the Mediterranean Sea (Kotnik et al., 2017) and worldwide (Fitzgerald et al., 2007).

Moreover, historical flooding events caused the dispersion of Hg contaminated material in the soils forming the alluvial plain of the Isonzo/Soča River (Acquavita et al., 2022) This plain represents the easternmost edge of the Friulian plain and is formed by alluvial megafans of sediments transported by local rivers (Cellina, Meduna, Tagliamento, Corno, Cormor, Torre, Natisone, Isonzo) during the last glacial maximum (Fontana et al., 2008). It is divided into two main geomorphological sectors (High and Low plain) by an east-west oriented Resurgence Belt (Cucchi et al., 2008; Treu et al., 2017). The widespread Hg contamination of this plain is confirmed by relatively high total Hg concentrations (up to 76 mg kg^{-1}) observed throughout the Isonzo River plain both in surface and deep soils, progressively decreasing as distance from the river increases (Acquavita et al., 2022; Piani et al., 2013).

Due to the prevalently anticlockwise water circulation of the Gulf of Trieste, Hg arriving at the Isonzo/Soča River mouth is deviated in south-west direction (Covelli et al., 2007). In this way

it can reach the Marano and Grado Lagoon, a shallow semi-enclosed environment extending on an area of ~160 km^2 between the mouths of Isonzo/Soča River and Tagliamento River and connected to the open sea by six tidal inlets (from west to east: Lignano, S. Andrea, Porto Buso, Morgo, Grado, Primero) (Ferrarin et al., 2010). Mercury enters the lagoon mainly through the eastern tidal inlets of Primero and Grado (Turritto et al., 2018) and is then removed through sedimentation, resulting in a decreasing trend of Hg concentration in surface sediments from east (14.4 mg kg^{-1}) to west (0.7 mg kg^{-1}) (Acquavita et al., 2012). The Hg contamination in this environment is particularly concerning given its high naturalistic value as transition habitat and nesting area for several bird species, evidenced by its designation as Special Protection Area ("Birds Directive", 2009/147/EC) and as Site of Community Importance (SCI - IT3320037; "Habitat Directive", 92/43/EEC) (Petranich et al., 2018b). Moreover, Hg contamination represents a concern also for the traditional economic activities still carried out within the Lagoon such as clam harvesting or aquaculture in confined fish farms (Acquavita et al., 2015; 2018).

The second main Hg source in the study area, the Torviscosa CAP, is located in the Low Friulian plain approximately 9 km north of the Marano and Grado Lagoon inside the industrial complex of Consorzio Industriale Aussa-Corno. In this plant, metallic Hg was used as the cathode in the electrolytic cells for the production of chlorine and caustic soda (NaOH) through the process first described by Castner and Kellner in 1892 (Lakshmanan and Murugesan, 2014). In this type of cell, Hg at the cathode forms an amalgam with sodium obtained from a brine saturated in NaCl. The amalgam then reacts with water in a "denuder" to form NaOH without consuming Hg. However, losses of this metal can occur during the process through emissions to air and water or its presence in products and wastes (Brinkmann et al., 2014). The annual production of the Torviscosa CAP initially stood at 4500 t (1950) but grew rapidly to 20,000 t in 1960. It was estimated that during this period about 20 kg day^{-1} of Hg were discharged in the local Banduzzi channel which connects the plant to the Aussa River, a resurgence river tributary of the Marano and Grado Lagoon in its inner central part. These releases decreased starting from 1970 (6-7 kg day^{-1}) until the installation of a modern wastewater treatment system in 1984, which likely stopped the direct discharge of this metal to the river. However, an overall estimated amount of 186 t of Hg has been lost in the environment during plant operations (Mattassi et al., 1991). Besides, emissions to air continued until the dismission of Hg cells in 2008: for example, between 2005 and 2007 Hg emissions to air were estimated between 50 and 100 kg y^{-1} (Acquavita et al., 2017).

As a result of the releases related to industrial activity, extremely high Hg concentrations (up to 1000 mg kg^{-1}) are reported for the sediments of the Banduzzi channel (Biasiol, 2015). Hg contamination due to the CAP can be detected also in water and sediments of downstream environments (Covelli et al., 2009) as far as the Marano and Grado Lagoon, although the influence of this contamination source is likely restricted to the area near the mouth of the Aussa River. This can be evidenced by the greater abundance of mobile forms of Hg in the sediments of this area compared to the predominance of non-mobile α-HgS of mining origin found in the easternmost part of the lagoon (Piani et al., 2005). Moreover, some areas of the dismissed CAP such as ex-cell house and distiller still represent a source of Hg^0 for the local atmosphere in function of meteorological conditions, resulting in high Hg^0 concentration in air (up to > 5000 ng m^{-3}) and in lichens collected nearby the plant area (Acquavita et al., 2017). Considering the high concentrations of Hg and other contaminants (e.g. PTEs, dioxins, PAHs; Ramieri et al., 2011) found in the surroundings of the CAP in soils, sediments, and groundwaters, the area was defined as a contaminated Site of National Interest (SIN n. 25 "Caffaro di Torviscosa") following the Italian Ministerial Decree 468/2001. The SIN originally included also the Marano and Grado Lagoon, but was later re-perimeterised through the Italian Ministerial Decree 222/M of 12/12/2012 on an area of 201 ha within the Torviscosa industrial complex (Ministero dell'Ambiente e della Sicurezza Energetica, 2022).

1.3 Study aims

Even though Hg contamination of soils, sediments, and waters of the Friuli Venezia Giulia Region has been studied in depth, little is known about the secondary Hg^0 emissions to the atmosphere from these contaminated surfaces. Existing data are mainly focused on atmospheric Hg^0 concentrations around anthropogenic point sources such as the Torviscosa CAP (Acquavita et al., 2017) or a waste incinerator plant in the western part of the Region (Fortuna et al., 2019; Tretiach et al., 2011), whereas direct measures of Hg^0 fluxes from natural water surfaces have been performed during only the diurnal period in some coastal marine environments of the Marano and Grado Lagoon and the Gulf of Trieste (Floreani et al., 2019).

To deepen the knowledge on Hg^0 evasion magnitude and dynamics in this highly contaminated coastal marine area, two sites monitored in the above cited study were selected for monitoring the Hg^0 fluxes at water-air interface during the entire day-night period. The aim of this part of the research was to investigate the variability of the phenomenon under different solar irradiation condition and likely different photo-induced formation of volatile Hg. Research

activity was focused on two environments characterised by different Hg contamination degree and hydrodynamic conditions, a fish farm of the Marano and Grado Lagoon (Val Noghera, VN), and the Bay of Piran (PR), in Slovenia. These sites were selected in order to evaluate the possible effect of both these parameters on Hg^0 fluxes. The Val Noghera fish farm is a confined area located in the south-eastern part of the lagoon. This ecosystem has limited water recirculation and exchanges with the open environment and can retain relatively high amounts of Hg in sediments. Moreover, this fish farm has been deeply studied previously for the evaluation of Hg and nutrient cycle at the sediment-water interface. Due to the surplus of organic matter (OM) and the frequent occurrence of hypoxic or anoxic conditions, some parts of the fish farm have been recognised as potential sites for Hg methylation (Petranich et al., 2018a, b). Conversely, the PR site is located in an open dynamic marine coastal environment in the southern part of the Gulf of Trieste, less subject to Hg supplies from the Isonzo River.
At both sites, measurements were conducted in summer, autumn, and spring in order to study the dynamics of Hg^0 fluxes in different periods of the year. No measurements were conducted in winter as existing data indicate that Hg^0 evasion in this season is relatively limited. Hg^0 fluxes were evaluated by means of a manually operated flux chamber coupled with a real-time Hg^0 analyser (Lumex RA-915M) at regular time intervals of 2 h. In parallel, the concentrations of the volatile fraction of Hg in surface water layer, operationally defined as DGM (Dissolved Gaseous Mercury), were determined together with monitoring the main meteorological and water physico-chemical parameters, in order to identify the main factors influencing gaseous exchanges of Hg^0 at the water-air interface.

A second part of the research was focused on the investigation of the effect of different past Hg supplies on present day Hg^0 evasion in freshwater environments subject to Hg contamination from different sources, namely Hg mining at Idrija and the chlor-alkali industry at Torviscosa.
To study the effect of Hg contamination from mining, measurements were conducted at the Solkan Reservoir (SK) in Slovenia along the Isonzo River. This reservoir is delimitated by a hydroelectric dam built between 1981 and 1984, which actively regulates the water current along the reservoir and can favour the accumulation of Hg transported by the river mostly in particulate form in the sediments of the basin (Hines et al., 2006).
The effect of past industrial Hg contamination on Hg^0 fluxes at water-air interface was assessed at the dockyard inside the Torviscosa chemical industrial pool, connected to Banduzzi channel, where the past discharges of the CAP occurred, and to the Aussa River by a shippable channel.

Despite being characterised by a relatively low hydrodynamism, this waterbody is affected by the saltwater intrusion in bottom water layer due to the "saltwedge" occurring from the Marano and Grado Lagoon into the Aussa River (Covelli et al., 2009). Moreover, the dockyard receives the present discharges of surrounding irrigation ditches, industrial wastewaters, and cooling waters of the local thermoelectric power plant (Regione Autonoma Friuli Venezia Giulia, 2012).

Fluxes of Hg^0 were measured also in a pristine environment with no known anthropogenic Hg sources, the Cavazzo Lake (CV, Italy), in order to evaluate Hg^0 exchanges in an area not subject to Hg contamination and to understand if the phenomenon is influenced by the same environmental factors. The Cavazzo Lake is located about 40 km northwest of the city of Udine in the Carnian Alps at 195 m a.s.l. and was formed during the last glacial maximum in a paleochannel of Tagliamento River dammed by end-moraine deposits (Marinelli, 1894; Venturini and Discenza, 2010). Natural freshwater inputs to the lake are represented by several seasonally active streams. In the 1950s the construction of the Somplago hydroelectric power plant on its northern shore has led to the connection of the lake with the feed basins upstream of the power plant and a consequent considerable increase in sediment inputs to the lake (Polonia et al., 2021).

Measurements of Hg^0 fluxes at water-air interface in these freshwater environments were performed during the diurnal period at regular time intervals of ~1 h using the same experimental approach adopted for coastal marine sites in the same seasons (summer, autumn, spring) and monitoring the same environmental parameters.

The last part of the research was focused on assessing Hg^0 exchanges at the soil-air interface in selected sites along the alluvial plain of Isonzo River, for which no information exists about potential releases of Hg^0 to the atmosphere from soil surfaces (Acquavita et al., 2022). Six sites characterised by a different degree of soil Hg contamination according to the recent characterisation performed by Acquavita et al. (2022) were selected in the municipalities of (from north to south) Savogna d'Isonzo (SAV and SVI), Sagrado (SAG), Turriaco (TUR), San Canzian d'Isonzo (SCZ) and Grado (FOS) both in the High (SAV, SVI, SAG) and Low plain (TUR, SCZ, FOS).

Measurements of Hg^0 fluxes were performed during diurnal period by means of a non-steady state flux chamber coupled with the same gaseous Hg analyser in order to take several replicated measures of fluxes from different soil plots in a short time interval and take into account the expected high variability of emissions even at small spatial scale (Rinklebe et al.,

2009). At each site, Hg^0 fluxes were evaluated in permanent meadows both from soil plots characterised by the native grass vegetation cover and plots where vegetation was previously removed. The aim of this distinction was to assess the influence of shading caused by the presence of vegetation on the Hg^0 evasion with respect to bare soils. The latter situation frequently occurs along the contaminated plain due to agricultural activities present over a large part of the area.

As no data were available about Hg^0 secondary emissions from these contaminated soils, to verify the temporal variability of the phenomenon measurement were conducted in summer, autumn, and winter. No measurements were performed in spring as both vegetation development and weather conditions in this season are similar to those encountered in autumn and consequently no significant differences in terms of fluxes are expected between these two periods.

In order to identify the main factors influencing Hg^0 fluxes in these terrestrial environments, the main meteorological parameters (UV radiation, air temperature) and soil temperature were monitored in field during all sampling period. At the end of each day, topsoil samples from the surficial layer most involved in gaseous exchanges with atmosphere (0-2 cm; Sigler and Lee, 2006) were collected for a simple soil characterisation (grain-size, pH, OM concentration) in order to assess the possible influence of soil physical characteristics on Hg^0 fluxes. Moreover, total Hg concentrations were also determined together with Hg speciation through thermo-desorption technique (Petranich et al., 2022) with the aim of assessing the influence of Hg contamination on the magnitude of Hg^0 fluxes and the possible influence of the occurrence of different Hg forms in the substrate.

More details about the environmental settings of all study areas are given in the Results section.

The expected results of this research project would give further information about the fate of Hg in these contaminated environments and the potential influence of past Hg contamination on present day Hg^0 fluxes and their effect on local atmosphere. Moreover, information obtained in this research would be useful to assess the importance of Hg^0 evasion in reducing the burden of Hg available in the substrate for transformations such as methylation, particularly in aquatic environments.

The identification of the most important factors influencing Hg^0 exchanges with the atmosphere would also be useful to evaluate the best mitigation strategies for Hg contamination in the studied environments. Finally, experimental field activity will provide indications about the effectiveness of the adopted experimental approaches for the assessment of Hg^0 evasion at

the substrate-atmosphere interface in Hg-contaminated sites. This aspect should be carefully evaluated in the risk assessment procedure at these sites in order to completely assess the potential exposure of local inhabitants or workers to Hg^0 through inhalation after its volatilisation from the substrate.

1.4 Mercury in the environment

Mercury (Hg) occurs naturally in all environmental compartments in, at least, relatively low amounts, with an estimated average concentration in the Earth's crust of 0.05 mg kg^{-1} (Canil et al., 2015; Rudnick and Gao, 2003). Three different oxidation states of Hg can be distinguished, 0, +2, and +1, the last of which is rather unstable and rarely detected under environmental conditions (Ullrich et al., 2001).

Several inorganic and organic compounds can be formed by Hg cations in the environment (Kubáň et al., 2007). The principal ore of Hg is cinnabar (α-HgS, Anthony et al., 2016), with a characteristic red colour known and used by humankind for more than 2300 years. There are several areas of world naturally enriched in Hg where α-HgS was extensively mined, and most of these are located along the so-called "mercuriferous belts" (Schroeder and Munthe, 1998; Selin, 2009): among these, can be mentioned the Hg mines of Almaden in Spain, the biggest α-HgS deposit worldwide (Higueras et al., 2013), Idrija in Slovenia (Gosar et al., 1997), Monte Amiata in Italy (Rimondi et al., 2012), New Idria and New Almaden in United States (Gustin et al., 2003), and Wanshan in China (Feng and Qiu, 2008). Moreover, divalent Hg (Hg^{2+}) can form inorganic complexes with various ligands, forming a wide range of inorganic compounds in water, soils, and sediments (e.g. $HgCl_2$, $Hg(OH)_2$, HgO, $HgSO_4$, …) (Terzano et al., 2010).

The organic compounds of Hg can be grouped in two categories: alkylmercurial compounds (including methylmercury, CH_3Hg^+ or MeHg, and ethylmercury, $C_2H_5Hg^+$) and arylmercurial compounds (e.g. phenylmercury, $C_6H_5Hg^+$). Among them, the most interesting from the environmental point of view is undoubtedly MeHg, easily bioaccumulated through the trophic webs due to its high liposolubility and slow excretion (Kidd et al., 2012) and which can cause significant toxic effects mostly on the nervous system of higher organisms (Fitzgerald and Clarkson, 1991).

Generally, the oxidised form Hg^{2+} in different chemical compounds represents the dominant form of this metal in terrestrial and aquatic environments, whereas the elemental form (Hg^0) is the dominant Hg specie in the atmosphere thanks to its high volatility and stability in gaseous form (Beckers and Rinklebe, 2017).

Anthropogenic activities have contributed to significantly increase the amounts of Hg mobilised to aquatic and terrestrial ecosystems (Driscoll et al., 2013). It has been estimated that human activities have released a total of about 1540 Gg of Hg into the environment, 73% of which after 1850 which is considered as the beginning of the industrial era. Moreover, direct discharges into soils and waterbodies represented a relevant part of anthropogenic releases of Hg in the environment, equal to about 2.3 times the amount emitted into the atmosphere (Streets et al., 2017).

Extending the attention over the last 500 years, Hg emissions in the environment have been dominated by those related to Hg mining and production, which however progressively declined during the last century, and to its use for the extraction of precious metals through the amalgamation technique (Outridge et al., 2018; Streets et al., 2019a). The intentional use of Hg in artisanal small-scale gold mining (ASGM) still nowadays represents the most relevant Hg emission source, estimated to account for the 37% of all Hg emitted in the atmosphere on a global level (Sundseth et al., 2017). Other than ASGM, today the main Hg emission source for the atmosphere is represented by the combustion of fossil fuels (especially coal) for heating and power generation due to its presence as an impurity in the fuel.

Currently, the major part of Hg emissions occurs in Asia (49%) followed by South-America and Sub-Saharan Africa (UN Environment, 2019), showing an increasing trend in industrialising country mainly as a result of fossil fuels combustion for energy production and industrial metal extraction, whereas emissions from Europe and North America are declining due to the progressive phase out of commercial use of Hg (Streets et al., 2019b) (Fig. 2).

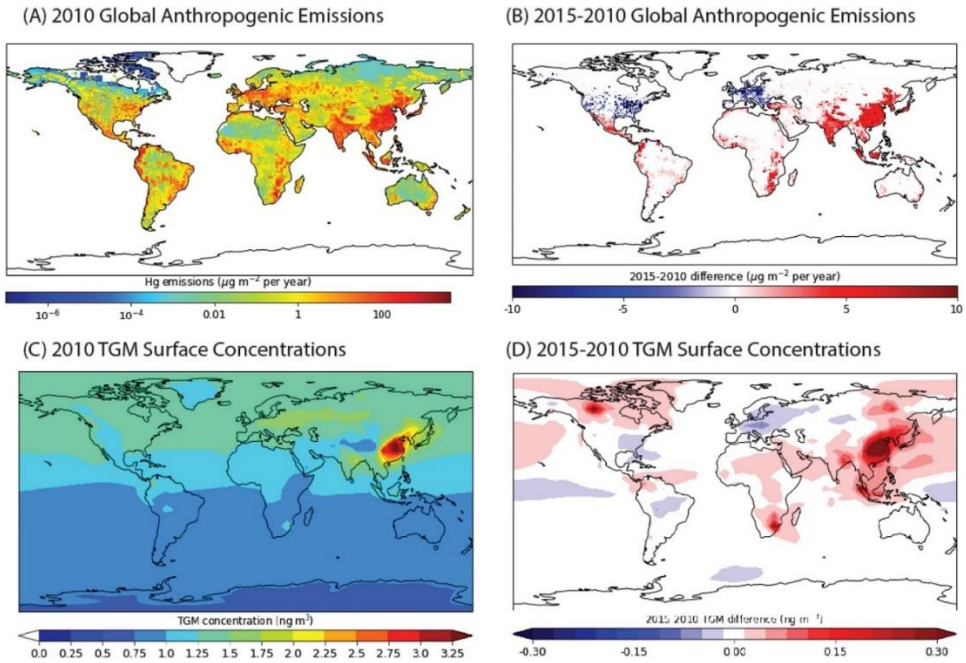

Figure 2:estimated global anthropogenic emissions and gaseous Hg atmospheric concentrations for 2010 and corresponding simulated trend between 2010 and 2015 estimates (Streets et al., 2019b).

Other processes that can cause the release of Hg in the atmosphere as a by-product of industrial activity are the production of cement, steel, and non-ferrous metals, biomass burning, and oil refining (Pacyna et al., 2010). Moreover, in the past Hg was largely intentionally used as catalyst in industrial processes such as chlor-alkali industry or vinyl-chloride monomer production, potentially leading to the release of relevant amounts of this metal in the surrounding environments (Acquavita et al., 2017; Huremović et al., 2017). In less advanced countries, Hg is still used in dental applications (amalgams), with possible releases into the environment following the cremation, and within batteries, measuring instruments (thermometers, barometers, manometers), lamps, pesticides, fungicides, laboratory reagents, drugs, cosmetics, and paints. The uncontrolled use of these products and the disposal and incineration of wastes containing Hg represent other sources of this metal for the environment (Fortuna et al., 2019; Horowitz et al., 2014; Meng et al., 2020; Pacyna et al., 2010; UN Environment, 2019).

1.4.1 Mercury toxicity

Hg has no known biological functions and the exposure to this metal in its various form, prevalently to the organic ones, can induce toxic effects on all organisms and their ecosystem processes (Gochfeld, 2003; Raj and Maiti, 2019).

At cellular level, Hg can cause changes in membranes permeability interfering with the transport of ions, alteration in macromolecules structure, interferences with functions of enzymes or polynucleotides, mitochondrial dysfunction and induction of generation of reactive oxygen species leading to increased oxidative stress (Rice et al., 2014; Schumacher and Abbott, 2017).

High Hg concentrations reduce soil fertility (Alloway, 2012) and are toxic for plants, resulting in symptoms such as reduce growth, poor root development, alteration of chlorophyll production and reduction of photosynthesis and respiration yields and of seeds viability and germination (Patra and Sharma, 2000; Raj and Maiti, 2019). Mercury is taken up by plants mainly under bioavailable Hg^{2+} forms through roots uptake and is accumulated in this organ thanks to its low translocation to shoots, interfering with the uptake of other nutrients such as potassium ion (K^+) (Chen and Yang, 2012; Raj and Maiti, 2019). In sites characterised by high Hg loadings through atmospheric depositions such as active mining sites, the uptake of Hg by plants is favoured by the higher bioavailability and mobility of recently deposed Hg together with direct uptake from the atmosphere in aboveground biomass (Ao et al., 2017; Paterson et al., 2006). This leads to higher bioaccumulation of this metal in plant tissues and to a potential exposure of population feeding on affected crops, as reported for some rice cultivations near mining sites in China (Ao et al., 2020, 2017; Qiu et al., 2013).

In higher organisms, Hg (mostly MeHg) is taken up mainly through the diet (biomagnification) and tends to accumulate mainly in muscle tissue, with gradually increasing concentration along the levels of the trophic web reaching, in apex predators, concentrations several orders of magnitude higher than those found in the environment (Morel et al., 1998). Organisms of higher trophic levels such as human beings are consequently more subject to negative effects of MeHg (Priyadarshanee et al., 2022).

The health of several wildlife species with key function in natural ecosystem can be significantly affected by MeHg exposure, representing a serious environmental concern (Driscoll et al., 2013). MeHg exposure of fish can compromise reproduction and embryonic development, interfere with biochemical processes and cause damage of cells and tissues, mostly in top predator species (Sandheinrich and Wiener, 2011). Moreover, high MeHg concentrations have been frequently reported also for piscivorous birds and mammals, resulting in hormonal changes, impairment of motor skills, decreases in reproduction and various neurotoxic and genotoxic outcomes (Driscoll et al., 2013; Wolfe et al., 1998).

For humans, dietary intake of MeHg is also the main exposure pathway to Hg, particularly for those populations that eat predominantly fish (Rice et al., 2014). The high MeHg accumulation

in fish as a result of high anthropogenic industrial discharges is for example the cause of the Hg poisoning of people which ingested contaminated fish occurred at Minamata (Japan) in 1956, which first highlighted the dangers of exposure to MeHg (Ekino et al., 2007; Harada, 1995).

Another exposure pathway is by inhalation, but it is generally restricted to workers employed in all those activities that involve the direct use of Hg or its release to the atmosphere as a by-product of work processes (Rice et al., 2014): for example, workers employed in ASGM are particularly subject to relevant Hg exposure (Gyamfi et al., 2020). However, the risk related to Hg inhalation should be carefully evaluated also for populations living nearby former Hg mining sites or factories were Hg was used as catalyst due to persistent high Hg concentrations in the atmosphere even after the closure of contamination source, if appropriate remediation action has not been taken (Esbrí et al., 2015; Fantozzi et al., 2021; McLagan et al., 2019). In this case, highest atmospheric Hg levels are usually recorded within narrow distances from the emission sources and periods of higher risk are those associated with low atmospheric dilution of emitted Hg^0, e.g. in absence of dilution due to scarce wind (Esbri et al., 2020).

The adverse effects of Hg on human health vary depending on its speciation (Fig. 3), the extent of exposure (intensity, frequency, and duration) and the age at which it occurs. These effects can be summarised as follows (Kim et al., 2016 and references therein):

- neurological effects: memory loss, mood changes, depression, irritation, and extremes of anger. These effects can occur at relatively low levels of exposure and have been recorded at urinary Hg^{2+} contents of less than 4 μg L^{-1} (Echeverria et al., 1998). Exposure to Hg could be linked to the occurrence of serious diseases such as Alzheimer's disease, erectism, dementia, Parkinson's disease, schizophrenia, and bipolar disorders. Finally, there is the suspicion that high MeHg levels in the fetus may damage the development of the nervous system, causing delays and difficulties in learning and thinking;
- kidney and liver damage: Hg is not entirely retained by the body and is partly eliminated. The organs involved in the elimination process are different depending on the Hg specie responsible of the exposure: in case of intoxication with inorganic forms of Hg, the removal occurs through the kidneys and can be up to 80% of the total amount absorbed, whereas organic Hg forms are removed by the liver and hardly exceeds 10%. However, high levels of exposure are required to cause a damage of this organs (Bernhoft, 2012; Zahir et al., 2005);

- cardiovascular effects: exposure to Hg can cause accelerated heart rate, irregular pulse, chest pain and palpitations. Exposure to MeHg through frequent fish consumption is of particular interest because it has been shown to be associated with the development of atherosclerosis and increased risk of cardiovascular diseases (Yoshizawa et al., 2002);
- effects on reproduction: Hg is capable of largely affecting reproductive functions in both men and women, causing reduced fertility and difficult in conception, miscarriages, reduction in the number and mobility of spermatozoa, mostly as a result of chronic exposure. Hg can also be transferred to the fetus through the placenta;
- genetic and epigenetic effects: exposure to both MeHg and Hg^{2+} might be associated with altered DNA methylation, interfering with transcription and protein synthesis (Goodrich et al., 2013).

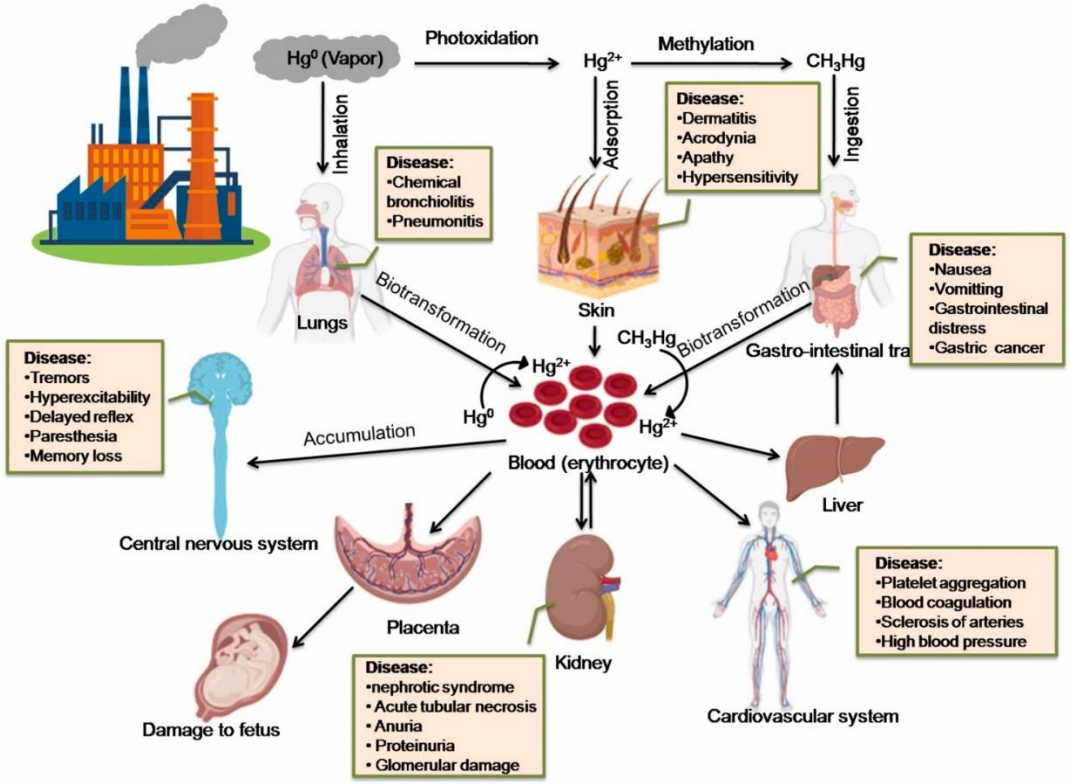

Figure 3: summary of Hg species distribution and transformations in human body and effects on different organs (Priyadarshanee et al., 2022)

In order to assess the possible risks for human health related to the presence of the various Hg forms in the environment and to identify the best remediation actions at global, regional, and local levels, it is necessary to better understand the phenomena of the biogeochemical cycle of this element, particularly those concerning emissions to the atmosphere from natural surfaces of legacy contaminated sites, which potentially represent relevant secondary sources of Hg^0

available for long-range transport (Gustin et al., 2003; Kocman et al., 2017; Osterwalder et al., 2019).

1.4.2 Mercury biogeochemical cycle in the environment

Mercury is subject to a complex natural biogeochemical cycle which involves every environmental compartment (Fig. 4).

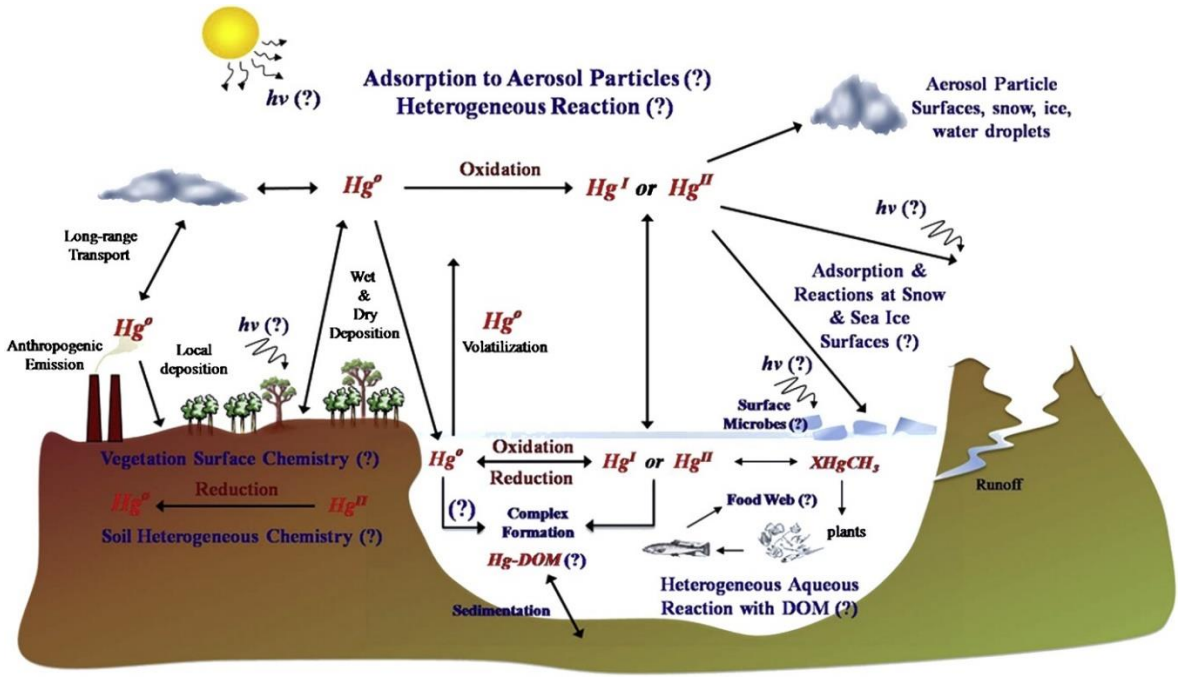

Figure 4: schematic representation of Hg biogeochemical cycle in the environment (Subir et al., 2011).

This biogeochemical cycle "begins" with the mobilization of Hg stored in deep lithospheric reservoirs mostly through volcanic and geothermal activity or emissions from naturally enriched areas as Hg^0 (Pirrone et al., 2010). Once emitted, Hg^0 enters in the global atmospheric pool and thanks to its volatility and stability in this compartment can be transported globally before being oxidised to Hg^{2+}, more soluble and subject to adsorption on particles or cloud and fog droplets and scavenging through dry and wet depositions (Amos et al., 2012; Ariya et al., 2015; Gustin et al., 2020; Lyman et al., 2020). Consequently, the atmosphere represents the main re-distribution pathway for Hg on global scale. By far the most abundant fraction of Hg in the atmosphere (usually ≥90% of the total) is represented by Hg^0, whereas the other fractions are represented by Hg^{2+} in several compounds and by Hg adsorbed on particulate matter (Hg-p) (Ie et al., 2022; Poissant et al., 2005; Ren et al., 2016). Hg^0 represents the form under which Hg is emitted in the atmosphere by natural sources, whereas the occurrence of Hg^{2+} and Hg-p forms is predominantly associated with anthropogenic activities (Liu et al., 2010; Schroeder

and Munthe, 1998; Selin, 2009) or can result from oxidation processes of Hg^0, particularly in presence of photochemical smog oxidants (Gabay et al., 2020).

The oxidation of Hg^0 to Hg^{2+} in the atmosphere and subsequent scavenging through depositions represent a key aspect of Hg biogeochemical cycle, but large uncertainties still persist on the redox chemistry of Hg in this compartment, e.g. about the predominant Hg oxidant. Several oxidant agents have been proposed such as ozone, bromine, chloride, hydrogen peroxide, hydroxyl and nitrate radicals, with bromine being the prime candidate (Lyman et al., 2020 and references). The role of bromine (and in general of halogens) in atmospheric Hg^0 oxidation may be confirmed by the high depositions of Hg observed corresponding with an increase in bromine concentrations, for example during the Atmospheric Mercury Depletion Events typically observed during Arctic spring (Brooks et al., 2006; Kamp et al., 2018; Skov et al., 2004). Moreover, Hg^0 oxidation seems to be favoured in marine boundary layer due to the higher concentration of halogens in marine aerosol (Griggs et al., 2020; Laurier et al., 2003). Due to their shorter residence time in the atmosphere, in the order of days or weeks, Hg^{2+} and Hg-p emitted by anthropogenic sources exert an impact more localised near the emission source (O'Connor et al., 2019; Schroeder and Munthe, 1998).

Once deposited on soils or waterbodies, Hg^{2+} can be reduced back to Hg^0 and re-emitted to atmosphere, becoming again available for long-range transport: these deposition-reemission cycles (or "hopping") contribute to further increase the spatial spreading of Hg in the environment, which can thus reach even remote and pristine areas (Agnan et al., 2016; Ci et al., 2011; Kurz et al., 2019). This atmospheric redistribution represents the predominant supply of Hg for remote environments (Selin, 2009). Consequently, Hg can persist and circulate within the atmosphere-pedosphere-hydrosphere-biosphere system for thousands of years as the ultimate sink for Hg, represented by burial in deep-sea sediments, occurs very slowly (Selin et al., 2008). This natural biogeochemical cycle of Hg has been deeply altered by the releases related to anthropogenic activities, which significantly increased both the amounts stored in the various environmental compartments and the amounts exchanged among them (Fig. 5): it has been estimated that present-day atmospheric deposition to natural surfaces are 3- to 5-fold higher than the pre-industrial levels (Mason and Sheu, 2002), and that a large component of these depositions (~60%) is attributable to Hg re-emitted from natural surfaces (Engstrom et al., 2014).

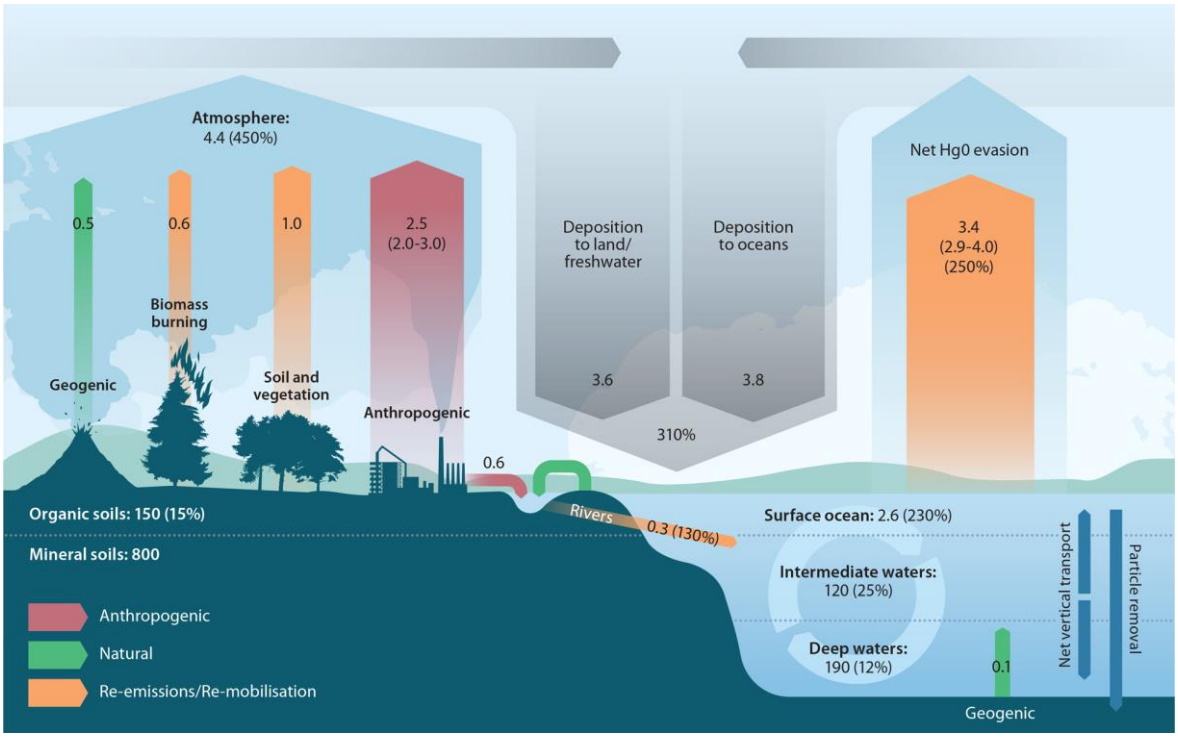

Figure 5: estimation of global Hg budgets in different environmental media. Percentages indicate the estimated increase from pre-anthropogenic levels due to human activities (Outridge et al., 2018).

Moreover, it is estimated that natural primary Hg emissions to atmosphere (volcanoes and geothermal activity) account for an overall amount of 80-600 Mg yr^{-1} and primary anthropogenic releases contribute for about 1900-2900 Mg yr^{-1}, whereas secondary emission from natural surfaces of previously emitted Hg contributes approximately 4520-4700 Mg yr^{-1} to the global atmospheric Hg pool (Driscoll et al., 2013). A large part of these re-emissions has been attributed to Hg previously mobilized by anthropogenic sources, but the discrimination from that deriving from natural primary emission is still difficult (Bishop et al., 2020).

Even though anthropogenic emissions are expected to decrease in the near future thanks to the implementation of emission control measures and phase-out of Hg use, particularly in the Northern Hemisphere (Horowitz et al., 2014; Lyman et al., 2020; Zhang et al., 2016), legacy emissions of Hg from natural surfaces would continue to affect the global Hg cycle for several tens to hundreds of years (Obrist et al., 2018). Moreover, the current global climate change could further influence the amount of Hg^0 re-emitted to the atmosphere, as confirmed by the modest decline of Hg^0 atmospheric concentration observed in the Arctic. This is likely a result of the reduced amount of sea-ice, which allows for greater gaseous exchanges at sea-air interface (Chen et al., 2015; Cole et al., 2013; DiMento et al., 2019; Kalinchuk et al., 2021). Additionally, increased permafrost thawing caused by global warming may cause a

considerable increase in the amount of Hg^0 released from soil surfaces in areas affected by this phenomenon (Ci et al., 2018; Dastoor et al., 2022).

1.4.3 Mercury in aquatic environment and water-air gaseous exchanges

As stated above, atmospheric depositions represent the most important and in many cases unique source of Hg for aquatic environments, particularly in open sea areas, oceans, and remote lakes (Fitzgerald et al., 1998; Mason and Sheu, 2002). Conversely, supplies related to direct discharges from anthropogenic activities or leaching and erosion of soils are usually restricted to rivers and coastal areas, particularly near relevant contamination sources (Amos et al., 2014; Feng et al., 2019; Xue et al., 2019). However, there is a growing body of evidence that for freshwater environments such as lakes supplies of Hg^{2+} associated with dissolved organic matter (DOM) of terrestrial origin as a result of catchment runoff may represent a largely underestimated source of potentially available Hg (Branfireun et al., 2020). Globally, estimated atmospheric depositions of Hg range between 4200 and 6800 Mg yr^{-1}, and about 30-70% of these goes to the oceans (Holmes et al., 2010; Lamborg et al., 2002; Strode et al., 2007). The ionic form Hg^{2+} has a pivotal role in the aquatic biogeochemical cycle of Hg (Fig. 6) as it is involved in several different processes leading to the production of Hg^0 through abiotic (photochemical) or biotic reduction and of MeHg through methylation, mainly in anoxic environments (Branfireun et al., 2020; Fitzgerald et al., 2007).

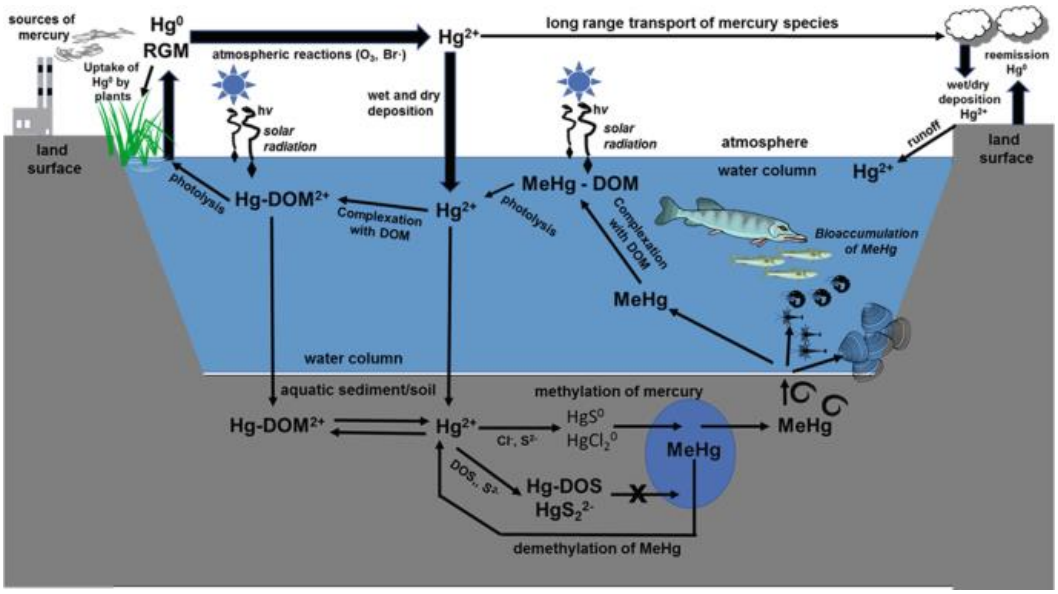

Figure 6: schematic representation of the main processes of Hg biogeochemical cycle in aquatic environments (Orem et al., 2019).

In the water column Hg^{2+} can interact with several inorganic and organic ligands, forming complexes with different stabilities. Among inorganic complexes, the Hg-hydroxides complexes are considered the most important in freshwater environments, whereas in marine environments Hg-chloride complexes become the dominant form due to the high concentrations of chlorides (Ravichandran, 2004). However, the highest stability constant between Hg inorganic complexes is attributable to Hg-sulphide complexes, which are predicted to be the most abundant Hg^{2+} inorganic form in marine sediments (Fitzgerald et al., 2007; Ravichandran, 2004). Similarly, among organic ligands those containing sulphur can bind Hg^{2+} more strongly than oxygen containing ligands: as a result, Hg^{2+} preferentially coordinates with functional groups of DOM containing reduced sulphur (e.g. thiols), forming stronger bounds than with oxygen- or nitrogen-containing functional groups (Ravichandran, 2004; Xia et al., 1999).

Depending on concentration and structure of DOM, the adsorption of Hg by DOM deeply influences the availability of this metal in the water column for the uptake by microorganisms (Graham et al., 2013) or for reduction to Hg^0 (Gu et al., 2011; Jiang et al., 2015). The formation of complexes between Hg^{2+} and various ligands can facilitate the adsorption of Hg on the particulate matter and its subsequent removal from the water column together with settling particles. This process is particularly important in coastal and freshwater settings, where particulate Hg represents the most abundant fraction (Fitzgerald et al., 2007; Sharif et al., 2014; Soerensen et al., 2010), whereas in open oceans the removal through this pathway occurs slower due to lower particle concentrations (Bowman et al., 2020). Moreover, the removal through particle scavenging is also affected by possible desorption of Hg during settling (Lamborg et al., 2016). Under low-oxygen conditions, Hg^{2+} is also easily scavenged through co-precipitation with iron (Fe) and manganese (Mn) oxy-hydroxides (Daye et al., 2015).

Under anoxic conditions, Hg^{2+} can be converted into its organic and more toxic and bioaccumulable form MeHg through the transfer of a methyl group from an organic compound to a metal ion (Morel et al., 1998). Methylation is believed to occur both in sediments and in water column (Eckley and Hintelmann, 2006) mainly as a biotic process initially associated with sulphate-reducing and iron(III)-reducing bacteria (Compeau and Bartha, 1985; Kerin et al., 2006) and more recently to all microorganisms (*Bacteria* and *Archaea*) that possesses the *hgcA* or *hgcB* genes (Parks et al., 2013), whereas the environmental significance of abiotic methylation in presence of methyl donors (e.g. methylcobalamin, humic material, methyltin) is still unclear (Beckers and Rinklebe, 2017). The genes responsible for Hg methylation have been detected in all anaerobic environments, including oxygenated layers of the open ocean

waters (Podar et al., 2015). Moreover, all anaerobic microenvironments in oxic water layers such as peryphyton, roots of macrophytes and settling particles may represent a source of MeHg for the water column through *in situ* production (Bouchet et al., 2018; Starr et al., 2022; Xiang et al., 2021), facilitating the bioaccumulation of produced MeHg through the trophic web (Pestana et al., 2019).

MeHg can also be degraded in aquatic environment through demethylation processes occurring either by a reductive pathway producing Hg^0 and CO_2 or by an oxidative pathway leading to the generation of Hg^{2+} and CO_2 (Barkay et al., 2003; Du et al., 2019). Demethylation can also be catalysed by incident solar radiation, especially at relatively low Hg concentrations in lake or lagoon waters (Klapstein and O'Driscoll, 2018; Seller et al., 1996), but there are still uncertainties as to whether photodemethylation leads to the production of Hg^0 or Hg^{2+} (Luo et al., 2020). Methylation and demethylation occur at the same time and their balance influence the net yield of MeHg production and its concentrations in the environment (Du et al., 2019; Hines et al., 2012).

The formation and evasion of Hg^0 in water can represent an important pathway to reduce the burden of Hg^{2+} available for the conversion to the organic form, contributing to limit the amount of Hg taken up by organisms and bioaccumulated through the trophic web (Horvat et al., 2003). Hg^0 generally represents only a fraction (~5-50%) of total Hg in water (Kotnik et al., 2017; O'Driscoll et al., 2003) but accounts for almost the total amount of the volatile fraction of Hg in water (operationally defined dissolved gaseous mercury, DGM; Rolfhus and Fitzgerald, 2001). The organic volatile form of this metal, dimethylmercury (DMeHg), due to its low stability in environmental conditions is detected only at extremely low concentrations and in deep oceans near the sediments where it is produced (Black et al., 2009; Horvat et al., 2003; Kotnik et al., 2017).

Hg^0 is formed in the water column through both abiotic (photochemical) and biotic reduction processes, with photoreduction largely considered the most important reaction in surface waters, where proceeds at faster rates than reduction by microorganisms (Lanzillotta et al., 2002; Soerensen et al., 2010). As a result, a typical pattern of Hg^0 concentrations is characterised by peak values during summer months and at midday, when solar irradiation is higher (Dill et al., 2006; Fantozzi et al., 2013b; Lanzillotta and Ferrara, 2001; Oh et al., 2011; Wollenberg and Peters, 2009).

Different pathways for Hg photoreduction have been proposed (Fig. 7). The interaction Hg-DOM plays a key role in the photoreduction of Hg^{2+} since DOM can absorb the energy of incoming solar radiation generating free electrons available to reduce Hg^{2+}, and this process is

favoured by the formation of weak complexes between the metal and functional groups of DOM (Costa and Liss, 1999; Luo et al., 2020; Zheng and Hintelmann, 2009). This effect is enhanced in presence of freshly produced DOM rich in chromophore groups, e.g. fulvic-like soil derived DOM (Fantozzi et al., 2007; Yang et al., 2020), or by the degradation of DOM, increasing the pool of photoreducible Hg^{2+} in water (Schartup et al., 2015).

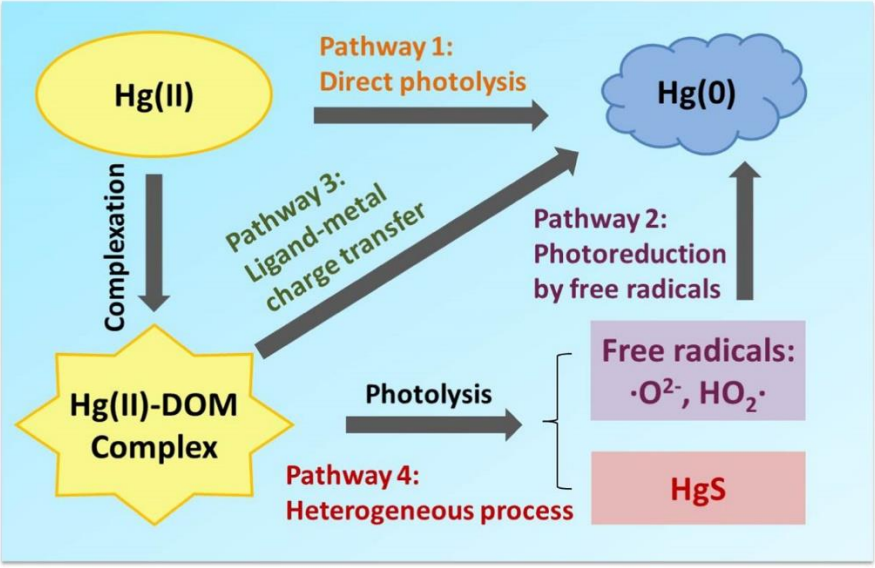

Figure 7: summary of possible Hg^{2+} photoreduction pathways in aquatic environments (Luo et al., 2020).

Ultraviolet (UV) radiation wavelengths are widely considered the most effective in promoting Hg photoreduction both in marine and freshwater environments (Amyot et al., 1997a; Oh et al., 2011) due to their high energy content and the higher absorption of this wavelength range by Hg complexes (Lee et al., 2019; Nriagu, 1994). However, Hg^{2+} can be reduced to Hg^0 through the interaction with particular fractions of DOM, e.g. humic substances, even in absence of light (Allard and Arsenie, 1991; Vudamala et al., 2017), even though DOM could have been photoactivated previously (Luo et al., 2022). On the other hand, the complexation with DOM can also decrease the availability of Hg^{2+} for photoreduction through the formation of strong bounds between Hg and reduced sulphur groups (Amyot et al., 2004; Gu et al., 2011) due to the higher energy required to break the Hg-S bound (Jeremiason et al., 2015). In a recent study, Wang et al. (2020) observed that the reduction of Hg^{2+} is inhibited at Hg/dissolved organic carbon (DOC) ratios above 1134 ng mg^{-1}, due to the dispersion of the incoming solar radiation on more Hg-DOM bounds. Moreover, an increase in DOM concentration could also limit the penetration of incident solar radiation through the water column, inhibiting the photochemical reactions (Castelle et al., 2009; Klapstein and O'Driscoll, 2018).

The formation of Hg^0 through biotic reduction seems to be related to detoxification pathways of Hg resistant bacteria (Barkay et al., 2003) through Hg reductase enzyme, but this reduction capacity has been observed also for microorganisms that do not possess the necessary gene (*merA*) to generate this enzyme, such as cyanobacteria (Kuss et al., 2015). Both prokaryotic and eukaryotic microorganisms have been proven to catalysed Hg^{2+} reduction (Mason et al., 1995), but in the latter case it is still not clear if the reduction occurs inside the cell or due to the excretion of reducing exudates (Liang et al., 2022). Moreover, biotic reduction may represent an important pathway for Hg^0 production in deep water layers and sediments, where UV radiation cannot penetrate (Fantozzi et al., 2009; Lepak et al., 2021).

The Hg^0 produced in deep water layers can then be transferred to surface water thanks to diffusion or advection related to water column mixing and upwelling induced by wind (Kuss et al., 2018; Wollenberg and Peters, 2009). When surface water is supersaturated in DGM relative to the atmosphere the volatilisation of this fraction of Hg through water-air interface can occur (Amyot et al., 1997b; Southworth et al., 2007), whereas if surface water is undersaturated in DGM depositions of Hg can be observed (Fu et al., 2013). This last situation can be caused by the occurrence of high atmospheric Hg concentrations related to the movement of air masses enriched in Hg^0 due to high emissions related to anthropogenic activities (Fu et al., 2010; Wang et al., 2016) or natural sources such as volcanic activity (Andersson et al., 2007).

Moreover, Hg^0 concentrations in surface water are the result of the net balance between Hg^{2+} reduction and Hg^0 oxidation reactions, which coexist in the environment and occur at comparable rates (O'Driscoll et al., 2018; Qureshi et al., 2010). Similar to reduction, oxidation is catalysed by incident solar radiation thanks to the photogeneration of oxidant radicals (He et al., 2014; Lalonde et al., 2004) and can overcome reduction when solar radiation weakens at sunset and during nights (Garcia et al., 2005). Oxidation is further enhanced in saltwater compared to freshwater environments due to the higher concentrations of halides (e.g. chlorides and bromides), which can both act as oxidants and stabilise oxidation products by forming complexes with the produced monovalent Hg^+ (Lalonde et al., 2001; Yamamoto, 1996). As a result, Hg^0 losses through oxidation in surface salt waters can be particularly high under strong solar irradiation conditions during summer (Ferrara et al., 2003) and overcome those through volatilization (Ci et al., 2016b; Lalonde et al., 2001). This makes marine environments more sensitive to Hg pollution than freshwater environments due to an increased residence time of Hg in the water column (Ci et al., 2016b).

The overall mass transfer of highly volatile gaseous species such as DGM at water-air interface depends on the rate of delivery of the dissolved gas to the surface water layer, which is related to mixing conditions, and on the rate of diffusion of the solute in the water matrix. This diffusion is in turn influenced by the viscosity of water and the solubility of the chemical species (Southworth et al., 2007; Tomažič et al., 2018) and represents the limiting step for Hg^0 exchanges due to the much lower resistance of the air boundary layer to Hg^0 diffusion (Zhu et al., 2016). As a result, parameters that influence the solubility of DGM such as temperature and salinity can deeply influence the rate of gaseous exchanges at the water-air interface (Kuss et al., 2009; Loux, 2004; Poissant et al., 2000).

Conditions of high wind speeds and subsequent turbulent mixing of the water column, waves, and currents can ensure supplies of photoreducible Hg^{2+} or directly DGM to shallow water layers, making it available for the evasion, particularly in coastal areas and lakes (Sharif et al., 2013; Wollenberg and Peters, 2009). Moreover, high wind speeds can also increase the exchange surface between water and air, promoting the gaseous exchanges (Fantozzi et al., 2013b).

1.4.4 Mercury in terrestrial environment and soil-air gaseous exchanges

Mercury biogeochemical cycle in terrestrial environment is characterised by a complex network of reactions involving gaseous exchanges with the atmosphere at the soil-air and plant-air interfaces, adsorption-desorption on mineral and organic soil surfaces, interconversion between different chemical forms and potential leaching and run-off to aquatic ecosystems (Fig. 8).

Nevertheless, soils represent the largest terrestrial pool of Hg (Grigal, 2003; Obrist, 2012). The majority of Hg in surface soils on global scale derives from atmospheric dry and wet depositions occurring directly on soils or indirectly through litterfall and throughfall from plants (Demers et al., 2013; Enrico et al., 2016), but there is still debate as to whether soils serve as a sink or secondary source of Hg for the atmosphere (Agnan et al., 2016; Bishop et al., 2020). It is estimated that due to anthropogenic activities the total amount of Hg stored in soils has doubled since pre-industrial period, reaching a global mass accumulated in soils assumed to be in the range of 250-1000 Gg (Amos et al., 2013; Obrist et al., 2018).

Typically, total Hg (THg) concentrations in background soils are not expected to exceed 0.1 mg kg^{-1} whereas in geologically enriched areas or near point sources this value can reach hundreds or thousands of mg kg^{-1} (Ballabio et al., 2021; Beckers and Rinklebe, 2017; Gosar et al., 2006; Higueras et al., 2006; Teršič et al., 2011). Naturally enriched areas are usually found

near the above cited "mercuriferous belts" and therefore the occurrence of high Hg concentrations outside these areas can quite reliably be identified as anthropogenic (Beckers and Rinklebe, 2017).

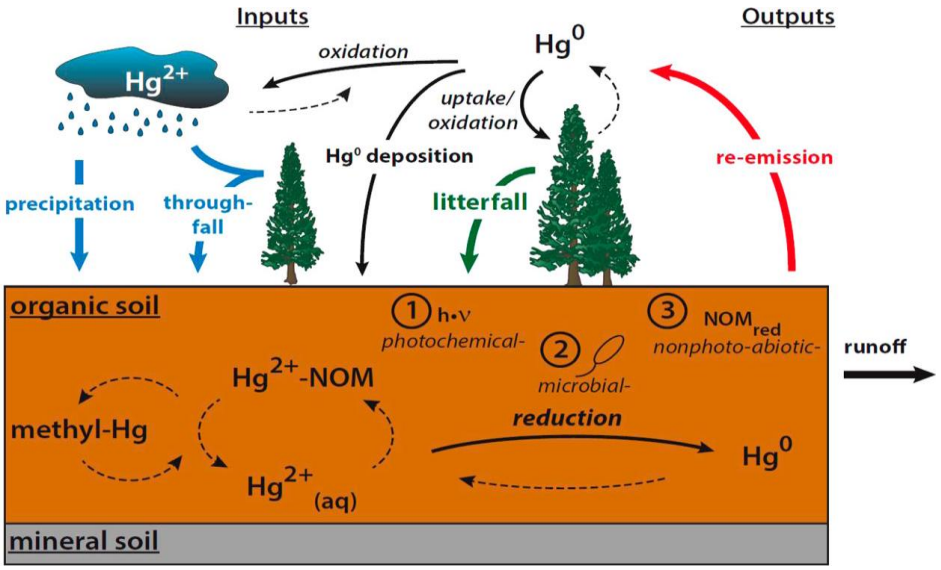

Figure 8: schematic representation of main processes of Hg biogeochemical cycle in terrestrial environments (Jiskra et al., 2015).

As for aquatic environments, Hg^{2+} represents the dominant form of Hg in soils, where can occur as 1) free ion dissolved in soil solution, 2) adsorbed non-specifically (weak electrostatic bond) or specifically (covalent bond), 3) chelated by different organic ligands or as mineral (Gabriel and Williamson, 2004; Schuster, 1991). Due to its high affinity for mineral surfaces and functional groups of organic matter, Hg^{2+} tends to be relatively immobile in soils compared to many other metals (O'Connor et al., 2019; Seo et al., 2008), forming many different inorganic and organic complexes. The formation of these complexes greatly influences Hg mobility and availability through the soil (Sysalová et al., 2017). Due to these differences in mobility and bioavailability of the various Hg species, the impact of Hg pollution cannot be properly assessed through the determination of total Hg concentrations only (Fernández-Martínez et al., 2019).

Generally, most of Hg supplied from atmospheric depositions is retained in organic upper soils thanks to the adsorption by OM (Baptista-Salazar et al., 2017; Grigal, 2003; Jiskra et al., 2015) mostly due to the high affinity of Hg for functional groups containing reduced sulphur such as thiols (Xia et al., 1999). When these groups become saturated, Hg^{2+} can be bound by soil OM through the formation of weaker complexes with oxygen or nitrogen containing functional groups such as alcohols, carboxylic acids or amines (Gismera et al., 2007). Organic Hg

complexes are usually characterised by a high degree of stability, only weakly affected by the pH, and low solubility in water (O'Connor et al., 2019). In addition, Hg^{2+} can be immobilized through sorption on soil matrix surfaces such as clay minerals, where Hg can form strong covalent bonds with oxygen atoms, and iron and manganese oxi-hydroxides (Coufalík et al., 2012; Jiskra et al., 2014; Yin et al., 1996).

Thanks to the high susceptibility of Hg^{2+} to be adsorbed through the formation of the above cited complexes with solid surfaces, only a small fraction of this metal typically occurs in the aqueous soil solution. As a result, Hg leaching rates are usually very low and influenced by Hg species found in soils (O'Connor et al., 2019; Palmieri et al., 2006). The speciation of Hg in soil solution is controlled by the physico-chemical characteristics of the soil such as pH, redox potential, and concentration of DOM, dissolved oxygen, and sulphides: under natural conditions, the most abundant forms of Hg occurring in soil solution are represented by $HgCl_2$, HgClOH and $Hg(OH)_2$ under acid, neutral and basic pH conditions respectively (Davis et al., 1997). These species can further be subject to sorption-desorption processes which influence their mobility through the soil: for example, the adsorption of Hg^{2+} or its complexes on hydrophilic fraction of colloidal organic matter can increase the availability of Hg forms and their mobility through the soil profile (O'Connor et al., 2019; Schuster, 1991).

Under anoxic conditions, sulphides represent the main inorganic ligand for Hg^{2+}, forming highly stable and insoluble compounds (Gabriel and Williamson, 2004) such as cinnabar (α-HgS) and metacinnabar (β-HgS), which are considered the less mobile and toxic Hg forms in soils (Gai et al., 2016; Sysalová et al., 2017). Cinnabar is usually the main form of this metal in naturally enriched substrates and in soils of former Hg mining sites due to both natural occurrence and anthropogenic discharge of mine tailings (Bavec and Gosar, 2016; Fernández-Martínez et al., 2019; Gustin et al., 2003; Pelcová et al., 2021). Conversely, β-HgS can be formed as a by-product during ore roasting processes in presence of impurities and occur in soils due to dumping of tailing material, as previously observed in areas interested by past metallurgical activities (Biester et al., 2000; Esbrí et al., 2010). Metacinnabar can also be formed directly in soils as a result of precipitation in presence of high sulphide concentrations (Skyllberg and Drott, 2010) or directly from Hg-thiolate organic complexes (Enescu et al., 2016).

Under anaerobic conditions, for example in permanently or periodically flooded soils, Hg^{2+} may also be converted to MeHg through microbial methylation by anaerobic bacteria (e.g. sulphate-reducing and iron-reducing bacteria or methanogens, Liu et al., 2014) in function of

its bioavailability, with lower rates of conversion for Hg complexed by high molecular weight OM or insoluble Hg-sulphide compounds (Gray et al., 2015; Skyllberg et al., 2006). Moreover, recent findings indicate that Hg methylation in soils is not restricted to wetlands and impoundments but can occur also in anoxic microenvironments within oxic soil layers (Shanley et al., 2020). Even though MeHg usually represents less than 2% of total Hg in soils (Schlüter, 2000), the mobilization of MeHg produced within soils can represent a relevant source of this bioaccumulable Hg form to aquatic environments through leaching and runoff (Bishop et al., 2020; Bravo et al., 2017).

Moreover, soils can also represent a significant source of Hg for the atmosphere through the emission of Hg^0. Elemental Hg in soil can derive from direct dry depositions from the atmosphere (Montoya et al., 2019), formation in soil through abiotic and biotic reduction reactions (Pannu et al., 2014) or direct discharge due to anthropogenic activities (Davis et al., 1997; Watson et al., 2015), e.g. after its use for amalgamation in ASGM (Dalziel and Tordon, 2014; Gustin et al., 2003). In extreme cases, droplets of liquid Hg^0 can be seen in highly contaminated sites (Davis et al., 1997; McLagan et al., 2019; Watson et al., 2015) but generally Hg^0 in aerobic soils is relatively quickly lost through evasion to the atmosphere, oxidation to Hg^{2+} favoured by high amounts of OM or sorption on solid soil surfaces (Palmieri et al., 2006; Windmöller et al., 2015).

Hg^0 evasion at the soil-air interface is generally regulated by complex site-specific interactions of various environmental factors such as solar radiation, soil and air temperatures, precipitation and soil moisture, vegetation cover, soil porosity, soil disturbance by biotic or anthropogenic activity, Hg concentration in soil and air (Beckers and Rinklebe, 2017).

The availability of Hg in the substrate usually represents the primary control on Hg^0 evasion at soil-air interface (Agnan et al., 2016), with higher Hg^0 emissions reported for surfaces characterised by higher Hg content in the substrate due geological enrichment or anthropogenic contamination (Coolbaugh et al., 2002; Gustin et al., 2003). However, the occurrence of extremely high atmospheric Hg concentration due to transport of air masses from areas characterised by strong Hg sources can suppress emissions also from high contaminated substrates and cause the occurrence of Hg deposition events (Eckley et al., 2015; Miller et al., 2011).

Incident solar radiation has a strong effect on Hg^0 evasion from soils as it can promote photoreduction of Hg^{2+} on soil surface and in first millimetres, the layer most involved in gaseous exchange with atmosphere (Bahlmann et al., 2006; Carpi and Lindberg, 1998; Zhou et

al., 2021), generally resulting in higher Hg^0 fluxes from irradiated than shaded soils, e.g. those in forested ecosystems (Wang et al., 2006).

The presence of vegetation deeply impacts the microclimatic conditions and air mixing of the boundary layer near soil surface, limiting the Hg^0 emissions mainly due to soil shading (Gustin et al., 2004): the limitation of soil Hg^0 fluxes by the presence of vegetation is confirmed by the strong increase in emissions generally observed e.g. after deforestation and biomass harvesting (Carpi et al., 2014; Eckley et al., 2021; Mazur et al., 2014).

The radiation in the UV wavelength range is considered the most effective in promoting the photoreduction of Hg^{2+} in soils (Choi and Holsen, 2009a; Moore and Carpi, 2005), but the formation of Hg^0 in soils can occur also in absence of radiation by means of biotic reduction. This occurs mainly through specific detoxification pathways of Hg-resistant microorganisms with the *mer* operon in their genome or non-specific reduction linked to microbial detoxification of reactive oxygen species (Fritsche et al., 2008; Osterwalder et al., 2019; Pannu et al., 2014). Finally, also direct interaction with specific fraction of soil OM, e.g. fulvic or humic acids can lead to Hg reduction, particularly if OM is rich in quinones as electron source (Zheng et al., 2012).

Moreover, solar irradiation can also promote soil heating, exerting a synergic control on Hg^0 fluxes with soil temperature (Lin et al., 2010). Higher soil temperatures can catalyse reaction rates of Hg^0 formation and lead to a higher diffusion of gases, favouring the migration of Hg^0 to the surface soil layers and its subsequent release to the atmosphere (Schlüter, 2000). An increase in soil temperature can also promote the desorption of Hg from soil surfaces thanks to higher thermal motion and promoted microbial activity (Pannu et al., 2014; Sigler and Lee, 2006).

The effect of temperature on soil Hg^0 fluxes can be understood through the calculation of the activation energy (Ea) associated with the gaseous releases (Kocman and Horvat, 2010). The Ea is defined as the energy that the system should absorb to initiate or increase the Hg^0 release from soil to the gaseous phase (Gustin et al., 2003; Lindberg et al., 1995). Assuming that Hg^0 release from soil occurs with a pseudo first order kinetics, the relationship between temperature and Hg^0 fluxes (F) can be quantitatively described through the Arrhenius equation (Ci et al., 2016a; Llanos et al., 2011):

$$\ln(F) = \ln(A) - \frac{E_a}{RT}$$

where *Ea* is the apparent activation energy, *T* is the absolute temperature, *R* is the gas constant and *A* is a pre-exponential factor and that can be visualised in a ln(F) vs 1/T plot. If the calculated Ea is higher than that needed for the evaporation of liquid Hg^0 (59 kJ mol^{-1}) emission of Hg from soil surface cannot be attributed solely to the direct physical evaporation of Hg^0 (Fu et al., 2008; Gustin et al., 2003; Kocman and Horvat, 2010). The lowest Ea values are commonly reported for soils characterised by the occurrence of Hg species more available for volatilisation such as Hg^0 (Schlüter, 2000) whereas higher energies are usually required to initiate evasion from substrates containing less mobile and reactive Hg forms like HgS (Gustin et al., 2002; Kocman and Horvat, 2010).

Sorption/desorption processes of Hg on soil organic and mineral surfaces play a key role in regulating the amount of this specie available for volatilisation (Gonzalez-Raymat et al., 2017) as desorbed Hg^{2+} in soil solution is generally more available for the reduction to Hg^0 than that strongly bound to OM (Jiskra et al., 2014; Pannu et al., 2014). As a result, an increase in soil OM can lead to a reduction in Hg^0 evasion to the atmosphere (Yang et al., 2007). Moreover, the vertical migration of Hg^0 can also be limited in clay soils due to higher compaction of particles and increased contact time between Hg^0 and mineral surfaces, resulting in higher sorption (Gonzalez-Raymat et al., 2017; Langston and Bebianno, 1998).
In the soil saturated zone, instead, the adsorption of Hg^{2+} on mineral surfaces mostly of iron(II)-bearing minerals can enhance the reduction of Hg^{2+} through electron transfer from Fe(II) and the subsequent transport of produced Hg^0 by groundwater movement (Debure et al., 2020; Ha et al., 2017; O'Loughlin et al., 2020). On the other hand, sorption of Hg^0 on mineral soil surfaces can contribute to limit its vertical diffusion through the pore space and consequently its evasion to the atmosphere (Yuan et al., 2019b; Zhou et al., 2021). This sorption can occur through van der Waals interactions with soil mineral surfaces, particularly effective in soils with high clay content due to the large surface area available for interactions (Xin et al., 2007), or through partitioning into the hydrophobic portion of soil OM as testified by its octanol-water partitioning coefficient (K_{OW}=4.17) higher than that of other soluble forms of Hg (Gonzalez-Raymat et al., 2017; Miller et al., 2007).
Finally, also variations in soil moisture content can significantly impact the Hg^0 evasion from soil into the atmosphere, with a general increase in Hg^0 fluxes as soil moisture increases (MacSween and Edwards, 2021; Song and Van Heyst, 2005; Wallschläger et al., 1999) until soil become saturated, condition in which fluxes are suppressed (Ericksen et al., 2005). This

flux enhancement, e.g. after a precipitation event, is generally higher for soils with a relatively low initial water content (Kocman and Horvat, 2010; Song and Van Heyst, 2005).

As summarised in Figure 9, this phenomenon has been linked to water infiltration through the soil column which can cause the displacement of Hg^0 from soil pore space and the desorption of Hg from solid surfaces due to its replacement by more polar water molecules, resulting in an immediate pulse of Hg^0 emission. The desorption continues as rainwater further infiltrates, but fluxes are suppressed due to soil saturation. After the rainfall cessation, the evasion can be increased by an increase of available energy (e.g. due to solar irradiation) for abiotic and biotic reduction of desorbed Hg^{2+} and, as soils dries, both Hg^{2+} and Hg^0 can be transferred to soil surface by water evaporation process and become more available for volatilisation. Finally, when soil becomes effectively dry, the Hg^0 emission is suppressed.

Vertical movement of Hg through the soil can also be further influenced by plant transpiration (Briggs and Gustin, 2013) and contribute to Hg^0 release to the atmosphere in function of plant seasonal activity (Cesário et al., 2021; Lindberg et al., 2002).

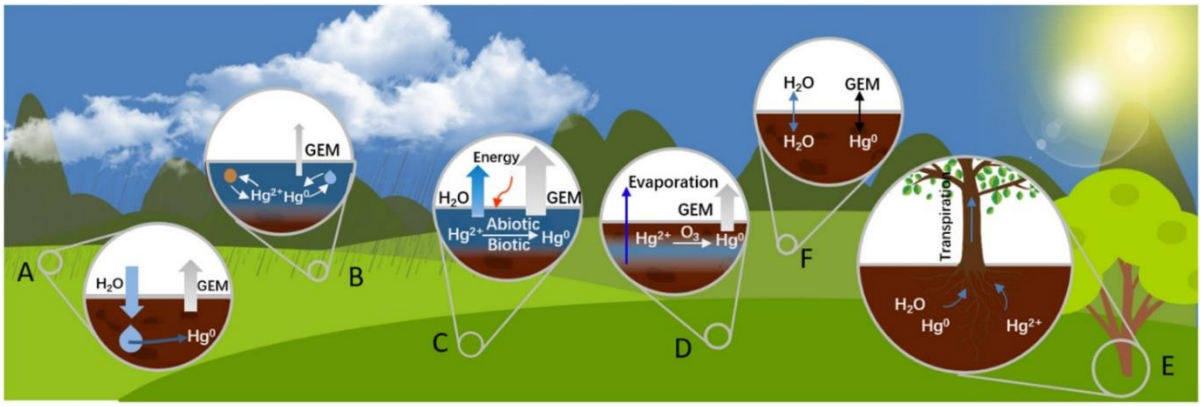

Figure 9: conceptual model of Hg volatilisation in response to rainfall events (O'Connor et al., 2019).

The presence of vegetation can strongly impact the gaseous exchanges of Hg between soils and the atmosphere mainly through soil shading, which limits the intensity of incident light on soil surface and the soil heating, resulting in reduced emissions of Hg^0 (Gustin et al., 2004; Stamenkovic et al., 2008).

Other than reducing emissions from soils, plants can contribute to reduce atmospheric Hg concentrations also through direct exchanges of Hg^0 with the atmosphere through stomatal uptake or cuticular adsorption of dry deposited Hg on leaf surfaces (Eckley et al., 2016; Stamenkovic and Gustin, 2009). Part of this Hg is fixed inside the leaf tissue (Heaton et al., 2005; Millhollen et al., 2006) and can reach the soil after tissue shed (litterfall) or biomass turnover (Rutter et al., 2011; Zhou and Obrist, 2021). This mechanism is particularly effective

in evergreen broadleaf ecosystems, characterised by high Hg deposition and low soil re-emission rates and frequently considered as net sinks for atmospheric Hg (Agnan et al., 2016; Blackwell and Driscoll, 2015; Yuan et al., 2019b; Zhou and Obrist, 2021).

Changes in vegetation cover caused by deforestation or simply by winter dormancy can switch ecosystem gaseous exchanges from net sinks to net sources of Hg^0 to the atmosphere as a result of increasing solar radiation reaching the soil surface (Feinberg et al., 2022; Yuan et al., 2019b). Moreover, recent findings increasingly seem to confirm that Hg^0 exchanges through stomata are bidirectional with a potential re-emission from leaf tissues to the atmosphere of adsorbed Hg^0 (Cesário et al., 2021; Yuan et al., 2019a). These fluxes are function of plant activity (e.g. stomatal opening) and atmospheric Hg^0 concentration, with emissions occurring over a certain compensation point (Naharro et al., 2020; Stamenkovic and Gustin, 2009). These gaseous exchanges are favoured by the low solubility and high vapour pressure of Hg^0, allowing a quick diffusion through mesophyll and leaf intercellular air space (Bash et al., 2007).

1.5 Methods for Hg^0 fluxes estimation

At present day, there are no standardised protocols or commercial flux systems available for the quantification of Hg^0 flux between the atmosphere and soil or water surfaces, hindering a reliable comparison between the results reported in various studies using different methods for flux estimation (Agnan et al., 2016; Sommar et al., 2020). Multiple experimental approaches have been used for the estimation of Hg^0 fluxes, which can be grouped in two main categories: enclosures with different type of flux chambers or various micrometeorological (MM) methods (Sommar et al., 2013; Zhu et al., 2015a).

Flux chambers are frequently used for direct estimation of Hg^0 releases from soils, water, and low-stand grass surfaces thanks to their relatively low cost, versatility, portability, and ease of use (Zhu et al., 2016). The simple operating principle of flux chambers is based on the isolation of a portion of atmosphere over the selected surfaces and the calculation of the flux based on the change of the concentration of the gaseous contaminant in the headspace. Based on operation principle, flux chamber can be classified as either steady-state (SS) or non-steady state (NSS) systems (Fig. 10) (Livingston and Hutchinson, 1995).

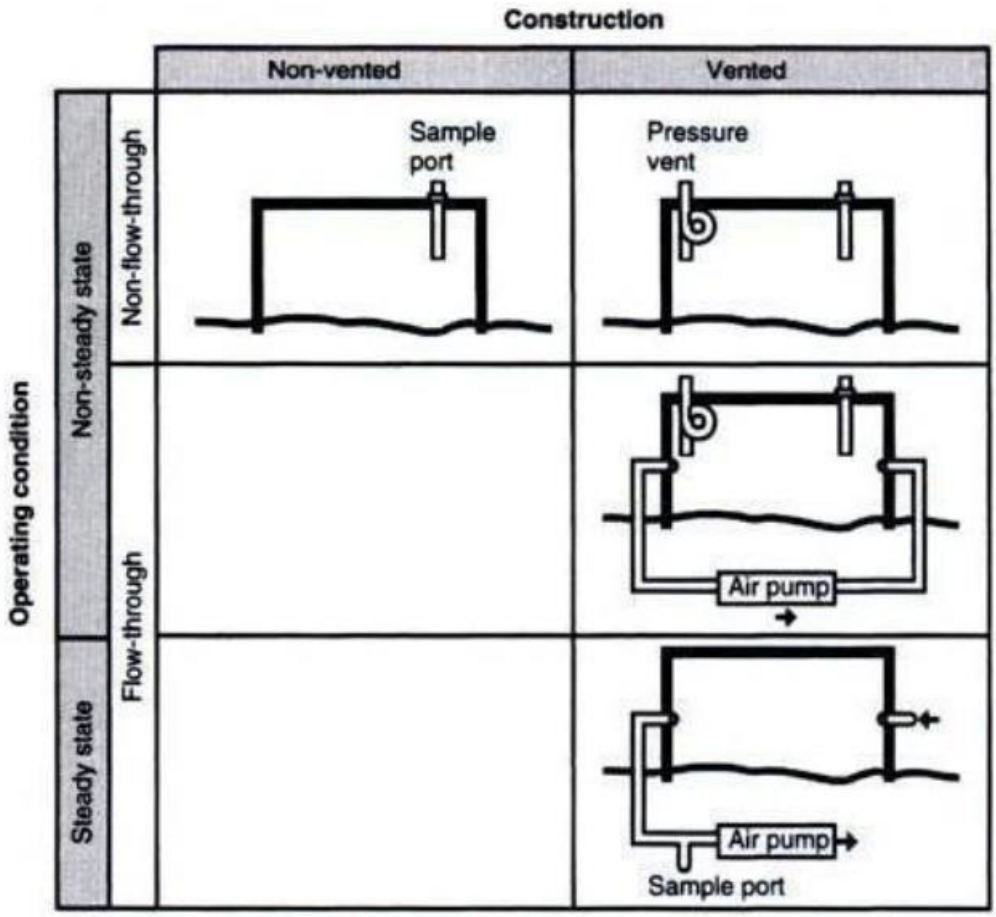

Figure 10: classification of different flux chamber types used for in field gas flux estimation (Livingston and Hutchinson, 1995).

Flux calculation with NSS systems is based on the rate of concentration increase of the gaseous analyte in the isolated atmosphere (dC/dt) during a known time of deployment of the chamber (Sommar et al., 2020), measured through inside air sampling for subsequent analysis or constant monitoring by means of online analysers. These systems can be further divided into static or dynamic depending on whether or not there is a continuous air circulation within them (Heinemeyer and McNamara, 2011; Oertel et al., 2016). In the last case, the system can be defined as "dynamic flow-through chambers", usually provided of venting systems to minimise the occurrence of pressure gradients between inside and outside the chamber (Livingston and Hutchinson, 1995). These systems are frequently used for the estimation of emissions from soils of greenhouse gases (e.g. CO_2, CH_4, N_2O) or for the assessment of soil respiration (Maier et al., 2022; Rochette et al., 1992), but apart from a few exceptions are rarely adopted for measuring Hg^0 fluxes at soil-air interface (Sommar et al., 2020).

The NSS approach has been more frequently adopted for the estimation of Hg^0 fluxes from soils in geothermal or volcanic areas, using both static non-flow-through chambers (Cabassi et al., 2021; Tassi et al., 2016) or dynamic flow-through chambers (Bagnato et al., 2014; Sun et

al., 2020), whereas other studies used dynamic closed chambers in contaminated (During et al., 2009; Rinklebe et al., 2010) or pristine areas (Kyllönen et al., 2012). The rate of concentration increase inside the chamber can be approximated by a linear regression for short deployment times in the order of minutes (Davidson et al., 2002; Kandel et al., 2016) like those commonly used for dynamic closed chambers with online gas analysers (Maier et al., 2022). Conversely, for long deployment times non-linear models are needed to reduce biases in flux estimation related to the built up of concentrations inside the chamber, which can strongly impact the concentration gradient with the soil and consequently reduce the diffusion of gaseous species to the air, altering the pre-deployment natural flux (Hutchinson and Mosier, 1981; Kutzbach et al., 2007; Pedersen et al., 2010; Yue et al., 2022).

The most widely chamber method for the estimation of Hg^0 fluxes from natural surfaces to the atmosphere is conversely represented by open steady-state flow-through chambers (Sommar et al., 2020). In this configuration, the chamber is continuously flushed with ambient air or inert gas at an appropriate constant flow rate depending on the chamber internal volume. The flow rate should ensure sufficiently fast turnover times of internal air, typically less than 1 min, to avoid excessive Hg^0 accumulation in the chamber headspace and the consequent increased boundary layer resistance to gaseous emission which can lead to a flux underestimation (Eckley et al., 2010; Sommar et al., 2020; Verginelli et al., 2018; Zhang et al., 2002). On the other hand, high flow rates through the chamber may increase the shear stress on the surface and the internal air mixing, resulting in greater concentration gradients which facilitate Hg^0 emissions potentially leading to overestimations of the real flux as calculated Hg^0 flux increases with increasing flow rate (Eckley et al., 2010; Wallschläger et al., 1999). Typically, high flushing rates and short turnover times are recommended for measuring fluxes from substrates characterised by high Hg concentration, whereas lower flow rates and higher turnover times can be used for low Hg substrates (Engle et al., 2006). Flux is then calculated considering the flow rate through the chamber and the difference between concentrations of target gas in the in-coming air and out-going air (Gao et al., 1997) alternatively measured at the inlet and at the outlet. This allows for a relatively high time resolution of flux measurements (typically 20 min; Sizmur et al., 2017) which makes chambers particularly suitable for the study of the processes underlying gas exchanges (Sommar et al., 2020).

Other than the flow rate and turnover time, also the shape of the chamber and the positions of inlet and outlet ports can significantly impact the magnitude of measured flux as the occurrence of turbulent mixing inside the chamber can result in artificial concentration gradients and lead to under- or overestimations of natural flux (Carpi and Lindberg, 1998; Eckley et al., 2010; Lin

et al., 2012). Different chamber shapes are reported in literature ranging from cylindrical chambers (Choi and Holsen, 2009b; Cizdziel et al., 2019; Eckley et al., 2010; Tao et al., 2017) to rectangular (Carpi and Lindberg, 1998; Kalinchuk et al., 2021; Sizmur et al., 2017; Wang et al., 2006) or aerodynamic designs (Gao et al., 1997; Lin et al., 2012; Osterwalder et al., 2018; Shi et al., 2020).

For the estimation of Hg^0 fluxes from natural surfaces to the atmosphere, chamber materials characterised by high solar radiation transmission should be preferred in order to allow the natural photoreduction of Hg^{2+} (Carpi et al., 2007; Zhu et al., 2015b); however, the material in which chamber is constructed should also be inert with respect to Hg, limiting its adsorption on chamber walls and allowing to achieve low blank fluxes, avoiding "memory effects" (Eckley et al., 2010; Ferrara and Mazzolai, 1998). Materials used in literature for chamber construction include Teflon (Carpi and Lindberg, 1998; Eckley et al., 2021; Sizmur et al., 2017), Plexiglas (Bagnato et al., 2013; Shi et al., 2020); quartz (Feng et al., 2008; Li et al., 2018; Zhou et al., 2017), and polycarbonate (Coolbaugh et al., 2002; Engle et al., 2001).

The approach of the open flux chamber (in this case also called "flux bag") can also be used for the estimation of Hg^0 exchanges between plants and atmosphere tightening the flux bag to the whole plant or to only part of it (Canário et al., 2017; Cesário et al., 2021; Graydon et al., 2006; Luo et al., 2016). In this case, chamber material should allow the transmission of photosynthetic active radiation (e.g. Tedlar) in order to limit the impact of isolation on plant physiology (Poissant et al., 2008).

The main limitations of flux chamber methods for the estimation of Hg^0 fluxes are the reduced footprint of the systems (generally < 0.1 m^2) and the modification of microclimatic conditions of the studied boundary layer caused by the deployment of the chamber, mostly in terms of temperature and exclusion of effects of wind and atmospheric turbulence, resulting in large uncertainties in scaling-up fluxes to ecosystem level (Zhu et al., 2016).

To overcome these limitations and quantify Hg^0 evasion on ecosystem scale, several MM methods have been developed based on measurements of Hg^0 concentrations at larger spatial scales, which cause only a marginal disturbance of natural environmental conditions (Osterwalder et al., 2018). Moreover, MM methods can also account for the effect of atmospheric turbulence and wind speeds, particularly important in influencing the rate of gaseous exchanges between atmosphere and natural surfaces (Sharif et al., 2013). These techniques can be grouped in 1) direct methods based on measurements of Hg^0 concentrations in air passing over a sampling point coupled with measurements of vertical wind speed and direction (eddy covariance or relaxed eddy accumulation) or 2) indirect methods in which Hg^0

diffusion is quantified on the basis of vertical concentration gradients (aerodynamic gradient or modified Bowen ratio methods) (Sommar et al., 2020).

In aquatic environments, MM models for the estimation of Hg^0 release are frequently based on the measurement of DGM concentrations in surface water and Hg^0 concentrations in the overlying air, with fluxes then calculated on the basis of Hg^0 diffusivity through the boundary layer between water and air. Due to the lower diffusivity of Hg^0 in water than in air, the diffusion within water boundary layer is considered the limiting step in this process, while the diffusion on the air side is frequently omitted in models (Andersson et al., 2007; Nerentorp Mastromonaco et al., 2017; Wängberg et al., 2001). The Hg^0 transfer velocity on the water side of boundary layer is parameterised in function of its specific Schmidt number (Sc), which represents the ratio between kinematic viscosity and diffusion coefficient of Hg^0 in water and is function of temperature and salinity (Kuss et al., 2009), and the wind speed usually measured at a height of 10 m (Tomažič et al., 2018).

The wind speed is used to calculate the friction velocity on the water surfaces with different parameterisation depending on model, e.g. linear (Liss and Merlivat, 1986), quadratic (Wanninkhof, 1992) or polynomial regression (Nightingale et al., 2000). The choice of the model can impact the calculation of Hg^0 transfer velocity and consequently strongly affects the obtained result (Nerentorp Mastromonaco et al., 2017). Moreover, for a precise flux quantification the application of these methods usually requires a fast response and synchronous measurement of several parameters in more locations (e.g. at different heights), which is difficult to achieve at the low concentrations usually observed for Hg^0 in the atmosphere excluding contaminated sites or using single analysers (Sommar et al., 2020; Zhu et al., 2016, 2015b). However, the use passive samplers placed in different point on an area or at different heights can at least partially reduce the uncertainties related to non-contemporary measurements (Jeon and Cizdziel, 2019; McLagan et al., 2019). Finally, MM techniques often require a relatively high expertise of the personnel and moderate to high computing capacity (Sommar et al., 2020).

2. Sampling strategy

A general summary of field activities and analysis performed for this research is reported in Figure 11.

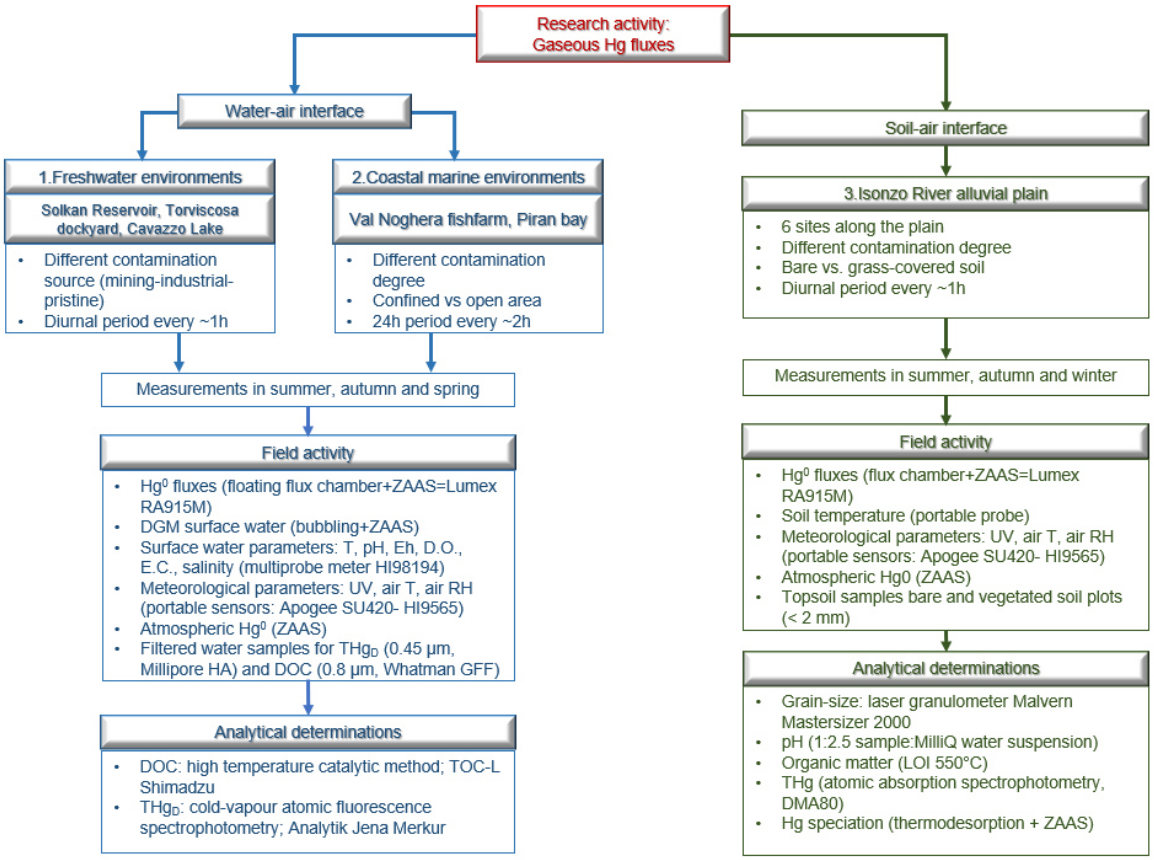

Figure 11: schematic description of sampling and laboratory activities performed during this research project both in aquatic and terrestrial environments.

The research activity was focused on the direct evaluation of Hg^0 releases into the atmosphere from various contaminated surfaces within the highly impacted area near the border between Italy and Slovenia and has been divided into two main topics. The first topic regards the evaluation of exchanges of Hg^0 at the water-air interface performed by means of a Plexiglas steady-state floating flux chamber (50x50x80 cm, Fig. 12) coupled with a real-time portable Hg^0 analyser (Lumex RA915M) through atomic absorption spectrophotometry with Zeeman background correction (ZAAS; Sholupov et al., 2004). This experimental setup is analogous to that used in a previous study conducted in a highly impacted coastal area, the Augusta Bay (Italy, Bagnato et al., 2013). Hg^0 fluxes (F) were then calculated according to equation (1):

$$F = \frac{(C_f - C_i)Q}{A} \qquad (1)$$

where (C_f-C_i) is the difference between Hg^0 concentrations in air entering and exiting the chamber measured at the beginning and at the end of each experiment, Q is the air flow rate through the chamber (10 L min^{-1}) and A is the basal area occupied by the chamber (0.25 m^2). Hg^0 fluxes at the water-air interface were evaluated in different seasons, namely summer, autumn, and spring, whereas no measurements were taken during winter; however, existing preliminary data obtained for some areas investigated in this work during a previous study (Floreani et al., 2019) suggest that Hg^0 emissions during this period are relatively lower than those observable during the rest of the year.

Figure 12: the floating flux chamber during a measurement at site VN.

As detailed previously, Hg^0 fluxes at the water-air interface were measured in coastal marine environments subject to different contamination degree and characterised by different hydrodynamic conditions (Val Noghera fishfarm, Bay of Piran) in order to study the processes related to gaseous exchanges of Hg during the entire day-night cycle in one of the coastal marine areas most impacted by Hg over the world, the Northern Adriatic Sea (Fitzgerald et al., 2007; Kotnik et al., 2017). Measurements were performed also in three freshwater environments subject to different Hg supplies (from mining at Solkan Reservoir and from chlor-alkali industry at Torviscosa Dockyard, compared with the pristine environment of Cavazzo Lake) in order to study the influence of past different Hg sources on present day emissions to the atmosphere. In the first case, Hg^0 fluxes were measured at regular time intervals of ~2 hours over the entire 24 h period for a total of 12/14 flux measurements for each

season, whereas in the latter case Hg^0 evasion was monitored during only the diurnal period at ~1 hour time intervals obtaining 6 distinct set of measurements for each selected season.
At the end of each flux measurement, a sample of surface water was collected for the determination of DGM concentrations through the method described by O'Driscoll et al. (2019). This method is based on the determination of equilibrium Hg^0 concentration in the headspace air of a close reactor where the water samples were bubbled through the Lumex analyser internal pump. Moreover, main physico-chemical parameters of the surface water and meteorological parameters were constantly monitored during field operations. Surface water samples were collected with the same time stamp of flux measurement for the determination of total dissolved Hg (THg_D) and dissolved organic carbon (DOC) concentrations as summarised in Figure 11.

The second research topic was focused on the study of processes that regulate Hg^0 evasion at the soil-air interface in 6 selected sites along the Isonzo River alluvial plain. In this case, Hg^0 fluxes were evaluated by means of a Plexiglas non-steady state (NSS) flux chamber (60x20x25 cm, Fig. 13) coupled with the same Lumex analyser in a closed circuit and with a design similar to the dynamic flux chambers (DFC) used in other studies reported in literature (Fantozzi et al., 2013a; García-Sánchez et al., 2006; Wang et al., 2006; Zhu et al., 2011). This approach allows for a more rapid (~5 min) estimation of Hg^0 fluxes at the soil-air interface, reducing the impact of chamber placing on microclimatic conditions of the studied surfaces and making possible to monitor the phenomenon at several points in a small time interval.
Hg^0 fluxes were calculated based on Hg^0 concentration linear increase inside the chamber during the time of the experiment (*dC/dt*) according to equation (2)

$$F = \frac{dC}{dt}\frac{V}{A} \quad (2)$$

where *V* is the internal volume of the chamber (0.03 m^3) and *A* is the basal area of the chamber (0.12 m^2).

In this study, Hg^0 fluxes were evaluated in each site from both soils covered by native grass vegetation and from bare soil plots where vegetation was removed before sampling. Similar to what performed in aquatic environments, Hg^0 fluxes were measured during the diurnal period at regular time intervals of ~1 hour taking 6/7 distinct set of measurements for every selected

site in three different seasons (summer, autumn, winter). Each set consisted of two replicate measurements of Hg^0 fluxes conducted alternatively from bare and vegetated soil plots. No measurements were performed in spring as weather conditions and vegetation development that can be found in this season are not very much dissimilar from those found in autumn. Consequently, it can be assumed that also Hg^0 fluxes do not significantly differ from those determined in this season. The main meteorological parameters were also constantly monitored during sampling periods in the terrestrial sites. At the end of each sampling day, a topsoil sample was collected from every studied plot for the determination of grain-size, pH, organic matter content, total Hg concentration and Hg speciation through thermo-desorption technique (Petranich et al., 2022).

Figure 13: the NSS flux chamber during a measurement at site SAV.

More in-depth details about sampling procedures and analytical determinations in the various contexts are reported in Chapter 3.

The QA/QC protocol for measurements of Hg^0 fluxes at the water-air interface involved performing field blanks at the beginning and at the end of each sampling day by sealing the chamber to a clean white polycarbonate surface. The Hg^0 concentrations measured inside the chamber headspace were not significantly different from those determined for the open air just before the blank measurement and, excluding measurements at Torviscosa, close to the limit of detection of the Lumex analyser (2 ng m^{-3}), resulting in negligible blank flux values (average±SD=0.76±0.73 ng m^{-2} h^{-1}, N=36). The same procedure was adopted for measurements of soil-air Hg^0 fluxes and also in this case relatively low blank flux values were

observed (average±SD=1.64±0.97 ng m^{-2} h^{-1}, N=18). Average blank values were considered as the minimum measurable flux and were then subtracted to the flux values obtained during field measurements.

In addition, as the NSS flux chamber used for the determination of soil-air Hg^0 fluxes was not tested before, we performed a series of tests to compare the performance of this configuration with those obtained with a "classical" open dynamic steady-state (SS) configuration of the same chamber. In this last configuration, calculation of Hg^0 fluxes is based on the difference between Hg^0 concentrations in air entering and exiting the chamber. A constant flow rate through the chamber (10 L min^{-1}) was maintained thanks to the Lumex analyser internal pump. Hg^0 concentrations were measured for 5 min alternatively at the outlet and at the inlet of the chamber by manually switching the connection tubes. Only the concentrations recorded after the achievement of a steady-state inside the chamber (after ~2 min) were considered (Fantozzi et al., 2013a), whereas the inlet concentrations were calculated as the average of measurements performed before and after those at the outlet.

After this procedure the chamber was removed from the soil surface and relocated on the same plot after 5 min for the determination of Hg^0 flux through the NSS approach. These tests were performed in field on 6 bare soil plots characterised by different total Hg concentrations in the surface layer (Tab. 1). Overall, 5 distinct set of measurements were performed during May 2021 on each plot under different UV irradiation conditions from morning to afternoon. The results showed a good agreement between the fluxes calculated with the two different configurations, without systematic over- or under-estimation of fluxes obtained with the NSS configuration with respect to the well-established SS technique (Fig. 14).

Table 1: total Hg concentrations in topsoils used for testing the different flux chamber configurations.

Plot	THg concentration (mg kg^{-1})
T1	0.28 ± 0.08
T2	2.94 ± 0.16
T3	6.17 ± 0.47
T4	14.32 ± 0.24
T5	18.59 ± 1.81
T6	20.87 ± 1.04

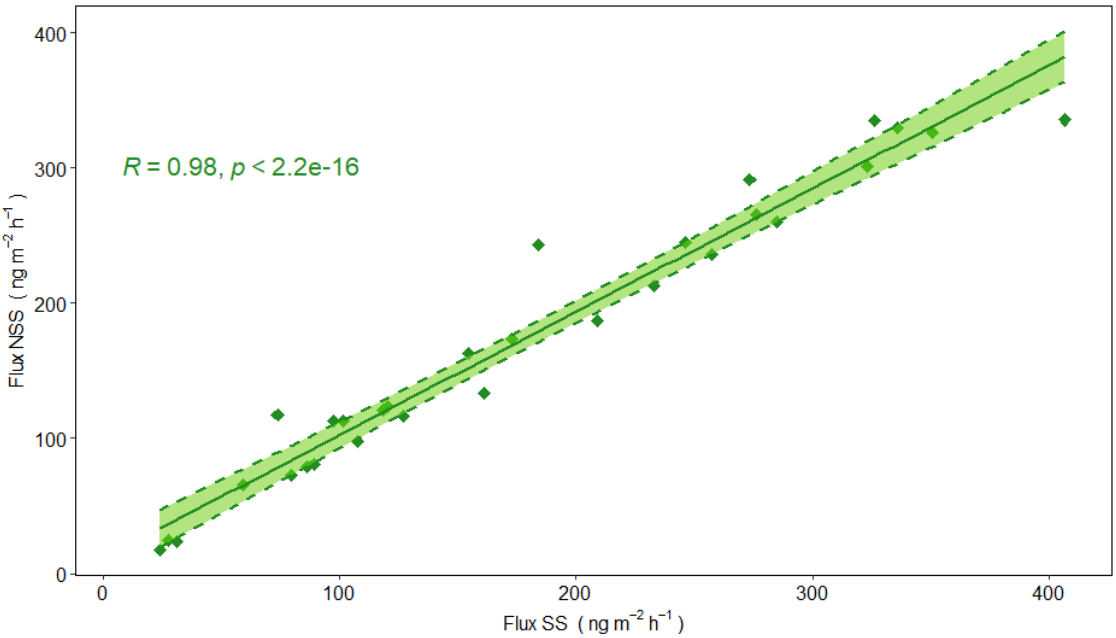

Figure 14: correlation between Hg^0 fluxes at soil-air interface measured with the open steady-state (SS) and closed non-steady-state (NSS) chamber configuration.

References

Acquavita, A., Biasiol, S., Lizzi, D., Mattassi, G., Pasquon, M., Skert, N., Marchiol, L., 2017. Gaseous Elemental Mercury Level and Distribution in a Heavily Contaminated Site: the Ex-chlor Alkali Plant in Torviscosa (Northern Italy). Water. Air. Soil Pollut. 228. https://doi.org/10.1007/s11270-016-3234-z

Acquavita, A., Brandolin, D., Cattaruzza, C., Felluga, A., Maddaleni, P., Meloni, C., Pasquon, M., Predonzani, S., Poli, L., Skert, N., Zanello, A., 2022. Mercury distribution and speciation in historically contaminated soils of the Isonzo River Plain (NE Italy). J. Soils Sediments 22, 79–92. https://doi.org/10.1007/s11368-021-03038-2

Acquavita, A., Covelli, S., Emili, A., Berto, D., Faganeli, J., Giani, M., Horvat, M., Koron, N.Ž., Rampazzo, F., 2012. Mercury in the sediments of the Marano and Grado Lagoon (northern Adriatic Sea): Sources, distribution and speciation. Estuar. Coast. Shelf Sci. 113, 20–31. https://doi.org/10.1016/j.ecss.2012.02.012

Agnan, Y., Le Dantec, T., Moore, C.W., Edwards, G.C., Obrist, D., 2016. New Constraints on Terrestrial Surface-Atmosphere Fluxes of Gaseous Elemental Mercury Using a Global Database. Environ. Sci. Technol. 50, 507–524. https://doi.org/10.1021/acs.est.5b04013

Allard, B., Arsenie, I., 1991. Abiotic reduction of mercury by humic substances in aquatic system - an important process for the mercury cycle. Water, Air, Soil Pollut. 56, 457–464. https://doi.org/10.1007/BF00342291

Alloway, B.J., 2012. Heavy metals in soils: trace metals and metalloids in soils and their bioavailability. Springer Science & Business Media, Dordrecht.

Amos, H.M., Jacob, D.J., Holmes, C.D., Fisher, J.A., Wang, Q., Yantosca, R.M., Corbitt, E.S., Galarneau, E., Rutter, A.P., Gustin, M.S., Steffen, A., Schauer, J.J., Graydon, J.A., Louis, V.L.S., Talbot, R.W., 2012. Gas-particle partitioning of atmospheric Hg (II) and its effect on global mercury deposition. Atmos. Chem. Phys. 591–603. https://doi.org/10.5194/acp-12-591-2012

Amos, H.M., Jacob, D.J., Kocman, D., Horowitz, H.M., Zhang, Y., Dutkiewicz, S., Horvat, M., Corbitt, E.S., Krabbenhoft, D.P., Sunderland, E.M., 2014. Global biogeochemical implications of mercury discharges from rivers and sediment burial. Environ. Sci. Technol. 48, 9514–9522. https://doi.org/10.1021/es502134t

Amos, H.M., Jacob, D.J., Streets, D.G., Sunderland, E.M., 2013. Legacy impacts of all-time anthropogenic emissions on the global mercury cycle. Global Biogeochem. Cycles 27, 410–421. https://doi.org/10.1002/gbc.20040

Amyot, M., Gill, G.A., Morel, F.M.M., 1997a. Production and loss of dissolved gaseous mercury in coastal seawater. Environ. Sci. Technol. 31, 3606–3611. https://doi.org/10.1021/es9703685

Amyot, M., Mierle, G., Lean, D., Mcqueen, D.J., 1997b. Effect of solar radiation on the formation of dissolved gaseous mercury in temperate lakes. Geochim. Cosmochim. Acta 61, 975–987. https://doi.org/10.1016/S0016-7037(96)00390-0

Amyot, M., Southworth, G., Lindberg, S.E., Hintelmann, H., Lalonde, J.D., Ogrinc, N., Poulain, A.J., Sandilands, K.A., 2004. Formation and evasion of dissolved gaseous mercury in large enclosures amended with 200HgCl2. Atmos. Environ. 38, 4279–4289. https://doi.org/10.1016/j.atmosenv.2004.05.002

Andersson, M.E., Gårdfeldt, K., Wängberg, I., Sprovieri, F., Pirrone, N., Lindqvist, O., 2007. Seasonal and daily variation of mercury evasion at coastal and off shore sites from the Mediterranean Sea. Mar. Chem. 104, 214–226. https://doi.org/10.1016/j.marchem.2006.11.003

Anthony, J.W., Bideaux, R.A., Bladh, K.W., Nichols, M.C., 2016. Handbook of Mineralogy. Mineralogical Society of America, Chantilly, VA 20151-1110, USA. https://doi.org/10.1111/j.2041-6962.1997.tb00844.x

Ao, M., Meng, B., Sapkota, A., Wu, Y., Qian, X., Qiu, G., Zhong, S., Shang, L., 2017. The influence of atmospheric Hg on Hg contaminations in rice and paddy soil in the Xunyang Hg mining district, China. Acta Geochim. 36, 181–189. https://doi.org/10.1007/s11631-017-0142-x

Ao, M., Xu, X., Wu, Y., Zhang, C., Meng, B., Shang, L., Liang, L., Qiu, R., Wang, S., Qian, X., Zhao, L., Qiu, G., 2020. Newly deposited atmospheric mercury in a simulated rice ecosystem in an active mercury mining region: High loading, accumulation, and availability. Chemosphere 238, 124630. https://doi.org/10.1016/j.chemosphere.2019.124630

Ariya, P.A., Amyot, M., Dastoor, A., Deeds, D., Feinberg, A., Kos, G., Poulain, A., Ryjkov, A., Semeniuk, K., Subir, M., Toyota, K., 2015. Mercury Physicochemical and Biogeochemical Transformation in the Atmosphere and at Atmospheric Interfaces: A Review and Future Directions. Chem. Rev. 115, 3760–3802. https://doi.org/10.1021/cr500667e

Bagnato, E., Barra, M., Cardellini, C., Chiodini, G., Parello, F., Sprovieri, M., 2014. First combined flux chamber survey of mercury and CO2 emissions from soil diffuse degassing at Solfatara of Pozzuoli crater, Campi Flegrei (Italy): Mapping and quantification of gas release. J. Volcanol. Geotherm. Res. 289, 26–40. https://doi.org/10.1016/j.jvolgeores.2014.10.017

Bagnato, E., Sproveri, M., Barra, M., Bitetto, M., Bonsignore, M., Calabrese, S., Di Stefano, V., Oliveri, E., Parello, F., Mazzola, S., 2013. The sea-air exchange of mercury (Hg) in the marine boundary layer of the Augusta basin (southern Italy): Concentrations and evasion flux. Chemosphere 93, 2024–2032. https://doi.org/10.1016/j.chemosphere.2013.07.025

Bahlmann, E., Ebinghaus, R., Ruck, W., 2006. Development and application of a laboratory flux measurement system (LFMS) for the investigation of the kinetics of mercury emissions from soils. J. Environ. Manage. 81, 114–125. https://doi.org/10.1016/j.jenvman.2005.09.022

Bakir, F., Damluji, S.F., Amin-Zaki, L., Murtadha, M., Khalidi, A., Al-Rawi, N.Y., Tikriti, S., Dhahir, H.I., Clarkson, T.W., Smith, J.C., Doherty, R.A., 1973. Methylmercury Poisoning in Iraq. Science (80-.). 181, 230–241. https://doi.org/10.1126/science.181.4096.230

Ballabio, C., Jiskra, M., Osterwalder, S., Borrelli, P., Montanarella, L., Panagos, P., 2021. A spatial assessment of mercury content in the European Union topsoil. Sci. Total Environ. 769, 144755. https://doi.org/10.1016/j.scitotenv.2020.144755

Bank, M.S., Vignati, D.A.L., Vigon, B., 2014. United Nations Environment Programme's Global Mercury Partnership: Science for successful implementation of the Minamata Convention. Environ. Toxicol. Chem. 33, 1199–1201. https://doi.org/10.1002/etc.2592

Baptista-Salazar, C., Richard, J.H., Horf, M., Rejc, M., Gosar, M., Biester, H., 2017. Grain-size dependence of mercury speciation in river suspended matter, sediments and soils in a mercury mining area at varying hydrological conditions. Appl. Geochemistry 81, 132–142. https://doi.org/10.1016/j.apgeochem.2017.04.006

Barkay, T., Miller, S.M., Summers, A.O., 2003. Bacterial mercury resistance from atoms to ecosystems. FEMS Microbiol. Rev. 27, 355–384. https://doi.org/10.1016/S0168-6445(03)00046-9

Bash, J.O., Bresnahan, P., Miller, D.R., 2007. Dynamic surface interface exchanges of mercury: A review and compartmentalized modeling framework. J. Appl. Meteorol. Climatol. 46, 1606–1618. https://doi.org/10.1175/JAM2553.1

Bavec, Š., Gosar, M., 2016. Speciation, mobility and bioaccessibility of Hg in the polluted urban soil of Idrija (Slovenia). Geoderma 273, 115–130. https://doi.org/10.1016/j.geoderma.2016.03.015

Beckers, F., Rinklebe, J., 2017. Cycling of mercury in the environment: Sources, fate, and human health implications: A review. Crit. Rev. Environ. Sci. Technol. 47, 693–794. https://doi.org/10.1080/10643389.2017.1326277

Bernhoft, R.A., 2012. Mercury toxicity and treatment: A review of the literature. J. Environ. Public Health 2012.

https://doi.org/10.1155/2012/460508

Biasiol, S., 2015. Utilizzo di moss bags per il monitoraggio della contaminazione da mercurio nel canale Banduzzi (Torviscosa). Thesis University of Udine.

Biester, H., Gosar, M., Covelli, S., 2000. Mercury speciation in sediments affected by dumped mining residues in the drainage area of the Idrija mercury mine, Slovenia. Environ. Sci. Technol. 34, 3330–3336. https://doi.org/10.1021/es991334v

Bishop, K., Shanley, J.B., Riscassi, A., de Wit, H.A., Eklöf, K., Meng, B., Mitchell, C., Osterwalder, S., Schuster, P.F., Webster, J., Zhu, W., 2020. Recent advances in understanding and measurement of mercury in the environment: Terrestrial Hg cycling. Sci. Total Environ. 721, 137647. https://doi.org/10.1016/j.scitotenv.2020.137647

Black, F.J., Conaway, C.H., Flegal, A.R., 2009. Stability of dimethyl mercury in seawater and its conversion to monomethyl mercury. Environ. Sci. Technol. 43, 4056–4062. https://doi.org/10.1021/es9001218

Blackwell, B.D., Driscoll, C.T., 2015. Deposition of mercury in forests along a montane elevation gradient. Environ. Sci. Technol. 49, 5363–5370. https://doi.org/10.1021/es505928w

Bouchet, S., Goñi-Urriza, M., Monperrus, M., Guyoneaud, R., Fernandez, P., Heredia, C., Tessier, E., Gassie, C., Point, D., Guédron, S., Achá, D., Amouroux, D., 2018. Linking Microbial Activities and Low-Molecular-Weight Thiols to Hg Methylation in Biofilms and Periphyton from High-Altitude Tropical Lakes in the Bolivian Altiplano. Environ. Sci. Technol. 52, 9758–9767. https://doi.org/10.1021/acs.est.8b01885

Bowman, K.L., Lamborg, C.H., Agather, A.M., 2020. A global perspective on mercury cycling in the ocean. Sci. Total Environ. 710, 136166. https://doi.org/10.1016/j.scitotenv.2019.136166

Branfireun, B.A., Cosio, C., Poulain, A.J., Riise, G., Bravo, A.G., 2020. Mercury cycling in freshwater systems - An updated conceptual model. Sci. Total Environ. 745, 140906. https://doi.org/10.1016/j.scitotenv.2020.140906

Bravo, A.G., Bouchet, S., Tolu, J., Björn, E., Mateos-Rivera, A., Bertilsson, S., 2017. Molecular composition of organic matter controls methylmercury formation in boreal lakes. Nat. Commun. 8, 14255. https://doi.org/10.1038/ncomms14255

Briggs, C., Gustin, M.S., 2013. Building upon the conceptual model for soil mercury flux: Evidence of a link between moisture evaporation and Hg evasion. Water. Air. Soil Pollut. 224, 1744. https://doi.org/10.1007/s11270-013-1744-5

Brinkmann, T., Giner Santonja, G., Schorcht, F., Roudier, S., Delgado Sancho, L., 2014. Best Available Techniques Reference Document for the Production of Chlor-alkali. European Commission, Joint Research Centre, Institute for Prospective Technological Studies. https://doi.org/10.2791/13138

Brooks, S.B., Saiz-Lopez, A., Skov, H., Lindberg, S.E., Plane, J.M.C., Goodsite, M.E., 2006. The mass balance of mercury in the springtime arctic environment. Geophys. Res. Lett. 33, L13812. https://doi.org/10.1029/2005GL025525

Cabassi, J., Lazzaroni, M., Giannini, L., Mariottini, D., Nisi, B., Rappuoli, D., Vaselli, O., 2022. Continuous and near real-time measurements of gaseous elemental mercury (GEM) from an Unmanned Aerial Vehicle: A new approach to investigate the 3D distribution of GEM in the lower atmosphere. Chemosphere 288, 132547. https://doi.org/10.1016/j.chemosphere.2021.132547

Cabassi, J., Venturi, S., Di Bennardo, F., Nisi, B., Tassi, F., Magi, F., Ricci, A., Picchi, G., Vaselli, O., 2021. Flux measurements of gaseous elemental mercury (GEM) from the geothermal area of "Le Biancane" natural park (Monterotondo Marittimo, Grosseto, Italy): Biogeochemical processes controlling GEM emission. J. Geochemical Explor. 228, 106824. https://doi.org/10.1016/j.gexplo.2021.106824

Canário, J., Poissant, L., Pilote, M., Caetano, M., Hintelmann, H., O'Driscoll, N.J., 2017. Salt-marsh plants as potential sources of Hg0 into the atmosphere. Atmos. Environ. 152, 458–464. https://doi.org/10.1016/j.atmosenv.2017.01.011

Canil, D., Crockford, P.W., Rossin, R., Telmer, K., 2015. Mercury in some arc crustal rocks and mantle peridotites and relevance to the moderately volatile element budget of the Earth. Chem. Geol. 396, 134–142. https://doi.org/10.1016/j.chemgeo.2014.12.029

Carpi, A., Fostier, A.H., Orta, O.R., dos Santos, J.C., Gittings, M., 2014. Gaseous mercury emissions from soil following forest loss and land use changes: Field experiments in the United States and Brazil. Atmos. Environ. 96, 423–429. https://doi.org/10.1016/j.atmosenv.2014.08.004

Carpi, A., Frei, A., Cocris, D., McCloskey, R., Contreras, E., Ferguson, K., 2007. Analytical artifacts produced by a polycarbonate chamber compared to a Teflon chamber for measuring surface mercury fluxes. Anal. Bioanal. Chem. 388, 361–365. https://doi.org/10.1007/s00216-006-1111-0

Carpi, A., Lindberg, S.E., 1998. Application of a Teflon® dynamic flux chamber for quantifying soil mercury flux: Tests and results over background soil. Atmos. Environ. 32, 873–882. https://doi.org/10.1016/S1352-

2310(97)00133-7

Castelle, S., Schäfer, J., Blanc, G., Dabrin, A., Lanceleur, L., Masson, M., 2009. Gaseous mercury at the air-water interface of a highly turbid estuary (Gironde Estuary, France). Mar. Chem. 117, 42–51. https://doi.org/10.1016/j.marchem.2009.01.005

Cesário, R., O'Driscoll, N.J., Justino, S., Wilson, C.E., Monteiro, C.E., Zilhão, H., Canário, J., 2021. Air concentrations of gaseous elemental mercury and vegetation-air fluxes within saltmarshes of the Tagus Estuary, Portugal. Atmosphere (Basel). 12, 228. https://doi.org/10.3390/atmos12020228

Chen, J., Yang, Z.M., 2012. Mercury toxicity, molecular response and tolerance in higher plants. BioMetals 25, 847–857. https://doi.org/10.1007/s10534-012-9560-8

Chen, L., Zhang, Y., Jacob, D.J., Soerensen, A.L., Fisher, J.A., Horowitz, H.M., Corbitt, E.S., Wang, X., 2015. A decline in Arctic Ocean mercury suggested by differences in decadal trends of atmospheric mercury between the Arctic and northern midlatitudes. Geophys. Res. Lett. 42, 6076–6083. https://doi.org/10.1002/2015GL064051

Chen, Y.S., Tseng, C.M., Reinfelder, J.R., 2020. Spatiotemporal Variations in Dissolved Elemental Mercury in the River-Dominated and Monsoon-Influenced East China Sea: Drivers, Budgets, and Implications. Environ. Sci. Technol. 54, 3988–3995. https://doi.org/10.1021/acs.est.9b06092

Choi, H.D., Holsen, T.M., 2009a. Gaseous mercury emissions from unsterilized and sterilized soils: The effect of temperature and UV radiation. Environ. Pollut. 157, 1673–1678. https://doi.org/10.1016/j.envpol.2008.12.014

Choi, H.D., Holsen, T.M., 2009b. Gaseous mercury fluxes from the forest floor of the Adirondacks. Environ. Pollut. 157, 592–600. https://doi.org/10.1016/j.envpol.2008.08.020

Ci, Z., Peng, F., Xue, X., Zhang, X., 2018. Temperature sensitivity of gaseous elemental mercury in the active layer of the Qinghai-Tibet Plateau permafrost. Environ. Pollut. 238, 508–515. https://doi.org/10.1016/j.envpol.2018.02.085

Ci, Z., Peng, F., Xue, X., Zhang, X., 2016a. Air-surface exchange of gaseous mercury over permafrost soil: An investigation at a high-altitude (4700 m.a.s.l.) and remote site in the central Qinghai-Tibet Plateau. Atmos. Chem. Phys. 16, 14741–14754. https://doi.org/10.5194/acp-16-14741-2016

Ci, Z., Zhang, X., Wang, Z., Niu, Z., 2011. Atmospheric gaseous elemental mercury (GEM) over a coastal/rural site downwind of East China: Temporal variation and long-range transport. Atmos. Environ. 45, 2480–2487. https://doi.org/10.1016/j.atmosenv.2011.02.043

Ci, Z., Zhang, X., Yin, Y., Chen, J., Wang, S., 2016b. Mercury Redox Chemistry in Waters of the Eastern Asian Seas: From Polluted Coast to Clean Open Ocean. Environ. Sci. Technol. 50, 2371–2380. https://doi.org/10.1021/acs.est.5b05372

Cizdziel, J. V., Zhang, Y., Nallamothu, D., Brewer, J.S., Gao, Z., 2019. Air/surface exchange of gaseous elemental mercury at different landscapes in Mississippi, USA. Atmosphere (Basel). 10, 538. https://doi.org/10.3390/atmos10090538

Cole, A.S., Steffen, A., Pfaffhuber, K.A., Berg, T., Pilote, M., Poissant, L., Tordon, R., Hung, H., 2013. Ten-year trends of atmospheric mercury in the high Arctic compared to Canadian sub-Arctic and mid-latitude sites. Atmos. Chem. Phys. 13, 1535–1545. https://doi.org/10.5194/acp-13-1535-2013

Compeau, G.C., Bartha, R., 1985. Sulfate-Reducing Bacteria: Principal Methylators of Mercury in Anoxic Estuarine Sediment. Appl. Environ. Microbiol. 50, 498–502. https://doi.org/10.1128/aem.50.2.498-502.1985

Conaway, C.H., Squire, S., Mason, R.P., Flegal, A.R., 2003. Mercury speciation in the San Francisco Bay estuary. Mar. Chem. 80, 199–225. https://doi.org/10.1016/S0304-4203(02)00135-4

Coolbaugh, M.F., Gustin, M.S., Rytuba, J.J., 2002. Annual emissions of mercury to the atmosphere from natural sources in Nevada and California. Environ. Geol. 42, 338–349. https://doi.org/10.1007/s00254-002-0557-4

Cossa, D., Knoery, J., Bănaru, D., Harmelin-Vivien, M., Sonke, J.E., Hedgecock, I.M., Bravo, A.G., Rosati, G., Canu, D., Horvat, M., Sprovieri, F., Pirrone, N., Heimbürger-Boavida, L.E., 2022. Mediterranean Mercury Assessment 2022: An Updated Budget, Health Consequences, and Research Perspectives. Environ. Sci. Technol. 56, 3840–3862. https://doi.org/10.1021/acs.est.1c03044

Costa, M., Liss, P.S., 1999. Photoreduction of mercury in sea water and its possible implications for Hg0 air-sea fluxes. Mar. Chem. 68, 87–95. https://doi.org/10.1016/S0304-4203(99)00067-5

Coufalík, P., Krásenský, P., Dosbaba, M., Komárek, J., 2012. Sequential extraction and thermal desorption of mercury from contaminated soil and tailings from Mongolia. Cent. Eur. J. Chem. 10, 1565–1573. https://doi.org/10.2478/s11532-012-0074-6

Covelli, S., Acquavita, A., Piani, R., Predonzani, S., De Vittor, C., 2009. Recent contamination of mercury in an estuarine environment (Marano lagoon, Northern Adriatic, Italy). Estuar. Coast. Shelf Sci. 82, 273–284.

https://doi.org/10.1016/j.ecss.2009.01.021

Covelli, S., Faganeli, J., Horvat, M., Brambati, A., 2001. Mercury contamination of coastal sediments as the result of long-term cinnabar mining activity (Gulf of Trieste, northern Adriatic sea). Appl. Geochemistry 16, 541–558. https://doi.org/10.1016/S0883-2927(00)00042-1

Covelli, S., Langone, L., Acquavita, A., Piani, R., Emili, A., 2012. Historical flux of mercury associated with mining and industrial sources in the Marano and Grado Lagoon (northern Adriatic Sea). Estuar. Coast. Shelf Sci. 113, 7–19. https://doi.org/10.1016/j.ecss.2011.12.038

Covelli, S., Piani, R., Acquavita, A., Predonzani, S., Faganeli, J., 2007. Transport and dispersion of particulate Hg associated with a river plume in coastal Northern Adriatic environments. Mar. Pollut. Bull. 55, 436–450. https://doi.org/10.1016/j.marpolbul.2007.09.006

Covelli, S., Piani, R., Kotnik, J., Horvat, M., Faganeli, J., Brambati, A., 2006. Behaviour of Hg species in a microtidal deltaic system: The Isonzo River mouth (northern Adriatic Sea). Sci. Total Environ. 368, 210–223. https://doi.org/10.1016/j.scitotenv.2005.09.089

Cucchi, F., Franceschini, G., Zini, L., 2008. Hydrogeochemical investigations and groundwater provinces of the Friuli Venezia Giulia Plain aquifers, northeastern Italy. Environ. Geol. 55, 985–999. https://doi.org/10.1007/s00254-007-1048-4

Custodio, D., Ebinghaus, R., Gerard Spain, T., Bieser, J., 2020. Source apportionment of atmospheric mercury in the remote marine atmosphere: Mace Head GAW station, Irish western coast. Atmos. Chem. Phys. 20, 7929–7939. https://doi.org/10.5194/acp-20-7929-2020

Dalziel, J., Tordon, R., 2014. Gaseous mercury flux measurements from two mine tailing sites in the Seal Harbour area of Nova Scotia. Geochemistry Explor. Environ. Anal. 14, 17–24. https://doi.org/10.1144/geochem2011-112

Dastoor, A., Angot, H., Bieser, J., Christensen, J.H., Douglas, T.A., Heimbürger-Boavida, L.E., Jiskra, M., Mason, R.P., McLagan, D.S., Obrist, D., Outridge, P.M., Petrova, M. V., Ryjkov, A., St. Pierre, K.A., Schartup, A.T., Soerensen, A.L., Toyota, K., Travnikov, O., Wilson, S.J., Zdanowicz, C., 2022. Arctic mercury cycling. Nat. Rev. Earth Environ. 3, 270–286. https://doi.org/10.1038/s43017-022-00269-w

Davidson, E.A., Savage, K., Verchot, L. V., Navarro, R., 2002. Minimizing artifacts and biases in chamber-based measurements of soil respiration. Agric. For. Meteorol. 113, 21–37. https://doi.org/10.1016/S0168-1923(02)00100-4

Davis, A., Bloom, N.S., Que Hee, S.S., 1997. The environmental geochemistry and bioaccessibility of mercury in soils and sediments: A review. Risk Anal. 17, 557–569. https://doi.org/10.1111/j.1539-6924.1997.tb00897.x

Daye, M., Kadlecova, M., Ouddane, B., 2015. Biogeochemical factors affecting the distribution, speciation, and transport of Hg species in the Deûle and Lys Rivers (Northern France). Environ. Sci. Pollut. Res. 22, 2708–2720. https://doi.org/10.1007/s11356-014-3528-x

Debure, M., Grangeon, S., Robinet, J.C., Madé, B., Fernández, A.M., Lerouge, C., 2020. Influence of soil redox state on mercury sorption and reduction capacity. Sci. Total Environ. 707, 136069. https://doi.org/10.1016/j.scitotenv.2019.136069

Demers, J.D., Blum, J.D., Zak, D.R., 2013. Mercury isotopes in a forested ecosystem: Implications for air-surface exchange dynamics and the global mercury cycle. Global Biogeochem. Cycles 27, 222–238. https://doi.org/10.1002/gbc.20021

Díez, S., 2009. Human Health Effects of Methylmercury Exposure BT - Reviews of Environmental Contamination and Toxicology, in: Whitacre, D.M. (Ed.), . Springer New York, New York, NY, pp. 111–132. https://doi.org/10.1007/978-0-387-09647-6_3

Dill, C., Kuiken, T., Zhang, H., Ensor, M., 2006. Diurnal variation of dissolved gaseous mercury (DGM) levels in a southern reservoir lake (Tennessee, USA) in relation to solar radiation. Sci. Total Environ. 357, 176–193. https://doi.org/10.1016/j.scitotenv.2005.04.011

DiMento, B.P., Mason, R.P., Brooks, S., Moore, C., 2019. The impact of sea ice on the air-sea exchange of mercury in the Arctic Ocean. Deep. Res. Part I Oceanogr. Res. Pap. 144, 28–38. https://doi.org/10.1016/j.dsr.2018.12.001

Dizdarevič, T., 2001. The influence of mercury production in Idrija mine on the environment in the Idrija region and over a broad area. RMZ - Mater. Geoenvironment 48, 56–64.

Driscoll, C.T., Mason, R.P., Chan, H.M., Jacob, D.J., Pirrone, N., 2013. Mercury as a global pollutant: Sources, pathways, and effects. Environ. Sci. Technol. 47, 4967–4983. https://doi.org/10.1021/es305071v

Du, H., Ma, M., Igarashi, Y., Wang, D., 2019. Biotic and Abiotic Degradation of Methylmercury in Aquatic Ecosystems: A Review. Bull. Environ. Contam. Toxicol. 102, 605–611. https://doi.org/10.1007/s00128-018-2530-2

During, A., Rinklebe, J., Böhme, F., Wennrich, R., Stärk, H.-J., Mothes, S., Du Laing, G., Schulz, E., Neue, H.-U., 2009. Mercury Volatilization from Three Floodplain Soils at the Central Elbe River, Germany. Soil Sediment Contam. An Int. J. 18, 429–444. https://doi.org/10.1080/15320380902962395

Echeverria, D., Aposhian, H.V., Woods, J.S., Heyer, N.J., Aposhian, M.M., Bittner, A.C.J., Mahurin, R.K., Cianciola, M., 1998. Neurobehavioral effects from exposure to dental amalgam Hg o : new distinctions between recent exposure and Hg body burden . FASEB J. 12, 971–980. https://doi.org/10.1096/fasebj.12.11.971

Eckley, C.S., Blanchard, P., McLennan, D., Mintz, R., Sekela, M., 2015. Soil-Air Mercury Flux near a Large Industrial Emission Source before and after Closure (Flin Flon, Manitoba, Canada). Environ. Sci. Technol. 49, 9750–9757. https://doi.org/10.1021/acs.est.5b01995

Eckley, C.S., Eagles-Smith, C., Tate, M.T., Krabbenhoft, D.P., 2021. Surface-air mercury fluxes and a watershed mass balance in forested and harvested catchments. Environ. Pollut. 277, 116869. https://doi.org/10.1016/j.envpol.2021.116869

Eckley, C.S., Gilmour, C.C., Janssen, S., Luxton, T.P., Randall, P.M., Whalin, L., Austin, C., 2020. The assessment and remediation of mercury contaminated sites: A review of current approaches. Sci. Total Environ. 707, 136031. https://doi.org/10.1016/j.scitotenv.2019.136031

Eckley, C.S., Gustin, M., Lin, C.J., Li, X., Miller, M.B., 2010. The influence of dynamic chamber design and operating parameters on calculated surface-to-air mercury fluxes. Atmos. Environ. 44, 194–203. https://doi.org/10.1016/j.atmosenv.2009.10.013

Eckley, C.S., Hintelmann, H., 2006. Determination of mercury methylation potentials in the water column of lakes across Canada. Sci. Total Environ. 368, 111–125. https://doi.org/10.1016/j.scitotenv.2005.09.042

Eckley, C.S., Parsons, M.T., Mintz, R., Lapalme, M., Mazur, M., Tordon, R., Elleman, R., Graydon, J.A., Blanchard, P., St Louis, V., 2013. Impact of closing Canada's largest point-source of mercury emissions on local atmospheric mercury concentrations. Environ. Sci. Technol. 47, 10339–10348. https://doi.org/10.1021/es401352n

Eckley, C.S., Tate, M.T., Lin, C.J., Gustin, M., Dent, S., Eagles-Smith, C., Lutz, M.A., Wickland, K.P., Wang, B., Gray, J.E., Edwards, G.C., Krabbenhoft, D.P., Smith, D.B., 2016. Surface-air mercury fluxes across Western North America: A synthesis of spatial trends and controlling variables. Sci. Total Environ. 568, 651–665. https://doi.org/10.1016/j.scitotenv.2016.02.121

Ekino, S., Susa, M., Ninomiya, T., Imamura, K., Kitamura, T., 2007. Minamata disease revisited: An update on the acute and chronic manifestations of methyl mercury poisoning. J. Neurol. Sci. 262, 131–144. https://doi.org/10.1016/j.jns.2007.06.036

Enescu, M., Nagy, K.L., Manceau, A., 2016. Nucleation of mercury sulfide by dealkylation. Sci. Rep. 6, 39359. https://doi.org/10.1038/srep39359

Engle, M.A., Gustin, M.S., Goff, F., Counce, D.A., Janik, C.J., Bergfeld, D., Rytuba, J.J., 2006. Atmospheric mercury emissions from substrates and fumaroles associated with three hydrothermal systems in the western United States. J. Geophys. Res. Atmos. 111. https://doi.org/10.1029/2005JD006563

Engle, M.A., Gustin, M.S., Zhang, H., 2001. Quantifying natural source mercury emissions from the Ivanhoe Mining District, north-central Nevada, USA. Atmos. Environ. 35, 3987–3997. https://doi.org/10.1016/S1352-2310(01)00184-4

Engstrom, D.R., Fitzgerald, W.F., Cooke, C.A., Lamborg, C.H., Drevnick, P.E., Swain, E.B., Balogh, S.J., Balcom, P.H., 2014. Atmospheric Hg emissions from preindustrial gold and silver extraction in the Americas: A reevaluation from lake-sediment archives. Environ. Sci. Technol. 48, 6533–6543. https://doi.org/10.1021/es405558e

Enrico, M., Roux, G. Le, Marusczak, N., Heimbürger, L.E., Claustres, A., Fu, X., Sun, R., Sonke, J.E., 2016. Atmospheric Mercury Transfer to Peat Bogs Dominated by Gaseous Elemental Mercury Dry Deposition. Environ. Sci. Technol. 50, 2405–2412. https://doi.org/10.1021/acs.est.5b06058

Ericksen, J.A., Gustin, M.S., Lindberg, S.E., Olund, S.D., Krabbenhoft, D.P., 2005. Assessing the potential for re-emission of mercury deposited in precipitation from arid soils using a stable isotope. Environ. Sci. Technol. 39, 8001–8007. https://doi.org/10.1021/es0505651

Esbrí, J.M., Bernaus, A., Ávila, M., Kocman, D., García-Noguero, E.M., Guerrero, B., Gaona, X., Álvarez, R., Perez-Gonzalez, G., Valiente, M., Higueras, P., Horvat, M., Loredo, J., 2010. XANES speciation of mercury in three mining districts - Almadén, Asturias (Spain), Idria (Slovenia). J. Synchrotron Radiat. 17, 179–186. https://doi.org/10.1107/S0909049510001925

Esbri, J.M., L. Higueras, P., Martínez-Coronado, A., Naharro, R., 2020. 4D dispersion of total gaseous mercury derived from a mining source: Identification of criteria to assess risks related to high concentrations of atmospheric mercury. Atmos. Chem. Phys. 20, 12995–13010. https://doi.org/10.5194/acp-20-12995-2020

Esbrí, J.M., López-Berdonces, M.A., Fernández-Calderón, S., Higueras, P., Díez, S., 2015. Atmospheric mercury pollution around a chlor-alkali plant in Flix (NE Spain): an integrated analysis. Environ. Sci. Pollut. Res. 22, 4842–4850. https://doi.org/10.1007/s11356-014-3305-x

Fantozzi, L., Ferrara, R., Dini, F., Tamburello, L., Pirrone, N., Sprovieri, F., 2013a. Study on the reduction of atmospheric mercury emissions from mine waste enriched soils through native grass cover in the Mt. Amiata region of Italy. Environ. Res. 125, 69–74. https://doi.org/10.1016/j.envres.2013.02.004

Fantozzi, L., Ferrara, R., Frontini, F.P., Dini, F., 2009. Dissolved gaseous mercury production in the dark: Evidence for the fundamental role of bacteria in different types of Mediterranean water bodies. Sci. Total Environ. 407, 917–924. https://doi.org/10.1016/j.scitotenv.2008.09.014

Fantozzi, L., Ferrara, R., Frontini, F.P., Dini, F., 2007. Factors influencing the daily behaviour of dissolved gaseous mercury concentration in the Mediterranean Sea. Mar. Chem. 107, 4–12. https://doi.org/10.1016/j.marchem.2007.02.008

Fantozzi, L., Guerrieri, N., Manca, G., Orrù, A., Marziali, L., 2021. An integrated investigation of atmospheric gaseous elemental mercury transport and dispersion around a chlor-alkali plant in the ossola valley (Italian central alps). Toxics 9, 172. https://doi.org/10.3390/toxics9070172

Fantozzi, L., Manca, G., Ammoscato, I., Pirrone, N., Sprovieri, F., 2013b. The cycling and sea-air exchange of mercury in the waters of the Eastern Mediterranean during the 2010 MED-OCEANOR cruise campaign. Sci. Total Environ. 448, 151–162. https://doi.org/10.1016/j.scitotenv.2012.09.062

Feinberg, A., Dlamini, T., Jiskra, M., Shah, V., Selin, N.E., 2022. Evaluating atmospheric mercury (Hg) uptake by vegetation in a chemistry-transport model. Environ. Sci. Process. Impacts 24, 1303–1318. https://doi.org/10.1039/d2em00032f

Feng, C., Pedrero, Z., Lima, L., Olivares, S., de la Rosa, D., Berail, S., Tessier, E., Pannier, F., Amouroux, D., 2019. Assessment of Hg contamination by a Chlor-Alkali Plant in riverine and coastal sites combining Hg speciation and isotopic signature (Sagua la Grande River, Cuba). J. Hazard. Mater. 371, 558–565. https://doi.org/10.1016/j.jhazmat.2019.02.092

Feng, X., Qiu, G., 2008. Mercury pollution in Guizhou, Southwestern China - An overview. Sci. Total Environ. 400, 227–237. https://doi.org/10.1016/j.scitotenv.2008.05.040

Feng, X., Wang, S., Qiu, G., He, T., Li, G., Li, Z., Shang, L., 2008. Total gaseous mercury exchange between water and air during cloudy weather conditions over Hongfeng reservoir, Guizhou, China. J. Geophys. Res. Atmos. 113. https://doi.org/10.1029/2007JD009600

Feng, X., Yan, H., Wang, S., Qiu, G., Tang, S., Shang, L., Dai, Q., Hou, Y., 2004. Seasonal variation of gaseous mercury exchange rate between air and water surface over Baihua reservoir, Guizhou, China. Atmos. Environ. 38, 4721–4732. https://doi.org/10.1016/j.atmosenv.2004.05.023

Fernández-Martínez, R., Esbrí, J.M., Higueras, P., Rucandio, I., 2019. Comparison of mercury distribution and mobility in soils affected by anthropogenic pollution around chloralkali plants and ancient mining sites. Sci. Total Environ. 671, 1066–1076. https://doi.org/10.1016/j.scitotenv.2019.03.348

Ferrara, R., Ceccarini, C., Lanzillotta, E., Gårdfeldt, K., Sommar, J., Horvat, M., Logar, M., Fajon, V., Kotnik, J., 2003. Profiles of dissolved gaseous mercury concentration in the Mediterranean seawater. Atmos. Environ. 37, 85–92. https://doi.org/10.1016/S1352-2310(03)00248-6

Ferrara, R., Mazzolai, B., 1998. A dynamic flux chamber to measure mercury emission from aquatic systems. Sci. Total Environ. 215, 51–57. https://doi.org/10.1016/S0048-9697(98)00117-X

Ferrarin, C., Umgiesser, G., Bajo, M., Bellafiore, D., De Pascalis, F., Ghezzo, M., Mattassi, G., Scroccaro, I., 2010. Hydraulic zonation of the lagoons of Marano and Grado, Italy. A modelling approach. Estuar. Coast. Shelf Sci. 87, 561–572. https://doi.org/10.1016/j.ecss.2010.02.012

Fitzgerald, W.F., Clarkson, T.W., 1991. Mercury and monomethylmercury: Present and future concerns. Environ. Health Perspect. 96, 159–166. https://doi.org/10.1289/ehp.9196159

Fitzgerald, W.F., Engstrom, D.R., Mason, R.P., Nater, E.A., 1998. The case for atmospheric mercury contamination in remote areas. Environ. Sci. Technol. 32, 1–7. https://doi.org/10.1021/es970284w

Fitzgerald, W.F., Lamborg, C.H., Hammerschmidt, C.R., 2007. Marine biogeochemical cycling of mercury. Chem. Rev. 107, 641–662. https://doi.org/10.1021/cr050353m

Floreani, F., Acquavita, A., Petranich, E., Covelli, S., 2019. Diurnal fluxes of gaseous elemental mercury from the water-air interface in coastal environments of the northern Adriatic Sea. Sci. Total Environ. 668, 925–935. https://doi.org/10.1016/j.scitotenv.2019.03.012

Fontana, A., Mozzi, P., Bondesan, A., 2008. Alluvial megafans in the Venetian-Friulian Plain (north-eastern Italy): Evidence of sedimentary and erosive phases during Late Pleistocene and Holocene. Quat. Int. 189, 71–90. https://doi.org/10.1016/j.quaint.2007.08.044

Fornasaro, S., Morelli, G., Rimondi, V., Fagotti, C., Friani, R., Lattanzi, P., Costagliola, P., 2022. Mercury

distribution around the Siele Hg mine (Mt. Amiata district, Italy) twenty years after reclamation: Spatial and temporal variability in soil, stream sediments, and air. J. Geochemical Explor. 232, 106886. https://doi.org/10.1016/j.gexplo.2021.106886

Fortuna, L., Carniel, F.C., Capozzi, F., 2019. Congruence Evaluation of Mercury Pollution Patterns Around a Waste Incinerator over a 16-Year-Long Period Using Different Biomonitors. Atmosphere (Basel). 10. https://doi.org/10.3390/atmos10040183

Fritsche, J., Obrist, D., Alewell, C., 2008. Evidence of microbial control of Hg0 emissions from uncontaminated terrestrial soils. J. Plant Nutr. Soil Sci. 171, 200–209. https://doi.org/10.1002/jpln.200625211

Fu, X., Feng, X., Guo, Y., Meng, B., Yin, R., Yao, H., 2013. Distribution and production of reactive mercury and dissolved gaseous mercury in surface waters and water/air mercury flux in reservoirs on Wujiang River, Southwest China. J. Geophys. Res. Atmos. 118, 3905–3917. https://doi.org/10.1002/jgrd.50384

Fu, X., Feng, X., Wang, S., 2008. Exchange fluxes of Hg between surfaces and atmosphere in the eastern flank of Mount Gongga, Sichuan province, southwestern China. J. Geophys. Res. Atmos. 113, D20306. https://doi.org/10.1029/2008JD009814

Fu, X., Feng, X., Zhang, G., Xu, W., Li, X., Yao, H., Liang, P., Li, J., Sommar, J., Yin, R., Liu, N., 2010. Mercury in the marine boundary layer and seawater of the South China Sea: Concentrations, sea/air flux, and implication for land outflow. J. Geophys. Res. Atmos. 115, 1–11. https://doi.org/10.1029/2009JD012958

Fu, X., Feng, X., Zhang, H., Yu, B., Chen, L., 2012. Mercury emissions from natural surfaces highly impacted by human activities in Guangzhou province, South China. Atmos. Environ. 54, 185–193. https://doi.org/10.1016/j.atmosenv.2012.02.008

Gabay, M., Raveh-Rubin, S., Peleg, M., Fredj, E., Tas, E., 2020. Is oxidation of atmospheric mercury controlled by different mechanisms in the polluted continental boundary layer vs. remote marine boundary layer? Environ. Res. Lett. 15, 064026. https://doi.org/10.1088/1748-9326/ab7b26

Gabriel, M.C., Williamson, D.G., 2004. Principal biogeochemical factors affecting the speciation and transport of mercury through the terrestrial environment. Environ. Geochem. Health 26, 421–434. https://doi.org/10.1007/s10653-004-1308-0

Gai, K., Hoelen, T.P., Hsu-Kim, H., Lowry, G. V., 2016. Mobility of Four Common Mercury Species in Model and Natural Unsaturated Soils. Environ. Sci. Technol. 50, 3342–3351. https://doi.org/10.1021/acs.est.5b04247

Gao, F., Yates, S.R., Yates, M. V., Gan, J., Ernst, F.F., 1997. Design, fabrication, and application of a dynamic chamber for measuring gas emissions from soil. Environ. Sci. Technol. 31, 148–153. https://doi.org/10.1021/es9602511

García-Sánchez, A., Contreras, F., Adams, M., Santos, F., 2006. Atmospheric mercury emissions from polluted gold mining areas (Venezuela). Environ. Geochem. Health 28, 529–540. https://doi.org/10.1007/s10653-006-9049-x

Garcia, E., Poulain, A.J., Amyot, M., Ariya, P.A., 2005. Diel variations in photoinduced oxidation of Hg0 in freshwater. Chemosphere 59, 977–981. https://doi.org/10.1016/j.chemosphere.2004.09.107

Gismera, M.J., Procopio, J.R., Sevilla, M.T., 2007. Characterization of mercury - Humic acids interaction by potentiometric titration with a modified carbon paste mercury sensor. Electroanalysis 19, 1055–1061. https://doi.org/10.1002/elan.200603821

Gochfeld, M., 2003. Cases of mercury exposure, bioavailability, and absorption. Ecotoxicol. Environ. Saf. 56, 174–179. https://doi.org/10.1016/S0147-6513(03)00060-5

Gonzalez-Raymat, H., Liu, G., Liriano, C., Li, Y., Yin, Y., Shi, J., Jiang, G., Cai, Y., 2017. Elemental mercury: Its unique properties affect its behavior and fate in the environment. Environ. Pollut. 229, 69–86. https://doi.org/10.1016/j.envpol.2017.04.101

Goodrich, J.M., Basu, N., Franzblau, A., Dolinoy, D.C., 2013. Mercury Biomarkers and DNA Methylation Among Michigan Dental Professionals. Environ. Mol. Mutagen. 54, 195–203. https://doi.org/10.1002/em.21763

Gosar, M., Pirc, S., Bidovec, M., 1997. Mercury in the Idrijca River sediments as a reflection of mining and smelting activities of the Idrija mercury mine. J. Geochemical Explor. 58, 125–131. https://doi.org/10.1016/S0375-6742(96)00064-7

Gosar, M., Šajn, R., Biester, H., 2006. Binding of mercury in soils and attic dust in the Idrija mercury mine area (Slovenia). Sci. Total Environ. 369, 150–162. https://doi.org/10.1016/j.scitotenv.2006.05.006

Gosar, M., Teršič, T., 2012. Environmental geochemistry studies in the area of Idrija mercury mine, Slovenia. Environ. Geochem. Health 34, 27–41. https://doi.org/10.1007/s10653-011-9410-6

Graham, A.M., Aiken, G.R., Gilmour, C.C., 2013. Effect of dissolved organic matter source and character on microbial Hg methylation in Hg-S-DOM solutions. Environ. Sci. Technol. 47, 5746–5754.

https://doi.org/10.1021/es400414a

Gray, J.E., Theodorakos, P.M., Fey, D.L., Krabbenhoft, D.P., 2015. Mercury concentrations and distribution in soil, water, mine waste leachates, and air in and around mercury mines in the Big Bend region, Texas, USA. Environ. Geochem. Health 37, 35–48. https://doi.org/10.1007/s10653-014-9628-1

Graydon, J.A., St. Louis, V.L., Lindberg, S.E., Hintelmann, H., Krabbenhoft, D.P., 2006. Investigation of mercury exchange between forest canopy vegetation and the atmosphere using a new dynamic chamber. Environ. Sci. Technol. 40, 4680–4688. https://doi.org/10.1021/es0604616

Grigal, D.F., 2003. Mercury Sequestration in Forests and Peatlands. J. Environ. Qual. 32, 393–405. https://doi.org/10.2134/jeq2003.3930

Griggs, T., Liu, L., Talbot, R.W., Torres, A., Lan, X., 2020. Comparison of atmospheric mercury speciation at a coastal and an urban site in Southeastern Texas, USA. Atmosphere (Basel). 11. https://doi.org/10.3390/ATMOS11010073

Grönlund, R., Edner, H., Svanberg, S., Kotnik, J., Horvat, M., 2005. Mercury emissions from the Idrija mercury mine measured by differential absorption lidar techniques and a point monitoring absorption spectrometer. Atmos. Environ. 39, 4067–4074. https://doi.org/10.1016/j.atmosenv.2005.03.027

Gu, B., Bian, Y., Miller, C.L., Dong, W., Jiang, X., Liang, L., 2011. Mercury reduction and complexation by natural organic matter in anoxic environments. Proc. Natl. Acad. Sci. U. S. A. 108, 1479–1483. https://doi.org/10.1073/pnas.1008747108

Gustin, M.S., Bank, M.S., Bishop, K., Bowman, K., Branfireun, B., Chételat, J., Eckley, C.S., Hammerschmidt, C.R., Lamborg, C., Lyman, S., Martínez-Cortizas, A., Sommar, J., Tsui, M.T.K., Zhang, T., 2020. Mercury biogeochemical cycling: A synthesis of recent scientific advances. Sci. Total Environ. 737, 139619. https://doi.org/10.1016/j.scitotenv.2020.139619

Gustin, M.S., Biester, H., Kim, C.S., 2002. Investigation of the light-enhanced emission of mercury from naturally enriched substrates. Atmos. Environ. 36, 3241–3254. https://doi.org/10.1016/S1352-2310(02)00329-1

Gustin, M.S., Coolbaugh, M.F., Engle, M.A., Fitzgerald, B.C., Keislar, R.E., Lindberg, S.E., Nacht, D.M., Quashnick, J., Rytuba, J.J., Sladek, C., Zhang, H., Zehner, R.E., 2003. Atmospheric mercury emissions from mine wastes and surrounding geologically enriched terrains. Environ. Geol. 43, 339–351. https://doi.org/10.1007/s00254-002-0630-z

Gustin, M.S., Ericksen, J.A., Schorran, D.E., Johnson, D.W., Lindberg, S.E., Coleman, J.S., 2004. Application of controlled mesocosms for understanding mercury air-soil-plant exchange. Environ. Sci. Technol. 38, 6044–6050. https://doi.org/10.1021/es0487933

Gyamfi, O., Sorenson, P.B., Darko, G., Ansah, E., Bak, J.L., 2020. Human health risk assessment of exposure to indoor mercury vapour in a Ghanaian artisanal small-scale gold mining community. Chemosphere 241. https://doi.org/10.1016/j.chemosphere.2019.125014

Ha, J., Zhao, X., Yu, R., Barkay, T., Yee, N., 2017. Hg(II) reduction by siderite (FeCO3). Appl. Geochemistry 78, 211–218. https://doi.org/10.1016/j.apgeochem.2016.12.017

Hammerschmidt, C.R., Fitzgerald, W.F., 2006. Methylmercury in freshwater fish linked to atmospheric mercury deposition. Environ. Sci. Technol. 40, 7764–7770. https://doi.org/10.1021/es061480i

Harada, M., 1995. Minamata Disease: Methylmercury Poisoning in Japan Caused by Environmental Pollution. Crit. Rev. Toxicol. 25, 1–24. https://doi.org/10.3109/10408449509089885

He, F., Zhao, W., Liang, L., Gu, B., 2014. Photochemical Oxidation of Dissolved Elemental Mercury by Carbonate Radicals in Water. Environ. Sci. Technol. Lett. 1, 499–503. https://doi.org/10.1021/ez500322f

Heaton, A.C.P., Rugh, C.L., Wang, N.J., Meagher, R.B., 2005. Physiological responses of transgenic merA-tobacco (Nicotiana tabacum) to foliar and root mercury exposure. Water. Air. Soil Pollut. 161, 137–155. https://doi.org/10.1007/s11270-005-7111-4

Heinemeyer, A., McNamara, N.P., 2011. Comparing the closed static versus the closed dynamic chamber flux methodology: Implications for soil respiration studies. Plant Soil 346, 145–151. https://doi.org/10.1007/s11104-011-0804-0

Higueras, P., Oyarzun, R., Lillo, J., Morata, D., 2013. Intraplate mafic magmatism, degasification, and deposition of mercury: The giant Almadén mercury deposit (Spain) revisited. Ore Geol. Rev. 51, 93–102. https://doi.org/10.1016/j.oregeorev.2012.12.004

Higueras, P., Oyarzun, R., Lillo, J., Sánchez-Hernández, J.C., Molina, J.A., Esbrí, J.M., Lorenzo, S., 2006. The Almadén district (Spain): Anatomy of one of the world's largest Hg-contaminated sites. Sci. Total Environ. 356, 112–124. https://doi.org/10.1016/j.scitotenv.2005.04.042

Hines, M.E., Faganeli, J., Adatto, I., Horvat, M., 2006. Microbial mercury transformations in marine, estuarine and freshwater sediment downstream of the Idrija Mercury Mine, Slovenia. Appl. Geochemistry 21, 1924–1939. https://doi.org/10.1016/j.apgeochem.2006.08.008

Hines, M.E., Poitras, E.N., Covelli, S., Faganeli, J., Emili, A., Žižek, S., Horvat, M., 2012. Mercury methylation and demethylation in Hg-contaminated lagoon sediments (Marano and Grado Lagoon, Italy). Estuar. Coast. Shelf Sci. 113, 85–95. https://doi.org/10.1016/j.ecss.2011.12.021

Holmes, C.D., Jacob, D.J., Corbitt, E.S., Mao, J., Yang, X., Talbot, R., Slemr, F., 2010. Global atmospheric model for mercury including oxidation by bromine atoms. Atmos. Chem. Phys. 10, 12037–12057. https://doi.org/10.5194/acp-10-12037-2010

Horowitz, H.M., Jacob, D.J., Amos, H.M., Streets, D.G., Sunderland, E.M., 2014. Historical mercury releases from commercial products: Global environmental implications. Environ. Sci. Technol. 48, 10242–10250. https://doi.org/10.1021/es501337j

Horvat, M., Kotnik, J., Logar, M., Fajon, V., Zvonarić, T., Pirrone, N., 2003. Speciation of mercury in surface and deep-sea waters in the Mediterranean Sea. Atmos. Environ. 37, 93–108. https://doi.org/10.1016/S1352-2310(03)00249-8

Huremović, J., Horvat, M., Kotnik, J., Kocman, D., Žižek, S., Ribeiro Guevara, S., Muhić-Šarac, T., Memić, M., 2017. Characterization of Mercury Contamination Surrounding a Chloralkali Production Facility in Tuzla, Bosnia and Herzegovina. Anal. Lett. 50, 1049–1064. https://doi.org/10.1080/00032719.2016.1205595

Hutchinson, G.L., Mosier, A.R., 1981. Improved Soil Cover Method for Field Measurement of Nitrous Oxide Fluxes. Soil Sci. Soc. Am. J. 45, 311–316. https://doi.org/https://doi.org/10.2136/sssaj1981.03615995004500020017x

Ie, I.R., Yuan, C.S., Lee, C.E., Chiang, K.C., Chen, T.W., Soong, K.Y., 2022. Chemical significance of atmospheric mercury at fishing port compared to urban and suburb in an offshore island. Atmos. Pollut. Res. 13, 101538. https://doi.org/10.1016/j.apr.2022.101538

Jeon, B., Cizdziel, J. V., 2019. Can the MerPAS Passive air sampler discriminate landscape, seasonal, and elevation effects on atmospheric mercury? A feasibility study in Mississippi, USA. Atmosphere (Basel). 10, 617. https://doi.org/10.3390/atmos10100617

Jeremiason, J.D., Portner, J.C., Aiken, G.R., Hiranaka, A.J., Dvorak, M.T., Tran, K.T., Latch, D.E., 2015. Photoreduction of Hg(II) and photodemethylation of methylmercury: the key role of thiol sites on dissolved organic matter. Environ. Sci. Process. Impacts 17, 1892–1903. https://doi.org/10.1039/C5EM00305A

Jiang, T., Skyllberg, U., Wei, S., Wang, D., Lu, S., Jiang, Z., Flanagan, D.C., 2015. Modeling of the structure-specific kinetics of abiotic, dark reduction of Hg(II) complexed by O/N and S functional groups in humic acids while accounting for time-dependent structural rearrangement. Geochim. Cosmochim. Acta 154, 151–167. https://doi.org/10.1016/j.gca.2015.01.011

Jiskra, M., Saile, D., Wiederhold, J.G., Bourdon, B., Björn, E., Kretzschmar, R., 2014. Kinetics of Hg(II) exchange between organic ligands, goethite, and natural organic matter studied with an enriched stable isotope approach. Environ. Sci. Technol. 48, 13207–13217. https://doi.org/10.1021/es503483m

Jiskra, M., Wiederhold, J.G., Skyllberg, U., Kronberg, R.M., Hajdas, I., Kretzschmar, R., 2015. Mercury Deposition and Re-emission Pathways in Boreal Forest Soils Investigated with Hg Isotope Signatures. Environ. Sci. Technol. 49, 7188–7196. https://doi.org/10.1021/acs.est.5b00742

Kalinchuk, V. V., Lopatnikov, E.A., Astakhov, A.S., Ivanov, M. V., Hu, L., 2021. Distribution of atmospheric gaseous elemental mercury (Hg(0)) from the Sea of Japan to the Arctic, and Hg(0) evasion fluxes in the Eastern Arctic Seas: Results from a joint Russian-Chinese cruise in fall 2018. Sci. Total Environ. 753, 142003. https://doi.org/10.1016/j.scitotenv.2020.142003

Kamp, J., Skov, H., Jensen, B., Sørensen, L.L., 2018. Fluxes of gaseous elemental mercury (GEM) in the High Arctic during atmospheric mercury depletion events (AMDEs). Atmos. Chem. Phys. 18, 6923–6938. https://doi.org/10.5194/acp-18-6923-2018

Kandel, T.P., Lærke, P.E., Elsgaard, L., 2016. Effect of chamber enclosure time on soil respiration flux: A comparison of linear and non-linear flux calculation methods. Atmos. Environ. 141, 245–254. https://doi.org/10.1016/j.atmosenv.2016.06.062

Kerin, E.J., Gilmour, C.C., Roden, E., Suzuki, M.T., Coates, J.D., Mason, R.P., 2006. Mercury methylation by dissimilatory iron-reducing bacteria. Appl. Environ. Microbiol. 72, 7919–7921. https://doi.org/10.1128/AEM.01602-06

Kidd, K.A., Muir, D.C.G., Evans, M.S., Wang, X., Whittle, M., Swanson, H.K., Johnston, T., Guildford, S., 2012. Biomagnification of mercury through lake trout (Salvelinus namaycush) food webs of lakes with different physical, chemical and biological characteristics. Sci. Total Environ. 438, 135–143. https://doi.org/10.1016/j.scitotenv.2012.08.057

Kim, K.H., Kabir, E., Jahan, S.A., 2016. A review on the distribution of Hg in the environment and its human health impacts. J. Hazard. Mater. 306, 376–385. https://doi.org/10.1016/j.jhazmat.2015.11.031

Klapstein, S.J., O'Driscoll, N.J., 2018. Methylmercury Biogeochemistry in Freshwater Ecosystems: A Review

Focusing on DOM and Photodemethylation. Bull. Environ. Contam. Toxicol. 100, 14–25. https://doi.org/10.1007/s00128-017-2236-x

Kocman, D., Horvat, M., 2010. A laboratory based experimental study of mercury emission from contaminated soils in the River Idrijca catchment. Atmos. Chem. Phys. 10, 1417–1426. https://doi.org/10.5194/acp-10-1417-2010

Kocman, D., Horvat, M., Pirrone, N., Cinnirella, S., 2013. Contribution of contaminated sites to the global mercury budget. Environ. Res. 125, 160–170. https://doi.org/10.1016/j.envres.2012.12.011

Kocman, D., Vreča, P., Fajon, V., Horvat, M., 2011. Atmospheric distribution and deposition of mercury in the Idrija Hg mine region, Slovenia. Environ. Res. 111, 1–9. https://doi.org/10.1016/j.envres.2010.10.012

Kocman, D., Wilson, S.J., Amos, H.M., Telmer, K.H., Steenhuisen, F., Sunderland, E.M., Mason, R.P., Outridge, P., Horvat, M., 2017. Toward an assessment of the global inventory of present-day mercury releases to freshwater environments. Int. J. Environ. Res. Public Health 14, 138. https://doi.org/10.3390/ijerph14020138

Kotnik, J., Horvat, M., Begu, E., Shlyapnikov, Y., Sprovieri, F., Pirrone, N., 2017. Dissolved gaseous mercury (DGM) in the Mediterranean Sea: Spatial and temporal trends. Mar. Chem. 193, 8–19. https://doi.org/10.1016/j.marchem.2017.03.002

Kotnik, J., Horvat, M., Dizdarevič, T., 2005. Current and past mercury distribution in air over the Idrija Hg mine region, Slovenia. Atmos. Environ. 39, 7570–7579. https://doi.org/10.1016/j.atmosenv.2005.06.061

Kubáň, Petr, Houserová, P., Kubáň, Pavel, Hauser, P.C., Vlastimil, K., 2007. Mercury speciation by CE: A review. Electrophoresis 28, 58–68. https://doi.org/10.1002/elps.200600457

Kudo, A., Miyahara, S., 1991. A Case History; Minamata Mercury Pollution in Japan – From Loss of Human Lives to Decontamination. Water Sci. Technol. 23, 283–290. https://doi.org/10.2166/wst.1991.0426

Kurz, A.Y., Blum, J.D., Washburn, S.J., Baskaran, M., 2019. Changes in the mercury isotopic composition of sediments from a remote alpine lake in Wyoming, USA. Sci. Total Environ. 669, 973–982. https://doi.org/10.1016/j.scitotenv.2019.03.165

Kuss, J., Holzmann, J., Ludwig, R., 2009. An elemental mercury diffusion coefficient for natural waters determined by molecular dynamics simulation. Environ. Sci. Technol. 43, 3183–3186. https://doi.org/10.1021/es8034889

Kuss, J., Krüger, S., Ruickoldt, J., Wlost, K.P., 2018. High-resolution measurements of elemental mercury in surface water for an improved quantitative understanding of the Baltic Sea as a source of atmospheric mercury. Atmos. Chem. Phys. 18, 4361–4376. https://doi.org/10.5194/acp-18-4361-2018

Kuss, J., Wasmund, N., Nausch, G., Labrenz, M., 2015. Mercury Emission by the Baltic Sea: A Consequence of Cyanobacterial Activity, Photochemistry, And Low-Light Mercury Transformation. Environ. Sci. Technol. 49, 11449–11457. https://doi.org/10.1021/acs.est.5b02204

Kutzbach, L., Schneider, J., Sachs, T., Giebels, M., Nykänen, H., Shurpali, N.J., Martikainen, P.J., Alm, J., Wilmking, M., 2007. CO2 flux determination by closed-chamber methods can be seriously biased by inappropriate application of linear regression. Biogeosciences 4, 1005–1025. https://doi.org/10.5194/bg-4-1005-2007

Kyllönen, K., Hakola, H., Hellén, H., Korhonen, M., Verta, M., 2012. Atmospheric mercury fluxes in a southern boreal forest and wetland. Water. Air. Soil Pollut. 223, 1171–1182. https://doi.org/10.1007/s11270-011-0935-1

Lakshmanan, S., Murugesan, T., 2014. The chlor-alkali process: Work in Progress. Clean Technol. Environ. Policy 16, 225–234. https://doi.org/10.1007/s10098-013-0630-6

Lalonde, J.D., Amyot, M., Kraepiel, A.M.L., Morel, F.M.M., 2001. Photooxidation of Hg(O) in artificial and natural waters. Environ. Sci. Technol. 35, 1367–1372. https://doi.org/10.1021/es001408z

Lalonde, J.D., Amyot, M., Orvoine, J., Morel, F.M.M., Auclair, J.C., Ariya, P.A., 2004. Photoinduced Oxidation of Hg0(aq) in the Waters from the St. Lawrence Estuary. Environ. Sci. Technol. 38, 508–514. https://doi.org/10.1021/es034394g

Lamborg, C.H., Fitzgerald, W.F., O'Donnell, J., Torgersen, T., 2002. A non-steady-state compartmental model of global-scale mercury biogeochemistry with interhemispheric atmospheric gradients. Geochim. Cosmochim. Acta 66, 1105–1118. https://doi.org/10.1016/S0016-7037(01)00841-9

Lamborg, C.H., Hammerschmidt, C.R., Bowman, K.L., 2016. An examination of the role of particles in oceanic mercury cycling. Philos. Trans. R. Soc. A Math. Phys. Eng. Sci. 374. https://doi.org/10.1098/rsta.2015.0297

Langston, W.J., Bebianno, M.J., 1998. Metal metabolism in aquatic environments. Springer Science & Business Media.

Lanzillotta, E., Ceccarini, C., Ferrara, R., 2002. Photo-induced formation of dissolved gaseous mercury in coastal and offshore seawater of the Mediterranean basin. Sci. Total Environ. 300, 179–187.

https://doi.org/10.1016/S0048-9697(02)00223-1

Lanzillotta, E., Ferrara, R., 2001. Daily trend of dissolved gaseous mercury concentration in coastal seawater of the Mediterranean basin. Chemosphere 45, 935–940. https://doi.org/10.1016/S0045-6535(01)00021-2

Laurier, F.J.G., Mason, R.P., Whalin, L., Kato, S., 2003. Reactive gaseous mercury formation in the North Pacific Ocean's marine boundary layer: A potential role of halogen chemistry. J. Geophys. Res. Atmos. 108, 4529. https://doi.org/10.1029/2003jd003625

Lee, J.I., Yang, J.H., Kim, P.R., Han, Y.J., 2019. Effects of organic carbon and UV wavelength on the formation of dissolved gaseous mercury in water under a controlled environment. Environ. Eng. Res. 24, 54–62. https://doi.org/10.4491/eer.2018.045

Lepak, R.F., Tate, M.T., Ogorek, J.M., DeWild, J.F., Peterson, B.D., Hurley, J.P., Krabbenhoft, D.P., 2021. Aqueous Elemental Mercury Production versus Mercury Inventories in the Lake Michigan Airshed: Deciphering the Spatial and Diel Controls of Mercury Gradients in Air and Water. ACS ES&T Water 1, 719–727. https://doi.org/10.1021/acsestwater.0c00187

Li, C., Liang, H., Liang, M., Chen, Y., Zhou, Y., 2018. Mercury emissions flux from various land uses in old mining area, Inner Mongolia, China. J. Geochemical Explor. 192, 132–141. https://doi.org/10.1016/j.gexplo.2018.06.011

Liang, X., Zhu, N., Johs, A., Chen, H., Pelletier, D.A., Zhang, L., Yin, X., Gao, Y., Zhao, J., Gu, B., 2022. Mercury Reduction, Uptake, and Species Transformation by Freshwater Alga Chlorella vulgaris under Sunlit and Dark Conditions . Environ. Sci. Technol. https://doi.org/10.1021/acs.est.1c06558

Lin, C.J., Gustin, M.S., Singhasuk, P., Eckley, C., Miller, M., 2010. Empirical models for estimating mercury flux from soils. Environ. Sci. Technol. 44, 8522–8528. https://doi.org/10.1021/es1021735

Lin, C.J., Zhu, W., Li, X., Feng, X., Sommar, J., Shang, L., 2012. Novel dynamic flux chamber for measuring air-surface exchange of Hg o from soils. Environ. Sci. Technol. 46, 8910–8920. https://doi.org/10.1021/es3012386

Lindberg, S.E., Dong, W., Meyers, T., 2002. Transpiration of gaseous elemental mercury through vegetation in a subtropical wetland in Florida. Atmos. Environ. 36, 5207–5219. https://doi.org/10.1016/S1352-2310(02)00586-1

Lindberg, S.E., Kim, K.H., Meyers, T.P., Owens, J.G., 1995. Micrometeorological Gradient Approach for Quantifying Air/Smface Exchange of Mercuiy Vapor: Tests over Contaminated Soils. Environ. Sci. Technol. 29, 126–135. https://doi.org/10.1021/es00001a016

Liss, P.S., Merlivat, L., 1986. Air-Sea Gas Exchange Rates: Introduction and Synthesis BT - The Role of Air-Sea Exchange in Geochemical Cycling, in: Buat-Ménard, P. (Ed.), . Springer Netherlands, Dordrecht, pp. 113–127. https://doi.org/10.1007/978-94-009-4738-2_5

Liu, B., Keeler, G.J., Timothy Dvonch, J., Barres, J.A., Lynam, M.M., Marsik, F.J., Morgan, J.T., 2010. Urban-rural differences in atmospheric mercury speciation. Atmos. Environ. 44, 2013–2023. https://doi.org/10.1016/j.atmosenv.2010.02.012

Liu, Y.R., Yu, R.Q., Zheng, Y.M., He, J.Z., 2014. Analysis of the microbial community structure by monitoring an Hg methylation gene (hgcA) in paddy soils along an Hg gradient. Appl. Environ. Microbiol. 80, 2874–2879. https://doi.org/10.1128/AEM.04225-13

Livingston, G.P., Hutchinson, G.L., 1995. Enclosure-based measurement of trace gas exchange: applications and sources of error, in: Matson, P.A., Harriss, R.C. (Eds.), Methods in Ecology. Biogenic Trace Gases: Measuring Emissions from Soil and Water. Blackwell Science Oxford, Malden, MA, pp. 14–51.

Llanos, W., Kocman, D., Higueras, P., Horvat, M., 2011. Mercury emission and dispersion models from soils contaminated by cinnabar mining and metallurgy. J. Environ. Monit. 13, 3460–3468. https://doi.org/10.1039/c1em10694e

Loux, N.T., 2004. A critical assessment of elemental mercury air/water exchange parameters. Chem. Speciat. Bioavailab. 16, 127–138. https://doi.org/10.3184/095422904782775018

Luo, H., Cheng, Q., He, D., Wang, X., Pan, X., 2022. Effects of photo-irradiation on mercury binding to dissolved organic matter: Insights from FT-IR and synchronous fluorescence two-dimensional correlation spectroscopy. Chemosphere 287, 132027. https://doi.org/10.1016/j.chemosphere.2021.132027

Luo, H., Cheng, Q., Pan, X., 2020. Photochemical behaviors of mercury (Hg) species in aquatic systems: A systematic review on reaction process, mechanism, and influencing factor. Sci. Total Environ. 720, 137540. https://doi.org/10.1016/j.scitotenv.2020.137540

Luo, Y., Duan, L., Driscoll, C.T., Xu, G., Shao, M., Taylor, M., Wang, S., Hao, J., 2016. Foliage/atmosphere exchange of mercury in a subtropical coniferous forest in south China. J. Geophys. Res. Biogeosciences 121, 2006–2016. https://doi.org/10.1002/2016JG003388

Lyman, S.N., Cheng, I., Gratz, L.E., Weiss-penzias, P., Zhang, L., 2020. An updated review of atmospheric

mercury. Sci. Total Environ. 707, 55–75. https://doi.org/10.1016/j.scitotenv.2019.135575

MacSween, K., Edwards, G.C., 2021. The role of precipitation and soil moisture in enhancing mercury air-surface exchange at a background site in south-eastern Australia. Atmos. Environ. 255, 118445. https://doi.org/10.1016/j.atmosenv.2021.118445

Maier, M., Weber, T.K.D., Fiedler, J., Fuß, R., Glatzel, S., Huth, V., Jordan, S., Jurasinski, G., Kutzbach, L., Schäfer, K., Weymann, D., Hagemann, U., 2022. Introduction of a guideline for measurements of greenhouse gas fluxes from soils using non-steady-state chambers. J. Plant Nutr. Soil Sci. 185, 447–461. https://doi.org/10.1002/jpln.202200199

Marinelli, O., 1894. Studi sul Lago di Cavazzo. Boll. Soc. Geogr. It. 43.

Marumoto, K., Imai, S., 2015. Determination of dissolved gaseous mercury in seawater of Minamata Bay and estimation for mercury exchange across air-sea interface. Mar. Chem. 168, 9–17. https://doi.org/10.1016/j.marchem.2014.09.007

Mason, R.P., Morel, F.M.M., Hemond, H.F., 1995. The role of microorganisms in elemental mercury formation in natural waters. Water, Air, Soil Pollut. 80, 775–787. https://doi.org/10.1007/BF01189729

Mason, R.P., Sheu, G.R., 2002. Role of the ocean in the global mercury cycle. Global Biogeochem. Cycles 16, 40-1-40–14. https://doi.org/10.1029/2001gb001440

Mattassi, G., Daris, F., Nedoclan, G., Crevatin, E., Modonutti, G.B., Lach, S., 1991. La qualità delle acque della Laguna di Marano. USL N°8 "Bassa Friulana."

Mazur, M., Mitchell, C.P.J., Eckley, C.S., Eggert, S.L., Kolka, R.K., Sebestyen, S.D., Swain, E.B., 2014. Gaseous mercury fluxes from forest soils in response to forest harvesting intensity: A field manipulation experiment. Sci. Total Environ. 496, 678–687. https://doi.org/10.1016/j.scitotenv.2014.06.058

McLagan, D.S., Monaci, F., Huang, H., Lei, Y.D., Mitchell, C.P.J., Wania, F., 2019. Characterization and Quantification of Atmospheric Mercury Sources Using Passive Air Samplers. J. Geophys. Res. Atmos. 124, 2351–2362. https://doi.org/10.1029/2018JD029373

Meng, X., Zhao, Y., Tang, W., Shan, B., 2020. Mercury pollution of riverine sediments in a typical irrigation area in the Beijing–Tianjin–Hebei region. Environ. Sci. Pollut. Res. 27, 8732–8739. https://doi.org/10.1007/s11356-019-07474-z

Miller, C.L., Mason, R.P., Gilmour, C.C., Heyes, A., 2007. Influence of dissolved organic matter on the complexation of mercury under sulfidic conditions. Environ. Toxicol. Chem. 26, 624–633. https://doi.org/10.1897/06-375R.1

Miller, M.B., Gustin, M.S., Eckley, C.S., 2011. Measurement and scaling of air-surface mercury exchange from substrates in the vicinity of two Nevada gold mines. Sci. Total Environ. 409, 3879–3886. https://doi.org/10.1016/j.scitotenv.2011.05.040

Millhollen, A.G., Gustin, M.S., Obrist, D., 2006. Foliar mercury accumulation and exchange for three tree species. Environ. Sci. Technol. 40, 6001–6006. https://doi.org/10.1021/es0609194

Ministero dell'Ambiente e della Sicurezza Energetica, 2022. Schede SIN: Caffaro di Torviscosa (già Laguna di Marano e Grado). [WWW Document]. URL https://bonifichesiticontaminati.mite.gov.it/sin-25/ (accessed 12.30.22).

Mlakar, I., 1974. Osnovni parametri proizvodnje rudnika Idrija skozi stoletja do danes. Idrij. razgledi 19, 1–40.

Montoya, A.J., Lena, J.C., Windmöller, C.C., 2019. Adsorption of gaseous elemental mercury on soils: Influence of chemical and/or mineralogical characteristics. Ecotoxicol. Environ. Saf. 170, 98–106. https://doi.org/10.1016/j.ecoenv.2018.11.054

Moore, C., Carpi, A., 2005. Mechanisms of the emission of mercury from soil: Role of UV radiation. J. Geophys. Res. Atmos. 110, D24302. https://doi.org/10.1029/2004JD005567

Morel, F.M.M., Kraepiel, A.M.L., Amyot, M., 1998. The chemical cycle and bioaccumulation of mercury. Annu. Rev. Ecol. Syst. 29, 543–566. https://doi.org/10.1146/annurev.ecolsys.29.1.543

Nacht, D.M., Gustin, M.S., Engle, M.A., Zehner, R.E., Giglini, A.D., 2004. Atmospheric Mercury Emissions and Speciation at the Sulphur Bank Mercury Mine Superfund Site, Northern California. Environ. Sci. Technol. 38, 1977–1983. https://doi.org/10.1021/es0304244

Naharro, R., Esbrí, J.M., Amorós, J.A., Higueras, P.L., 2020. Experimental assessment of the daily exchange of atmospheric mercury in Epipremnum aureum. Environ. Geochem. Health 42, 3185–3198. https://doi.org/10.1007/s10653-020-00557-8

Nerentorp Mastromonaco, M.G., Gårdfeldt, K., Wängberg, I., 2017. Seasonal and spatial evasion of mercury from the western Mediterranean Sea. Mar. Chem. 193, 34–43. https://doi.org/10.1016/j.marchem.2017.02.003

Nightingale, D., Malin, G., Law, C.S., Watson, J., Liss, S., Liddicoat, I., Boutin, J., Upstill-Goddard, C., 2000. In situ evaluation of air-sea gas exchange parameterizations using novel conservative and volatile tracers.

North 14, 373–387.

Nriagu, J.O., 1994. Mechanistic steps in the photoreduction of mercury in natural waters. Sci. Total Environ. 154, 1–8.

O'Connor, D., Hou, D., Ok, Y.S., Mulder, J., Duan, L., Wu, Q., Wang, S., Tack, F.M.G., Rinklebe, J., 2019. Mercury speciation, transformation, and transportation in soils, atmospheric flux, and implications for risk management: A critical review. Environ. Int. 126, 747–761. https://doi.org/10.1016/j.envint.2019.03.019

O'Driscoll, N.J., Beauchamp, S., Siciliano, S.D., Rencz, A.N., Lean, D.R.S., 2003. Continuous analysis of dissolved gaseous mercury (DGM) and mercury flux in two freshwater lakes in Kejimkujik Park, Nova Scotia: Evaluating mercury flux models with quantitative data. Environ. Sci. Technol. 37, 2226–2235. https://doi.org/10.1021/es025944y

O'Driscoll, N.J., Covelli, S., Petranich, E., Floreani, F., Klapstein, S., Acquavita, A., 2019. Dissolved Gaseous Mercury Production at a Marine Aquaculture Site in the Mercury-Contaminated Marano and Grado Lagoon, Italy. Bull. Environ. Contam. Toxicol. 103. https://doi.org/10.1007/s00128-019-02621-1

O'Driscoll, N.J., Vost, E., Mann, E., Klapstein, S., Tordon, R., Lukeman, M., 2018. Mercury photoreduction and photooxidation in lakes: Effects of filtration and dissolved organic carbon concentration. J. Environ. Sci. (China) 68, 151–159. https://doi.org/10.1016/j.jes.2017.12.010

O'Loughlin, E.J., Boyanov, M.I., Kemner, K.M., Thalhammer, K.O., 2020. Reduction of Hg (II) by Fe (II)-bearing smectite clay minerals. Minerals 10, 1079.

Obrist, D., 2012. Mercury distribution across 14 U.S. forests. Part II: Patterns of methyl mercury concentrations and areal mass of total and methyl mercury. Environ. Sci. Technol. 46, 5921–5930. https://doi.org/10.1021/es2045579

Obrist, D., Kirk, J.L., Zhang, L., Sunderland, E.M., Jiskra, M., Selin, N.E., 2018. A review of global environmental mercury processes in response to human and natural perturbations: Changes of emissions, climate, and land use. Ambio 47, 116–140. https://doi.org/10.1007/s13280-017-1004-9

Oertel, C., Matschullat, J., Zurba, K., Zimmermann, F., Erasmi, S., 2016. Greenhouse gas emissions from soils—A review. Chemie der Erde 76, 327–352. https://doi.org/10.1016/j.chemer.2016.04.002

Oh, S., Kim, M.K., Lee, Y.M., Zoh, K.D., 2011. Effect of abiotic and biotic factors on the photo-induced production of dissolved gaseous mercury. Water. Air. Soil Pollut. 220, 353–363. https://doi.org/10.1007/s11270-011-0759-z

Olofsson, M., Sommar, J., Om, E.L., Andersson, M., Angberg, I.W., 2005. Application of Relaxed Eddy Accumulation Technique. Water. Air. Soil Pollut. 167, 331–352.

Orem, W.H., Krabbenhoft, D.P., Poulin, B.A., Aiken, G.R., 2019. Aquatic Cycling of Mercury, in: Rumbold, D.G., Pollman, C.D., Axelrad, D.M. (Eds.), Mercury and the Everglades. A Synthesis and Model for Complex Ecosystem Restoration. Springer International Publishing, Cham, pp. 1–12. https://doi.org/10.1007/978-3-030-32057-7_1

Osterwalder, S., Huang, J.H., Shetaya, W.H., Agnan, Y., Frossard, A., Frey, B., Alewell, C., Kretzschmar, R., Biester, H., Obrist, D., 2019. Mercury emission from industrially contaminated soils in relation to chemical, microbial, and meteorological factors. Environ. Pollut. 250, 944–952. https://doi.org/10.1016/j.envpol.2019.03.093

Osterwalder, S., Sommar, J., Åkerblom, S., Jocher, G., Fritsche, J., Nilsson, M.B., Bishop, K., Alewell, C., 2018. Comparative study of elemental mercury flux measurement techniques over a Fennoscandian boreal peatland. Atmos. Environ. 172, 16–25. https://doi.org/10.1016/j.atmosenv.2017.10.025

Outridge, P.M., Mason, R.P., Wang, F., Guerrero, S., Heimbürger-Boavida, L.E., 2018. Updated Global and Oceanic Mercury Budgets for the United Nations Global Mercury Assessment 2018. Environ. Sci. Technol. 52, 11466–11477. https://doi.org/10.1021/acs.est.8b01246

Pacyna, E.G., Pacyna, J.M., Sundseth, K., Munthe, J., Kindbom, K., Wilson, S., Steenhuisen, F., Maxson, P., 2010. Global emission of mercury to the atmosphere from anthropogenic sources in 2005 and projections to 2020. Atmos. Environ. 44, 2487–2499. https://doi.org/10.1016/j.atmosenv.2009.06.009

Palmieri, H.E.L., Nalini, H.A., Leonel, L. V., Windmöller, C.C., Santos, R.C., de Brito, W., 2006. Quantification and speciation of mercury in soils from the Tripuí Ecological Station, Minas Gerais, Brazil. Sci. Total Environ. 368, 69–78. https://doi.org/10.1016/j.scitotenv.2005.09.085

Pannu, R., Siciliano, S.D., O'Driscoll, N.J., 2014. Quantifying the effects of soil temperature, moisture and sterilization on elemental mercury formation in boreal soils. Environ. Pollut. 193, 138–146. https://doi.org/10.1016/j.envpol.2014.06.023

Parks, J.M., Johs, A., Podar, M., Bridou, R., Hurt, R.A., Smith, S.D., Tomanicek, S.J., Qian, Y., Brown, S.D., Brandt, C.C., Palumbo, A. V., Smith, J.C., Wall, J.D., Elias, D.A., Liang, L., 2013. The genetic basis for bacterial mercury methylation. Science (80-.). 339, 1332–1335. https://doi.org/10.1126/science.1230667

Paterson, M.J., Blanchfield, P.J., Podemski, C., Hintelmann, H.H., Gilmour, C.C., Harris, R., Ogrinc, N., Rudd, J.W.M., Sandilands, K.A., 2006. Bioaccumulation of newly deposited mercury by fish and invertebrates: An enclosure study using stable mercury isotopes. Can. J. Fish. Aquat. Sci. 63, 2213–2224. https://doi.org/10.1139/F06-118

Patra, M., Sharma, A., 2000. Mercury toxicity in plants. Bot. Rev. 66, 379–422. https://doi.org/10.1007/BF02868923

Pavoni, E., Crosera, M., Petranich, E., Oliveri, P., Klun, K., Faganeli, J., Covelli, S., Adami, G., 2020. Trace elements in the estuarine systems of the Gulf of Trieste (northern Adriatic Sea): A chemometric approach to depict partitioning and behaviour of particulate, colloidal and truly dissolved fractions. Chemosphere 252, 126517. https://doi.org/10.1016/j.chemosphere.2020.126517

Pavoni, E., Petranich, E., Signore, S., Fontolan, G., Covelli, S., 2021. The legacy of the idrija mine twenty-five years after closing: Is mercury in the water column of the gulf of trieste still an environmental issue? Int. J. Environ. Res. Public Health 18, 10192. https://doi.org/10.3390/ijerph181910192

Pedersen, A.R., Petersen, S.O., Schelde, K., 2010. A comprehensive approach to soil-atmosphere trace-gas flux estimation with static chambers. Eur. J. Soil Sci. 61, 888–902. https://doi.org/10.1111/j.1365-2389.2010.01291.x

Pelcová, P., Ridošková, A., Hrachovinová, J., Grmela, J., 2021. Evaluation of mercury bioavailability to vegetables in the vicinity of cinnabar mine. Environ. Pollut. 283, 117092. https://doi.org/10.1016/j.envpol.2021.117092

Pestana, I.A., Almeida, M.G., Bastos, W.R., Souza, C.M.M., 2019. Total Hg and methylmercury dynamics in a river-floodplain system in the Western Amazon: Influence of seasonality, organic matter and physical and chemical parameters. Sci. Total Environ. 656, 388–399. https://doi.org/10.1016/j.scitotenv.2018.11.388

Petranich, E., Covelli, S., Acquavita, A., De Vittor, C., Faganeli, J., Contin, M., 2018a. Benthic nutrient cycling at the sediment-water interface in a lagoon fish farming system (northern Adriatic Sea, Italy). Sci. Total Environ. 644, 137–149. https://doi.org/10.1016/j.scitotenv.2018.06.310

Petranich, E., Covelli, S., Acquavita, A., Faganeli, J., Horvat, M., Contin, M., 2018b. Evaluation of mercury biogeochemical cycling at the sediment–water interface in anthropogenically modified lagoon environments. J. Environ. Sci. (China) 68, 5–23. https://doi.org/10.1016/j.jes.2017.11.014

Petranich, E., Predonzani, S., Acquavita, A., Mashyanov, N., Covelli, S., 2022. Rapid thermoscanning technique for direct analysis of mercury species in contaminated sediments : From pure compounds to real sample application. Appl. Geochemistry 143, 105393. https://doi.org/10.1016/j.apgeochem.2022.105393

Piani, A., Acquavita, A., Catalano, L., Contin, M., Mattassi, G., De Nobili, M., 2013. Effects of long term Hg contamination on soil mercury speciation and soil biological activities. E3S Web Conf. 1, 1–4. https://doi.org/10.1051/e3sconf/20130108001

Piani, R., Covelli, S., Biester, H., 2005. Mercury contamination in Marano Lagoon (Northern Adriatic sea, Italy): Source identification by analyses of Hg phases. Appl. Geochemistry 20, 1546–1559. https://doi.org/10.1016/j.apgeochem.2005.04.003

Pirrone, N., Cinnirella, S., Feng, X., Finkelman, R.B., Friedli, H.R., Leaner, J., Mason, R., Mukherjee, A.B., Stracher, G.B., Streets, D.G., Telmer, K., 2010. Global mercury emissions to the atmosphere from anthropogenic and natural sources. Atmos. Chem. Phys. 10, 5951–5964. https://doi.org/10.5194/acp-10-5951-2010

Podar, M., Gilmour, C.C., Brandt, C.C., Soren, A., Brown, S.D., Crable, B.R., Palumbo, A. V., Somenahally, A.C., Elias, D.A., 2015. Global prevalence and distribution of genes and microorganisms involved in mercury methylation. Sci. Adv. 1, e1500675. https://doi.org/10.1126/sciadv.1500675

Poissant, L., Amyot, M., Pilote, M., Lean, D., 2000. Mercury water - Air exchange over the upper St. Lawrence River and Lake Ontario. Environ. Sci. Technol. 34, 3069–3078. https://doi.org/10.1021/es990719a

Poissant, L., Pilote, M., Beauvais, C., Constant, P., Zhang, H.H., 2005. A year of continuous measurements of three atmospheric mercury species (GEM, RGM and Hgp) in southern Québec, Canada. Atmos. Environ. 39, 1275–1287. https://doi.org/10.1016/j.atmosenv.2004.11.007

Poissant, L., Pilote, M., Yumvihoze, E., Lean, D., 2008. Mercury concentrations and foliage/atmosphere fluxes in a maple forest ecosystem in Québec, Canada. J. Geophys. Res. Atmos. 113, D10307. https://doi.org/10.1029/2007JD009510

Polonia, A., Albertazzi, S., Bellucci, L.G., Bonetti, C., Bonetti, J., Giorgetti, G., Giuliani, S., Correa, M.L., Mayr, C., Peruzza, L., Stanghellini, G., Gasperini, L., 2021. Decoding a complex record of anthropogenic and natural impacts in the Lake of Cavazzo sediments, NE Italy. Sci. Total Environ. 787, 147659. https://doi.org/10.1016/j.scitotenv.2021.147659

Polyzou, C., Loupa, G., Trepekli, A., Rapsomanikis, S., 2019. Fluxes of gaseous elemental mercury on a

Mediterranean coastal grassland. Atmosphere (Basel). 10, 485. https://doi.org/10.3390/atmos10090485

Priyadarshanee, M., Chatterjee, S., Rath, S., Dash, H.R., Das, S., 2022. Cellular and genetic mechanism of bacterial mercury resistance and their role in biogeochemistry and bioremediation. J. Hazard. Mater. 423, 126985. https://doi.org/10.1016/j.jhazmat.2021.126985

Qiu, G., Feng, X., Meng, B., Zhang, C., Gu, C., Du, B., Lin, Y., 2013. Environmental geochemistry of an abandoned mercury mine in Yanwuping, Guizhou Province, China. Environ. Res. 125, 124–130. https://doi.org/10.1016/j.envres.2013.01.008

Qureshi, A., O'Driscoll, N.J., Macleod, M., Neuhold, Y.M., Hungerbühler, K., 2010. Photoreactions of mercury in surface ocean water: Gross reaction kinetics and possible pathways. Environ. Sci. Technol. 44, 644–649. https://doi.org/10.1021/es9012728

Raj, D., Maiti, S.K., 2019. Sources, toxicity, and remediation of mercury: an essence review. Environ. Monit. Assess. 191, 566. https://doi.org/10.1007/s10661-019-7743-2

Ramieri, E., Barbanti, A., Picone, M., Menchini, G., Bressan, E., Dal Forno, E., 2011. Integrated plan for the sustainable management of the Lagoon of Marano and Grado. Littoral 2010, 05008. https://doi.org/10.1051/litt/201105008

Ravichandran, M., 2004. Interactions between mercury and dissolved organic matter - A review. Chemosphere 55, 319–331. https://doi.org/10.1016/j.chemosphere.2003.11.011

RegioneAutonomaFriuliVeneziaGiulia, 2012. Piano Regionale Di Tutela Delle Acque.

Ren, X., Luke, W.T., Kelley, P., Cohen, M.D., Artz, R., Olson, M.L., Schmeltz, D., Puchalski, M., Goldberg, D.L., Ring, A., Mazzuca, G.M., Cummings, K.A., Wojdan, L., Preaux, S., Stehr, J.W., 2016. Atmospheric mercury measurements at a suburban site in the Mid-Atlantic United States: Inter-annual, seasonal and diurnal variations and source-receptor relationships. Atmos. Environ. 146, 141–152. https://doi.org/10.1016/j.atmosenv.2016.08.028

Rice, K.M., Walker, E.M., Wu, M., Gillette, C., Blough, E.R., 2014. Environmental mercury and its toxic effects. J. Prev. Med. Public Heal. 47, 74–83. https://doi.org/10.3961/jpmph.2014.47.2.74

Rimondi, V., Gray, J.E., Costagliola, P., Vaselli, O., Lattanzi, P., 2012. Concentration, distribution, and translocation of mercury and methylmercury in mine-waste, sediment, soil, water, and fish collected near the Abbadia San Salvatore mercury mine, Monte Amiata district, Italy. Sci. Total Environ. 414, 318–327. https://doi.org/10.1016/j.scitotenv.2011.10.065

Rinklebe, J., During, A., Overesch, M., Du Laing, G., Wennrich, R., Stärk, H.J., Mothes, S., 2010. Dynamics of mercury fluxes and their controlling factors in large Hg-polluted floodplain areas. Environ. Pollut. 158, 308–318. https://doi.org/10.1016/j.envpol.2009.07.001

Rinklebe, J., During, A., Overesch, M., Wennrich, R., Stärk, H.J., Mothes, S., Neue, H.U., 2009. Optimization of a simple field method to determine mercury volatilization from soils-Examples of 13 sites in floodplain ecosystems at the Elbe River (Germany). Ecol. Eng. 35, 319–328. https://doi.org/10.1016/j.ecoleng.2008.04.019

Robins, N.A., Hagan, N., Halabi, S., Hsu-Kim, H., Gonzales, R.D.E., Morris, M., Woodall, G., Richter, D. de B., Heine, P., Zhang, T., Bacon, A., Vandenberg, J., 2012. Estimations of historical atmospheric mercury concentrations from mercury refining and present-day soil concentrations of total mercury in Huancavelica, Peru. Sci. Total Environ. 426, 146–154. https://doi.org/10.1016/j.scitotenv.2012.03.082

Rochette, P., Gregorich, E.G., Desjardins, R.L., 1992. Comparison of static and dynamic closed chambers for measurement of soil respiration under field conditions. Can. J. Soil Sci. 72, 605–609. https://doi.org/10.4141/cjss92-050

Rolfhus, K.R., Fitzgerald, W.F., 2001. The evasion and spatial/temporal distribution of mercury species in Long Island Sound, CT-NY. Geochim. Cosmochim. Acta 65, 407–418. https://doi.org/10.1016/S0016-7037(00)00519-6

Rudnick, R.L., Gao, S., 2003. Composition of the Continental Crust, in: Holland, H.D., Turekian, K.K. (Eds.), Treatise on Geochemistry. Elsevier, Amsterdam.

Rutter, A.P., Schauer, J.J., Shafer, M.M., Creswell, J.E., Olson, M.R., Robinson, M., Collins, R.M., Parman, A.M., Katzman, T.L., Mallek, J.L., 2011. Dry deposition of gaseous elemental mercury to plants and soils using mercury stable isotopes in a controlled environment. Atmos. Environ. 45, 848–855. https://doi.org/10.1016/j.atmosenv.2010.11.025

Saiz-Lopez, A., Sitkiewicz, S.P., Roca-Sanjuán, D., Oliva-Enrich, J.M., Dávalos, J.Z., Notario, R., Jiskra, M., Xu, Y., Wang, F., Thackray, C.P., Sunderland, E.M., Jacob, D.J., Travnikov, O., Cuevas, C.A., Acuña, A.U., Rivero, D., Plane, J.M.C., Kinnison, D.E., Sonke, J.E., 2018. Photoreduction of gaseous oxidized mercury changes global atmospheric mercury speciation, transport and deposition. Nat. Commun. 9, 4796. https://doi.org/10.1038/s41467-018-07075-3

Sandheinrich, M.B., Wiener, J.G., 2011. Methylmercury in Freshwater Fish. Environ. Contam. Biota 169–192. https://doi.org/10.1201/b10598-5

Schartup, A.T., Ndu, U., Balcom, P.H., Mason, R.P., Sunderland, E.M., 2015. Contrasting effects of marine and terrestrially derived dissolved organic matter on mercury speciation and bioavailability in seawater. Environ. Sci. Technol. 49, 5965–5972. https://doi.org/10.1021/es506274x

Schlüter, K., 2000. Review: Evaporation of mercury from soils. An integration and synthesis of current knowledge. Environ. Geol. 39, 249–271. https://doi.org/10.1007/s002540050005

Schroeder, W.H., Munthe, J., 1998. Atmospheric Mercury-An Overview. Atmos. Environ. 32, 809–822.

Schumacher, L., Abbott, L.C., 2017. Effects of methyl mercury exposure on pancreatic beta cell development and function. J. Appl. Toxicol. 37, 4–12. https://doi.org/10.1002/jat.3381

Schuster, E., 1991. The behavior of mercury in the soil with special emphasis on complexation and adsorption processes - A review of the literature. Water, Air, Soil Pollut. 56, 667–680. https://doi.org/10.1007/BF00342308

Selin, H., Keane, S.E., Wang, S., Selin, N.E., Davis, K., Bally, D., 2018. Linking science and policy to support the implementation of the Minamata Convention on Mercury. Ambio 47, 198–215. https://doi.org/10.1007/s13280-017-1003-x

Selin, N.E., 2009. Global Biogeochemical Cycling of Mercury: A Review. Annu. Rev. Environ. Resour. 34, 43–63. https://doi.org/10.1146/annurev.environ.051308.084314

Selin, N.E., Jacob, D.J., Yantosca, R.M., Strode, S., Jaeglé, L., Sunderland, E.M., 2008. Global 3-D land-ocean-atmosphere model for mercury: Present-day versus preindustrial cycles and anthropogenic enrichment factors for deposition. Global Biogeochem. Cycles 22, GB2011. https://doi.org/10.1029/2007GB003040

Seller, P., Kelly, C.A., Rudd, J.W.M., Mac Hutchon, A.R., 1996. Photodegradation of methylmercury in lakes. Nature 380, 694–697. https://doi.org/10.1038/380694a0

Seo, D.C., Yu, K., DeLaune, R.D., 2008. Comparison of monometal and multimetal adsorption in Mississippi River alluvial wetland sediment: Batch and column experiments. Chemosphere 73, 1757–1764. https://doi.org/10.1016/j.chemosphere.2008.09.003

Shanley, J.B., Marvin-DiPasquale, M., Lane, O., Arendt, W., Hall, S., McDowell, W.H., 2020. Resolving a paradox—high mercury deposition, but low bioaccumulation in northeastern Puerto Rico. Ecotoxicology 29, 1207–1220. https://doi.org/10.1007/s10646-019-02108-z

Sharif, A., Monperrus, M., Tessier, E., Bouchet, S., Pinaly, H., Rodriguez-Gonzalez, P., Maron, P., Amouroux, D., 2014. Fate of mercury species in the coastal plume of the Adour River estuary (Bay of Biscay, SW France). Sci. Total Environ. 496, 701–713. https://doi.org/10.1016/j.scitotenv.2014.06.116

Sharif, A., Tessier, E., Bouchet, S., Monperrus, M., Pinaly, H., Amouroux, D., 2013. Comparison of different air-water gas exchange models to determine gaseous mercury evasion from different european coastal lagoons and estuaries. Water. Air. Soil Pollut. 224. https://doi.org/10.1007/s11270-013-1606-1

Shi, T., Gong, Y., Ma, J., Wu, H., Yang, S., Ju, T., Qu, Y., Liu, L., 2020. Soil-air exchange of mercury from agricultural fields in Zhejiang, East China: Seasonal variations, influence factors, and models of fluxes. Chemosphere 249, 126063. https://doi.org/10.1016/j.chemosphere.2020.126063

Sholupov, S., Pogarev, S., Ryzhov, V., 2004. Zeeman atomic absorption spectrometer RA-915 + for direct determination of mercury in air and complex matrix samples 85, 473–485. https://doi.org/10.1016/j.fuproc.2003.11.003

Sigler, J.M., Lee, X., 2006. Gaseous mercury in background forest soil in the northeastern United States. J. Geophys. Res. Biogeosciences 111, G02007. https://doi.org/10.1029/2005JG000106

Sizmur, T., McArthur, G., Risk, D., Tordon, R., O'Driscoll, N.J., 2017. Gaseous mercury flux from salt marshes is mediated by solar radiation and temperature. Atmos. Environ. 153, 117–125. https://doi.org/10.1016/j.atmosenv.2017.01.024

Skov, H., Christensen, J.H., Goodsite, M.E., Heidam, N.Z., Jensen, B., Wåhlin, P., Geernaert, G., 2004. Fate of Elemental Mercury in the Arctic during Atmospheric Mercury Depletion Episodes and the Load of Atmospheric Mercury to the Arctic. Environ. Sci. Technol. 38, 2373–2382. https://doi.org/10.1021/es030080h

Skyllberg, U., Bloom, P.R., Qian, J., Lin, C.M., Bleam, W.F., 2006. Complexation of mercury(II) in soil organic matter: EXAFS evidence for linear two-coordination with reduced sulfur groups. Environ. Sci. Technol. 40, 4174–4180. https://doi.org/10.1021/es0600577

Skyllberg, U., Drott, A., 2010. Competition between disordered iron sulfide and natural organic matter associated thiols for mercury(II) - An EXAFS study. Environ. Sci. Technol. 44, 1254–1259. https://doi.org/10.1021/es902091w

Soerensen, A.L., Mason, R.P., Balcom, P.H., Sunderland, E.M., 2013. Drivers of surface ocean mercury

concentrations and air-sea exchange in the West Atlantic Ocean. Environ. Sci. Technol. 47, 7757–7765. https://doi.org/10.1021/es401354q

Soerensen, A.L., Sunderland, E.M., Holmes, C.D., Jacob, D.J., Yantosca, R.M., Skov, H., Christensen, J.H., Strode, S.A., Mason, R.P., 2010. An improved global model for air-sea exchange of mercury: High concentrations over the North Atlantic. Environ. Sci. Technol. 44, 8574–8580. https://doi.org/10.1021/es102032g

Sommar, J., Osterwalder, S., Zhu, W., 2020. Recent advances in understanding and measurement of Hg in the environment: Surface-atmosphere exchange of gaseous elemental mercury (Hg0). Sci. Total Environ. 721, 137648. https://doi.org/10.1016/j.scitotenv.2020.137648

Sommar, J., Zhu, W., Lin, C.J., Feng, X., 2013. Field approaches to measure hg exchange between natural surfaces and the atmosphere - A review. Crit. Rev. Environ. Sci. Technol. 43, 1657–1739. https://doi.org/10.1080/10643389.2012.671733

Song, X., Van Heyst, B., 2005. Volatilization of mercury from soils in response to simulated precipitation. Atmos. Environ. 39, 7494–7505. https://doi.org/10.1016/j.atmosenv.2005.07.064

Southworth, G., Lindberg, S., Hintelmann, H., Amyot, M., Poulain, A., Bogle, M.A., Peterson, M., Rudd, J., Harris, R., Sandilands, K., Krabbenhoft, D., Olsen, M., 2007. Evasion of added isotopic mercury from a northern temperate lake. Environ. Toxicol. Chem. 26, 53–60. https://doi.org/10.1897/06-148R.1

Stamenkovic, J., Gustin, M.S., 2009. Nonstomatal versus stomatal uptake of atmospheric mercury. Environ. Sci. Technol. 43, 1367–1372. https://doi.org/10.1021/es801583a

Stamenkovic, J., Gustin, M.S., Arnone, J.A., Johnson, D.W., Larsen, J.D., Verburg, P.S.J., 2008. Atmospheric mercury exchange with a tallgrass prairie ecosystem housed in mesocosms. Sci. Total Environ. 406, 227–238. https://doi.org/10.1016/j.scitotenv.2008.07.047

Starr, L.D., McCarthy, M.J., Hammerschmidt, C.R., Subramaniam, A., Despins, M.C., Montoya, J.P., Newell, S.E., 2022. Mercury methylation linked to nitrification in the tropical North Atlantic Ocean. Mar. Chem. 247, 104174. https://doi.org/10.1016/j.marchem.2022.104174

Streets, D.G., Horowitz, H.M., Jacob, D.J., Lu, Z., Levin, L., Ter Schure, A.F.H., Sunderland, E.M., 2017. Total Mercury Released to the Environment by Human Activities. Environ. Sci. Technol. 51, 5969–5977. https://doi.org/10.1021/acs.est.7b00451

Streets, D.G., Horowitz, H.M., Lu, Z., Levin, L., Thackray, C.P., Sunderland, E.M., 2019a. Five hundred years of anthropogenic mercury: Spatial and temporal release profiles. Environ. Res. Lett. 14, 084004. https://doi.org/10.1088/1748-9326/ab281f

Streets, D.G., Horowitz, H.M., Lu, Z., Levin, L., Thackray, C.P., Sunderland, E.M., 2019b. Global and regional trends in mercury emissions and concentrations, 2010–2015. Atmos. Environ. 201, 417–427. https://doi.org/10.1016/j.atmosenv.2018.12.031

Strode, S.A., Jaeglé, L., Selin, N.E., Jacob, D.J., Park, R.J., Yantosca, R.M., Mason, R.P., Slemr, F., 2007. Air-sea exchange in the global mercury cycle. Global Biogeochem. Cycles 21, 1–12. https://doi.org/10.1029/2006GB002766

Subir, M., Ariya, P.A., Dastoor, A.P., 2011. A review of uncertainties in atmospheric modeling of mercury chemistry I. Uncertainties in existing kinetic parameters - Fundamental limitations and the importance of heterogeneous chemistry. Atmos. Environ. 45, 5664–5676. https://doi.org/10.1016/j.atmosenv.2011.04.046

Sun, Y., Guo, Z., Du, J., Zhao, W., 2020. Diffuse emission and transport of gaseous elemental mercury (GEM) in the Mapamyum geothermal system, Western Tibet (China). J. Volcanol. Geotherm. Res. 397, 106825. https://doi.org/10.1016/j.jvolgeores.2020.106825

Sundseth, K., Pacyna, J.M., Pacyna, E.G., Pirrone, N., Thorne, R.J., 2017. Global sources and pathways of mercury in the context of human health. Int. J. Environ. Res. Public Health 14. https://doi.org/10.3390/ijerph14010105

Sysalová, J., Kučera, J., Drtinová, B., Červenka, R., Zvěřina, O., Komárek, J., Kameník, J., 2017. Mercury species in formerly contaminated soils and released soil gases. Sci. Total Environ. 584–585, 1032–1039. https://doi.org/10.1016/j.scitotenv.2017.01.157

Tao, Z., Liu, Y., Zhou, M., Chai, X., 2017. Exchange pattern of gaseous elemental mercury in landfill: mercury deposition under vegetation coverage and interactive effects of multiple meteorological conditions. Environ. Sci. Pollut. Res. 24, 26586–26593. https://doi.org/10.1007/s11356-017-0275-9

Tassi, F., Cabassi, J., Calabrese, S., Nisi, B., Venturi, S., Capecchiacci, F., Giannini, L., Vaselli, O., 2016. Diffuse soil gas emissions of gaseous elemental mercury (GEM) from hydrothermal-volcanic systems: An innovative approach by using the static closed-chamber method. Appl. Geochemistry 66, 234–241. https://doi.org/10.1016/j.apgeochem.2016.01.002

Teršič, T., Gosar, M., Biester, H., 2011. Distribution and speciation of mercury in soil in the area of an ancient

mercury ore roasting site, Frbejžene trate (Idrija area, Slovenia). J. Geochemical Explor. 110, 136–145. https://doi.org/10.1016/j.gexplo.2011.05.002

Terzano, R., Santoro, A., Spagnuolo, M., Vekemans, B., Medici, L., Janssens, K., Göttlicher, J., Denecke, M.A., Mangold, S., Ruggiero, P., 2010. Solving mercury (Hg) speciation in soil samples by synchrotron X-ray microspectroscopic techniques. Environ. Pollut. 158, 2702–2709. https://doi.org/10.1016/j.envpol.2010.04.016

Tomažič, Š., Ličer, M., Žagar, D., 2018. Numerical modelling of mercury evasion in a two-layered Adriatic Sea using a coupled atmosphere-ocean model. Mar. Pollut. Bull. 135, 1164–1173. https://doi.org/10.1016/j.marpolbul.2018.08.064

Travnikov, O., 2005. Contribution of the intercontinental atmospheric transport to mercury pollution in the Northern Hemisphere. Atmos. Environ. 39, 7541–7548. https://doi.org/10.1016/j.atmosenv.2005.07.066

Tretiach, M., Candotto Carniel, F., Loppi, S., Carniel, A., Bortolussi, A., Mazzilis, D., Del Bianco, C., 2011. Lichen transplants as a suitable tool to identify mercury pollution from waste incinerators: A case study from NE Italy. Environ. Monit. Assess. 175, 589–600. https://doi.org/10.1007/s10661-010-1553-x

Treu, F., Zini, L., Zavagno, E., Biolchi, S., Boccali, C., Gregorič, A., Napolitanoc, R., Urbancd, J., Zuecco, G., Cucchi, F., 2017. Intrinsic vulnerability of the Isonzo/Soča high plain aquifer (NE Italy - W Slovenia). J. Maps 13, 799–810. https://doi.org/10.1080/17445647.2017.1384935

Turritto, A., Acquavita, A., Bezzi, A., Covelli, S., Fontolan, G., Petranich, E., Piani, R., Pillon, S., 2018. Suspended particulate mercury associated with tidal fluxes in a lagoon environment impacted by cinnabar mining activity (northern Adriatic Sea). J. Environ. Sci. (China) 68, 100–113. https://doi.org/10.1016/j.jes.2017.12.009

Ullrich, S.M., Tanton, T.W., Abdrashitova, S.A., 2001. Mercury in the aquatic environment: A review of factors affecting methylation. Crit. Rev. Environ. Sci. Technol. 31, 241–293. https://doi.org/10.1080/20016491089226

UN Environment, 2019. Global Mercury Assessment 2018. UN Environment Programme, Chemicals and Health Branch, Geneva, Switzerland.

Vaselli, O., Higueras, P., Nisi, B., María Esbrí, J., Cabassi, J., Martínez-Coronado, A., Tassi, F., Rappuoli, D., 2013. Distribution of gaseous Hg in the Mercury mining district of Mt. Amiata (Central Italy): A geochemical survey prior the reclamation project. Environ. Res. 125, 179–187. https://doi.org/10.1016/j.envres.2012.12.010

Venturini, C., Discenza, K., 2010. Stratigrafia e paleo-idrografia del Friuli centrale (Prealpi Carniche) Miocene superiore-Pliocene inferiore. Gortania Udine 30, 31–52.

Verginelli, I., Pecoraro, R., Baciocchi, R., 2018. Using dynamic flux chambers to estimate the natural attenuation rates in the subsurface at petroleum contaminated sites. Sci. Total Environ. 619–620, 470–479. https://doi.org/10.1016/j.scitotenv.2017.11.100

Vudamala, K., Chakraborty, P., Sailaja, B.B.V., 2017. An insight into mercury reduction process by humic substances in aqueous medium under dark condition. Environ. Sci. Pollut. Res. 24, 14499–14507. https://doi.org/10.1007/s11356-017-8979-4

Wallschläger, D., Turner, R.R., London, J., Ebinghaus, R., Kock, H.H., Sommar, J., Xiao, Z., 1999. Factors affecting the measurement of mercury emissions from soils with flux chambers. J. Geophys. Res. Atmos. 104, 21859–21871. https://doi.org/10.1029/1999JD900314

Wang, C., Ci, Z., Wang, Z., Zhang, X., 2016. Air-sea exchange of gaseous mercury in the East China Sea. Environ. Pollut. 212, 535–543. https://doi.org/10.1016/j.envpol.2016.03.016

Wang, D., He, L., Shi, X., Wei, S., Feng, X., 2006. Release flux of mercury from different environmental surfaces in Chongqing, China. Chemosphere 64, 1845–1854. https://doi.org/10.1016/j.chemosphere.2006.01.054

Wang, S., Feng, X., Qiu, G., Wei, Z., Xiao, T., 2005. Mercury emission to atmosphere from Lanmuchang Hg-Tl mining area, Southwestern Guizhou, China. Atmos. Environ. 39, 7459–7473. https://doi.org/10.1016/j.atmosenv.2005.06.062

Wang, Z., Fei, Z., Wu, Q., Yin, R., 2020. Evaluation of the effects of Hg/DOC ratios on the reduction of Hg(II) in lake water. Chemosphere 253, 126634. https://doi.org/10.1016/j.chemosphere.2020.126634

Wang, Z., Zhang, G., Chen, X., Zhao, Q., Wang, W., Sheng, L., Bian, H., Li, Z., Wang, D., 2019. Measurement and Scaling of Mercury on Soil and Air in a Historical Artisanal Gold Mining Area in Northeastern China. Chinese Geogr. Sci. 29, 245–257. https://doi.org/10.1007/s11769-019-1026-2

Wängberg, I., Schmolke, S., Schager, P., Munthe, J., Ebinghaus, R., Iverfeldt, Å., 2001. Estimates of air-sea exchange of mercury in the Baltic Sea. Atmos. Environ. 35, 5477–5484. https://doi.org/10.1016/S1352-2310(01)00246-1

Wanninkhof, R., 1992. Relationship between wind speed and gas exchange over the ocean. J. Geophys. Res. 97,

7373–7382. https://doi.org/10.1029/92JC00188

Watson, D., Miller, C., Lester, B., Lowe, K., Southworth, G., Bogle, M.A., Liang, L., Pierce, E., 2015. Mercury source zone identification using soil vapor sampling and analysis. Front. Environ. Sci. Eng. 9, 596–604. https://doi.org/10.1007/s11783-014-0709-2

Windmöller, C.C., Durão, W.A., de Oliveira, A., do Valle, C.M., 2015. The redox processes in Hg-contaminated soils from Descoberto (Minas Gerais, Brazil): Implications for the mercury cycle. Ecotoxicol. Environ. Saf. 112, 201–211. https://doi.org/10.1016/j.ecoenv.2014.11.009

Wolfe, M.F., Schwarzbach, S., Sulaiman, R.A., 1998. Effects of mercury on wildlife: A comprehensive review. Environ. Toxicol. Chem. 17, 146–160. https://doi.org/10.1897/1551-5028(1998)017<0146:EOMOWA>2.3.CO;2

Wollenberg, J.L., Peters, S.C., 2009. Mercury emission from a temperate lake during autumn turnover. Sci. Total Environ. 407, 2909–2918. https://doi.org/10.1016/j.scitotenv.2008.12.017

World Health Organization, 2020. Chemicals of major public health concerns [WWW Document]. URL https://www.who.int/teams/environment-climate-change-and-health/chemical-safety-and-health/health-impacts/chemicals (accessed 1.3.23).

Xia, K., Skyllberg, U.L., Bleam, W.F., Bloom, P.R., Nater, E.A., Helmke, P.A., 1999. X-ray absorption spectroscopic evidence for the complexation of Hg(II) by reduced sulfur in soil humic substances. Environ. Sci. Technol. 33, 257–261. https://doi.org/10.1021/es980433q

Xiang, Y., Liu, G., Yin, Y., Cai, Y., 2021. Periphyton as an important source of methylmercury in Everglades water and food web. J. Hazard. Mater. 410, 124551. https://doi.org/10.1016/j.jhazmat.2020.124551

Xin, M., Gustin, M., Johnson, D., 2007. Laboratory investigation of the potential for re-emission of atmospherically derived Hg from soils. Environ. Sci. Technol. 41, 4946–4951. https://doi.org/10.1021/es062783f

Xue, W., Kwon, S.Y., Grasby, S.E., Sunderland, E.M., Pan, X., Sun, R., Zhou, T., Yan, H., Yin, R., 2019. Anthropogenic influences on mercury in Chinese soil and sediment revealed by relationships with total organic carbon. Environ. Pollut. 255, 113186. https://doi.org/10.1016/j.envpol.2019.113186

Yamamoto, M., 1996. Stimulation of elemental mercury oxidation in the presence of chloride ion in aquatic environments. Chemosphere 32, 1217–1224. https://doi.org/10.1016/0045-6535(96)00008-2

Yang, J., Kim, J., Soerensen, A.L., Lee, W., Han, S., 2020. The role of fluorescent dissolved organic matter on mercury photoreduction rates: A case study of three temperate lakes. Geochim. Cosmochim. Acta 277, 192–205. https://doi.org/10.1016/j.gca.2020.03.027

Yang, Y. kui, Zhang, C., Shi, X. jun, Lin, T., Wang, D. yong, 2007. Effect of organic matter and pH on mercury release from soils. J. Environ. Sci. 19, 1349–1354. https://doi.org/10.1016/S1001-0742(07)60220-4

Yin, Y., Allen, H.E., Li, Y., Huang, C.P., Sanders, P.F., 1996. Adsorption of Mercury(II) by Soil: Effects of pH, Chloride, and Organic Matter. J. Environ. Qual. 25, 837–844. https://doi.org/https://doi.org/10.2134/jeq1996.00472425002500040027x

Yoshizawa, K., Rimm, E.B., Morris, J.S., Spate, V.L., Hsieh, C., Spiegelman, D., Stampfer, M.J., Willett, W.C., 2002. Mercury and the Risk of Coronary Heart Disease in Men. N. Engl. J. Med. 347, 1755–1760. https://doi.org/10.1056/NEJMoa021437

Yuan, W., Sommar, J., Lin, C.J., Wang, X., Li, K., Liu, Y., Zhang, H., Lu, Z., Wu, C., Feng, X., 2019a. Stable Isotope Evidence Shows Re-emission of Elemental Mercury Vapor Occurring after Reductive Loss from Foliage. Environ. Sci. Technol. 53, 651–660. https://doi.org/10.1021/acs.est.8b04865

Yuan, W., Wang, X., Lin, C.J., Sommar, J., Lu, Z., Feng, X., 2019b. Process factors driving dynamic exchange of elemental mercury vapor over soil in broadleaf forest ecosystems. Atmos. Environ. 219, 117047. https://doi.org/10.1016/j.atmosenv.2019.117047

Yue, H., Liu, C., Zhang, W., Dannenmann, M., Wang, X., Yao, Z., Song, C., Butterbach-Bahl, K., 2022. How to Improve Cumulative Methane and Nitrous Oxide Flux Estimations of the Non-Steady-State Chamber Method? J. Geophys. Res. Biogeosciences 127, e2021JG006641. https://doi.org/10.1029/2021JG006641

Zahir, F., Rizwi, S.J., Haq, S.K., Khan, R.H., 2005. Low dose mercury toxicity and human health. Environ. Toxicol. Pharmacol. 20, 351–360. https://doi.org/10.1016/j.etap.2005.03.007

Zhang, H., Lindberg, S.E., Barnett, M.O., Vette, A.F., Gustin, M.S., 2002. Dynamic flux chamber measurement of gaseous mercury emission fluxes over soils. Part 1: simulation of gaseous mercury emissions from soils using a two-resistance exchange interface model. Atmos. Environ. 36, 835–846.

Zhang, Y., Jacob, D.J., Horowitz, H.M., Chen, L., Amos, H.M., Krabbenhoft, D.P., Slemr, F., St. Louis, V.L., Sunderland, E.M., 2016. Observed decrease in atmospheric mercury explained by global decline in anthropogenic emissions. Proc. Natl. Acad. Sci. U. S. A. 113, 526–531. https://doi.org/10.1073/pnas.1516312113

Zheng, W., Hintelmann, H., 2009. Mercury isotope fractionation during photoreduction in natural water is controlled by its Hg/DOC ratio. Geochim. Cosmochim. Acta 73, 6704–6715. https://doi.org/10.1016/j.gca.2009.08.016

Zheng, W., Liang, L., Gu, B., 2012. Mercury reduction and oxidation by reduced natural organic matter in anoxic environments. Environ. Sci. Technol. 46, 292–299. https://doi.org/10.1021/es203402p

Zhou, J., Obrist, D., 2021. Global Mercury Assimilation by Vegetation. Environ. Sci. Technol. 55, 14245–14257. https://doi.org/10.1021/acs.est.1c03530

Zhou, J., Wang, Z., Zhang, X., Driscoll, C.T., 2021. Measurement of the Vertical Distribution of Gaseous Elemental Mercury Concentration in Soil Pore Air of Subtropical and Temperate Forests. Environ. Sci. Technol. 55, 2132–2142. https://doi.org/10.1021/acs.est.0c05204

Zhou, J., Wang, Z., Zhang, X., Sun, T., 2017. Investigation of factors affecting mercury emission from subtropical forest soil: A field controlled study in southwestern China. J. Geochemical Explor. 176, 128–135. https://doi.org/10.1016/j.gexplo.2015.10.007

Zhu, J., Wang, D., Liu, X., Zhang, Y., 2011. Mercury fluxes from air/surface interfaces in paddy field and dry land. Appl. Geochemistry 26, 249–255. https://doi.org/10.1016/j.apgeochem.2010.11.025

Zhu, W., Li, Z., Li, P., Yu, B., Lin, C.J., Sommar, J., Feng, X., 2018. Re-emission of legacy mercury from soil adjacent to closed point sources of Hg emission. Environ. Pollut. 242, 718–727. https://doi.org/10.1016/j.envpol.2018.07.002

Zhu, W., Lin, C.J., Wang, X., Sommar, J., Fu, X., Feng, X., 2016. Global observations and modeling of atmosphere-surface exchange of elemental mercury: A critical review. Atmos. Chem. Phys. 16, 4451–4480. https://doi.org/10.5194/acp-16-4451-2016

Zhu, W., Sommar, J., Lin, C.J., Feng, X., 2015a. Mercury vapor air-surface exchange measured by collocated micrometeorological and enclosure methods – Part I: Data comparability and method characteristics. Atmos. Chem. Phys. 15, 685–702. https://doi.org/10.5194/acp-15-685-2015

Zhu, W., Sommar, J., Lin, C.J., Feng, X., 2015b. Mercury vapor air-surface exchange measured by collocated micrometeorological and enclosure methods - Part II: Bias and uncertainty analysis. Atmos. Chem. Phys. 15, 5359–5376. https://doi.org/10.5194/acp-15-5359-2015

Žibret, G., Gosar, M., 2006. Calculation of the mercury accumulation in the Idrijca River alluvial plain sediments. Sci. Total Environ. 368, 291–297. https://doi.org/10.1016/j.scitotenv.2005.09.086

3. Results

3.1 Preamble

In this chapter the results and discussion related to the present research project are reported through three manuscripts and a brief appendix as follows:

1. The first manuscript is entitled "*Dissolved gaseous mercury production and sea-air exchange at impacted coastal environments of the Northern Adriatic Sea*" has been submitted and is currently Under Review by the journal Environmental Pollution. This manuscript provides the first evidences about the processes and dynamics which affect the occurrence and production of dissolved gaseous mercury in the surface water layer and its gaseous exchanges at the water-air interface over the entire 24h diurnal cycle in two coastal environments of the highly impacted area of the Northern Adriatic Sea. For this part of the research, the activity was focused on the highly Hg-impacted confined environment of the Val Noghera fish farm in the Marano and Grado Lagoon (Italy) and on the open marine coastal area of the Bay of Piran (Slovenia), the latter chosen as a relative pristine area of the northernmost part of the Adriatic Sea. The main aim of the study was to investigate how the different degree of Hg contamination and the different hydrodynamic conditions found at the two selected sites affect the magnitude of gaseous exchanges of Hg between the water and the atmosphere in different seasons (summer, autumn, spring). Moreover, the results provide evidences about the ability of these gaseous exchanges to limit the burden of Hg in the water column and about the possibility to enhance this process through a higher hydrodynamims at the fish farm as a mitigation strategy for Hg contamination.

2. The second manuscript, entitled "*Gaseous mercury exchange from water-air interface in differently impacted freshwater environments*" has been published by the journal International Journal of Environmental Research and Public Health. The manuscript is focused on the evaluation of the impact of legacy Hg contamination on present day Hg^0 fluxes at the water-air interface in impacted freshwater environments, also investigating the possible differences related to the different contamination source. For this purpose, two sites were selected: the Solkan Reservoir (Slovenia) along the Isonzo River for Hg contamination of mining origin and the Torviscosa Dockyard (Italy), near the former

local chlor-alkali plant, for contamination of industrial origin. Measurements were conducted over the diurnal period in different seasons (summer, autumn, spring) to elucidate the variability of the evasion under different conditions. A third site with no known Hg sources, the Cavazzo Lake (Italy), was selected as natural background of this area. Moreover, the influence of variable physico-chemical conditions of the water column at the various sites on Hg^0 releases was also assessed. This study provides further data about the fate of Hg supplied to these aquatic environments decades after the phase out of the primary contamination sources.

3. The third manuscript, entitled "*Gaseous mercury evasion from bare and grass-covered soils contaminated by mining and ore roasting (Isonzo River alluvial plain, Northeastern Italy)*" has been published by the journal Environmental Pollution. The manuscript provides the first direct evidences about secondary releases of Hg^0 at the soil-air interface in 6 selected sites along the Isonzo River alluvial plain. These sites are characterised by a different degree of Hg contamination of the soil as a result of historical flooding events of the Isonzo River, which lead to a widespread dispersion of Hg-contaminated material coming from the upstream Idrija Hg mining district (Slovenia). Fluxes of Hg^0 were measured in different seasons (summer, autumn, winter) to elucidate the temporal variability of the evasion. The influence of soil physico-chemical characteristics and Hg total concentration and speciation was also evaluated. Finally, measurements were taken from both bare and grass-covered soil plots, providing information about the importance of the presence of vegetation and its growing stage on limiting Hg^0 effluxes to the atmosphere and the possible use of vegetation as a cost-effective mitigation strategy for Hg contaminated terrestrial sites.

4. In the last part of this chapter, the atmospheric concentrations of Hg^0 (in this case operationally defined GEM: Gaseous Elemental Mercury) recorded during sampling activity performed at all sites investigated in the previous parts are briefly reported. The aim of these measurements was to assess the level of GEM in the atmosphere at these sites in order to understand if they can be influenced by the releases from the investigated contaminated surfaces.

3.2 Article I: Hg^0 fluxes at water-air interface in coastal environments

Dissolved gaseous mercury production and sea-air gaseous exchange in impacted coastal environments of the Northern Adriatic Sea

Federico Floreani[a,b]*, Nicolò Barago[a], Jadran Faganeli[c], Stefano Covelli[a]

[a]*Department of Mathematics & Geosciences, University of Trieste, Via E. Weiss 2, 34128 Trieste, Italy.*

[b]*Department of Life Sciences, University of Trieste, Via L. Giorgieri 5, 34127 Trieste, Italy*

[c]*Marine Biology Station, National Institute of Biology, Fornace 41, 6330 Piran, Slovenia*

*Corresponding author: Federico Floreani

Department of Mathematics and Geosciences

University of Trieste

Via E. Weiss 2, 34128 Trieste (Italy)

e-mail: federico.floreani@phd.units.it

(manuscript submitted to *Environmental Pollution*)

Abstract

Coastal aquatic environments are particularly vulnerable to mercury (Hg) pollution as they are potentially subject to relevant supplies from direct discharges and riverine transport. The formation of dissolved gaseous mercury (DGM) and its subsequent evasion into the atmosphere can reduce the amount of Hg in the water column. The northern Adriatic Sea is well known for Hg contamination largely due to historical Hg mining which took place in Idrija (Slovenia). In this work, the diurnal patterns of both DGM production and gaseous Hg fluxes at the water-air interface were seasonally evaluated in two selected environments within this area, a highly Hg-impacted, confined fish farm (VN: Val Noghera, Italy) and an open coastal zone less impacted by Hg inputs (PR: Bay of Piran, Slovenia). Substantial DGM production was observed at VN (range=126.0-711.3 pg L^{-1}) driven by both strong photoreduction and possibly dark biotic reduction, resulting in higher values in spring and summer and comparable concentrations throughout both day and night. Significantly lower DGM was observed at PR (range=21.8-183.4 pg L^{-1}). Surprisingly, comparable Hg fluxes were found at the two sites (range VN=7.43-41.17 ng m^{-2} h^{-1}, PR=0-81.49 ng m^{-2} h^{-1}), likely due to enhanced gaseous exchanges at PR thanks to high water turbulence and to the strong limitation of evasion at VN by water stagnation and competition with high DGM oxidation in saltwater. Slight differences between the temporal variation of DGM and fluxes further confirmed that Hg evasion is more controlled by factors such as water temperature and mixing conditions than DGM concentrations alone. These results indicate that static water conditions should be avoided, as by limiting volatilisation they can increase the amount of Hg retained in water which may be available for methylation and trophic transfer, mostly in marine impacted coastal sites where oxidation to ionic Hg may be favoured.

Keywords: *Idrija mercury mine; mercury evasion; fish farm; flux chamber; water-air exchange*

.

1. Introduction

Mercury (Hg) is a toxic element which occurs naturally under different inorganic and organic forms in every environmental compartment, at least at relatively low concentrations (Beckers and Rinklebe, 2017). A peculiarity of this metal is the high vapour pressure and low solubility of its elemental form, often referred to as gaseous elemental mercury (Hg^0 or GEM). This specie usually represents more than 90% of the Hg occurring in the atmosphere and can persist for more than 1 year in this compartment (Ariya et al., 2015; Ren et al., 2016; Saiz-Lopez et al., 2018). This long residence time allows Hg^0 to be subject to long-range atmospheric transport before being removed through dry or wet depositions mostly after oxidation to the more soluble ionic form (Hg^{2+}) (Ariya et al., 2015; Custodio et al., 2020; Zhang et al., 2012). Moreover, after deposition, Hg^{2+} can be reduced to Hg^0 and re-emitted into the atmosphere, further enhancing its dispersion throughout the environment (Fitzgerald et al., 1998; Strode et al., 2007; Zheng and Hintelmann, 2009). Historical emissions related to various anthropogenic activities (e.g. mining, coal combustion, metal production, … (UNEP, 2019)) have contributed to significantly increase the amount of Hg involved in these exchanges compared to pre-industrial levels (Enrico et al., 2017; Mason and Sheu, 2002). As a result, Hg pollution has been recognised as a global concern by the Minamata Convention in 2013 (Selin et al., 2018).

Aquatic ecosystems are particularly sensitive to Hg pollution due to the possible conversion of inorganic Hg to the organic form methylmercury (MeHg), which can be easily bioaccumulated and biomagnified in food webs and can have notable toxic effects on biota and humans mainly on the nervous system (Díez, 2009; Morel et al., 1998). MeHg is mainly produced in anoxic sediments and water layers by several microorganisms (Fitzgerald et al., 2007; Parks et al., 2013), although several pathways for Hg methylation, even in oxic water layers, have recently been identified (Wang et al., 2022). Moreover, coastal and marginal sea environments are considered more vulnerable to Hg pollution as they represent hot spots for Hg methylation due to both the high Hg loadings related to both atmospheric depositions and direct riverine inputs (Amos et al., 2014; Kotnik et al., 2015; Xue et al., 2019) and the high nutrient concentrations along with rates of microbial activity (Hammerschmidt and Fitzgerald, 2004).
The formation of Hg^0 and subsequent evasion at the water-air interface can represent a relevant pathway for reducing the amount of Hg^{2+} available for methylation into the aquatic environment (Horvat et al., 2003). Considering that Hg^0 is the largely predominant constituent of the volatile Hg fraction in water, with volatile organic dimethylmercury (DMeHg) occurring

only at extremely low concentrations in deep water layers and rarely detected in surface waters (Black et al., 2009; Cossa et al., 2009; Kotnik et al., 2017), hereafter it will be referred to as DGM (Dissolved Gaseous Mercury), commonly used to indicate the operationally defined gaseous Hg fraction in water. In surface seawater, DGM is produced through abiotic (photochemical) and biotic reduction of Hg^{2+} (Amyot et al., 1997; Kuss et al., 2015; Qureshi et al., 2010), with photoreduction considered the dominant pathway due to its higher rates (Soerensen et al., 2010). An important control on photoreduction rates is exerted by dissolved organic matter (DOM), which, depending on its concentration and structure, can: i) promote reaction rates acting as a photosensitiser, particularly if it is rich in chromophores (Costa and Liss, 1999; Fantozzi et al., 2007), ii) form strong complexes with Hg^{2+} due to its high affinity for reduced sulphur groups (e.g. thiols), rendering it non-photoreducible (O'Driscoll et al., 2018), iii) reduce light penetration through the water column and the efficacy of photochemical reactions (Castelle et al., 2009). Moreover, DGM can be produced even in the absence of light through "dark reduction" reactions mediated by microbial activity (Fantozzi et al., 2009) or by interaction with a particular fraction of organic matter (OM) e.g. humic substances (Allard and Arsenie, 1991). These processes are generally more important in deep water layers and sediments (Amyot et al., 1997; Lepak et al., 2021). However, DGM in water can be re-oxidised to non-volatile Hg^{2+} mainly through photochemical reactions occurring at the same time as photoreduction (Whalin et al., 2007) and enhanced in salt water by the presence of halides (e.g. Cl^-, Br^-) (Ci et al., 2016). When the balance between production through reduction and losses through oxidation leads to a super-saturation of DGM in surface water, evasion into the atmosphere can take place (Southworth et al., 2007) as a function of both DGM availability and physical forcing such as temperature, water turbulence, mixing or currents (Lindberg and Zhang, 2000; Sharif et al., 2013).

The northernmost part of the Adriatic Sea (Gulf of Trieste, Italy) is one of the coastal marine areas most impacted by anthropogenic releases of Hg in the world (Fitzgerald et al., 2007). The main source of Hg in this area is the transport of Hg-enriched sedimentary material by the Isonzo River as a consequence of the dispersion into the environment of large amounts of this element (>35,000 t, Dizdarevič, 2001; Gosar et al., 1997)) due to historical cinnabar mining in Idrija (Slovenia) which lasted for approximately 500 years (Covelli et al., 2001). As a result of the erosion and leaching of contaminated surfaces, the Isonzo River still carries notable amounts of Hg into the Gulf of Trieste, even 25 years after the mine closure, mostly after intense rain events (Covelli et al., 2007; Baptista-Salazar et al., 2017). At the mouth of the

Isonzo River, the contaminated material is diverted westward by the prevalent anticlockwise water circulation of the Gulf and enters the Marano and Grado Lagoon, where Hg can accumulate in sediments mainly in the eastern section (Acquavita et al., 2012). A second anthropogenic source of Hg is related to past uncontrolled discharges from the 1940s to the 1980s of processing and seepage wastewaters from a chlor-alkali plant (Torviscosa, Italy) into the Aussa River and consequently into the lagoon (Covelli et al., 2009). Mercury contamination of this lagoon is of particular concern considering that traditional aquaculture in the form of fish farms cover approximately 14% of its area (Acquavita et al., 2015). These fish farms are closed environments, isolated from the rest of the lagoon by man-made embankments, having only limited water exchanges with the external lagoon (Petranich et al., 2018a).

At present, only limited information restricted to the daylight hours exists regarding Hg^0 exchanges at the water-air interface in this area (Floreani et al., 2019). Understanding the processes that control Hg speciation and gaseous exchanges at the water-air interface in coastal areas subject to notable Hg supplies related to anthropogenic activities is of particular interest in order to evaluate the ability of gaseous exchange to reduce the burden of Hg available to methylation and trophic transfer, mostly in environments characterised by limited water exchanges. In-depth knowledge of these processes may also be useful to better assess the impact of Hg pollution on ecosystems and human health, also helping define possible mitigation strategies (Bouchet et al., 2011; Clarke et al., 2023; Hsu-Kim et al., 2018). The purpose of this work is to further improve the understanding of Hg cycling in this contaminated area through the parallel evaluation of DGM dynamics and Hg^0 fluxes over the entire diurnal cycle during different periods of the year. Both a highly impacted and confined area (the Val Noghera fish farm in the Marano and Grado Lagoon, Italy) and a *quasi*-pristine open coastal zone of the Gulf of Trieste (the Bay of Piran, Slovenia) less subjected to riverine Hg inputs (Fig.1) were selected in order to understand the impact of the degree of contamination and different hydrodynamic conditions on Hg^0 production and evasion. The expected results will provide further information regarding DGM production in this area and its connection with Hg^0 exchange and on the main factor influencing the variability of these processes.

2. Materials and Methods

2.1 Environmental settings

The Val Noghera fish farm is located in the central part of the Marano and Grado Lagoon (Northern Adriatic Sea, Italy), one of the best preserved wetland transitional environments in the entire Mediterranean area, covering an area of approximately 160 km^2 between the Tagliamento and Isonzo River deltas (Fig. 1).

Figure 1: study area and sampling sites (satellite images from Bing).

The Val Noghera fish farm extends over a total area of 2.7 km^2, most of which is occupied by shallow waters and saltmarshes, having become a habitat for many bird species. The fish farm is divided into two main sectors: the eastern part (2.1 km^2) was created in the 1960s and is still used for aquaculture, with active water recirculation through sluice gates, whereas the western part (0.6 km^2), dating from the early 19th century, is no longer used for fishing and is characterised by extremely limited water recycling and recirculation. More details about the

hydrogeology and management of these environments have been reported in previous works (Petranich et al., 2018a, 2018b). Our sampling site (VN) is located in a channel of the older sector of the fish farm, characterised by a relatively shallow water column (~2 m) and Hg concentrations in sediments ranging between 2.15 and 5.10 mg kg^{-1} (Petranich et al., 2018b).
The Bay of Piran is a semi-enclosed area located in the southern part of the Gulf of Trieste, close to the border between Slovenia and Croatia (Fig. 1), and covers an area of approximately 19 km^2. It is a typical marine area with a maximum depth of ~15 m, influenced by the irregular supply of freshwater from the Dragonja River to its inner sector, with an average discharge of 4 m^3 s^{-1} (Cozzi et al., 2012; Ogorelec et al., 1991; Pavoni et al., 2020). Thanks to the limited Hg supplies from the northern part of the Gulf, the concentrations of this metal reported for sediments of the bay are relatively low (<0.5 mg kg^{-1}, Covelli et al., 2001; Faganeli et al., 1991). Measurements at this site (PR) were performed in the northern part of the bay near the local Marine Biology Station.
The climate of the area can be defined as oceanic mesotemperate (Pesaresi et al., 2014) with relatively warm temperatures throughout the entire year with occasional droughts in summer. Sea breezes blowing from the north-east during the night and morning (2-3 m s^{-1}) and from the sea in the afternoon (3-4 m s^{-1}) strongly affect the temperature regime (ARPAFVG-OSMER, 2014) together with the occurrence of a strong north-easterly Bora wind, mostly during winter (Boldrin et al., 2009). The highest water temperatures are observed in July, reaching values above 30°C inside the lagoon (Ferrarin et al., 2010).

2.2 Sampling strategy

Three distinct sampling campaigns to determine Hg^0 fluxes at the water-air interface were performed for both sites during the period of the year characterised by higher UV irradiation and temperature, which may favour the gaseous exchanges of Hg between the aquatic and atmospheric compartment (Cizdziel et al., 2019; Ferrara et al., 2000; Nerentorp Mastromonaco et al., 2017). More specifically, measurements were performed during late spring (VN: May 2022; PR: June 2021), summer (VN: August 2020; PR: August 2019) and autumn (VN: November 2020, PR: November 2021), whereas no measurements were carried out in winter due to logistical difficulties; however, previously published data report that Hg^0 emission during the winter period in these sites might be relatively low compared to those observed in other seasons (Floreani et al., 2019). The variation of Hg^0 fluxes during the entire 24h period was assessed by means of a floating flux chamber (FC), taking 11 to 14 distinct sets of measurements at regular time intervals of ~2 h during each sampling campaign. It was,

however, sometimes necessary to lengthen this time interval at the Piran site due to the relatively high wave motion observed *in situ*, a condition not suitable for the application of the adopted experimental approach (Bagnato et al., 2013; Fantozzi et al., 2007).

Continuous measurements of incident UV radiation in the wavelength band between 250 and 400 nm, recognised as the most effective in promoting Hg photoreduction (Amyot et al., 1997; Qureshi et al., 2010), were conducted using a specific sensor (SU-420, Apogee Instruments, Logan, UT, USA) installed at a height of ~2 m near sampling points in unshaded areas. The sensor has a resolution of 0.1 W m^{-2} and recorded 1 data per minute as an average of the value of the readings taken every 1 sec. Average UV intensity, corresponding exactly to the duration of every single flux measurement, was then calculated. Air temperature and relative humidity were monitored in the field through a portable thermohygrometer (HI9565, Hanna Instruments, Padova, Italy).

The main physico-chemical parameters of the surface water layer (temperature, pH, oxidation-reduction potential (ORP), conductivity, salinity, and dissolved oxygen (DO_2)) were monitored in parallel with Hg^0 flux measurements by means of a portable multiprobe meter (HI98194, Hanna Instruments, Padova, Italy).

After each flux measurement, surface water samples were collected for the determination of DOC, total dissolved Hg (THg_D), and DGM concentrations. Aliquots for the determination of DOC (V=5 mL) were filtered through pre-combusted (450°C) glass microfiber filters (Whatman GF/F, 0.8 μm pore size) and collected in glass containers, whereas mixed cellulose ester membrane filters (Millipore Millex HA, 0.45 μm pore size) were used to collect water samples for THg_D analysis (V=100 mL) in pre-conditioned borosilicate bottles, immediately oxidised through the addition of 0.5 mL of bromine chloride (BrCl). All samples were stored in the dark and transported to the laboratory, where the aliquots for THg_D were stored at 4°C, whereas aliquots for DOC determination were frozen until analysed. Finally, DGM concentrations were determined following incubation in the field of 1 L unfiltered water samples as reported hereafter.

2.3 Analytical determinations

Concentrations of DOC were determined by means of a Total Carbon Analyzer TOC-L (Shimadzu, Japan) using a high-temperature catalytic method (Sugimura and Suzuki, 1988). Instrument calibration was performed using potassium phthalate, whereas quality control was ensured by the analysis of certified surface seawater reference material (Consensus Reference Material, Hansell lab-University of Miami, Florida). The method is characterised by a precision

of < 3% expressed as %RSD.

The determination of THg_D was conducted by means of a specific detector (Mercur, Analytik Jena, Jena, Germany) after a pre-reduction of the sample with NH_2OH-HCl (30%, 0.25 mL) followed by a reduction with $SnCl_2$ 2% in HCl 4% using the cold vapour atomic fluorescence spectrometry technique (CV-AFS), in accordance with EPA Method 1631e (United States Environmental Protection Agency, 2002). Instrument calibration was performed by generating a calibration curve from NIST 3133 certified reference solution at different dilution levels. The limit of detection (LOD) and the limit of quantification (LOQ) calculated on the basis of the standard deviations of ten reagent blanks were 0.69 ng L^{-1} and 2.31 ng L^{-1}, respectively.

The method employed for DGM determination has been extensively described elsewhere (O'Driscoll et al., 2019). Briefly, the 1 L aliquots were gently transferred to a borosilicate bubbler and continuously bubbled for 15 min in a closed loop circuit under low light conditions, creating an equilibrium between aqueous DGM and Hg^0 in the headspace. This allows for the rapid extraction of DGM from the water (>90% of DGM with sparging time of 5 min (O'Driscoll et al., 2003)). The bubbler was connected with a real-time Hg^0 analyser (Lumex RA915M, Lumex Instruments, St. Petersburg, Russia) which was used to maintain the air flow through the bubbler by means of the Lumex internal pump and to record Hg^0 concentrations in the air in the headspace. The Lumex analyser is based on the atomic absorption spectrophotometry technique with Zeeman correction for background absorption and high frequency modulated light polarisation (ZAAS-HFM; Sholupov et al., 2004). The instrument allows for the determination of gaseous Hg in air in a wide range of concentrations (from 2 to 30,000 ng m^{-3}) with an accuracy of 20%. The instrument is calibrated annually by the parent company and calibration was controlled in the field by a self-checking program measuring gaseous Hg in an internal accessory cell containing a known quantity of Hg: the obtained relative deviations were always less than ±6%. DGM concentrations were calculated using the air Hg^0 concentrations at equilibrium and the dimensionless Henry's law constant in function of the temperature of the water sample (Andersson et al., 2008; O'Driscoll et al., 2019). The system was checked through blanks performed by bubbling MilliQ water, resulting in Hg^0 concentrations in air lower than the LOD of the Lumex Instrument (2 ng m^{-3}).

2.4 Hg^0 fluxes at the water-air interface

For the assessment of Hg^0 fluxes at the water-air interface, a Plexiglas floating FC coupled with the Lumex analyser was employed following the approach described by Bagnato et al. (2013). Briefly, the chamber is open at the bottom to allow the diffusion of Hg^0 from the confined sea surface and has a square base of 50x50 cm and an overall height of 80 cm. For the determination of Hg^0 fluxes, the FC was mounted on a floating board of sintered expanded polystyrene incorporated into an aluminium structure. The FC was manually lowered onto the surface of the water with the lower edges immersed 30 cm in the water in order to avoid the entry of air from outside the chamber by ensuring a tight seal with the surface of the sea (Bagnato et al., 2013). During measurements, the headspace of the chamber was constantly flushed through the Lumex internal pump at its specific constant rate of approximately 10 L min^{-1}. This rate is high enough to avoid an excessive build-up of Hg^0 concentrations in the enclosed air which can suppress the evasion from the water surface (Eckley et al., 2010; Floreani et al., 2022), and Hg^0 concentrations inside the FC were continuously recorded (1 s interval). After FC deployment, internal Hg^0 concentrations reached a steady-state within approximately 10 min, and FC was removed from the surface of the sea after each sampling. The relatively short sampling time allowed for a reduction in the influence of FC on the microenvironment near the sea surface, as long deployment times can modify ambient conditions near the surface enclosed by the chamber leading to biases in flux estimations (Eckley et al., 2010; Zhu et al., 2016).

The achieved equilibrium concentrations (C_o), corrected for the initial Hg^0 amount in air entering the chamber (C_i), were used for the calculation of fluxes (F) according to Eq. (1) (Bagnato et al., 2013; Kalinchuk et al., 2021):

$$F = \frac{(C_o - C_i)\, Q}{A} \tag{1}$$

where Q is the air flow rate through the chamber (in $m^3\ s^{-1}$) and A is the basal area of the chamber (0.25 m^2). The QA/QC protocol involved the use of blanks performed in the field by placing the chamber on a clean white polycarbonate surface which showed negligible values and internal Hg^0 concentrations close to the Lumex limit of detection (2 ng m^{-3}). Before and after each sampling campaign the chamber was cleaned with a diluted laboratory detergent and carefully rinsed several times with MilliQ water.

2.5 Statistical analysis

For statistical analysis, *R Software 4.1.3* (R Foundation for Statistical Computing, Vienna, Austria) and the *ggplot2* package (Wickham et al., 2016) were used. The normal distribution of data was assessed using the Shapiro-Wilk test. As sample data were found to be not normally distributed, the non-parametric Kendall rank correlation coefficient was used to evaluate the strength of the associations between variables. Furthermore, the non-parametric Kruskal-Wallis test (K-W) was utilised to assess the occurrence of statistically significant differences between two or more groups of independent variables. If statistically significant differences were found, Dunn's post-hoc test was performed to identify which groups of data differed.

3. Results and Discussion

A summary of data collected during the different sampling campaigns at both selected sites is depicted in Table 1. There were optimal weather conditions throughout sampling days, with only an intermittent light cloud cover during morning periods of summer sampling at VN, which did not significantly affect the incident UV radiation recorded during flux measurements, and a short rain event at 2:00 am during summer at PR.

3.1 Total dissolved mercury (THg_D)

Dissolved Hg concentrations in the surface water at VN were significantly higher (K-W, $p<0.0001$) than those observed at PR in all seasons. Overall, THg_D concentrations at VN ranged between 5.18 and 30.95 ng L^{-1} (average=13.38±6.64 ng L^{-1}, n=40): these values are within the range previously reported for this area (3.39-71.46 ng L^{-1}) (Floreani et al., 2019) and below the European Environmental Quality Standard (EQS) for Hg in surface water (70 ng L^{-1}, Directive 2008/105/CE). The highest THg_D concentrations were recorded in summer and the lowest in autumn (Fig. S1a), likely as a result of diffusive effluxes of Hg species from contaminated sediments into the water column as a function of temperature or release from the degradation of organic matter (Cossa et al., 2009; Covelli et al., 2008; Schartup et al., 2015) previously observed at this site (Petranich et al., 2018b). These effluxes may have influenced THg_D concentration in the entire water column due to shallow depth (~2 m), resulting in irregular fluctuations of THg_D during sampling periods. Conversely, THg_D concentrations at PR were less variable than those found at VN and usually < 5 ng L^{-1} (average=1.97±1.24 ng L^{-1}, n=35), with only one sample exceeding this amount (spring t0: THg_D=6.45 ng L^{-1}). At this site, no significant differences were observed between values found in the various seasons (Fig. S1b).

Table 1: Summary of data collected during the sampling campaigns at the selected sites. Data are reported as mean±SD (min-max); n.a.=not available. Wind data provided as hourly averages by Weather Forecast Regional Observatory of Friuli Venezia Giulia region (OSMER-ARPA FVG) and Slovenian Environmental Agency (ARSO) through database OMNIA (http://www.meteo.fvg.it/).

	Val Noghera (VN)			**Bay of Piran (PR)**		
	Summer (n=13)	Autumn (n=14)	Spring (n=13)	Summer (n=11)	Autumn (n=13)	Spring (n=12)
Air temp. (°C)	25.2±4.2 *(19.7-32.5)*	13.8±5.7 *(8.3-21.9)*	21.4±4.3 *(15.5-27.8)*	21.0±3.7 *(16.0-25.2)*	11.5±3.6 *(7.5-17.3)*	22.1±3.6 *(17.6-28.5)*
UV radiation (W m^{-2})	15.3±18.0 *(0.0-49.3)*	6.4±8.2 *(0.0-19.8)*	20.7±20.5 *(0.0-50.4)*	15.7±16.6 *(0.0-47.7)*	3.8±5.0 *(0.0-12.6)*	16.6±19.8 *(0.0-48.8)*
Wind speed (m s^{-1})	2.6±1.6 *(0.4-5.4)*	1.6±1.0 *(0.1-3.6)*	1.7±1.2 *(0.2-4.0)*	2.3±0.7 *(1.1-3.4)*	3.3±1.1 *(1.5-5.2)*	2.6±1.1 *(0.6-4.2)*
Water temp. (°C)	25.31±0.78 *(24.31-26.55)*	13.16±0.78 *(11.97-14.42)*	23.68±1.44 *(21.35-26.11)*	24.45±0.62 *(23.50-25.80)*	15.38±0.44 *(14.87-16.14)*	22.42±0.47 *(21.93-23.28)*
Salinity (PSU)	38.48±0.23 *(37.85-38.74)*	24.13±0.25 (23.37-24.40)	35.19±0.09 *(34.98-35.32)*	34.73±0.60 *(34.00-35.50)*	35.74±0.22 *(35.26-36.03)*	37.90±0.37 *(37.31-38.51)*
Dissolved O_2 (mg L^{-1})	5.88±1.37 *(4.15-8.32)*	7.97±0.44 *(6.93-8.41)*	6.55±1.35 *(4.01-8.38)*	5.45±0.80 *(5.08-5.90)*	8.52±0.35 *(7.55-8.93)*	6.28±0.36 *(5.72-6.92)*
DOC (mg L^{-1})	10.7±0.7 *(10.1-12.0)*	5.7±0.4 *(5.1-6.5)*	n.a.	n.a.	1.4±0.2 *(1.2-1.9)*	1.8±0.3 *(1.5-2.5)*
THg_D (ng L^{-1})	21.07±4.38 *(15.38-30.95)*	7.26±2.39 *(5.18-14.92)*	12.27±2.99 *(7.69-19.08)*	1.36±0.43 *(0.80-2.10)*	2.29±1.34 *(< 0.69- 4.31)*	2.00±1.50 *(0.91-6.45)*
DGM (pg L^{-1})	253.4±45.7 (176.9-367.3)	179.1±27.7 (126.0-224.2)	430.2±134.0 (243.5-711.3)	42.0±12.9 (28.6-68.7)	29.7±8.0 (21.8-52.6)	107.5±37.1 *(65.5-183.4)*
DGM/TDHg (%)	1.14±0.22 *(0.81-1.59)*	2.61±0.63 *(1.12-3.42)*	3.57±0.93 *(1.66-5.43)*	2.90±1.18 *(0.53-4.89)*	1.91±1.46 *(0.55-6.07)*	6.70±3.19 *(2.35-12.08)*
Hg^0 flux (ng m^{-2} h^{-1})	21.35±6.81 *(9.42-34.38)*	12.25±4.32 *(8.04-24.72)*	23.60±10.85 *(7.43-41.17)*	36.58±25.15 *(2.25-81.49)*	11.32±9.85 *(0.0-38.42)*	18.37±22.01 *(2.38-79.96)*

Moreover, a THg_D concentration of 10.40 ng L^{-1} was detected in summer in the sample collected at 07:30 am, which can be considered an outlier ($p<0.05$, Dixon Q test) and was not used for further elaboration. These concentrations are higher than the average THg_D estimated for the surface water of the Mediterranean Sea (0.17±0.05 ng L^{-1}) (Cossa et al., 2022) and are comparable to the values reported for the Gulf of Trieste (0.12-4.90 ng L^{-1}) (Faganeli et al., 2003), but are generally lower than those observable in the northern part of the Gulf near the mouth of the Isonzo River (0.46-15.4 ng L^{-1}) (Covelli et al., 2006), more affected by the riverine Hg inputs from drainage from the area around Idrija (Faganeli et al., 2003).

3.2 Dissolved gaseous mercury (DGM)

The concentrations of DGM at the fish farm site varied between 126.0 and 711.3 pg L^{-1} (average=278.5±135.1 pg L^{-1}, n=40) and were comparable to those previously reported for this site (200.3-321.5 pg L^{-1}) (O'Driscoll et al., 2019) and for the open Marano and Grado Lagoon (17.3-795.0 pg L^{-1}) (Emili et al., 2012). As expected, DGM concentrations encountered at Piran were significantly lower than those obtained at VN in every season (K-W, $p<0.0001$) and ranged between 21.8 and 183.4 pg L^{-1} (average=59.4±41.4 pg L^{-1}, n=36), in good agreement with values previously recorded in another study conducted near our sampling station (33.2-168.0 pg L^{-1}) (Kotnik et al., 2022) and within the range reported in the literature for the Gulf of Trieste (40-860 pg L^{-1}) (Andersson et al., 2007; Bratkič et al., 2013; Covelli et al., 2006; Kotnik et al., 2015).

The higher DGM concentrations found at VN are undoubtedly related to the higher degree of Hg contamination at this site, resulting in higher THg_D concentrations and the subsequent greater abundance of Hg forms available for the conversion to DGM. The weak but positive correlation observed between THg_D and DGM concentration at VN ($\tau=0.30$, $p<0.01$, n=40) may confirm a common source of these two species or that THg_D is the substrate for DGM formation (Marumoto and Imai, 2015). Conversely, no relationship between these two parameters was detected at PR likely due to the relatively constant THg_D concentrations recorded at this site. However, DGM accounted for only a relatively small portion of THgD (0.81-5.43% at VN and 0.53-12.08% at PR) in agreement with percentages reported in other studies (Cheng et al., 2019; Conaway et al., 2003; Kotnik et al., 2015; Soerensen et al., 2013; C. Wang et al., 2020) and consequently even the relatively low THgD concentrations recorded at PR did not likely represent a limiting factor for DGM production (Castelle et al., 2009). DGM concentrations found in this work are generally higher than those reported in the literature for other coastal areas subject to lower Hg supplies than the Gulf of Trieste, such as

the Tagus Estuary (13.4-40.0 pg L^{-1}) (Cesário et al., 2017a), Arcachon Bay (5-193 pg L^{-1}) (Bouchet et al., 2011), the Gironde Estuary (2-150 pg L^{-1}) (Castelle et al., 2009), and the Thau Lagoon (15.1-63.1 pg L^{-1}) (Sharif et al., 2013).

At both sites, significant differences were observed between DGM concentrations determined during the various seasons, with maximum and minimum values recorded during spring and autumn sampling, respectively (Fig. 2a, S2).

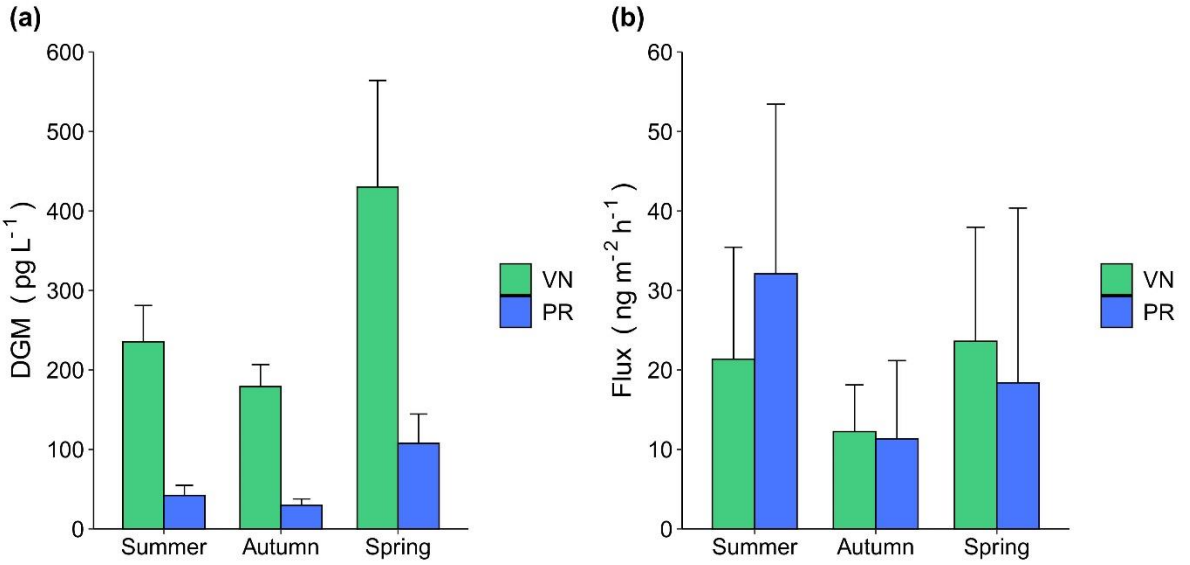

Figure 2: overall average values over the various seasons of (a) DGM concentrations and (b) Hg0 fluxes in the two selected sampling sites, Val Noghera fish farm (VN) and the Bay of Piran (PR).

It must be emphasised that spring measurements were performed late in the season and thus characterised by relatively high values of both UV radiation and water temperature, comparable to those recorded in summer (Table 1), which likely promoted higher DGM production. This hypothesis may be supported by the overall weak positive relationships found between DGM concentrations and incident UV radiation at both sites (VN: τ=0.24, $p<0.05$, n=40; PR: τ=0.40, $p<0.001$, n=36 Fig. S3). Taking into consideration data recorded during daylight hours, slightly better relationships were observed (VN: τ=0.42, $p<0.01$, n=23; PR: τ=0.42, $p<0.01$, n=20) further confirming the role of UV irradiation on DGM production. Many studies observed the occurrence of highest seasonal DGM concentration during period of high insolation and temperatures, promoting both photochemical and biotic reduction (Baeyens and Leermakers, 1998; Ci et al., 2011; Rolfhus and Fitzgerald, 2001; Wang et al., 2016; C. Wang et al., 2020). It is widely accepted that photoreduction is a key process in the formation of DGM in surface waters (Ci et al., 2016; Costa and Liss, 1999; Lanzillotta et al., 2002; Soerensen et al., 2013) and that UV radiation wavelengths are the most effective in promoting this reaction (Amyot et al., 1997; Lee et al., 2019). Various mechanisms have been proposed for the photochemical

reduction of Hg^{2+}, including direct photolysis and secondary photochemical processes mediated by photo-produced reducing agents (e.g. oxygen radical species) or by ligand-metal charge transfer in Hg-DOM complexes (Luo et al., 2020).

The interaction between Hg and DOM plays a key role in the activation of photochemical Hg^{2+} reduction, as a relevant fraction of the photoreducible Hg^{2+} present in the water column could be associated with functional groups of DOM in weakly bound complexes (O'Driscoll et al., 2018; Zheng and Hintelmann, 2009): if it is rich in chromophoric groups, DOM can absorb incident radiation and transfer its energy to adsorbed Hg^{2+}, favouring its reduction (Costa and Liss, 1999; Fantozzi et al., 2013, 2007). As a result, an increase in DOM concentration can promote the photo-induced formation of DGM, especially at low THg_D/DOC ratios (Z. Wang et al., 2020) such as those observed in this study and confirmed by the positive relationships found between DOC and DGM concentrations both at VN and PR (VN: τ=0.44, $p<0.01$, n=27, n=; PR: τ=0.37, $p<0.05$, n=25, Fig. S3). However, modification of DOM related to photobleaching might reduce this effect over time as a result of a progressive increase in the relative abundance of thiol functional groups and of the proportion of Hg^{2+} strongly bound to these sites, less available to photoreduction (Luo et al., 2020). This may help explain the seasonal trend in DGM concentration progressively decreasing from late spring to late autumn particularly at site VN, characterised by higher DOC concentrations in the water (Tab. 1) likely because of OM degradation, efflux from sediments and the excretion of photosynthetases (Petranich et al., 2018a). This is in agreement with a progressive decrease in Hg^{2+} photoreduction rates due to a progressive DOM photobleaching, as observed in other studies (Amyot et al., 2004; Costa and Liss, 1999; O'Driscoll et al., 2022). Moreover, the strong mineralisation of organic matter occurring at this site (Petranich et al., 2018a) may also have contributed to enhance the reducible pool of Hg^{2+} in water (Schartup et al., 2015; Živković et al., 2022). The occurrence of strong OM mineralisation in the fish farm (VN) was likely confirmed by trends of DO_2 concentrations, characterised by a progressive decrease during the afternoon and night until reaching moderate hypoxic conditions ($DO_2 < 5$ mg L^{-1}) in the early morning likely as a result of high oxygen consumption coupled with the low hydrodynamics typical of this site (De Vittor et al., 2012; Petranich et al., 2018a). This diurnal pattern was more evident during summer and spring measurements, whereas in autumn higher and less variable DO_2 concentrations were observed coupled with relatively lower DOC concentrations. Considering the PR site, a recent study (Bratkič et al., 2018) found a peak in photochemical reduction during spring in the nearby waters of the Gulf of Trieste, which may explain the high spring DGM concentrations recorded in our work. A second peak in Hg^{2+} reduction was

identified in autumn and related to phytoplankton (diatomaceous) bloom and associated bacterial taxa which contain known Hg reducers such as *Rhodobacteraceaea* and *Gammaproteobacteria*; this autumn Hg^{2+} reduction peak may potentially explain the relatively high DGM observed in our study in November, only slightly lower than those found in summer (Fig. S2b). The overall positive relationship found in this study between DGM concentrations and water temperature can further support a link between DGM production and biological activity, whose rates are strongly related to temperature (Ahn et al., 2010; Chen et al., 2020). Microorganisms can contribute to DGM formation through both direct Hg^{2+} reduction and the excretion of exudates able to reduce Hg^{2+}, sometimes after light activation (Lanzillotta et al., 2004; Liang et al., 2022; Mason et al., 1995; Wu and Wang, 2014). Even though the relative importance of these two pathways is still poorly understood (Grégoire and Poulain, 2014; Liang et al., 2022), recent findings indicate that biotic mediated Hg^{2+} reduction with or without light account for a relevant fraction of DGM production in water (Kuss et al., 2015). Direct biotic Hg^{2+} reduction can occur even in the absence of light throughout the whole day and water column, consequently representing an important pathway for DGM production in bottom water layers and sediments (Fantozzi et al., 2009; Lepak et al., 2021; Poulain et al., 2004). This process is mainly catalysed by mercury reductase enzyme present in the cytoplasm of Hg-resistant bacteria as a result of the expression of *mer* operon (Barkay et al., 2003). Considering the high Hg concentrations found at VN, the possible presence of Hg-resistant bacteria able to reduce Hg^{2+}, previously documented for the nearby sediments of the Marano and Grado Lagoon (Baldi et al., 2012), could potentially explain the diurnal trend observed for DGM at this site, characterised in all seasons by DGM values during the night which were comparable to those observed during day (Fig. 3, S4a).

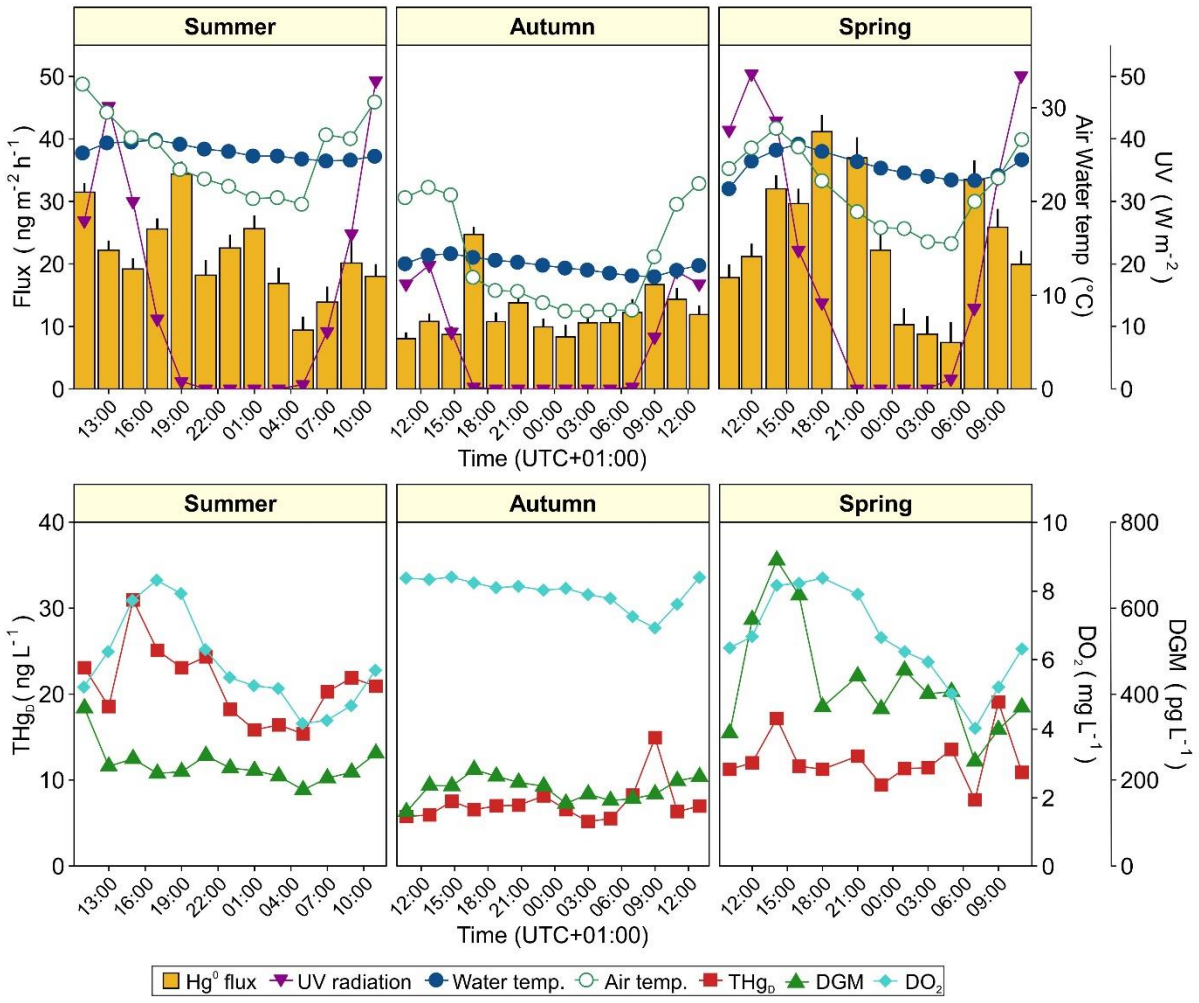

Figure 3: diurnal patterns of Hg^0 fluxes, UV radiation, water and air temperatures, THg_D, DGM, and dissolved oxygen (DO_2) concentrations in the different seasons at Val Noghera fish farm (VN).

The positive relationship between DGM concentration and water temperature found at this site (Fig. S3) may further confirm this hypothesis since temperature represents the primary control on Hg^{2+} dark reduction (Lamborg et al., 2021). However, it cannot be excluded that these relatively high nocturnal DGM concentrations are related to other processes, such as dark abiotic reduction mediated by organic matter (e.g. humic substances) or demethylation. Humic substances can directly reduce Hg^{2+} in the absence of light thanks to the interaction with reducing intermediates such as quinones (Allard and Arsenie, 1991; O'Driscoll et al., 2004; Vudamala et al., 2017), and this effect may have been favoured by the relative high DOC concentration observed at VN (Tab. 1). Moreover, previous studies have indicated that both reductive and oxidative demethylation could occur in VN sediments (Petranich et al., 2018b) producing either Hg^0 or Hg^{2+} available for reduction. Finally, effluxes from anoxic sediments due to the dissolution of Hg adsorbent compounds such as iron or manganese hydroxides are also possible (Bouffard and Amyot, 2009), considering the shallow depth (~2 m) of the water

column at this site. Sediment benthic fluxes may have influenced also the amount of Hg^{2+} in the water column available for reduction as Hg can be released from sediments both in Hg^{2+} or Hg^0 form (Acquavita et al., 2021). However, it should be noted that during the day DGM concentrations at VN roughly followed the pattern of UV radiation with a slight delay, confirming the previous observations made at this site (O'Driscoll et al., 2019) and indicating that under light conditions, the formation of DGM in the water column may be largely related to photo-induced processes. A better agreement between UV radiation and DGM variation was observed at the Bay of Piran (PR), with peak DGM concentrations observed in the central part of the day in all seasons and lower and relatively constant concentrations during the night (Fig. 4, S4b), with minimum values recorded between 4 and 6 am.

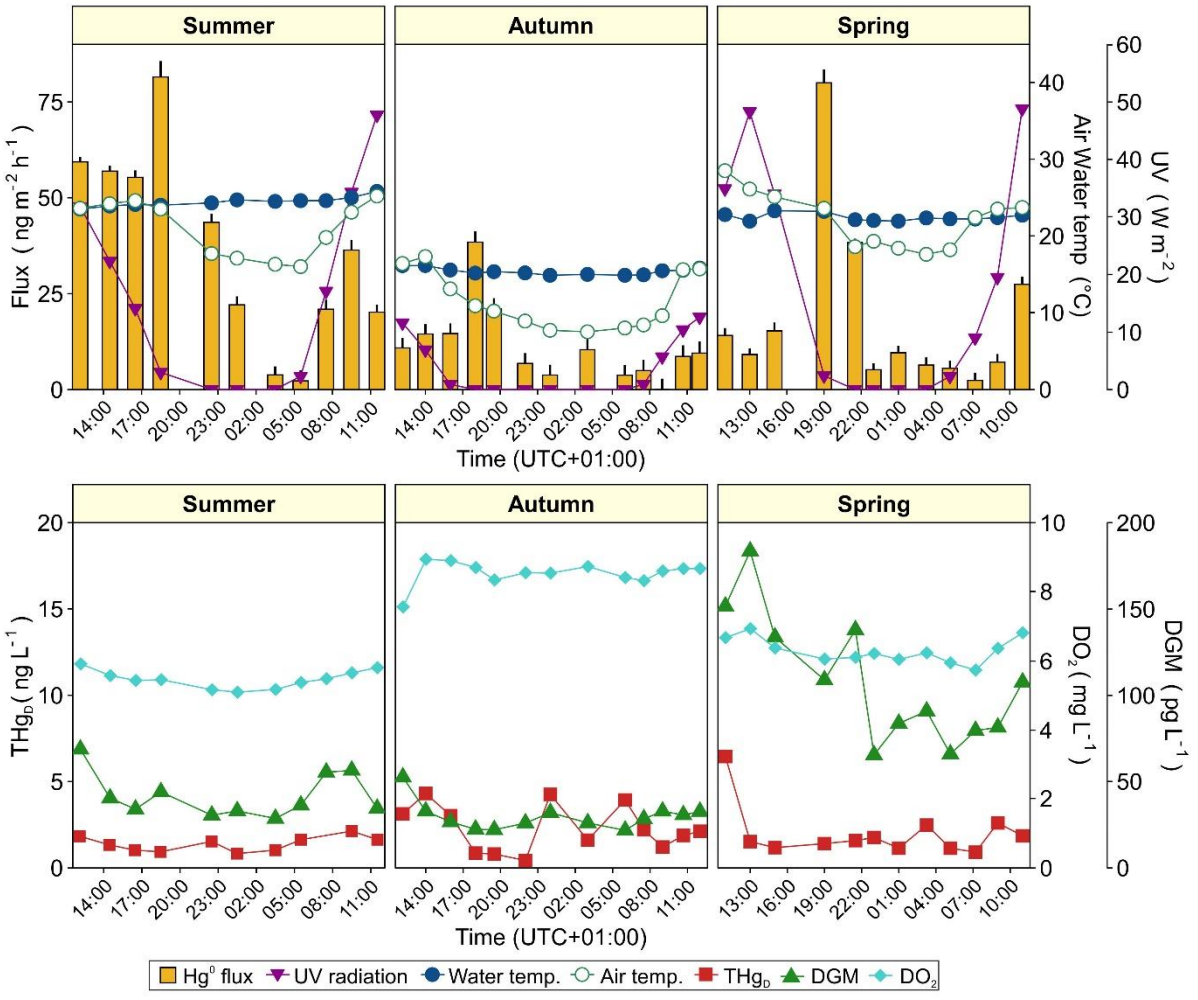

Figure 4: diurnal patterns of Hg^0 fluxes, UV radiation, water and air temperatures, THg_D, DGM, and dissolved oxygen (DO_2) concentrations in the different seasons at the Bay of Piran (PR). Note differences in scale on the y-axis compared to the VN sampling station in Fig. 3.

These results further confirm the relevance of photochemical processes at this site. However, considering the higher hydrodynamics observed at PR compared to VN, it cannot be excluded that the irregular variability of DGM concentrations observed during the sampling periods could also be related to supplies from outside the bay (Kotnik et al., 2022), which can recharge or deplete the pool of volatile Hg available for evasion into the atmosphere.

3.3 Hg^0 fluxes at the water-air interface

The Hg^0 fluxes recorded at the Val Noghera (VN) fish farm during this study varied between 7.43 and 41.17 ng m^{-2} h^{-1}, with an overall average of 18.90±9.05 ng m^{-2} h^{-1} (n=40), whereas at Piran (PR) Hg^0 emission showed a greater variability, ranging between 0 and 81.49 ng m^{-2} h^{-1} with an overall average of 21.39±21.90 ng m^{-2} h^{-1} (n=36). Considering the significantly higher DGM concentrations observed at VN than at PR, the comparable and in some cases slightly higher fluxes calculated for this latter site were unexpected. This discrepancy may be explained by the different hydrodynamism of the selected sites. The PR site was located in an open coastal area subject to marked water turbulence due to waves and tides which could have favoured the release of Hg^0 at the water-air interface extending the surface boundary layer (Ferrara et al., 2000; Zappa et al., 2003). This enhancement is effective mostly when surface water is super-saturated in DGM with respect to the atmosphere (Castelle et al., 2009) which is likely what occurred in this study taking into consideration both the measured DGM concentrations and the low atmospheric Hg concentrations usually occurring at this site (Floreani et al., 2019). Under these circumstances, gaseous exchanges can be more regulated by turbulent mixing conditions rather than the concentration gradient between the water and air (Lindberg and Meyers, 1995; Poissant et al., 2000). Moreover, spikes of high Hg^0 emission at PR (81.49 ng m^{-2} h^{-1} at 6:30 pm in summer and 79.96 ng m^{-2} h^{-1} at 7:00 pm in spring) were recorded in parallel with increased wave motion observed in the field despite the low UV irradiation with the subsequent photo-production of DGM and the alteration of micro-environmental conditions caused by placing the FC, which should diminish the influence of turbulence (Bagnato et al., 2013). This hypothesis could be confirmed by the relative good agreement between temporal patterns of Hg^0 fluxes and surface current speeds recorded by oceanographic buoy Vida, located offshore near our sampling site (Bratkič et al., 2018) particularly in summer (Fig. 5). However, high current speeds not always resulted in increases in Hg^0 fluxes, as observed e.g. for the last measure in summer. This could be explained by a different current direction which could have favoured a lower supply of Hg to our sampling site, as confirmed by the observed contemporary decrease in DGM concentration. Moreover, in spring the peak of Hg^0 emission

corresponded with an increase in wave height, but the same effect was not observable in summer likely due to a lower availability of DGM. Unfortunately, oceanographic data are not available for the autumn campaign.

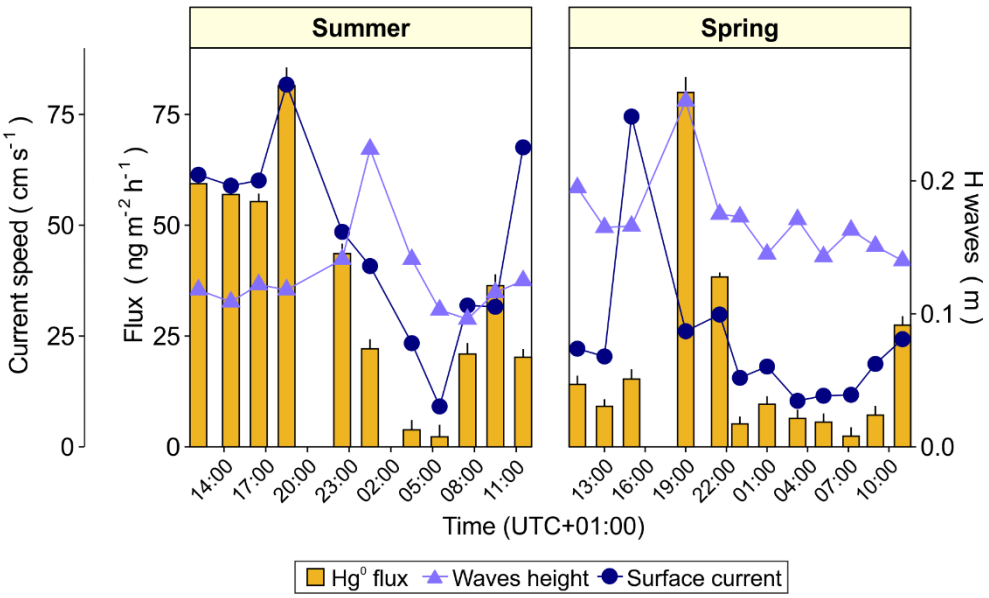

Figure 5: diurnal patterns of Hg^0 fluxes recorded at Bay of Piran in summer and spring and of surface current speeds and wave heights recorded at nearby oceanographic buoy Vida of Marine Biology Station of Piran.

Conversely, VN site in the confined environment of the fish farm was characterised by extremely scarce water movement and the occurrence of stable surface layer conditions may have strongly limited Hg^0 emissions (Osterwalder et al., 2021).

The calculated fluxes are in good agreement with the estimated Hg^0 emission rate for the Northern Adriatic Sea (28.4±4.7 ng m^{-2} h^{-1}) (Andersson et al., 2007) and by far exceed the estimated annual atmospheric depositions of Hg in this area (1.98-3.25 ng m^{-2} h^{-1}) (Tomažič et al., 2018) or in nearby inland area of Iskrba (SLO) (wet deposition=0.34-1.14 ng m^{-2} h^{-1}) (Sprovieri et al., 2017), confirming that these environments may represent a source of Hg for nearby coastal environments under favourable wind conditions (Barago et al., 2020; Wängberg et al., 2008). For example, Hg concentrations detected in lichens collected over the entire Marano and Grado Lagoon (Floreani et al., 2020) roughly followed the same spatial pattern of Hg contamination in sediments, further confirming that Hg^0 evasion from the substrate can heavily impact the atmospheric level of this metal over our study area. Generally, Hg^0 fluxes recorded in our study were comparable to those estimated for other coastal environments and marginal seas surrounded by notable anthropogenic sources of Hg (e.g. Augusta Bay, Italy; San Francisco Bay, USA; Minamata Bay, Japan; Yellow Sea, China; Tab. 2), highlighting the importance of the discharges of this metal from past human activities in promoting the

occurrence of high DGM concentrations in surface water and its subsequent release into the atmosphere. Moreover, fluxes calculated in this study are higher than those commonly reported for offshore areas (Tab. 2), where Hg amounts involved in exchanges between environmental compartments are generally lower than coastal areas due to lower supplies of this metal from river transport and/or direct anthropogenic discharges (Amos et al., 2014; Fitzgerald et al., 2007; Marumoto and Imai, 2015). However, it must be stressed that comparison among Hg fluxes reported in different studies should be interpreted with great caution as a standard protocol for measurements does not yet exist (Eckley et al., 2010; Sommar et al., 2020). Hg^0 fluxes at the water-air interface can be directly evaluated through the use of FCs or computed through several gas-exchange models. In the first case, differences in size, shape, and turnover time of air inside the chamber could significantly affect the calculated flux value (Eckley et al., 2010; Zhu et al., 2015) whereas the choice of gas-exchange model could lead to different Hg^0 flux estimations due to different parametrisation of Hg transfer velocities from water (Nerentorp Mastromonaco et al., 2017; Osterwalder et al., 2021; Sharif et al., 2013).

The same experimental approach used in the present study was previously adopted in a preliminary investigation of Hg^0 fluxes at the water-air interface in different coastal areas of the northern Adriatic Sea (Floreani et al., 2019). Two of the sites investigated in the cited study correspond to those selected in this work and generally showed higher emissions likely due to the fact that measurements were performed only during the diurnal period when a greater DGM formation is expected, as partially confirmed by our results. Even though DGM was not measured in the cited study, the higher THg_D concentrations recorded in particular at VN also suggest a greater abundance of substrate available for the reduction of Hg^{2+} to DGM and its subsequent release to the atmosphere. Moreover, our results are comparable to fluxes previously measured with the same experimental approach in freshwater environments upstream from our study area, the Solkan Reservoir along the Isonzo River (21.88±11.55 ng m^{-2} h^{-1}) and the dockyard of the Torviscosa chlor-alkali plant (19.01±12.65 ng m^{-2} h^{-1}) (Floreani et al., 2022), impacted by the same contamination sources responsible for Hg inputs into the Gulf of Trieste and the Marano and Grado Lagoon.

Table 2: Comparison of Hg^0 fluxes obtained in this study and over various other coastal and open sea environments. n.a. = not available, FC = flux chamber, MM = micrometeorological model.

Site	Hg^0 flux (ng m^{-2} h^{-1})		Method	Reference
	av±std	Min-Max		
Coastal sites				
Val Noghera	18.90±9.05	7.43-41.17	FC	This study
Piran Bay	21.39±21.90	0-81.49	FC	This study
Val Noghera	35.6±12.6	16.4-64.0	FC	(Floreani et al., 2019)
Piran Bay	32.2±16.6	6.0 - 68.0	FC	(Floreani et al., 2019)
Gulf of Trieste	5.13±n.a.	n.a.	MM	(Kotnik et al., 2022)
N Adriatic	28.4±4.7	23.7-33.2	MM	(Andersson et al., 2007)
Augusta Bay	23.1±24	3.2-72.1	FC	(Bagnato et al., 2013)
Tyrrhenian Sea (near CAP)	n.a.	8.2-44	FC	(Ferrara and Mazzolai, 1998)
Sardinia coast	3.61±0.98	2.36-4.75	FC	(Gårdfeldt et al., 2003)
Arcachon Bay	4.3±n.a.	0.4-14.5	MM	(Bouchet et al., 2011)
Minamata Bay	5.4±6.3	0.1-33	MM	(Marumoto and Imai, 2015)
Tokyo Bay	5.8±5.0	0.1-22.1	MM	(Narukawa et al., 2006)
Jiaozhou bay	0.67±n.a.	-0.15-2.21	FC	(Xu et al., 2012)
Bohai Sea	0.8±1.5	-6.1-12.8	MM	(C. Wang et al., 2020)
Swedish coastal area	0.61±n.a.	-0.61-8.8	FC	(Gårdfeldt et al., 2001)
Long Island Sound	0.7±0.5	0.1-10.3	MM	(Rolfhus and Fitzgerald, 2001)
San Francisco Bay	n.a.	2.5-46.0	MM	(Conaway et al., 2003)
Offshore marginal seas				
Western Mediterranean Sea	4.5±5.1	-5.6-33.8	MM	(Nerentorp Mastromonaco et al., 2017)
Eastern Mediterranean Sea	2.2±1.5	0.2-4.9	MM	(Fantozzi et al., 2013)
Baltic Sea	1.3±1.6	-0.13-1.87	MM	(Kuss et al., 2018)
North Sea	6.2±5.3	0.5-19.9	MM	(Baeyens and Leermakers, 1998)
South China Sea	4.5±3.4	0.2-15.3	MM	(Fu et al., 2010)
East China Sea	4.1±3.2	0.2-14.8	MM	(Wang et al., 2016)
Yellow Sea	18.3±11.8	3.2-44.0	MM	(Ci et al., 2011)
Western Pacific marginal seas	1.7±0.6	0.6-2.5	FC	(Kalinchuk, 2023)
Eastern Arctic Seas	0.67±0.13	0.28-1.35	FC	(Kalinchuk et al., 2021)
Open ocean				
Arctic Ocean	0.65±0.19	0.33-0.82	FC	(Kalinchuk et al., 2021)
Atlantic Ocean	n.a.	2.1-6.8	MM	(Soerensen et al., 2013)
Eastern North Atlantic Ocean	0.6±0.7	n.a.	MM	(Mason et al., 2017)
Western North Atlantic Ocean	1.2±1.6	n.a.	MM	(Mason et al., 2017)
Pacific Ocean	n.a.	0.7-8.7	MM	(Soerensen et al., 2014)
South Pacific Ocean	0.7±0.6	n.a.	MM	(Mason et al., 2017)

Considering the seasonal variation, no significant difference between Hg^0 fluxes at the two selected sites was detected in any season (Fig. 2b, S5). At VN, the highest Hg^0 fluxes were observed in spring and the lowest in autumn following the same pattern of DGM concentrations (Fig. 2). The positive relationship observed between DGM concentration and Hg^0 fluxes at this site (τ=0.43, p<0.001, n=40, Fig. 6) further confirms the importance of the availability of the volatile Hg^0 to support relevant emissions into the atmosphere (Baeyens and Leermakers, 1998; Kalinchuk et al., 2021; Osterwalder et al., 2021).

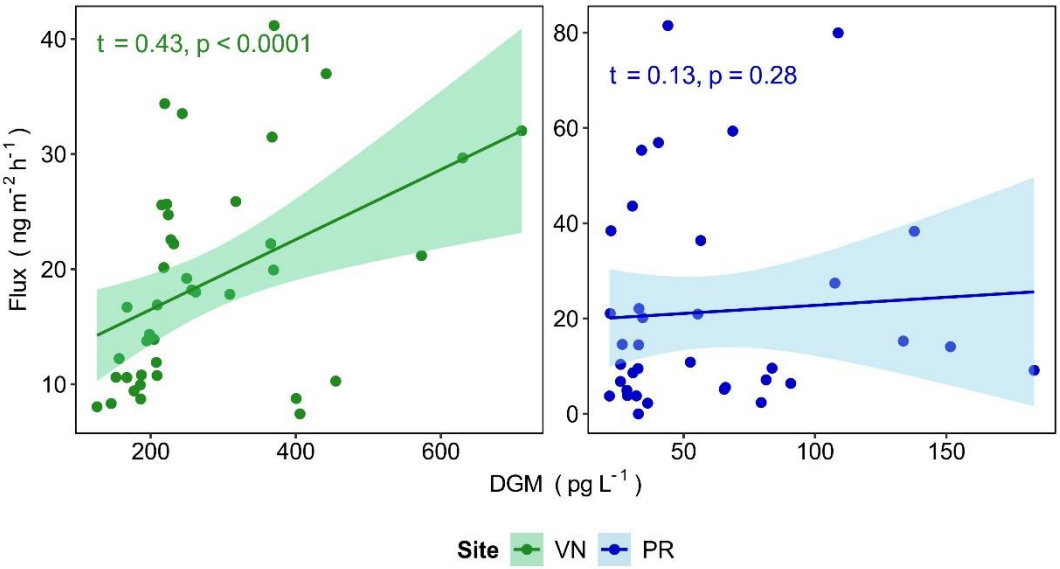

Figure 6: overall correlation between DGM concentrations and Hg^0 fluxes at the selected sampling sites, Val Noghera fish farm (VN) and the Bay of Piran (PR). Kendall's rank correlation coefficient (τ) and 95% confidence intervals are reported.

However, Hg^0 fluxes calculated for the spring were comparable to those observed in summer despite the significantly lower DGM concentrations found in this last period (Fig. S3a, S5a). A potential explanation for this trend lies in the lower water temperatures recorded during spring compared to summer, which may have limited gaseous evasion due to lower diffusivity and the higher solubility of DGM under these conditions (Andersson et al., 2008; Kuss et al., 2009; Sanemasa, 1975). Indeed, an overall positive relationship between fluxes and water temperature at VN (τ=0.39, p<0.001, n=40, Fig. S6) was observed, confirming that this parameter plays a key role in controlling the magnitude of Hg^0 evasion into the atmosphere, as observed in numerous studies (Bouchet et al., 2011; Chen et al., 2020; Kalinchuk, 2023; Kalinchuk et al., 2021; Poissant et al., 2000; Soerensen et al., 2013; C. Wang et al., 2020). An overall weak positive relationship between Hg^0 fluxes and surface water temperatures was also found at PR (τ=0.29, p<0.01, n=36, Fig. S6). In this case, as also seen at VN, higher water

temperatures in summer could help explain the different seasonal variation between DGM concentration and Hg^0 fluxes. Indeed, the lowest average emission was observed in autumn and the highest in summer despite DGM concentrations lower than those observed in spring (Fig. 2), even though, as stated above, fluxes at this site may have been deeply influenced by water turbulence.

At the fish farm, Hg^0 fluxes could also have been limited by the competition of the evasion process with the re-oxidation of DGM to non-volatile Hg^{2+}, which can occur at the same time as the reduction under sunlight, mainly due to photochemical reactions leading to the production of oxidants such as single oxygen or hydroxyl or carbonate radicals (Garcia et al., 2005; He et al., 2014; Luo et al., 2020). Moreover, oxidation rates can be significantly enhanced with increasing salinity, even in the absence of light (Ci et al., 2016; Lalonde et al., 2001) thanks to the presence of halides (e.g. Cl^-, Br^-) which can react with hydroxyl radical to form additional oxidants (Whalin et al., 2007) or stabilise Hg oxidation products through the formation of non-photoreducible complexes (Qureshi et al., 2010; Yamamoto, 1996). Previous studies have indicated that losses of DGM through photo-oxidation in saltwater can be dominant compared to volatilisation (Ci et al., 2016; Lalonde et al., 2004). An increase in DGM oxidation rates and decrease in volatilisation can increase the amount of Hg retained in the water column, mostly in static water environments such as the fish farm (VN), whereas in more dynamic conditions, such as those encountered at PR, most of the produced DGM can be readily lost to the atmosphere (Clarke et al., 2023; Zhang et al., 2021). In addition, considering the high DOC concentrations observed in this site, a potential contribution of direct adsorption of DGM on functional groups of OM in reducing the amounts available for volatilisation cannot be ruled out, as previous studies indicate that a relevant fraction of elemental Hg can occur in this phase in natural waters (Wang et al., 2015). Finally, during spring sampling at VN, a notable macrophyte bloom was observed in the field, coupled with the formation of a transparent biological film on the surface of the water, which may have further limited the diffusion of Hg^0 into the atmosphere (Osterwalder et al., 2021). All these aspects could lead to a longer residence time of Hg in the water column, potentially resulting in its greater availability for methylation after oxidation, even in microenvironments in oxic water layers such as periphyton, roots of macrophytes, and settling particles, and in a favoured incorporation into the trophic web (Branfireun et al., 2020; Colombo et al., 2013; Cossa et al., 2009; Jung et al., 2022; Zhang et al., 2021). This aspect may be a great concern in this environment due to the frequent occurrence of environmental conditions favourable for Hg methylation such as reduced DO_2 levels (Petranich et al., 2018b). Moreover, Hg^0 may also be directly subject to

biotic or abiotic methylation (Gonzalez-Raymat et al., 2017; Yin et al., 2014) mostly in the presence of halogens and under conditions of strong solar irradiation (Castro et al., 2011) like those which occurred in this study in spring, coupled with relatively low volatilisation, but it is still unclear if these reactions occur under environmental conditions (Gonzalez-Raymat et al., 2017). This may be cause for concern for the health of aquatic ecosystem and should be further investigated in future also taking into consideration potential demethylation processes favoured by incident UV radiation (Klapstein and O'Driscoll, 2018).

Considering the diurnal variability of Hg^0 fluxes (Fig. 3-4), positive values were calculated for all measurements at both sites except for PR at 7:30 am in autumn with night-time fluxes generally slightly lower than those observed during the day (Fig. 7), indicating a constant super-saturation in DGM in the surface waters (Nerentorp Mastromonaco et al., 2017; Wang et al., 2016) supported by the efficient above-described DGM production or transport processes even in the absence of light. This applies especially to the fish farm site (VN), whereas at PR slightly higher differences between day and night Hg^0 fluxes were generally observed likely confirming a greater importance of photochemical processes as already observed for DGM. Interestingly, the peak Hg^0 fluxes at VN were always recorded at sunset, corresponding to the inversion of the temperature gradient between the air and water, which may have influenced the transfer velocity of DGM between these two compartments (Poissant et al., 2000; Vette et al., 2002). Generally, at both sites, fluxes gradually decreased during the night, reaching the minimum before sunrise followed by a relatively sharp increase in the morning, roughly following a temporal pattern similar to that observed for DGM concentrations, confirming that factors influencing DGM formation also impact gaseous evasion at the water-air interface (Cesário et al., 2017b).

However, some differences between temporal patterns of DGM and fluxes were observed: fluxes at VN generally showed a decrease from late morning to afternoon coupled with increasing DGM concentration, whereas at PR, the progressive reduction of fluxes during the night was accompanied by relatively constant DGM values. These findings suggest that evasion is more regulated by physical parameters influencing air-sea gaseous exchanges rather than DGM concentrations alone (Lindberg and Zhang, 2000), as confirmed by the weak relationship between these two parameters at PR (Fig. 6), and that DGM supplies in these sites can easily overcome losses through volatilisation.

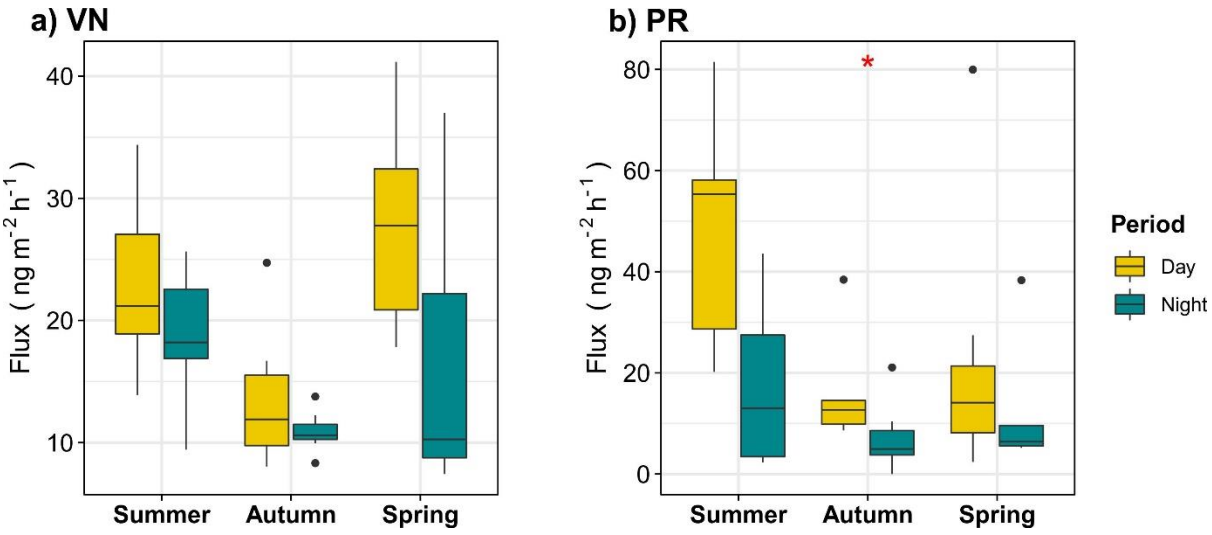

Figure 7: distribution of Hg^0 fluxes recorded during day and night at the two sites, Val Noghera fish farm (VN) and the Bay of Piran (PR). Note the difference in Y-axis scale.

4. Conclusions

A significant production of DGM was observed in this study at the Val Noghera (VN) fish farm, likely as a result of the combination of photoreduction of Hg^{2+} during the day and abiotic and biotic reduction reactions during night and day, which can occur both in shallow water and in contaminated sediments. The comparable DGM concentrations observed during night and day may confirm the importance of processes leading to DGM production in the absence of solar radiation at this site. Moreover, strong mineralisation of abundant OM present at this site could have further contributed to increase the amount of Hg^{2+} available for reduction reactions. Lower THg_D and DGM concentrations were observed at PR, confirming the lower degree of contamination of this part of the Gulf of Trieste. The highest average DGM concentrations at both sites were observed during spring and the lowest in autumn following the same temporal pattern of UV radiation: this suggests that photoreduction likely represented the dominant DGM production pathway.

Relatively high Hg^0 fluxes were recorded at both sites, highlighting that the contaminated coastal area of the northern Adriatic Sea can potentially represent a secondary source of Hg into the atmosphere. Generally, higher Hg^0 fluxes were observed in summer likely due to higher water temperatures which decrease DGM solubility. Moreover, positive fluxes were observed during all sampling periods, thus suggesting a continuous supply of DGM even during the night, which would be able to replace DGM lost through volatilisation. Temporal patterns of Hg^0 fluxes only partially corresponded to those of DGM concentrations, confirming that gaseous exchanges are the result of a complex site-specific interaction between many

physico-chemical factors. However, despite the significantly high DGM concentration observed at the fish farm, Hg^0 fluxes were comparable to those calculated for the Bay of Piran. This unexpected result may be explained by the different hydrodynamism of the water column at the selected sites: the high water turbulence observed at PR likely promoted a higher rate of Hg^0 emission, whereas water stagnation at VN may have strongly limited gaseous exchanges at this site together with expected high Hg oxidation rates in static saltwater environments, likely favouring the higher retention of Hg in the water column. Therefore, these results suggest that enhancing water turbulence in confined coastal marine environments could represent a simple mitigation action to increase the amount of Hg lost by the system through volatilisation, thereby reducing the burden available for methylation and incorporation into food webs. Therefore, Hg^0 fluxes should be accurately monitored in this kind of environment which is particularly vulnerable to Hg contamination, as understanding the entity and dynamics of this phenomenon under various conditions could be helpful to assess the ability of these ecosystems to recover from historical and/or contemporary supplies of this metal related to anthropogenic activities.

Further research is needed to verify this hypothesis, e.g. coupling Hg^0 fluxes and MeHg concentration measurements at the fish farm under different hydrodynamic conditions. On the other hand, considering the shallow water depth and the methylation potential observed at VN (Petranich et al., 2018b), evasion of gaseous DMeHg cannot be excluded and should be evaluated as it can represent a source of organic Hg for coastal terrestrial environments (Coale et al., 2018).

Acknowledgements

This work is part of the Ph.D. thesis written by Federico Floreani at the University of Trieste; the Ph.D. fellowship was funded by PO FRIULI VENEZIA GIULIA-FONDO SOCIALE EUROPEO 2014/2020. The authors are very grateful to Alessandro Acquavita for his valuable technical assistance during sampling operations and his useful suggestions. A special thanks to Claudio Furlanut, Marco Cambi and the entire staff at Val Noghera Fish Farm for their fundamental logistical support and kind hospitality at the fish farm during field work. Thanks also to Elisa Petranich and to students Gabriele Faoro and Federico Vito Zotta for their support in sampling operations. We acknowledge Katja Klun for providing DOC analysis. OSMER-ARPA FVG and ARSO are acknowledged for providing the meteorological wind data. We warmly thank Karry Close for proofreading the manuscript.

References

Acquavita, A., Aleffi, I.F., Benci, C., Bettoso, N., Crevatin, E., Milani, L., Tamberlich, F., Toniatti, L., Barbieri, P., Licen, S., Mattassi, G., 2015. Annual characterization of the nutrients and trophic state in a Mediterranean coastal lagoon: The Marano and Grado Lagoon (northern Adriatic Sea). Reg. Stud. Mar. Sci. 2, 132–144. https://doi.org/10.1016/j.rsma.2015.08.017

Acquavita, A., Covelli, S., Emili, A., Berto, D., Faganeli, J., Giani, M., Horvat, M., Koron, N.Ž., Rampazzo, F., 2012. Mercury in the sediments of the Marano and Grado Lagoon (northern Adriatic Sea): Sources, distribution and speciation. Estuar. Coast. Shelf Sci. 113, 20–31. https://doi.org/10.1016/j.ecss.2012.02.012

Acquavita, A., Floreani, F., Covelli, S., 2021. Occurrence and speciation of arsenic and mercury in alluvial and coastal sediments. Curr. Opin. Environ. Sci. Heal. 22, 100272. https://doi.org/10.1016/j.coesh.2021.100272

Ahn, M.C., Kim, B., Holsen, T.M., Yi, S.M., Han, Y.J., 2010. Factors influencing concentrations of dissolved gaseous mercury (DGM) and total mercury (TM) in an artificial reservoir. Environ. Pollut. 158, 347–355. https://doi.org/10.1016/j.envpol.2009.08.036

Allard, B., Arsenie, I., 1991. Abiotic reduction of mercury by humic substances in aquatic system - an important process for the mercury cycle. Water, Air, Soil Pollut. 56, 457–464. https://doi.org/10.1007/BF00342291

Amos, H.M., Jacob, D.J., Kocman, D., Horowitz, H.M., Zhang, Y., Dutkiewicz, S., Horvat, M., Corbitt, E.S., Krabbenhoft, D.P., Sunderland, E.M., 2014. Global biogeochemical implications of mercury discharges from rivers and sediment burial. Environ. Sci. Technol. 48, 9514–9522. https://doi.org/10.1021/es502134t

Amyot, M., Gill, G.A., Morel, F.M.M., 1997. Production and loss of dissolved gaseous mercury in coastal seawater. Environ. Sci. Technol. 31, 3606–3611. https://doi.org/10.1021/es9703685

Amyot, M., Southworth, G., Lindberg, S.E., Hintelmann, H., Lalonde, J.D., Ogrinc, N., Poulain, A.J., Sandilands, K.A., 2004. Formation and evasion of dissolved gaseous mercury in large enclosures amended with 200HgCl2. Atmos. Environ. 38, 4279–4289. https://doi.org/10.1016/j.atmosenv.2004.05.002

Andersson, M.E., Gårdfeldt, K., Wängberg, I., Sprovieri, F., Pirrone, N., Lindqvist, O., 2007. Seasonal and daily variation of mercury evasion at coastal and off shore sites from the Mediterranean Sea. Mar. Chem. 104, 214–226. https://doi.org/10.1016/j.marchem.2006.11.003

Andersson, M.E., Gårdfeldt, K., Wängberg, I., Strömberg, D., 2008. Determination of Henry's law constant for elemental mercury. Chemosphere 73, 587–592. https://doi.org/10.1016/j.chemosphere.2008.05.067

Ariya, P.A., Amyot, M., Dastoor, A., Deeds, D., Feinberg, A., Kos, G., Poulain, A., Ryjkov, A., Semeniuk, K., Subir, M., Toyota, K., 2015. Mercury Physicochemical and Biogeochemical Transformation in the Atmosphere and at Atmospheric Interfaces: A Review and Future Directions. Chem. Rev. 115, 3760–3802. https://doi.org/10.1021/cr500667e

ARPAFVG-OSMER, 2014. Il clima del Friuli Venezia Giulia.

Baeyens, W., Leermakers, M., 1998. Elemental mercury concentrations and formation rates in the Scheldt estuary and the North Sea. Mar. Chem. 60, 257–266. https://doi.org/10.1016/S0304-4203(97)00102-3

Bagnato, E., Sproveri, M., Barra, M., Bitetto, M., Bonsignore, M., Calabrese, S., Di Stefano, V., Oliveri, E., Parello, F., Mazzola, S., 2013. The sea-air exchange of mercury (Hg) in the marine boundary layer of the Augusta basin (southern Italy): Concentrations and evasion flux. Chemosphere 93, 2024–2032. https://doi.org/10.1016/j.chemosphere.2013.07.025

Baldi, F., Gallo, M., Marchetto, D., Fani, R., Maida, I., Horvat, M., Fajon, V., Zizek, S., Hines, M., 2012. Seasonal mercury transformation and surficial sediment detoxification by bacteria of Marano and Grado lagoons. Estuar. Coast. Shelf Sci. 113, 105–115. https://doi.org/10.1016/j.ecss.2012.02.008

Baptista-Salazar, C., Richard, J.H., Horf, M., Rejc, M., Gosar, M., Biester, H., 2017. Grain-size dependence of mercury speciation in river suspended matter, sediments and soils in a mercury mining area at varying hydrological conditions. Appl. Geochemistry 81, 132–142. https://doi.org/10.1016/j.apgeochem.2017.04.006

Barago, N., Floreani, F., Acquavita, A., Esbrí, J.M., Covelli, S., Higueras, P., 2020. Spatial and temporal trends of gaseous elemental mercury over a highly impacted coastal environment (Northern Adriatic, Italy). Atmosphere (Basel). 11, 935. https://doi.org/10.3390/atmos11090935

Barkay, T., Miller, S.M., Summers, A.O., 2003. Bacterial mercury resistance from atoms to ecosystems. FEMS Microbiol. Rev. 27, 355–384. https://doi.org/10.1016/S0168-6445(03)00046-9

Beckers, F., Rinklebe, J., 2017. Cycling of mercury in the environment: Sources, fate, and human health implications: A review. Crit. Rev. Environ. Sci. Technol. 47, 693–794. https://doi.org/10.1080/10643389.2017.1326277

Black, F.J., Conaway, C.H., Flegal, A.R., 2009. Stability of dimethyl mercury in seawater and its conversion to monomethyl mercury. Environ. Sci. Technol. 43, 4056–4062. https://doi.org/10.1021/es9001218

Boldrin, A., Carniel, S., Giani, M., Marini, M., Bernardi Aubry, F., Campanelli, A., Grilli, F., Russo, A., 2009. Effects of bora wind on physical and biogeochemical properties of stratified waters in the northern Adriatic. J. Geophys. Res. 114, C08S92. https://doi.org/10.1029/2008jc004837

Bouchet, S., Tessier, E., Monperrus, M., Bridou, R., Clavier, J., Thouzeau, G., Amouroux, D., 2011. Measurements of gaseous mercury exchanges at the sediment-water, water-atmosphere and sediment-atmosphere interfaces of a tidal environment (Arcachon Bay, France). J. Environ. Monit. 13, 1351–1359. https://doi.org/10.1039/c0em00358a

Bouffard, A., Amyot, M., 2009. Importance of elemental mercury in lake sediments. Chemosphere 74, 1098–1103. https://doi.org/10.1016/j.chemosphere.2008.10.045

Branfireun, B.A., Cosio, C., Poulain, A.J., Riise, G., Bravo, A.G., 2020. Mercury cycling in freshwater systems - An updated conceptual model. Sci. Total Environ. 745, 140906. https://doi.org/10.1016/j.scitotenv.2020.140906

Bratkič, A., Ogrinc, N., Kotnik, J., Faganeli, J., Žagar, D., Yano, S., Tada, A., Horvat, M., 2013. Mercury speciation driven by seasonal changes in a contaminated estuarine environment. Environ. Res. 125, 171–178. https://doi.org/10.1016/j.envres.2013.01.004

Bratkič, A., Tinta, T., Koron, N., Guevara, S.R., Begu, E., Barkay, T., Horvat, M., Falnoga, I., Faganeli, J., 2018. Mercury transformations in a coastal water column (Gulf of Trieste, northern Adriatic Sea). Mar. Chem. 200, 57–67. https://doi.org/10.1016/j.marchem.2018.01.001

Castelle, S., Schäfer, J., Blanc, G., Dabrin, A., Lanceleur, L., Masson, M., 2009. Gaseous mercury at the air-water interface of a highly turbid estuary (Gironde Estuary, France). Mar. Chem. 117, 42–51. https://doi.org/10.1016/j.marchem.2009.01.005

Castro, L., Dommergue, A., Larose, C., Ferrari, C., Maron, L., 2011. A Theoretical study of abiotic methylation reactions of gaseous elemental mercury by halogen-containing molecules. J. Phys. Chem. A 115, 5602–5608. https://doi.org/10.1021/jp200643n

Cesário, R., Hintelmann, H., O'Driscoll, N.J., Monteiro, C.E., Caetano, M., Nogueira, M., Mota, A.M., Canário, J., 2017a. Biogeochemical Cycle of Mercury and Methylmercury in Two Highly Contaminated Areas of Tagus Estuary (Portugal). Water. Air. Soil Pollut. 228, 257. https://doi.org/10.1007/s11270-017-3442-1

Cesário, R., Poissant, L., Pilote, M., O'Driscoll, N.J., Mota, A.M., Canário, J., 2017b. Dissolved gaseous mercury formation and mercury volatilization in intertidal sediments. Sci. Total Environ. 603–604, 279–289. https://doi.org/10.1016/j.scitotenv.2017.06.093

Chen, Y.S., Tseng, C.M., Reinfelder, J.R., 2020. Spatiotemporal Variations in Dissolved Elemental Mercury in the River-Dominated and Monsoon-Influenced East China Sea: Drivers, Budgets, and Implications. Environ. Sci. Technol. 54, 3988–3995. https://doi.org/10.1021/acs.est.9b06092

Cheng, G., Li, D., Li, Y., 2019. Distribution of dissolved gaseous mercury (DGM)and its controlling factors in the Yellow Sea and Bohai Sea. Ecotoxicol. Environ. Saf. 180, 715–722. https://doi.org/10.1016/j.ecoenv.2019.05.049

Ci, Z., Zhang, X., Yin, Y., Chen, J., Wang, S., 2016. Mercury Redox Chemistry in Waters of the Eastern Asian Seas: From Polluted Coast to Clean Open Ocean. Environ. Sci. Technol. 50, 2371–2380. https://doi.org/10.1021/acs.est.5b05372

Ci, Z.J., Zhang, X.S., Wang, Z.W., Niu, Z.C., Diao, X.Y., Wang, S.W., 2011. Distribution and air-sea exchange of mercury (Hg) in the Yellow Sea. Atmos. Chem. Phys. 11, 2881–2892. https://doi.org/10.5194/acp-11-2881-2011

Cizdziel, J. V., Zhang, Y., Nallamothu, D., Brewer, J.S., Gao, Z., 2019. Air/surface exchange of gaseous elemental mercury at different landscapes in Mississippi, USA. Atmosphere (Basel). 10, 538. https://doi.org/10.3390/atmos10090538

Clarke, R.G., Klapstein, S.J., Keenan, R., O'Driscoll, N.J., 2023. Mercury photoreduction and photooxidation kinetics in estuarine water: Effects of salinity and dissolved organic matter. Chemosphere 312, 137279. https://doi.org/10.1016/j.chemosphere.2022.137279

Coale, K.H., Heim, W.A., Negrey, J., Weiss-Penzias, P., Fernandez, D., Olson, A., Chiswell, H., Byington, A., Bonnema, A., Martenuk, S., Newman, A., Beebe, C., Till, C., 2018. The distribution and speciation of mercury in the California current: Implications for mercury transport via fog to land. Deep. Res. Part II Top. Stud. Oceanogr. 151, 77–88. https://doi.org/10.1016/j.dsr2.2018.05.012

Colombo, M.J., Ha, J., Reinfelder, J.R., Barkay, T., Yee, N., 2013. Anaerobic oxidation of Hg(0) and methylmercury formation by Desulfovibrio desulfuricans ND132. Geochim. Cosmochim. Acta 112, 166–177. https://doi.org/10.1016/j.gca.2013.03.001

Conaway, C.H., Squire, S., Mason, R.P., Flegal, A.R., 2003. Mercury speciation in the San Francisco Bay estuary. Mar. Chem. 80, 199–225. https://doi.org/10.1016/S0304-4203(02)00135-4

Cossa, D., Averty, B., Pirrone, N., 2009. The origin of methylmercury in open mediterranean waters. Limnol. Oceanogr. 54, 837–844. https://doi.org/10.4319/lo.2009.54.3.0837

Cossa, D., Knoery, J., Bănaru, D., Harmelin-Vivien, M., Sonke, J.E., Hedgecock, I.M., Bravo, A.G., Rosati, G., Canu, D., Horvat, M., Sprovieri, F., Pirrone, N., Heimbürger-Boavida, L.E., 2022. Mediterranean Mercury Assessment 2022: An Updated Budget, Health Consequences, and Research Perspectives. Environ. Sci. Technol. 56, 3840–3862. https://doi.org/10.1021/acs.est.1c03044

Costa, M., Liss, P.S., 1999. Photoreduction of mercury in sea water and its possible implications for Hg0 air-sea fluxes. Mar. Chem. 68, 87–95. https://doi.org/10.1016/S0304-4203(99)00067-5

Covelli, S., Acquavita, A., Piani, R., Predonzani, S., De Vittor, C., 2009. Recent contamination of mercury in an estuarine environment (Marano lagoon, Northern Adriatic, Italy). Estuar. Coast. Shelf Sci. 82, 273–284. https://doi.org/10.1016/j.ecss.2009.01.021

Covelli, S., Faganeli, J., De Vittor, C., Predonzani, S., Acquavita, A., Horvat, M., 2008. Benthic fluxes of mercury species in a lagoon environment (Grado Lagoon, Northern Adriatic Sea, Italy). Appl. Geochemistry 23, 529–546. https://doi.org/10.1016/j.apgeochem.2007.12.011

Covelli, S., Faganeli, J., Horvat, M., Brambati, A., 2001. Mercury contamination of coastal sediments as the result of long-term cinnabar mining activity (Gulf of Trieste, northern Adriatic sea). Appl. Geochemistry 16, 541–558. https://doi.org/10.1016/S0883-2927(00)00042-1

Covelli, S., Piani, R., Acquavita, A., Predonzani, S., Faganeli, J., 2007. Transport and dispersion of particulate Hg associated with a river plume in coastal Northern Adriatic environments. Mar. Pollut. Bull. 55, 436–450. https://doi.org/10.1016/j.marpolbul.2007.09.006

Covelli, S., Piani, R., Kotnik, J., Horvat, M., Faganeli, J., Brambati, A., 2006. Behaviour of Hg species in a microtidal deltaic system: The Isonzo River mouth (northern Adriatic Sea). Sci. Total Environ. 368, 210–223. https://doi.org/10.1016/j.scitotenv.2005.09.089

Cozzi, S., Falconi, C., Comici, C., Čermelj, B., Kovac, N., Turk, V., Giani, M., 2012. Recent evolution of river discharges in the Gulf of Trieste and their potential response to climate changes and anthropogenic pressure. Estuar. Coast. Shelf Sci. 115, 14–24. https://doi.org/10.1016/j.ecss.2012.03.005

Custodio, D., Ebinghaus, R., Gerard Spain, T., Bieser, J., 2020. Source apportionment of atmospheric mercury in the remote marine atmosphere: Mace Head GAW station, Irish western coast. Atmos. Chem. Phys. 20, 7929–7939. https://doi.org/10.5194/acp-20-7929-2020

De Vittor, C., Faganeli, J., Emili, A., Covelli, S., Predonzani, S., Acquavita, A., 2012. Benthic fluxes of oxygen, carbon and nutrients in the Marano and Grado Lagoon (northern Adriatic Sea, Italy). Estuar. Coast. Shelf Sci. 113, 57–70. https://doi.org/10.1016/j.ecss.2012.03.031

Díez, S., 2009. Human Health Effects of Methylmercury Exposure BT - Reviews of Environmental Contamination and Toxicology, in: Whitacre, D.M. (Ed.), . Springer New York, New York, NY, pp. 111–132. https://doi.org/10.1007/978-0-387-09647-6_3

Dizdarevič, T., 2001. The influence of mercury production in Idrija mine on the environment in the Idrija region and over a broad area. RMZ - Mater. Geoenvironment 48, 56–64.

Eckley, C.S., Gustin, M., Lin, C.J., Li, X., Miller, M.B., 2010. The influence of dynamic chamber design and operating parameters on calculated surface-to-air mercury fluxes. Atmos. Environ. 44, 194–203. https://doi.org/10.1016/j.atmosenv.2009.10.013

Emili, A., Acquavita, A., Koron, N., Covelli, S., Faganeli, J., Horvat, M., Žižek, S., Fajon, V., 2012. Benthic flux measurements of Hg species in a northern Adriatic lagoon environment (Marano and Grado Lagoon, Italy). Estuar. Coast. Shelf Sci. 113, 71–84. https://doi.org/10.1016/j.ecss.2012.05.018

Enrico, M., Le Roux, G., Heimbürger, L.E., Van Beek, P., Souhaut, M., Chmeleff, J., Sonke, J.E., 2017. Holocene Atmospheric Mercury Levels Reconstructed from Peat Bog Mercury Stable Isotopes. Environ. Sci. Technol. 51, 5899–5906. https://doi.org/10.1021/acs.est.6b05804

Faganeli, J., Horvat, M., Covelli, S., Fajon, V., Logar, M., Lipej, L., Cermelj, B., 2003. Mercury and methylmercury in the Gulf of Trieste (northern Adriatic Sea). Sci. Total Environ. 304, 315–326. https://doi.org/10.1016/S0048-9697(02)00578-8

Faganeli, J., Planinc, R., Pezdič, Smodiš, B., Stegnar, P., Ogorelec, B., 1991. Marine geology of the Gulf of Trieste (northern Adriatic): Geochemical aspects. Mar. Geol. 99, 93–108. https://doi.org/10.1016/0025-3227(91)90085-I

Fantozzi, L., Ferrara, R., Frontini, F.P., Dini, F., 2009. Dissolved gaseous mercury production in the dark: Evidence for the fundamental role of bacteria in different types of Mediterranean water bodies. Sci. Total Environ. 407, 917–924. https://doi.org/10.1016/j.scitotenv.2008.09.014

Fantozzi, L., Ferrara, R., Frontini, F.P., Dini, F., 2007. Factors influencing the daily behaviour of dissolved gaseous mercury concentration in the Mediterranean Sea. Mar. Chem. 107, 4–12.

https://doi.org/10.1016/j.marchem.2007.02.008

Fantozzi, L., Manca, G., Ammoscato, I., Pirrone, N., Sprovieri, F., 2013. The cycling and sea-air exchange of mercury in the waters of the Eastern Mediterranean during the 2010 MED-OCEANOR cruise campaign. Sci. Total Environ. 448, 151–162. https://doi.org/10.1016/j.scitotenv.2012.09.062

Ferrara, R., Mazzolai, B., 1998. A dynamic flux chamber to measure mercury emission from aquatic systems. Sci. Total Environ. 215, 51–57. https://doi.org/10.1016/S0048-9697(98)00117-X

Ferrara, R., Mazzolai, B., Lanzillotta, E., Nucaro, E., Pirrone, N., 2000. Temporal trends in gaseous mercury evasion from the Mediterranean seawaters. Sci. Total Environ. 259, 183–190. https://doi.org/10.1016/S0048-9697(00)00581-7

Ferrarin, C., Umgiesser, G., Bajo, M., Bellafiore, D., De Pascalis, F., Ghezzo, M., Mattassi, G., Scroccaro, I., 2010. Hydraulic zonation of the lagoons of Marano and Grado, Italy. A modelling approach. Estuar. Coast. Shelf Sci. 87, 561–572. https://doi.org/10.1016/j.ecss.2010.02.012

Fitzgerald, W.F., Engstrom, D.R., Mason, R.P., Nater, E.A., 1998. The case for atmospheric mercury contamination in remote areas. Environ. Sci. Technol. 32, 1–7. https://doi.org/10.1021/es970284w

Fitzgerald, W.F., Lamborg, C.H., Hammerschmidt, C.R., 2007. Marine biogeochemical cycling of mercury. Chem. Rev. 107, 641–662. https://doi.org/10.1021/cr050353m

Floreani, F., Acquavita, A., Barago, N., Klun, K., Faganeli, J., Covelli, S., 2022. Gaseous Mercury Exchange from Water – Air Interface in Differently Impacted Freshwater Environments. Int. J. Environ. Res. Public Health 19, 8149.

Floreani, F., Acquavita, A., Petranich, E., Covelli, S., 2019. Diurnal fluxes of gaseous elemental mercury from the water-air interface in coastal environments of the northern Adriatic Sea. Sci. Total Environ. 668, 925–935. https://doi.org/10.1016/j.scitotenv.2019.03.012

Floreani, F., Barago, N., Acquavita, A., Covelli, S., Skert, N., Higueras, P., 2020. Spatial distribution and biomonitoring of atmospheric mercury concentrations over a contaminated coastal lagoon (Northern Adriatic, Italy). Atmosphere (Basel). 11, 1280. https://doi.org/10.3390/atmos11121280

Fu, X., Feng, X., Zhang, G., Xu, W., Li, X., Yao, H., Liang, P., Li, J., Sommar, J., Yin, R., Liu, N., 2010. Mercury in the marine boundary layer and seawater of the South China Sea: Concentrations, sea/air flux, and implication for land outflow. J. Geophys. Res. Atmos. 115, 1–11. https://doi.org/10.1029/2009JD012958

Garcia, E., Poulain, A.J., Amyot, M., Ariya, P.A., 2005. Diel variations in photoinduced oxidation of Hg0 in freshwater. Chemosphere 59, 977–981. https://doi.org/10.1016/j.chemosphere.2004.09.107

Gårdfeldt, K., Feng, X., Sommar, J., Lindqvist, O., 2001. Total gaseous mercury exchange between air and water at river and sea surfaces in Swedish coastal regions. Atmos. Environ. 35, 3027–3038. https://doi.org/https://doi.org/10.1016/S1352-2310(01)00106-6

Gårdfeldt, K., Sommar, J., Ferrara, R., Ceccarini, C., Lanzillotta, E., Munthe, J., Wängberg, I., Lindqvist, O., Pirrone, N., Sprovieri, F., Pesenti, E., Strömberg, D., 2003. Evasion of mercury from coastal and open waters of the Atlantic Ocean and the Mediterranean Sea. Atmos. Environ. 37, 73–84. https://doi.org/10.1016/S1352-2310(03)00238-3

Gonzalez-Raymat, H., Liu, G., Liriano, C., Li, Y., Yin, Y., Shi, J., Jiang, G., Cai, Y., 2017. Elemental mercury: Its unique properties affect its behavior and fate in the environment. Environ. Pollut. 229, 69–86. https://doi.org/10.1016/j.envpol.2017.04.101

Gosar, M., Pirc, S., Bidovec, M., 1997. Mercury in the Idrijca River sediments as a reflection of mining and smelting activities of the Idrija mercury mine. J. Geochemical Explor. 58, 125–131. https://doi.org/10.1016/S0375-6742(96)00064-7

Grégoire, D.S., Poulain, A.J., 2014. A little bit of light goes a long way: The role of phototrophs on mercury cycling. Metallomics 6, 396–407. https://doi.org/10.1039/c3mt00312d

Hammerschmidt, C.R., Fitzgerald, W.F., 2004. Geochemical Controls on the Production and Distribution of Methylmercury in Near-Shore Marine Sediments. Environ. Sci. Technol. 38, 1487–1495. https://doi.org/10.1021/es034528q

He, F., Zhao, W., Liang, L., Gu, B., 2014. Photochemical Oxidation of Dissolved Elemental Mercury by Carbonate Radicals in Water. Environ. Sci. Technol. Lett. 1, 499–503. https://doi.org/10.1021/ez500322f

Horvat, M., Kotnik, J., Logar, M., Fajon, V., Zvonarić, T., Pirrone, N., 2003. Speciation of mercury in surface and deep-sea waters in the Mediterranean Sea. Atmos. Environ. 37, 93–108. https://doi.org/10.1016/S1352-2310(03)00249-8

Hsu-Kim, H., Eckley, C.S., Achá, D., Feng, X., Gilmour, C.C., Jonsson, S., Mitchell, C.P.J., 2018. Challenges and opportunities for managing aquatic mercury pollution in altered landscapes. Ambio 47, 141–169. https://doi.org/10.1007/s13280-017-1006-7

Jung, E., Kim, H., Yun, D., Rahman, M.M., Lee, J.H., Kim, S., Kim, C.K., Han, S., 2022. Importance of hydraulic

residence time for methylmercury accumulation in sediment and fish from artificial reservoirs. Chemosphere 293, 133545. https://doi.org/10.1016/j.chemosphere.2022.133545

Kalinchuk, V. V., 2023. Gaseous elemental mercury and its evasion fluxes in the marine boundary layer of the marginal seas of the northwestern Pacific: Results from two cruises in September–December 2019. Sci. Total Environ. 858, 159711. https://doi.org/10.1016/j.scitotenv.2022.159711

Kalinchuk, V. V., Lopatnikov, E.A., Astakhov, A.S., Ivanov, M. V., Hu, L., 2021. Distribution of atmospheric gaseous elemental mercury (Hg(0)) from the Sea of Japan to the Arctic, and Hg(0) evasion fluxes in the Eastern Arctic Seas: Results from a joint Russian-Chinese cruise in fall 2018. Sci. Total Environ. 753, 142003. https://doi.org/10.1016/j.scitotenv.2020.142003

Klapstein, S.J., O'Driscoll, N.J., 2018. Methylmercury Biogeochemistry in Freshwater Ecosystems: A Review Focusing on DOM and Photodemethylation. Bull. Environ. Contam. Toxicol. 100, 14–25. https://doi.org/10.1007/s00128-017-2236-x

Kotnik, J., Horvat, M., Begu, E., Shlyapnikov, Y., Sprovieri, F., Pirrone, N., 2017. Dissolved gaseous mercury (DGM) in the Mediterranean Sea: Spatial and temporal trends. Mar. Chem. 193, 8–19. https://doi.org/10.1016/j.marchem.2017.03.002

Kotnik, J., Horvat, M., Ogrinc, N., Fajon, V., Žagar, D., Cossa, D., Sprovieri, F., Pirrone, N., 2015. Mercury speciation in the Adriatic Sea. Mar. Pollut. Bull. 96, 136–148. https://doi.org/10.1016/j.marpolbul.2015.05.037

Kotnik, J., Žagar, D., Novak, G., Ličer, M., Horvat, M., 2022. Dissolved Gaseous Mercury (DGM) in the Gulf of Trieste, Northern Adriatic Sea. J. Mar. Sci. Eng. 10, 587. https://doi.org/10.3390/jmse10050587

Kuss, J., Holzmann, J., Ludwig, R., 2009. An elemental mercury diffusion coefficient for natural waters determined by molecular dynamics simulation. Environ. Sci. Technol. 43, 3183–3186. https://doi.org/10.1021/es8034889

Kuss, J., Krüger, S., Ruickoldt, J., Wlost, K.P., 2018. High-resolution measurements of elemental mercury in surface water for an improved quantitative understanding of the Baltic Sea as a source of atmospheric mercury. Atmos. Chem. Phys. 18, 4361–4376. https://doi.org/10.5194/acp-18-4361-2018

Kuss, J., Wasmund, N., Nausch, G., Labrenz, M., 2015. Mercury Emission by the Baltic Sea: A Consequence of Cyanobacterial Activity, Photochemistry, And Low-Light Mercury Transformation. Environ. Sci. Technol. 49, 11449–11457. https://doi.org/10.1021/acs.est.5b02204

Lalonde, J.D., Amyot, M., Kraepiel, A.M.L., Morel, F.M.M., 2001. Photooxidation of Hg(O) in artificial and natural waters. Environ. Sci. Technol. 35, 1367–1372. https://doi.org/10.1021/es001408z

Lalonde, J.D., Amyot, M., Orvoine, J., Morel, F.M.M., Auclair, J.C., Ariya, P.A., 2004. Photoinduced Oxidation of Hg0(aq) in the Waters from the St. Lawrence Estuary. Environ. Sci. Technol. 38, 508–514. https://doi.org/10.1021/es034394g

Lamborg, C.H., Hansel, C.M., Bowman, K.L., Voelker, B.M., Marsico, R.M., Oldham, V.E., Swarr, G.J., Zhang, T., Ganguli, P.M., 2021. Dark Reduction Drives Evasion of Mercury From the Ocean. Front. Environ. Chem. 2, 659085. https://doi.org/10.3389/fenvc.2021.659085

Lanzillotta, E., Ceccarini, C., Ferrara, R., 2002. Photo-induced formation of dissolved gaseous mercury in coastal and offshore seawater of the Mediterranean basin. Sci. Total Environ. 300, 179–187. https://doi.org/10.1016/S0048-9697(02)00223-1

Lanzillotta, E., Ceccarini, C., Ferrara, R., Dini, F., Frontini, F.P., Banchetti, R., 2004. Importance of the biogenic organic matter in photo-formation of dissolved gaseous mercury in a culture of the marine diatom Chaetoceros sp. Sci. Total Environ. 318, 211–221. https://doi.org/10.1016/S0048-9697(03)00400-5

Lee, J.I., Yang, J.H., Kim, P.R., Han, Y.J., 2019. Effects of organic carbon and UV wavelength on the formation of dissolved gaseous mercury in water under a controlled environment. Environ. Eng. Res. 24, 54–62. https://doi.org/10.4491/eer.2018.045

Lepak, R.F., Tate, M.T., Ogorek, J.M., DeWild, J.F., Peterson, B.D., Hurley, J.P., Krabbenhoft, D.P., 2021. Aqueous Elemental Mercury Production versus Mercury Inventories in the Lake Michigan Airshed: Deciphering the Spatial and Diel Controls of Mercury Gradients in Air and Water. ACS ES&T Water 1, 719–727. https://doi.org/10.1021/acsestwater.0c00187

Liang, X., Zhu, N., Johs, A., Chen, H., Pelletier, D.A., Zhang, L., Yin, X., Gao, Y., Zhao, J., Gu, B., 2022. Mercury Reduction, Uptake, and Species Transformation by Freshwater Alga Chlorella vulgaris under Sunlit and Dark Conditions . Environ. Sci. Technol. https://doi.org/10.1021/acs.est.1c06558

Lindberg, S.E., Zhang, H., 2000. Air/water exchange of mercury in the Everglades II: Measuring and modeling evasion of mercury from surface waters in the Everglades Nutrient Removal Project. Sci. Total Environ. 259, 135–143. https://doi.org/10.1016/S0048-9697(00)00586-6

Lindberg, S.I.S., Meyers, T.P., 1995. Evasion of mercury vapor from the surface of a recently limed acid lake

forest in Sweden. Water. Air. Soil Pollut. 85, 725–730.

Luo, H., Cheng, Q., Pan, X., 2020. Photochemical behaviors of mercury (Hg) species in aquatic systems: A systematic review on reaction process, mechanism, and influencing factor. Sci. Total Environ. 720, 137540. https://doi.org/10.1016/j.scitotenv.2020.137540

Marumoto, K., Imai, S., 2015. Determination of dissolved gaseous mercury in seawater of Minamata Bay and estimation for mercury exchange across air-sea interface. Mar. Chem. 168, 9–17. https://doi.org/10.1016/j.marchem.2014.09.007

Mason, R.P., Hammerschmidt, C.R., Lamborg, C.H., Bowman, K.L., Swarr, G.J., Shelley, R.U., 2017. The air-sea exchange of mercury in the low latitude Pacific and Atlantic Oceans. Deep. Res. Part I Oceanogr. Res. Pap. 122, 17–28. https://doi.org/10.1016/j.dsr.2017.01.015

Mason, R.P., Morel, F.M.M., Hemond, H.F., 1995. The role of microorganisms in elemental mercury formation in natural waters. Water, Air, Soil Pollut. 80, 775–787. https://doi.org/10.1007/BF01189729

Mason, R.P., Sheu, G.R., 2002. Role of the ocean in the global mercury cycle. Global Biogeochem. Cycles 16, 40-1-40–14. https://doi.org/10.1029/2001gb001440

Morel, F.M.M., Kraepiel, A.M.L., Amyot, M., 1998. The chemical cycle and bioaccumulation of mercury. Annu. Rev. Ecol. Syst. 29, 543–566. https://doi.org/10.1146/annurev.ecolsys.29.1.543

Narukawa, M., Sakata, M., Marumoto, K., Asakura, K., 2006. Air-sea exchange of mercury in Tokyo Bay. J. Oceanogr. 62, 249–257. https://doi.org/10.1007/s10872-006-0049-3

Nerentorp Mastromonaco, M.G., Gårdfeldt, K., Wängberg, I., 2017. Seasonal and spatial evasion of mercury from the western Mediterranean Sea. Mar. Chem. 193, 34–43. https://doi.org/10.1016/j.marchem.2017.02.003

O'Driscoll, N.J., Beauchamp, S., Siciliano, S.D., Rencz, A.N., Lean, D.R.S., 2003. Continuous analysis of dissolved gaseous mercury (DGM) and mercury flux in two freshwater lakes in Kejimkujik Park, Nova Scotia: Evaluating mercury flux models with quantitative data. Environ. Sci. Technol. 37, 2226–2235. https://doi.org/10.1021/es025944y

O'Driscoll, N.J., Christensen, T.M., Mann, E.A., Keenan, R., Klapstein, S.J., 2022. Temporal Changes in Photoreducible Mercury, Photoreduction Rates, and the Role of Dissolved Organic Matter in Freshwater Lakes. Bull. Environ. Contam. Toxicol. 108, 635–640. https://doi.org/10.1007/s00128-021-03422-1

O'Driscoll, N.J., Covelli, S., Petranich, E., Floreani, F., Klapstein, S., Acquavita, A., 2019. Dissolved Gaseous Mercury Production at a Marine Aquaculture Site in the Mercury-Contaminated Marano and Grado Lagoon, Italy. Bull. Environ. Contam. Toxicol. 103. https://doi.org/10.1007/s00128-019-02621-1

O'Driscoll, N.J., Lean, D.R.S., Loseto, L.L., Carignan, R., Siciliano, S.D., 2004. Effect of Dissolved Organic Carbon on the Photoproduction of Dissolved Gaseous Mercury in Lakes: Potential Impacts of Forestry. Environ. Sci. Technol. 38, 2664–2672. https://doi.org/10.1021/es034702a

O'Driscoll, N.J., Vost, E., Mann, E., Klapstein, S., Tordon, R., Lukeman, M., 2018. Mercury photoreduction and photooxidation in lakes: Effects of filtration and dissolved organic carbon concentration. J. Environ. Sci. (China) 68, 151–159. https://doi.org/10.1016/j.jes.2017.12.010

Ogorelec, B., Mišič, M., Faganeli, J., 1991. Marine geology of the Gulf of Trieste (northern Adriatic): Sedimentological aspects. Mar. Geol. 99, 79–92. https://doi.org/10.1016/0025-3227(91)90084-H

Osterwalder, S., Nerentorp, M., Zhu, W., Jiskra, M., Nilsson, E., Nilsson, M.B., Rutgersson, A., Soerensen, A.L., Sommar, J., Wallin, M.B., Wängberg, I., Bishop, K., 2021. Critical Observations of Gaseous Elemental Mercury Air-Sea Exchange. Global Biogeochem. Cycles 35, e2020GB006742. https://doi.org/10.1029/2020GB006742

Parks, J.M., Johs, A., Podar, M., Bridou, R., Hurt, R.A., Smith, S.D., Tomanicek, S.J., Qian, Y., Brown, S.D., Brandt, C.C., Palumbo, A. V., Smith, J.C., Wall, J.D., Elias, D.A., Liang, L., 2013. The genetic basis for bacterial mercury methylation. Science (80-.). 339, 1332–1335. https://doi.org/10.1126/science.1230667

Pavoni, E., Crosera, M., Petranich, E., Oliveri, P., Klun, K., Faganeli, J., Covelli, S., Adami, G., 2020. Trace elements in the estuarine systems of the Gulf of Trieste (northern Adriatic Sea): A chemometric approach to depict partitioning and behaviour of particulate, colloidal and truly dissolved fractions. Chemosphere 252, 126517. https://doi.org/10.1016/j.chemosphere.2020.126517

Pesaresi, S., Galdenzi, D., Biondi, E., Casavecchia, S., 2014. Bioclimate of Italy: Application of the worldwide bioclimatic classification system. J. Maps 10, 538–553. https://doi.org/10.1080/17445647.2014.891472

Petranich, E., Covelli, S., Acquavita, A., De Vittor, C., Faganeli, J., Contin, M., 2018a. Benthic nutrient cycling at the sediment-water interface in a lagoon fish farming system (northern Adriatic Sea, Italy). Sci. Total Environ. 644, 137–149. https://doi.org/10.1016/j.scitotenv.2018.06.310

Petranich, E., Covelli, S., Acquavita, A., Faganeli, J., Horvat, M., Contin, M., 2018b. Evaluation of mercury biogeochemical cycling at the sediment–water interface in anthropogenically modified lagoon environments. J. Environ. Sci. (China) 68, 5–23. https://doi.org/10.1016/j.jes.2017.11.014

Poissant, L., Amyot, M., Pilote, M., Lean, D., 2000. Mercury water - Air exchange over the upper St. Lawrence River and Lake Ontario. Environ. Sci. Technol. 34, 3069–3078. https://doi.org/10.1021/es990719a

Poulain, A.J., Amyot, M., Findlay, D., Telor, S., Barkay, T., Hintelmann, H., 2004. Biological and photochemical production of dissolved gaseous mercury in a boreal lake. Limnol. Oceanogr. 49, 2265–2275. https://doi.org/10.4319/lo.2004.49.6.2265

Qureshi, A., O'Driscoll, N.J., Macleod, M., Neuhold, Y.M., Hungerbühler, K., 2010. Photoreactions of mercury in surface ocean water: Gross reaction kinetics and possible pathways. Environ. Sci. Technol. 44, 644–649. https://doi.org/10.1021/es9012728

Ren, X., Luke, W.T., Kelley, P., Cohen, M.D., Artz, R., Olson, M.L., Schmeltz, D., Puchalski, M., Goldberg, D.L., Ring, A., Mazzuca, G.M., Cummings, K.A., Wojdan, L., Preaux, S., Stehr, J.W., 2016. Atmospheric mercury measurements at a suburban site in the Mid-Atlantic United States: Inter-annual, seasonal and diurnal variations and source-receptor relationships. Atmos. Environ. 146, 141–152. https://doi.org/10.1016/j.atmosenv.2016.08.028

Rolfhus, K.R., Fitzgerald, W.F., 2001. The evasion and spatial/temporal distribution of mercury species in Long Island Sound, CT-NY. Geochim. Cosmochim. Acta 65, 407–418. https://doi.org/10.1016/S0016-7037(00)00519-6

Saiz-Lopez, A., Sitkiewicz, S.P., Roca-Sanjuán, D., Oliva-Enrich, J.M., Dávalos, J.Z., Notario, R., Jiskra, M., Xu, Y., Wang, F., Thackray, C.P., Sunderland, E.M., Jacob, D.J., Travnikov, O., Cuevas, C.A., Acuña, A.U., Rivero, D., Plane, J.M.C., Kinnison, D.E., Sonke, J.E., 2018. Photoreduction of gaseous oxidized mercury changes global atmospheric mercury speciation, transport and deposition. Nat. Commun. 9, 4796. https://doi.org/10.1038/s41467-018-07075-3

Sanemasa, I., 1975. The solubility of elemental mercury vapor in water. Bull. Chem. Soc. Jpn. 48, 1795–1798.

Schartup, A.T., Ndu, U., Balcom, P.H., Mason, R.P., Sunderland, E.M., 2015. Contrasting effects of marine and terrestrially derived dissolved organic matter on mercury speciation and bioavailability in seawater. Environ. Sci. Technol. 49, 5965–5972. https://doi.org/10.1021/es506274x

Selin, H., Keane, S.E., Wang, S., Selin, N.E., Davis, K., Bally, D., 2018. Linking science and policy to support the implementation of the Minamata Convention on Mercury. Ambio 47, 198–215. https://doi.org/10.1007/s13280-017-1003-x

Sharif, A., Tessier, E., Bouchet, S., Monperrus, M., Pinaly, H., Amouroux, D., 2013. Comparison of different air-water gas exchange models to determine gaseous mercury evasion from different european coastal lagoons and estuaries. Water. Air. Soil Pollut. 224. https://doi.org/10.1007/s11270-013-1606-1

Sholupov, S., Pogarev, S., Ryzhov, V., 2004. Zeeman atomic absorption spectrometer RA-915 + for direct determination of mercury in air and complex matrix samples 85, 473–485. https://doi.org/10.1016/j.fuproc.2003.11.003

Soerensen, A.L., Mason, R.P., Balcom, P.H., Jacob, D.J., Zhang, Y., Kuss, J., Sunderland, E.M., 2014. Elemental mercury concentrations and fluxes in the tropical atmosphere and Ocean. Environ. Sci. Technol. 48, 11312–11319. https://doi.org/10.1021/es503109p

Soerensen, A.L., Mason, R.P., Balcom, P.H., Sunderland, E.M., 2013. Drivers of surface ocean mercury concentrations and air-sea exchange in the West Atlantic Ocean. Environ. Sci. Technol. 47, 7757–7765. https://doi.org/10.1021/es401354q

Soerensen, A.L., Sunderland, E.M., Holmes, C.D., Jacob, D.J., Yantosca, R.M., Skov, H., Christensen, J.H., Strode, S.A., Mason, R.P., 2010. An improved global model for air-sea exchange of mercury: High concentrations over the North Atlantic. Environ. Sci. Technol. 44, 8574–8580. https://doi.org/10.1021/es102032g

Sommar, J., Osterwalder, S., Zhu, W., 2020. Recent advances in understanding and measurement of Hg in the environment: Surface-atmosphere exchange of gaseous elemental mercury (Hg0). Sci. Total Environ. 721, 137648. https://doi.org/10.1016/j.scitotenv.2020.137648

Southworth, G., Lindberg, S., Hintelmann, H., Amyot, M., Poulain, A., Bogle, M.A., Peterson, M., Rudd, J., Harris, R., Sandilands, K., Krabbenhoft, D., Olsen, M., 2007. Evasion of added isotopic mercury from a northern temperate lake. Environ. Toxicol. Chem. 26, 53–60. https://doi.org/10.1897/06-148R.1

Sprovieri, F., Pirrone, N., Bencardino, M., D'Amore, F., Angot, H., Barbante, C., Brunke, E.G., Arcega-Cabrera, F., Cairns, W., Comero, S., Del Carmen Diéguez, M., Dommergue, A., Ebinghaus, R., Bin Feng, X., Fu, X., Elizabeth Garcia, P., Manfred Gawlik, B., Hageström, U., Hansson, K., Horvat, M., Kotnik, J., Labuschagne, C., Magand, O., Martin, L., Mashyanov, N., Mkololo, T., Munthe, J., Obolkin, V., Ramirez Islas, M., Sena, F., Somerset, V., Spandow, P., Vardè, M., Walters, C., Wängberg, I., Weigelt, A., Yang, X., Zhang, H., 2017. Five-year records of mercury wet deposition flux at GMOS sites in the Northern and Southern hemispheres. Atmos. Chem. Phys. 17, 2689–2708. https://doi.org/10.5194/acp-17-2689-2017

Strode, S.A., Jaeglé, L., Selin, N.E., Jacob, D.J., Park, R.J., Yantosca, R.M., Mason, R.P., Slemr, F., 2007. Air-sea exchange in the global mercury cycle. Global Biogeochem. Cycles 21, 1–12. https://doi.org/10.1029/2006GB002766

Sugimura, Y., Suzuki, Y., 1988. A high-temperature catalytic oxidation method for the determination of non-volatile dissolved organic carbon in seawater by direct injection of a liquid sample. Mar. Chem. 24, 105–131. https://doi.org/https://doi.org/10.1016/0304-4203(88)90043-6

Tomažič, Š., Ličer, M., Žagar, D., 2018. Numerical modelling of mercury evasion in a two-layered Adriatic Sea using a coupled atmosphere-ocean model. Mar. Pollut. Bull. 135, 1164–1173. https://doi.org/10.1016/j.marpolbul.2018.08.064

UN Environment, 2019. Global Mercury Assessment 2018. UN Environment Programme, Chemicals and Health Branch, Geneva, Switzerland.

United States Environmental Protection Agency, 2002. Method 1631, Revision E: Mercury in Water by Oxidation, Purge and Trap, and Cold Vapor Atomic Fluorescence Spectrometry. Off. Water, Off. Sci. Technol. Eng. Anal. Div. (4303), 1200 Pennsylvania Ave. NW, Washington, D.C. 1–34.

Vette, A.F., Landis, M.S., Keeler, G.J., 2002. Deposition and emission of gaseous mercury to and from Lake Michigan during the Lake Michigan Mass Balance Study (July, 1994-October, 1995). Environ. Sci. Technol. 36, 4525–4532. https://doi.org/10.1021/es0112184

Vudamala, K., Chakraborty, P., Sailaja, B.B.V., 2017. An insight into mercury reduction process by humic substances in aqueous medium under dark condition. Environ. Sci. Pollut. Res. 24, 14499–14507. https://doi.org/10.1007/s11356-017-8979-4

Wang, C., Ci, Z., Wang, Z., Zhang, X., 2016. Air-sea exchange of gaseous mercury in the East China Sea. Environ. Pollut. 212, 535–543. https://doi.org/10.1016/j.envpol.2016.03.016

Wang, C., Wang, Z., Zhang, X., 2020. Characteristics of the air–sea exchange of gaseous mercury and deposition flux of atmospheric mercury at an island near the boundary of the Bohai Sea and Yellow Sea. Atmos. Environ. 232, 117547. https://doi.org/10.1016/j.atmosenv.2020.117547

Wang, K., Liu, G., Cai, Y., 2022. Possible pathways for mercury methylation in oxic marine waters. Crit. Rev. Environ. Sci. Technol. 52, 3997–4015. https://doi.org/10.1080/10643389.2021.2008753

Wang, Y., Li, Y., Liu, G., Wang, D., Jiang, G., Cai, Y., 2015. Elemental Mercury in Natural Waters: Occurrence and Determination of Particulate Hg(0). Environ. Sci. Technol. 49, 9742–9749. https://doi.org/10.1021/acs.est.5b01940

Wang, Z., Fei, Z., Wu, Q., Yin, R., 2020. Evaluation of the effects of Hg/DOC ratios on the reduction of Hg(II) in lake water. Chemosphere 253, 126634. https://doi.org/10.1016/j.chemosphere.2020.126634

Wängberg, I., Munthe, J., Amouroux, D., Andersson, M.E., Fajon, V., Ferrara, R., Gårdfeldt, K., Horvat, M., Mamane, Y., Melamed, E., Monperrus, M., Ogrinc, N., Yossef, O., Pirrone, N., Sommar, J., Sprovieri, F., 2008. Atmospheric mercury at mediterranean coastal stations. Environ. Fluid Mech. 8, 101–116. https://doi.org/10.1007/s10652-007-9047-2

Whalin, L., Kim, E.H., Mason, R., 2007. Factors influencing the oxidation, reduction, methylation and demethylation of mercury species in coastal waters. Mar. Chem. 107, 278–294. https://doi.org/10.1016/j.marchem.2007.04.002

Wickham, H., Chang, W., Henry, L., Pendersen, T.L., Takahashi, K., Wilke, C., Woo, K., Yutani, H., Dunnington, D., 2016. ggplot2: elegant graphics for data analysis. Springer-Verlag, New York. https://doi.org/ggplot2.tidyverse.org

Wu, Y., Wang, W.X., 2014. Intracellular speciation and transformation of inorganic mercury in marine phytoplankton. Aquat. Toxicol. 148, 122–129. https://doi.org/10.1016/j.aquatox.2014.01.005

Xu, L.Q., Liu, R.H., Wang, J.Y., Tan, H.W., Tang, A.K., Yu, P., 2012. Mercury Emission Flux in the Jiaozhou Bay Measured by Flux Chamber. Procedia Environ. Sci. 13, 1500–1506. https://doi.org/10.1016/j.proenv.2012.01.142

Xue, W., Kwon, S.Y., Grasby, S.E., Sunderland, E.M., Pan, X., Sun, R., Zhou, T., Yan, H., Yin, R., 2019. Anthropogenic influences on mercury in Chinese soil and sediment revealed by relationships with total organic carbon. Environ. Pollut. 255, 113186. https://doi.org/10.1016/j.envpol.2019.113186

Yamamoto, M., 1996. Stimulation of elemental mercury oxidation in the presence of chloride ion in aquatic environments. Chemosphere 32, 1217–1224. https://doi.org/10.1016/0045-6535(96)00008-2

Yin, Y., Li, Y., Tai, C., Cai, Y., Jiang, G., 2014. Fumigant methyl iodide can methylate inorganic mercury species in natural waters. Nat. Commun. 5, 4633. https://doi.org/10.1038/ncomms5633

Zappa, C.J., Raymond, P.A., Terray, E.A., McGillis, W.R., 2003. Variation in Surface Turbulence and the Gas Transfer Velocity over a Tidal Cycle in a Macro-tidal Estuary. Estuaries 26, 1401–1415. https://doi.org/10.1007/BF02803649

Zhang, L., Blanchard, P., Gay, D.A., Prestbo, E.M., Risch, M.R., Johnson, D., Narayan, J., Zsolway, R., Holsen, T.M., Miller, E.K., Castro, M.S., Graydon, J.A., St. Louis, V.L., Dalziel, J., 2012. Estimation of speciated and total mercury dry deposition at monitoring locations in eastern and central North America. Atmos. Chem. Phys. 12, 4327–4340. https://doi.org/10.5194/acp-12-4327-2012

Zhang, X., Guo, Y., Liu, G., Liu, Y., Song, M., Shi, J., Hu, L., Li, Y., Yin, Y., Cai, Y., Jiang, G., 2021. Dark Reduction of Mercury by Microalgae-Associated Aerobic Bacteria in Marine Environments. Environ. Sci. Technol. 55, 14258–14268. https://doi.org/10.1021/acs.est.1c03608

Zheng, W., Hintelmann, H., 2009. Mercury isotope fractionation during photoreduction in natural water is controlled by its Hg/DOC ratio. Geochim. Cosmochim. Acta 73, 6704–6715. https://doi.org/10.1016/j.gca.2009.08.016

Zhu, W., Lin, C.J., Wang, X., Sommar, J., Fu, X., Feng, X., 2016. Global observations and modeling of atmosphere-surface exchange of elemental mercury: A critical review. Atmos. Chem. Phys. 16, 4451–4480. https://doi.org/10.5194/acp-16-4451-2016

Zhu, W., Sommar, J., Lin, C.J., Feng, X., 2015. Mercury vapor air-surface exchange measured by collocated micrometeorological and enclosure methods – Part I: Data comparability and method characteristics. Atmos. Chem. Phys. 15, 685–702. https://doi.org/10.5194/acp-15-685-2015

Živković, I., Humphreys, M.P., Achterberg, E.P., Dumousseaud, C., Woodward, E.M.S., Bojanić, N., Šolić, M., Bratkič, A., Kotnik, J., Vahčič, M., Obu Vazner, K., Begu, E., Fajon, V., Shlyapnikov, Y., Horvat, M., 2022. Enhanced mercury reduction in the South Atlantic Ocean during carbon remineralization. Mar. Pollut. Bull. 178, 113644. https://doi.org/10.1016/j.marpolbul.2022.113644

Supplementary material

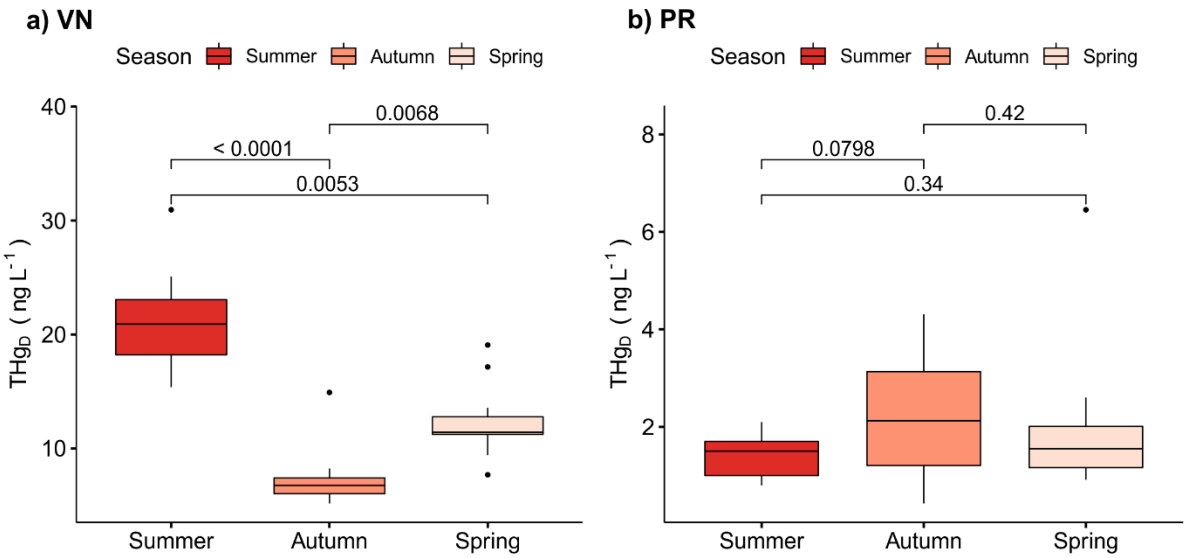

Figure S1: *variation of THg$_D$ concentrations in the various seasons at the two selected sites, Val Noghera fishfarm (VN) and Bay of Piran (PR). The p-values of pairwise Dunn's post-hoc test are reported. (Note the difference in Y-axis scales).*

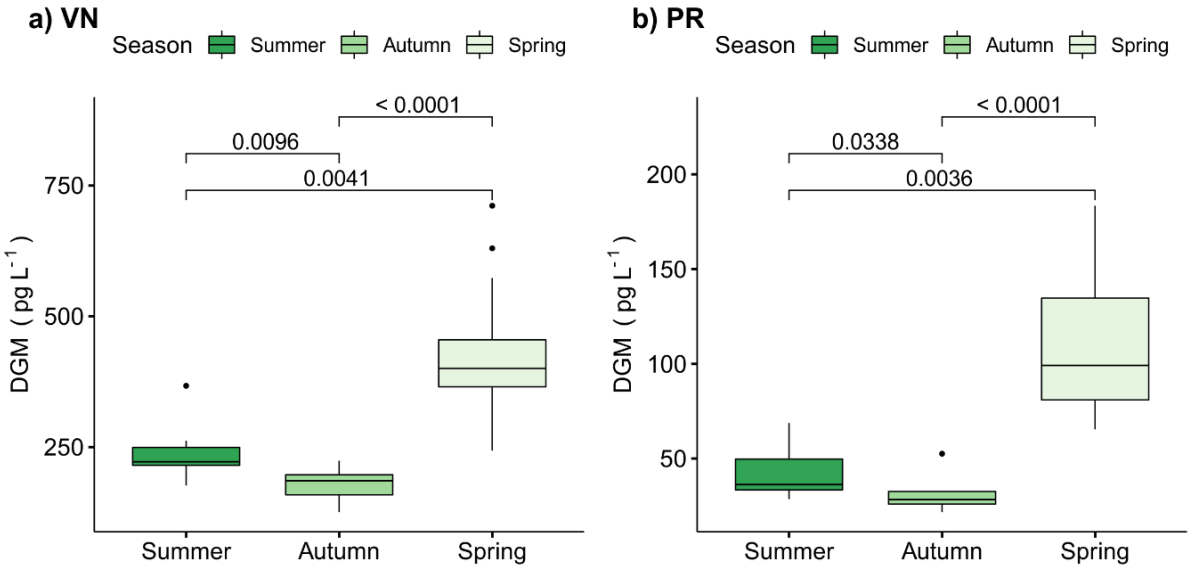

Figure S2: *variation of DGM concentrations in the various seasons at the two selected sites, Val Noghera fishfarm (VN) and Bay of Piran (PR). The p-values of pairwise Dunn's post-hoc test are reported. (Note the difference in Y-axis scales).*

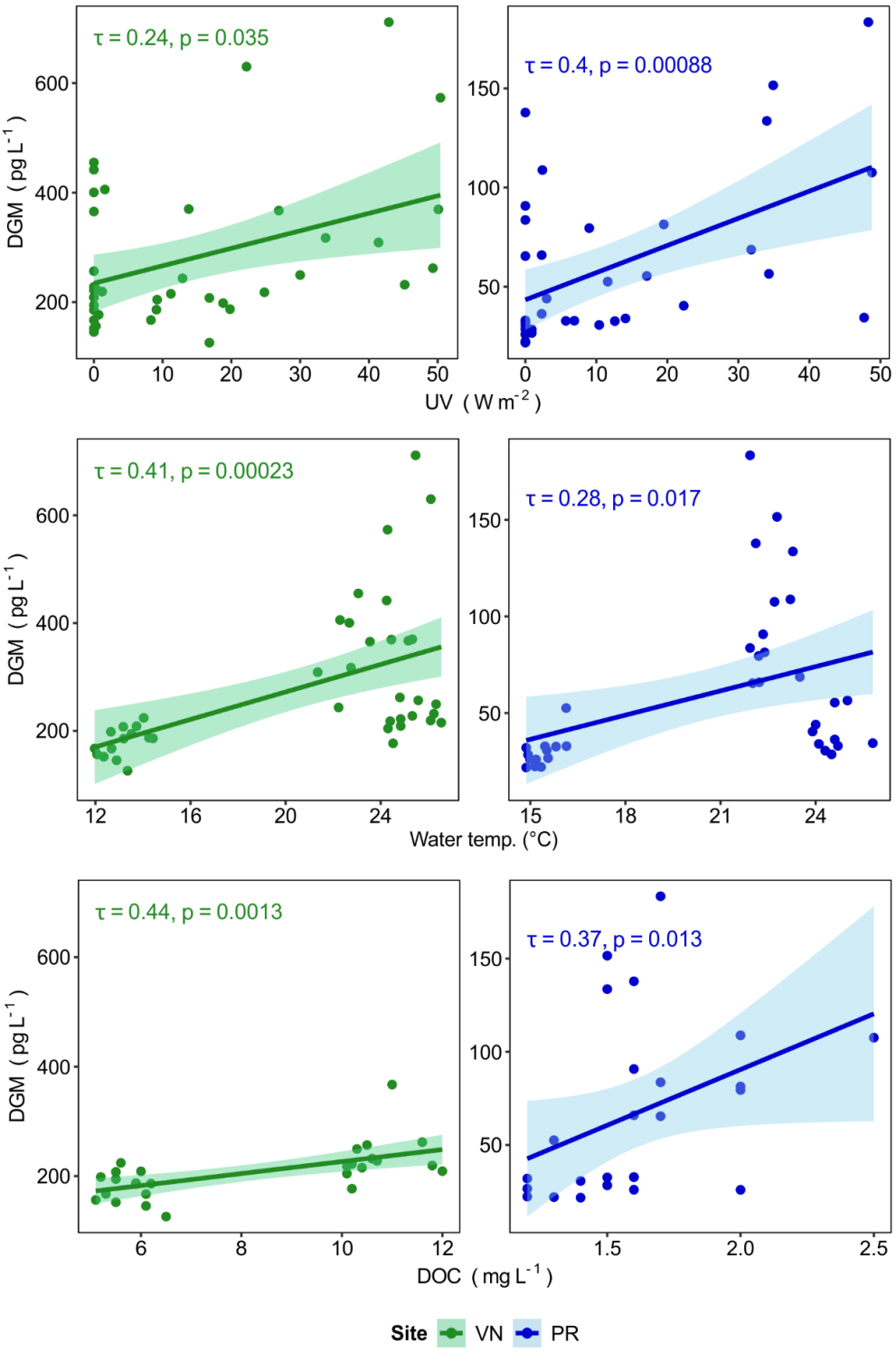

Figure S3: *overall correlation between DGM concentrations and UV radiation, water temperature, DOC concentrations at the two selected sites, Val Noghera fishfarm (VN) and Bay of Piran (PR).*

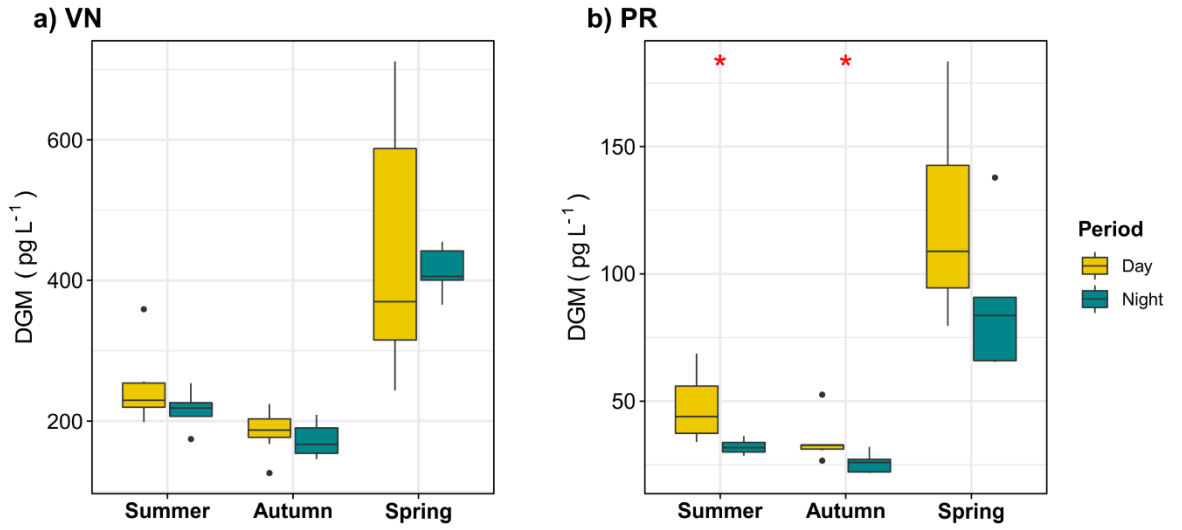

Figure S4: *distribution of DGM concentrations determined during day and night periods at the two sites, Val Noghera fishfarm (VN) and Bay of Piran (PR). Asterisks indicate statistically significant differences according to Kruskal-Wallis test (*p <0.05). (Note the difference in Y-axis scales).*

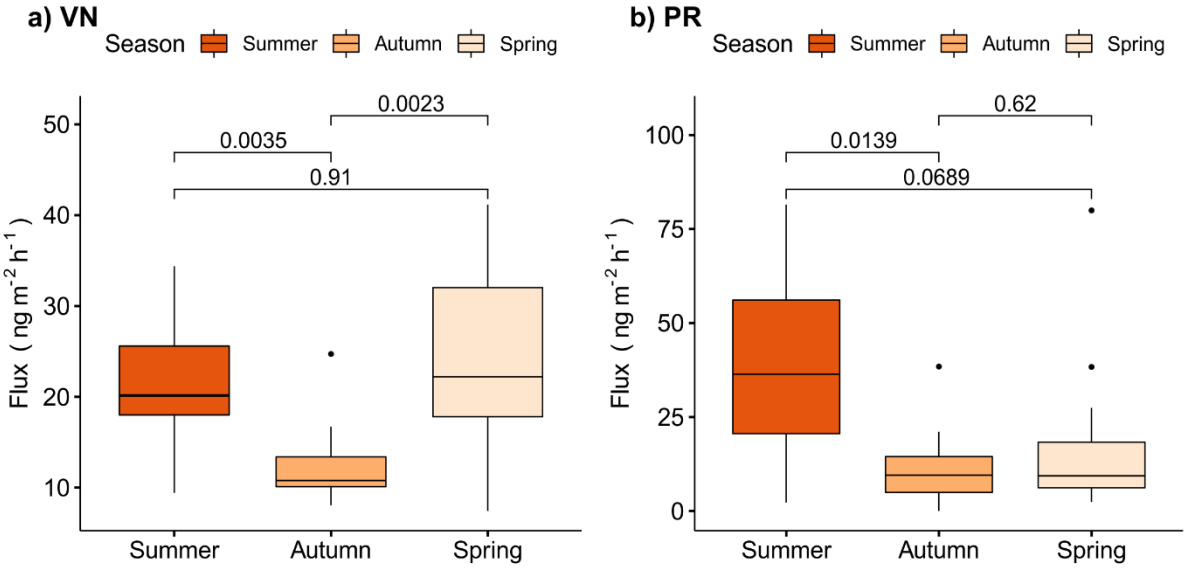

Figure S5: *variation of Hg^0 fluxes in the various seasons at the two selected sites, Val Noghera fishfarm (VN) and Bay of Piran (PR). The p-values of pairwise Dunn's post-hoc test are reported. (Note the difference in Y-axis scales).*

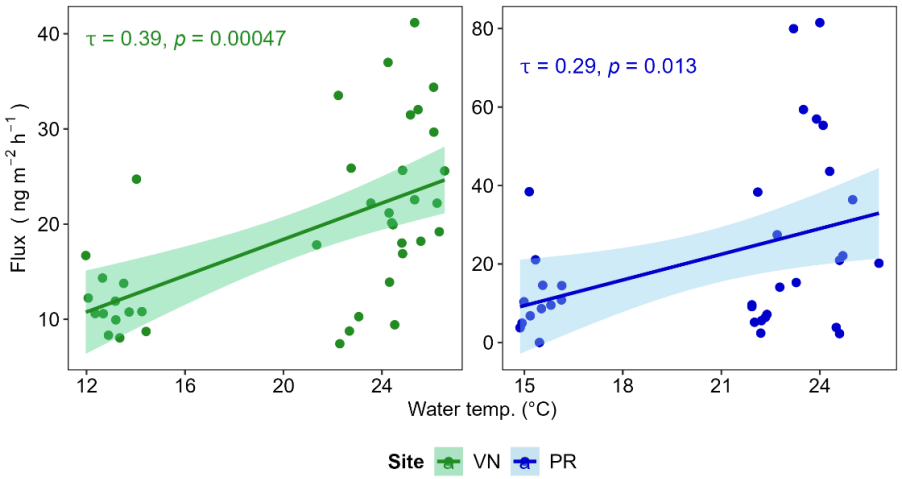

Figure S6: *overall correlation between water temperatures and Hg^0 fluxes at the selected sampling sites, Val Noghera fishfarm (VN) and Bay of Piran (PR). Kendall's rank correlation coefficient (τ) and 95% confidence intervals are reported.*

3.3 Article II: Hg^0 fluxes at water-air interface in freshwater environments

Gaseous mercury exchange from water-air interface in differently impacted freshwater environments.

Federico Floreani[1,2]*, Alessandro Acquavita[3], Nicolò Barago[1], Katja Klun[4], Jadran Faganeli[4], Stefano Covelli[1]

[1]Department of Mathematics & Geosciences, University of Trieste, Via E. Weiss 2, 34128 Trieste, Italy.

[2]Department of Life Sciences, University of Trieste, Via L. Giorgieri 5, 34127 Trieste, Italy

[3]ARPA FVG Regional Agency for Environmental Protection of Friuli Venezia Giulia, Via Cairoli 14, 33057, Palmanova (Udine), Italy

[4]Marine Biology Station, National Institute of Biology, Fornace 41, 6330 Piran, Slovenia

International Journal of
Environmental Research and Public Health

MDPI

Article

Gaseous Mercury Exchange from Water–Air Interface in Differently Impacted Freshwater Environments

Federico Floreani [1,2,*], Alessandro Acquavita [3], Nicolò Barago [1], Katja Klun [4], Jadran Faganeli [4] and Stefano Covelli [1]

1 Department of Mathematics & Geosciences, University of Trieste, Via Weiss 2, 34128 Trieste, Italy; nicolo.barago@phd.units.it (N.B.); covelli@units.it (S.C.)
2 Department of Life Sciences, University of Trieste, Via Giorgieri 5, 34127 Trieste, Italy
3 ARPA FVG Regional Agency for Environmental Protection of Friuli Venezia Giulia, Via Cairoli 14, 33057 Palmanova, Italy; alessandro.acquavita@arpa.fvg.it
4 Marine Biology Station, National Institute of Biology, Fornace 41, 6330 Piran, Slovenia; katja.klun@nib.si (K.K.); jadran.faganeli@nib.si (J.F.)
* Correspondence: federico.floreani@phd.units.it

Abstract: Gaseous exchanges of mercury (Hg) at the water–air interface in contaminated sites strongly influence its fate in the environment. In this study, diurnal gaseous Hg exchanges were seasonally evaluated by means of a floating flux chamber in two freshwater environments impacted by anthropogenic sources of Hg, specifically historical mining activity (Solkan Reservoir, Slovenia) and the chlor-alkali industry (Torviscosa dockyard, Italy), and in a pristine site, Cavazzo Lake (Italy). The highest fluxes (21.88 ± 11.55 ng m^{-2} h^{-1}) were observed at Solkan, coupled with high dissolved gaseous mercury (DGM) and dissolved Hg (THg_D) concentrations. Conversely, low vertical mixing and saltwater intrusion at Torviscosa limited Hg mobility through the water column, with higher Hg concentrations in the deep layer near the contaminated sediments. Consequently, both DGM and THg_D in surface water were generally lower at Torviscosa than at Solkan, resulting in lower fluxes (19.01 ± 12.65 ng m^{-2} h^{-1}). However, at this site, evasion may also be limited by high atmospheric Hg levels related to dispersion of emissions from the nearby chlor-alkali plant. Surprisingly, comparable fluxes (15.56 ± 12.78 ng m^{-2} h^{-1}) and Hg levels in water were observed at Cavazzo, suggesting a previously unidentified Hg input (atmospheric depositions or local geology). Overall, at all sites the fluxes were higher in the summer and correlated to incident UV radiation and water temperature due to enhanced photo production and diffusivity of DGM, the concentrations of which roughly followed the same seasonal trend.

Keywords: Idrija mercury mine; chlor-alkali plant; mercury evasion; dissolved gaseous mercury; flux chamber; water-air exchange

Citation: Floreani, F.; Acquavita, A.; Barago, N.; Klun, K.; Faganeli, J.; Covelli, S. Gaseous Mercury Exchange from Water–Air Interface in Differently Impacted Freshwater Environments. *Int. J. Environ. Res. Public Health* **2022**, *19*, 8149. https://doi.org/10.3390/ijerph19138149

Academic Editor: Paul B. Tchounwou

Received: 20 May 2022
Accepted: 30 June 2022
Published: 2 July 2022

1. Introduction

A key aspect of the Hg biogeochemical cycle is represented by gaseous exchanges between the atmosphere and natural surfaces. In the atmosphere, Hg can persist for more than 1 year due to the high volatility and low solubility of its elemental form (Hg^0 or GEM, Gaseous Elemental Mercury) [1], which undergoes long-range transport before being converted to the oxidised, more soluble and easily removable form (Hg^{2+}) [2,3]. In this way, Hg can reach and impact remote ecosystems far from the points of emission [4]. Direct atmospheric depositions and local supplies deriving from industrial discharge, surface run-off, soil erosion, and leaching are frequently considered the predominant forms of Hg input to freshwater ecosystems [5–8]. In aquatic environments, both inorganic and organic complexes of Hg^{2+} prevail, depending on pH and redox conditions [9], and their fate is deeply influenced by reactions and transformations involving the Hg^{2+} pool [10]. For example, deposited Hg can be promptly re-emitted to the atmosphere when reduced

to Hg^0 [11,12]. This recycling prolongs the lifespan of Hg in surface reservoirs, enhances its global distribution [13], and, particularly in aquatic ecosystems, contributes to limiting the amount of Hg available for the production/bioaccumulation/biomagnification of the neurotoxic species methylmercury (MeHg) [5,14–16]. In natural waters the volatile fraction of Hg, usually referred to as dissolved gaseous mercury (DGM), can account for 1–50% of the total Hg [17–19] and is mainly constituted by Hg^0 produced through abiotic (photochemical) or biotic reduction of Hg^{2+}. Photoreduction is considered the dominant process in surface waters [20] where it proceeds at higher rates than biotic reduction mediated by heterotrophic bacteria or algae [21,22]. The high energetic UV radiation (UV-A = 315–400 nm, UV-B = 280–315 nm) is highly effective in promoting DGM production [23–25], especially in waterbodies with low levels of dissolved organic carbon (DOC), where a high level of UV penetration through the water column is possible [26,27]. The direct photolysis of Hg^{2+} or the reduction mediated by dissolved organic matter (DOM) are the proposed mechanisms for Hg photoreduction [28], but the role of the latter is still unclear: Mercury complexation by DOM can indeed increase photoreduction by favouring the transfer of solar energy [29], but the formation of strong complexes between Hg^{2+} and reduced sulphur groups [30] can lower the amount of this metal available for photoreactions [31]. In the water column, DGM can be re-oxidised to Hg^{2+} with slower rates than photoreduction [32] mainly through photochemical pathways enhanced by the formation of oxidant radical species [24,33].

When the balance between reduction and oxidation in surface water leads to DGM supersaturation, evasion to the atmosphere can take place [34]. Even though emissions are strongly influenced by the concentration of DGM [35], gaseous Hg evasion to the atmosphere also depends on temperature and turbulent mixing induced by wind [36–38].

The estimate of gaseous Hg exchange from the surface of the water is of paramount importance to assess the fate of Hg in contaminated sites, as legacy emissions will continue to affect its cycling among ecosystems even for centuries [39]. Consequently, the Minamata Convention on Mercury highlighted the need to monitor Hg levels and processes in the environment, with particular focus on contaminated sites [40]. In this framework, the aim of this study was to evaluate gaseous Hg exchanges at the water–air interface (WAI) by means of a floating flux chamber (FC) coupled with a real-time GEM analyser in parallel with total dissolved Hg (THg_D) and DGM concentrations in two freshwater sites impacted by past anthropogenic activities (mining vs. chlor-alkali industry). In addition, a third site with no known Hg sources was selected as a pristine environment (Figure 1). Sampling was performed during the diurnal period in different seasons to elucidate the variability of the phenomenon in connection with the physico-chemical parameters of water and the meteorological conditions.

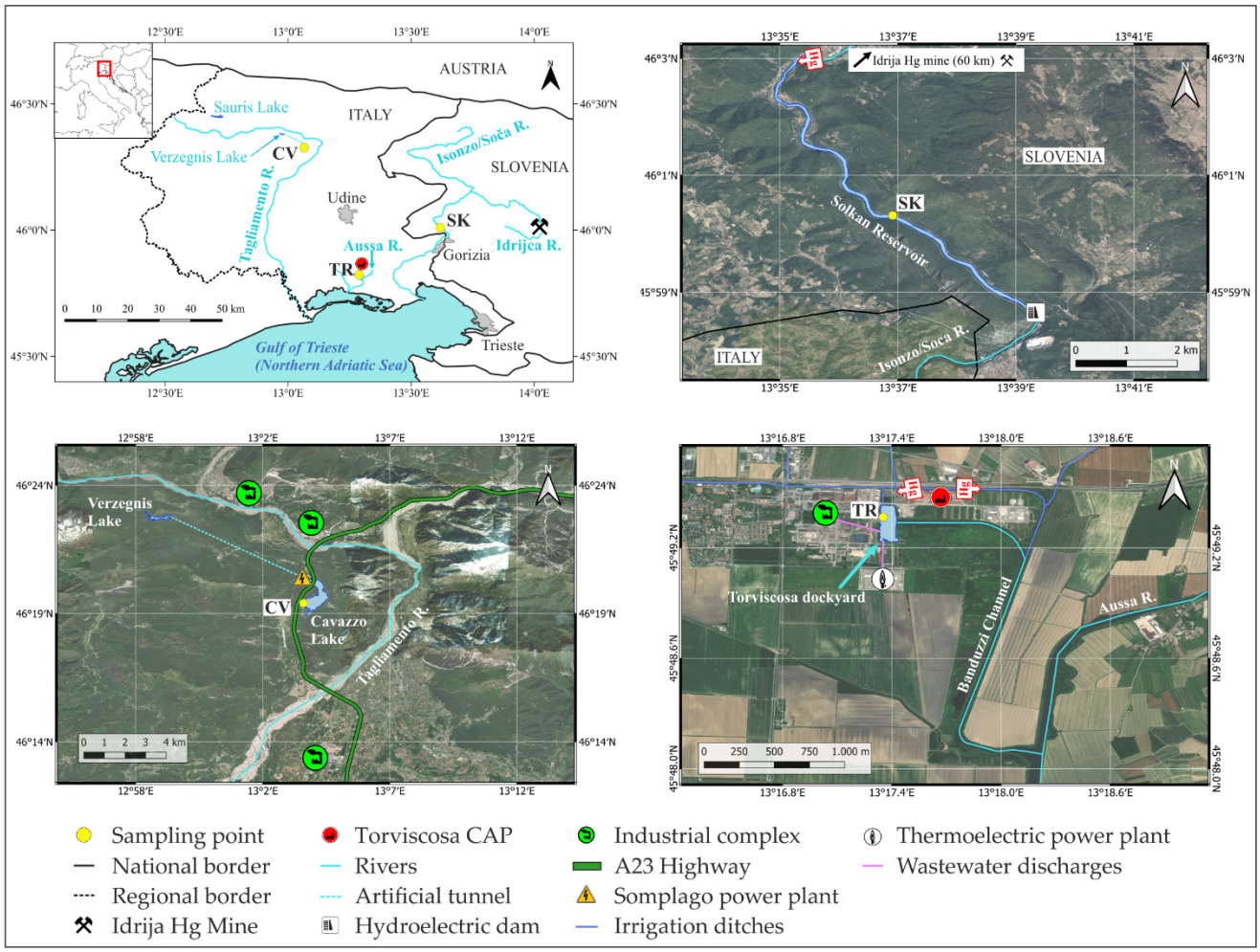

Figure 1. Study area and selected study sites.

2. Materials and Methods

2.1. Environmental Settings

The Torviscosa dockyard (site TR) is located inside the industrial complex in the low alluvial Friulian plain (NE Italy), the characteristics of which are described elsewhere [41,42]. Industrial activity started in 1937 with the production of cellulose from cane (*Arundo donax* sp.) coupled with a chlor-alkali plant (CAP) using Hg-cells in 1949 [43]. The dockyard extends 380 m N-S and 120 m E-W, with a variable water depth of between 0.3 and 6 m. Freshwater supplies come from numerous irrigation ditches which empty into a main drainage channel, where in the past CAP discharges converged and connected to the northern part of the dockyard. The site is also subject to the influence of the tide from the nearby Marano and Grado lagoon through the Aussa River, with the formation of a "saltwedge" [43]. Moreover, the current sewer drain of the industrial complex and the discharge of cooling waters from the local thermoelectric power plant are located in the southern part of the dockyard [44] and probably influence local water circulation, as a weak surface water current coming from this area was observed in field under ebb tide conditions, whereas a substantial stagnation was encountered during flood tide. The entire area of the complex was subject to the notable input of several contaminants (e.g., PTEs, dioxins, PAHs; [45]) and is currently classified as a contaminated site of national interest following Italian Ministerial Decrees 468/2001 and 222/2012. Mercury contamination is mainly attributable to the past uncontrolled discharges of the CAP: it was estimated that ~186 tons of Hg were discharged into the Aussa River between 1949 and 1984, when a modern wastewater system treatment was installed [43,46]. As a result, extremely high

concentrations of this metal are reported for sediments, waters, and air within the industrial complex [47], as well as for the fluvial waters and sediments of the Aussa River [43].

The Isonzo/Soča is a 138 km long alpine river with a catchment area of 3452 km^2 and represents the main freshwater input for the Gulf of Trieste, northern Adriatic Sea [48]. The hydrological regime is torrential and characterised by maximum flows in April and October/November, and minimum flows in February and August [49]. The course of the river is highly influenced by the presence of hydropower generating dams, which also strongly impacted sediment transport and aquatic ecosystems [50,51]. One of these dams delimits the Solkan artificial reservoir (SK, Figure 1), located about 40 km from the river mouth. The Solkan reservoir was dammed in 1984, has a maximum depth of 20 m, and a length of ~8 km [52]. The mean annual river discharge detected downstream from the reservoir is 80.4 m^3 s^{-1} [49]. The Isonzo/Soča River represents the main source of Hg into the Gulf of Trieste [53] due to the contaminated material supplied by one of its tributaries, the Idrijca River, which flows through the heavily contaminated historical Idrija Hg mining district [54]. Even though mining ceased in 1996, significant amounts of Hg are still delivered to the Adriatic Sea, mainly in particulate form due to the erosion of contaminated soils, riverbanks, and sediments [55,56], particularly during extreme rain events [57,58]. Covelli et al. [55,57] reported Hg concentrations at the Isonzo/Soča River mouth of 0.46–17.01 ng L^{-1} and of 0.83–112 ng L^{-1} in the dissolved phase and particulate phase, respectively, whereas higher values were found in the Idrijca River waters, particularly during intense rain events (dissolved Hg = 0.57–359 ng L^{-1} [59]; particulate Hg = 0.43–702 ng L^{-1} [56]). As a result of enhanced sedimentation caused by damming, sediments in artificial reservoirs can trap a significant amount of the pollutants transported by rivers [60]; for the Solkan reservoir, Hg concentrations found in sediments range between 5 and 20 mg kg^{-1} [50].

Cavazzo Lake (CV, Figure 1) is a natural freshwater basin located 195 m a.s.l. in the Carnian Alps (NE Italy). It occupies an area of approximately 1.3 km^2 and has a maximum depth of 38 m in its central part [61,62]. The lake was formed after the Last Glacial Maximum along the palaeochannel of the Tagliamento River in a secondary fluvio-glacial valley carved by glaciers and dammed by end moraine deposits [63,64]. Current natural freshwater supplies are constituted by several seasonally active streams. The lake was subject to notable anthropogenic impacts in the last decades that modified its catchment area: the building of the Somplago hydroelectric power plant, the concurrent digging of an outflow channel (1953–1958), and the construction of a highway viaduct (1973–1979) [62]. The Somplago power plant is fed by an artificial channel that receives water from two upstream artificial basins, Sauris Lake (977 m a.s.l.) and Verzegnis Lake (473 m a.s.l.), and drives cold water through a tunnel into Cavazzo Lake in its northern part [65]. Moreover, this channel strongly increased the sedimentary load to the lake, and sediments deposed after the 1950s show enrichments in Al, Ti, Fe, Sr, S, Zr, Zn, and Pb relative to pristine conditions; this is likely due to the different lithological characteristic of the catchments of the artificial lakes and direct anthropogenic discharges and emissions related to motor vehicle traffic and nearby industrial activities, since two industrial complexes (including plants for wood processing and metal, paper, cement, and steel production) are located within 10 km of the lake [62].

2.2. Sampling and Analyses

Gaseous Hg fluxes at the WAI were evaluated during summer (July 2020), autumn (October 2020), and spring (May 2021), while it was not possible to take measurements during winter due to restrictions related to the SARS-CoV2 outbreak. A plexiglass open-bottom floating flux chamber (FC) consisting of one section 50 × 50 × 50 cm, which sits on the surface, and another section 50 × 50 × 30 cm, which is submerged in the water [66–68], coupled with a real-time gaseous Hg analyser (Lumex RA915M, Lumex, St. Petersburg, Russia) was used [69]. The instrument facilitates the determination of GEM in the air over

a wide range of concentration (from 2 to 30,000 ng m^{-3}). Calibration is annually performed by the parent company and checked in the field using an internal reference cell.

Six distinct sets of measurements were taken per day at each study site (from T0 to T5) at regular intervals of 60–90 min. Operatively, the FC was placed on a floating foam board and then manually lowered to the water surface. During sampling, air was drawn through the FC by means of the Lumex internal pump at a constant rate (10 L min^{-1}), and GEM concentrations in the headspace were continuously recorded (1 s interval). The adopted flow rate is in the range of those previously used with a similarly shaped flux chamber, ranging between 5 and 20 L min^{-1} in ocean [68] and coastal contaminated environments [66,67], respectively. In this study, the flow rate is lower than those adopted in contaminated settings, since lower Hg concentrations were expected at Cavazzo and reduced flow rates are recommended in this case [70]; however, since a constant flow rate should be used when comparing different locations [71], the value adopted was kept high enough to avoid a potential excessive buildup of gaseous Hg inside the chamber at the sites of Solkan and Torviscosa, which could suppress the emissions. After deployment, the steady state of internal GEM was rapidly achieved (~10 min). At the end of each measure, the chamber was removed from the water, thus limiting its disturbance on the environmental parameters of the surface layer. Moreover, the immersion of the edges of the chamber for 30 cm in water ensures a tight seal, preventing the entry of outside air. Together with the relatively large size of the chamber, this also reduces the influence of other parameters, such as turbulent mixing and waves. However, all measurements were taken under relatively calm conditions, which were optimal for this technique [66]. Gaseous Hg fluxes (F, in ng m^{-2} h^{-1}) were then calculated according to the following equation [72]:

$$F = \frac{(C_o - C_i) \times Q}{A} \quad (1)$$

where Q is the air flow rate through the chamber, A is the surface area of the chamber (0.25 m^2), and $C_o - C_i$ is the difference between GEM concentrations in air exiting and entering the chamber (in ng m^{-3}). Chamber blanks were checked in the field at the beginning of each sampling day by sealing the FC bottom to a clean polycarbonate surface and they showed negligible values. After each sampling day, the FC was extensively cleaned with diluted laboratory detergent and rinsed several times with MilliQ water.

Atmospheric GEM levels were monitored at the beginning and the end of each sampling day for 20 min using the same sampling interval (1 s) by means of the same analyser; values below the limit of detection (LOD) were set to 1 ng m^{-3} (1/2 LOD) according to the medium bound approach [73].

The intensity of incoming UV radiation in the wavelength range between 250 and 400 nm was monitored in the field by means of a specific sensor (SU-420, Apogee Instruments, Logan, UT, USA) with a resolution of 0.1 W m^{-2}. The sensor was installed at ~2 m above ground in unshaded areas close to the sampling points and controlled by means of a laptop computer using Apogee Connect V1.05.003 software (Apogee Instruments, Logan, UT, USA). Data logging was programmed to record data at 1 min intervals as average values of readings were taken continuously every 1 s. Air temperature and relative humidity were also measured in the field using a portable thermohygrometer (HI9565, Hanna Instruments, Padova, Italy).

Temperature, pH, ORP, conductivity, salinity, and dissolved oxygen of surface water were measured in parallel with gaseous Hg fluxes by means of a portable multiprobe meter (HI98194, Hanna Instruments, Padova, Italy). Water samples were collected to determine dissolved organic carbon and gaseous mercury (DOC and DGM), and total dissolved Hg (THg_D). During summer and spring at site TR, additional water samples taken from the bottom water layer (~2.5 m) were collected using a Niskin bottle.

Water samples for DOC were filtered through pre-combusted (450 °C) Whatman GF/F filters (0.8 µm pore size), collected in glass containers, and frozen until analysis. Analytical determination was performed following a high-temperature catalytic method [74] using a

TOC-L Shimadzu analyser calibrated with potassium phthalate and checked via an analysis of certified reference material (Consensus Reference Material, University of Miami, Florida).

DGM was measured following the method described by O'Driscoll et al. [75] on a 1 L fixed volume of water bubbled in a glass container under low light conditions connected with the Lumex analyser in a closed loop circuit. The calculation of DGM (2) was performed on the basis of the equilibrium GEM concentration (GEM_{eq}) and the dimensionless Henry's law constant for Hg (H′) calculated in function of the water temperature [76]:

$$DGM = \frac{GEM_{eq}}{H'} \quad (2)$$

Samples for THg_D were filtered through Millipore Millex HA membrane filters (0.45 µm pore size) into pre-conditioned borosilicate bottles, immediately oxidised by the addition of BrCl (0.5 mL/100 mL sample), and preserved at +4 °C until analysis. Final determinations were conducted according to EPA Method 1631e using the cold vapour atomic fluorescence spectrometry technique (CV-AFS) with a specifically designed detector (Mercur, Analytik Jena, Jena, Germany). The instrument was calibrated using NIST 3133 certificated solution at different dilution levels and characterised by a LOD of 0.63 ng L^{-1} and a limit of quantification (LOQ) of 2.11 ng L^{-1} calculated on the basis of the standard deviations of ten reagent blanks.

Statistical analyses were performed using *R Software 4.1.3* (R Foundation for Statistical Computing, Vienna, Austria [77,78]). The Shapiro–Wilk test [79] was used to test the normal distribution of data and the non-parametric Kruskal-Wallis H test (K-W) to determine whether there were statistically significant differences between two or more groups of an independent variable after testing the normality [80]. As the occurrence of significant differences between data from different seasons was ascertained, Dunn's post hoc test [81] was performed using the "FSA" R package [82] to identify which groups differ. Finally, the non-parametric Kendall rank correlation coefficient was used to evaluate the associations among variables.

3. Results

A summary of data collected from all seasons at the selected sites is reported in Tables S1–S3. The variation in gaseous Hg fluxes at the WAI, together with DGM concentrations and incident UV radiation during the sampling periods, are depicted in Figure 2. All sampling campaigns were conducted under conditions of low wind speed and low water turbulence, optimal for the deployment of the flux chamber: hourly data recorded at selected monitoring stations near the sampling points showed that 52% of mean wind speeds during sampling periods were lower than 2 m s^{-1}, whereas only one average value was above 5.5 m s^{-1} ("moderate breeze" according to the Beaufort scale, Tables S1–S3). Wind data were provided by the Weather Forecast Regional Observatory of the Friuli Venezia Giulia region (OSMER-ARPA FVG) and the Slovenian Environmental Agency (ARSO) through the database "OMNIA" [83].

3.1. Summer

Measurements were performed on days characterised by sunny weather conditions and the absence of clouds, as evidenced by the UV incident radiation patterns (Figure 2a–c). The UV irradiation reached peaks at noon above 50 W m^{-2} at each site. As expected, the highest water temperatures were also observed during this season, slightly higher at TR (range = 19.37–22.90 °C) than the other two sites, where values ranged between 15.96 and 18.68 °C. DOC levels were comparable among all sites, with the highest value recorded at TR (average = 1.5 ± 0.7 mg L^{-1}) and the lowest at CV (average = 1.0 ± 0.2 mg L^{-1}).

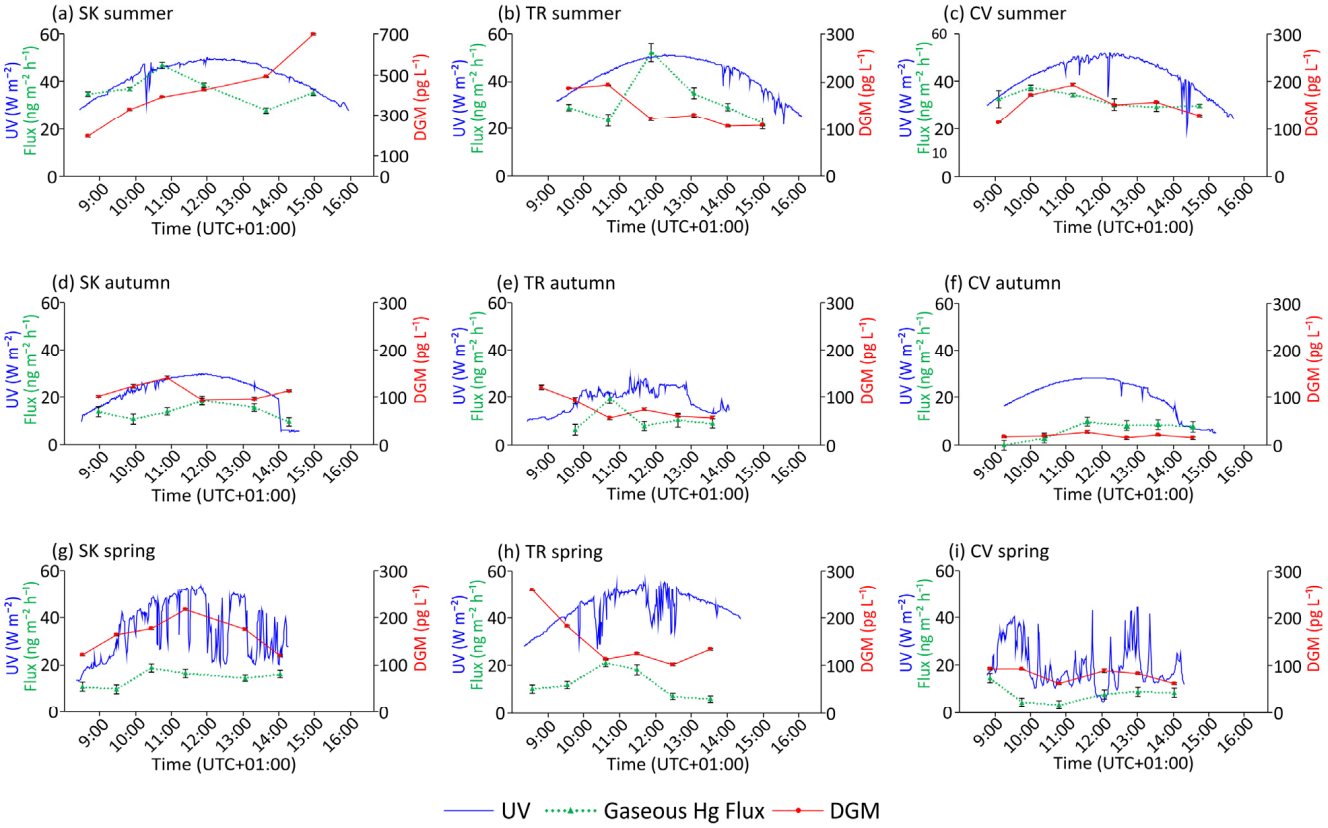

Figure 2. Variation in UV radiation, DGM concentration, and gaseous Hg flux during sampling periods in the different selected sites.

Overall, the highest THg_D concentrations in water (Figure S1) were observed at site SK (range = 13.27–32.22 ng L^{-1}), which also displayed a strong variability during the sampling period. Both TR and CV showed a diurnal variability characterised by minimum values in the central part of the day and a peak at T5 (TR = 10.66 ng L^{-1}, CV = 16.46 ng L^{-1}), and the concentrations were, on average, lower than those found at SK. Similarly, DGM concentrations were also higher at SK where an increasing trend was observed during the whole sampling period, from 197.5 to 696.1 pg L^{-1}. At TR and CV, the levels of DGM were comparable, although with different trends: in the first case the peaks were found in the morning (T0 and T1) followed by a sharp decrease to relatively constant values in the afternoon; in the second case DGM followed the incoming UV radiation pattern, reaching a peak of 194.0 pg L^{-1} at T2 and then decreasing in the afternoon.

As was the case for THg_D and DGM, gaseous Hg evasion fluxes at the WAI were also the highest in summer, ranging on average from 36.65 ± 6.15 ng m^{-2} h^{-1} found at SK to 32.45 ± 3.17 ng m^{-2} h^{-1} at CV, and with the maximum generally recorded at T2, shortly before the peak of radiation, followed by a decrease during the afternoon. At CV, gaseous Hg fluxes showed a smaller variability during the sampling period; in this case, values found in the afternoon were also lower, whereas the maximum was found at T1 in the middle of the morning (10 a.m. local solar time).

Overall, atmospheric GEM showed average values below 3 ng m^{-3}, higher at SK (2.77 ± 0.98 ng m^{-3}) than TR (1.92 ± 0.95 ng m^{-3}) and CV (1.30 ± 0.61 ng m^{-3}). Due to a technical issue, at the TR site only the afternoon measurement is available.

3.2. Autumn

Optimal weather conditions occurred during autumn sampling at SK and almost all day at CV, where increasing clouds were observed at the end of the sampling period (Figure 2d–f). In both cases, it is notable that the last measures were taken under conditions

of reduced irradiation. At TR, there was irregular cloud cover during the day, but it did not significantly affect the absolute value of incident UV radiation; the peaks were comparable at all sites and slightly below 30 W m^{-2}, obviously lower than those recorded in summer. As expected, water temperatures were lower than those found in summer at all sites and showed a low diurnal variability (<1 °C). Similar to summer, temperatures were about 2 °C higher at TR than at other sites (range = 13.86–14.87 °C). On average, DOC was higher than that observed in summer at both SK and CV (1.2 ± 0.2 mg L^{-1} and 1.5 ± 0.7 mg L^{-1}, respectively), whereas at TR a decrease was observed (average = 1.0 ± 0.3 mg L^{-1}).

THg_D levels were generally lower than those obtained for summer, especially at TR, where all values were below 2.65 ng L^{-1} (T2) (Figure S1). The highest concentrations were found at SK (maximum of 7.37 ng L^{-1}). DGM concentration was also lower than in summer, especially at SK, which is the site where the highest value of this season was recorded (range = 95.9–142.2 pg L^{-1}), whereas the lowest concentrations were found at CV (range = 55.8–66.4 pg L^{-1}). Here, the diurnal trend was comparable to that found in summer, although with less pronounced variability; the same is true for TR, where after a peak of 122.6 pg L^{-1} at T0, DGM dropped to values comparable to those observed in the lake. Conversely, at SK the diurnal variability was characterised by lower values of DGM after the peak recorded at T2.

Generally, gaseous Hg fluxes at the WAI in autumn were lower than in summer at SK and, in particular, at CV, as confirmed by the average diurnal values of 14.07 ± 3.19 ng m^{-2} h^{-1} and 7.46 ± 2.63 ng m^{-2} h^{-1}, respectively. It is notable that no gaseous Hg emission was detected at T0 in CV. In both cases, the diurnal trends of the gaseous Hg fluxes, especially at SK, were characterised by an upward increase to a peak around noon followed by an irregular decrease in the afternoon. Finally, gaseous Hg fluxes calculated for TR showed an irregular variability around values intermediate between SK and CV.

TR was also characterised by a high variability of atmospheric GEM, ranging from <2 ng m^{-3} to 543.61 ng m^{-3}, with the maximum detected in the morning. Atmospheric GEM concentrations found at other sites were significantly lower (<3 ng m^{-3} on average) and less variable.

3.3. Spring

During May 2021, weather conditions were mostly sunny at TR and variable at SK, but the absolute values of peak UV radiation were comparable to those observed in summer. Unfortunately, sampling at CV was conducted under more extended cloud cover (Figure 2g–i). Water temperatures at SK and CV were comparable to those found in autumn, ranging between 9.35 °C (CV at T5) and 10.48 °C (SK at T3), whereas values measured at TR were higher than the previous season (range = 16.11–16.80 °C). DOC concentration at CV was, on average, close to that observed in autumn (1.5 ± 0.5 mg L^{-1}), whereas both SK (average = 0.9 ± 0.3 mg L^{-1}) and TR (average = 0.8 ± 0.3 mg L^{-1}) were the lowest of all sampling campaigns.

THg_D showed a clear variability during the diurnal period (Figure S1), with higher concentrations generally found in the afternoon. Absolute values ranged from <0.63 ng L^{-1} (CV at T1) to 9.96 ng L^{-1} (SK at T4), and only at TR showed an increase compared to autumn. Conversely, DGM concentrations were generally higher than those found in autumn, although they did not reach the levels found during summer, except for the maximum value recorded at TR (259.7 pg L^{-1}), which was also the maximum recorded in this season. At SK and CV, DGM followed the UV radiation pattern despite the cloud cover at the latter site, whereas at TR, the trend was the same as other seasons with higher values in the morning.

Generally, the average diurnal gaseous Hg fluxes were of the same order of magnitude as those found in autumn: the lowest fluxes were calculated for CV (8.02 ± 3.96 ng m^{-2} h^{-1}), whereas the impacted sites SK and TR were comparable (14.91 ± 3.51 ng m^{-2} h^{-1} and 12.68 ± 6.08 ng m^{-2} h^{-1}, respectively). These latter sites also showed a similar variability over the sampling period, with the gaseous Hg evasion peak reached at T2 (between 10:30

and 11:00 local solar time). At site CV, gaseous Hg fluxes followed an opposite diurnal trend, with an initial decrease in the morning followed by an increasing trend in the afternoon.

Atmospheric GEM levels were the highest of all sampling campaigns, with average values of 4.61 ± 4.09 ng m^{-3} at SK and 3.61 ± 2.67 ng m^{-3} at CV. Extremely high values were again obtained at TR in the morning (up to 344.08 ng m^{-3}).

4. Discussion

Gaseous Hg evasion fluxes at the WAI displayed the highest average value at the Solkan Reservoir (SK, 21.88 ± 11.55 ng m^{-2} h^{-1}), which was impacted by historical Hg mining activity. This site was also characterised by both the highest THg_D (10.35 ± 8.29 ng L^{-1}, range = 2.27–32.22 ng L^{-1}) and DGM concentrations (232.6 ± 167.4 pg L^{-1}, range = 95.9–696.1 pg L^{-1}), which were comparable to those previously reported at the mouth of the Isonzo/Soča River [55,84], but generally lower than those of the Idrijca River [56], which flows through the Idrija mining district. Gaseous Hg evasion was slightly lower at the Torviscosa industrial site (TR, 19.01 ± 12.65 ng m^{-2} h^{-1}), where lower DGM levels (125.4 ± 52.9 pg L^{-1}, range = 58.1–259.7 pg L^{-1}) were found, likely as a result of the reduced availability of THg_D in the surface water layer (5.69 ± 3.51 ng L^{-1}, range = 1.61–13.68 ng L^{-1}), particularly if compared to values previously found downstream in the Aussa River (4.1–52.4 ng L^{-1}, [43]). Surprisingly, the gaseous Hg fluxes at Cavazzo Lake (i.e., the pristine area) (CV, 15.56 ± 12.78 ng m^{-2} h^{-1}) were similar to those obtained at the other sites, and both DGM (97.7 ± 44.7 pg L^{-1}; range = 55.8–194 pg L^{-1}) and THg_D (5.46 ± 4.51 ng L^{-1}, range ≤ 0.63–18.16 ng L^{-1}) were comparable to those observed at TR. To our knowledge, Hg supplies to Cavazzo Lake are unknown, thus it can be hypothesised that they may be related to emissions from the industrial complexes located about 10 km and downwind from the lake [85–87], but at present no data are available to confirm this hypothesis. In addition, DGM concentrations at CV were also comparable to those found in environments subjected to various anthropogenic sources (e.g., Juam Reservoir = 20–109 pg L^{-1}, [85]; Hongfeng Reservoir = 18–109 pg L^{-1}, [88]; and Big Dam West Lake = 32.4–182.6 pg L^{-1}, [17]), but higher than those commonly reported for background lakes in North America (≤60 pg L^{-1}; [22,34,89–91]). It should be noted that a geological origin of Hg from the catchment area of the hydroelectrical power plant cannot be excluded: the area is characterised by the presence of Triassic dolostones and limestones with bituminous levels rich in organic matter and carbon intervals [92]. These levels were exploited in the past for coal mining [93,94] and could potentially contain variable amounts of Hg, as reported for other bituminous coal from other areas in the world [95,96]. The increased sediment load to the lake generated by the discharge of the power plant potentially caused the subsequent rise in Hg inputs, as also observed for sulphur and organic carbon [62].

Overall, gaseous Hg fluxes are comparable to or slightly higher than those reported for other freshwater environments (Table 1) subject to Hg supplies from different sources (i.e., domestic and industrial wastewater discharge, atmospheric deposition on the local or long range scale [88,97,98]), but higher than those observed over various natural freshwater systems in North America (e.g., [34,37,99]).

Unfortunately, no measurements were conducted during the night and this could have led to an overestimation of the calculated daily gaseous Hg fluxes [91,97]. In addition, the methods employed for flux measurements add a certain degree of variability. In detail, micrometeorological models generally tend to underestimate the fluxes with respect to flux chamber deployments [17,19,100], but also differences in size, shape, and air turnover time within the chambers used can lead to different results [71]. Thus, our results are directly comparable with those reported using the same experimental approach for the Marano and Grado Lagoon [67], which is downstream from the sites selected in this work and is subject to the same Hg contamination sources (CAP and Hg mining at Idrija). The fluxes found in the lagoon environment were generally higher (range = 11.38–97.38 ng m^{-2} h^{-1}), likely due to the more elevated contamination of THg_D present in the water column and available for photoreduction to DGM. In our study, weak but statistically significant positive correlations

between THg_D and DGM concentrations were found both at SK ($\tau = 0.40$, $p < 0.05$) and TR ($\tau = 0.41$, $p < 0.05$), whereas this relationship was not significant at CV ($\tau = 0.13$, $p = 0.45$). Cavazzo Lake was the only site where a negative relationship between THg_D and DOC concentrations was observed ($\tau = -0.43$, $p < 0.05$). A possible explanation for these results could be related to an enhanced adsorption of Hg by organic matter and a subsequent reduced availability for photoreduction [28,31]; considering that DOC concentrations were comparable in all investigated sites, this effect may be caused by a different structure of the organic matter, e.g., a reduced content of chromophoric groups or a higher abundance of thiols [24], able to strongly bind Hg [30]. The enrichment of sulphur observed in the lake [62] may support this hypothesis, but further study is needed to better clarify the role of organic matter in Hg photochemistry in this environment.

Table 1. Comparison of gaseous Hg fluxes obtained in this study and over various freshwater systems. n.a. = not available, n.s. = not specified.

Measurement Site	Main Hg Source	Gaseous Hg Flux ($ng\ m^{-2}\ h^{-1}$)		Method	References
		Mean ± SD	Min–Max		
Solkan Reservoir (SLO)	Hg mining	21.88 ± 11.55	9.96–46.77	DFC	This study
Torviscosa dockyard (ITA)	CAP discharge	19.01 ± 12.65	6.21–52.71	DFC	This study
Lake of Cavazzo (ITA)	Unknown	15.56 ± 12.78	0–37.59	DFC	This study
Baihua Reservoir (CHI)	Organic chemical plant	7.6 ± 2.1	0–50.5	DFC	[98]
Hongfeng Reservoir (CHI)	Atmospheric depositions	5.4 ± 2.3	0.002–36.1	DFC	[88]
Wujiangdu Reservoir (CHI)	Wastewater discharge	-	−11.2–67.2	DFC	[101]
Suofengying Reservoir (CHI)	Wastewater discharge	-	−6.7–23.9	DFC	[101]
Big Dam West (CAN)	Atmospheric depositions	5.4 ± n.a.	0.8–43.8	DFC	[97]
North Cranberry (CAN)	Atmospheric depositions	1.1 ± n.a.	−2.0–13.5	DFC	[97]
Lake Lacawac (USA)	Atmospheric depositions	-	0.14–20.95	DFC	[102]
Puzzle Lake (CAN)	Atmospheric depositions	3.8 ± 2.6	−4.55–9.00	DFC	[17]
Lake Velenje (SLO)	Atmospheric depositions	5.9 ± n.a.	5.3–6.6	DFC	[100]
Lake Ontario (CAN-USA)	n.s.	-	0–9.07	MM	[37]
Lake Michigan (USA)	n.s.	-	0.6–1.6	MM	[34]
Cane Creek Lake (USA)	n.s.	-	0.6–1.2	DFC	[99]
Arbutus Lake (USA)	n.s.	1.6 ± 0.7	-	MM	[91]
Swedish River (SWE)	(Remote area)	11 ± n.a.	−2.5–88.9	DFC	[103]
Lake Gardsjon (SWE)	n.s.	8.5 ± 6.5	-	DFC	[36]
Florida Everglades (USA)	n.s.	1.2 ± 4.9	-	DFC	[104]

Generally, the gaseous Hg fluxes at the WAI were significantly higher in summer ($p < 0.05$, Dunn's test) than autumn and spring at all sites (Figure 3).

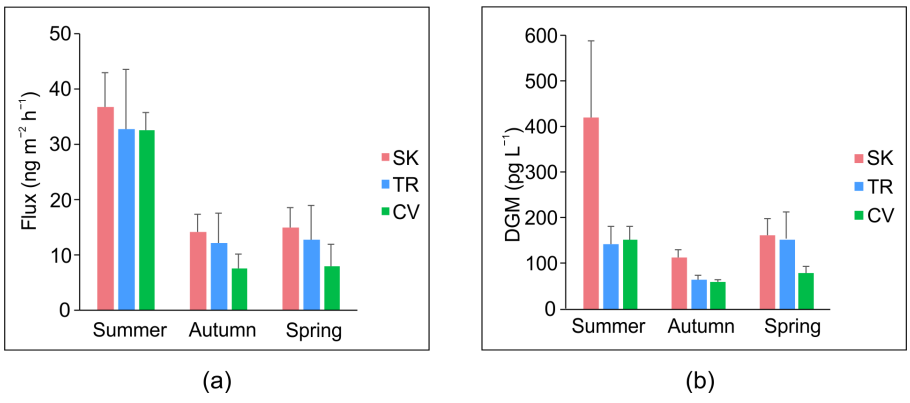

Figure 3. Average diurnal values over the various seasons and selected sampling sites of (**a**) gaseous Hg fluxes, (**b**) DGM concentrations.

The highest values of gaseous Hg fluxes found in summer are related to the intensity of the incident solar radiation, as observed in several studies conducted in both marine (e.g., [67,68,105]) and freshwater environments (e.g., [19,98,99]); in fact, solar radiation is a key factor in promoting a faster rate of DGM production in warmer periods via the photoreduction of Hg^{2+} in surface waters and the subsequent evasion to the atmosphere [26,106–108]. This was also confirmed in this study, as high DGM concentrations were detected in summer and the lowest in autumn in parallel with UV radiation intensity, which is most effective in systems with low DOC content that in turn allow for higher light penetration [24,26]. In this work, UV radiation and DGM contents were significantly correlated at both SK ($\tau = 0.62$, $p < 0.001$) and CV ($\tau = 0.62$, $p < 0.001$), but not at TR (Figure S2b) likely due to other atmospheric Hg inputs as discussed below. Similarly, gaseous Hg fluxes at SK and CV were significantly correlated with DGM concentrations (Figure 4), confirming the importance of this latter volatile form in Hg release at the WAI [19], even though it always accounted for less than 10% of THg_D. This value is in agreement with those usually reported for lake water ([35] and references therein).

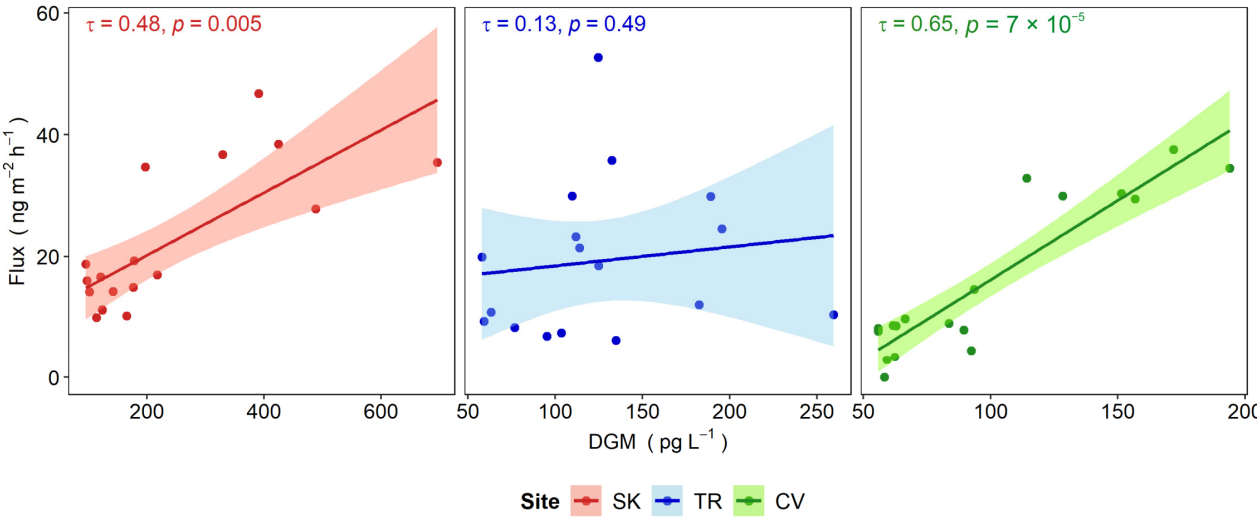

Figure 4. Correlation between DGM concentrations and gaseous Hg fluxes for the selected sampling sites. Kendall's rank correlation coefficients (τ) and 95% confidence intervals are reported.

As previously mentioned, at site TR no significant correlation between gaseous Hg fluxes and DGM was found, thus suggesting that Hg evasion in this site could be subject to different controls than the amount of DGM [99]. In this site, the strong UV irradiation in spring, with levels similar to summer conditions, potentially enhanced DGM production in addition to low DOC concentration, which could have favoured a higher penetration of radiation [31]. However, the reduced gaseous Hg evasion in spring lies in lower water temperatures compared to summer, as this parameter can significantly affect the equilibrium between water and air, enhancing the solubility of DGM at lower temperatures [98,109]. The positive influence of temperatures on gaseous Hg evasion has been observed in several studies (e.g., [101,103,110]), as was also found in this work (Figure 5).

In addition, gaseous Hg evasion at TR could also be limited by the presence of high atmospheric GEM and by the low dynamicity of the system. During each sampling campaign in this site, the highest DGM concentrations were observed in conjunction with relatively low gaseous Hg evasion and high GEM levels in the atmosphere (>500 ng m^{-3}), these latter likely due to the wind driven dispersion of the emissions from the old buildings of the dismissed CAP [47]. High atmospheric GEM can hinder evasion from water surfaces, decreasing the degree of saturation in DGM [34,101], and can also represent a source of Hg for surface water through direct dry depositions [111]. This experimental evidence is supported by the relatively high Hg concentrations found in lichens collected downwind

from the CAP [112]. In addition, the water column at site TR suffers from low mixing and thermoaline stratification with the occurrence of a "saltwedge", as previously observed in the connected Aussa River [43]. The stratification could limit the diffusion of DGM produced at the bottom of the dockyard as the result of dark abiotic and biotic reduction in the bottom water layer and contaminated sediments.

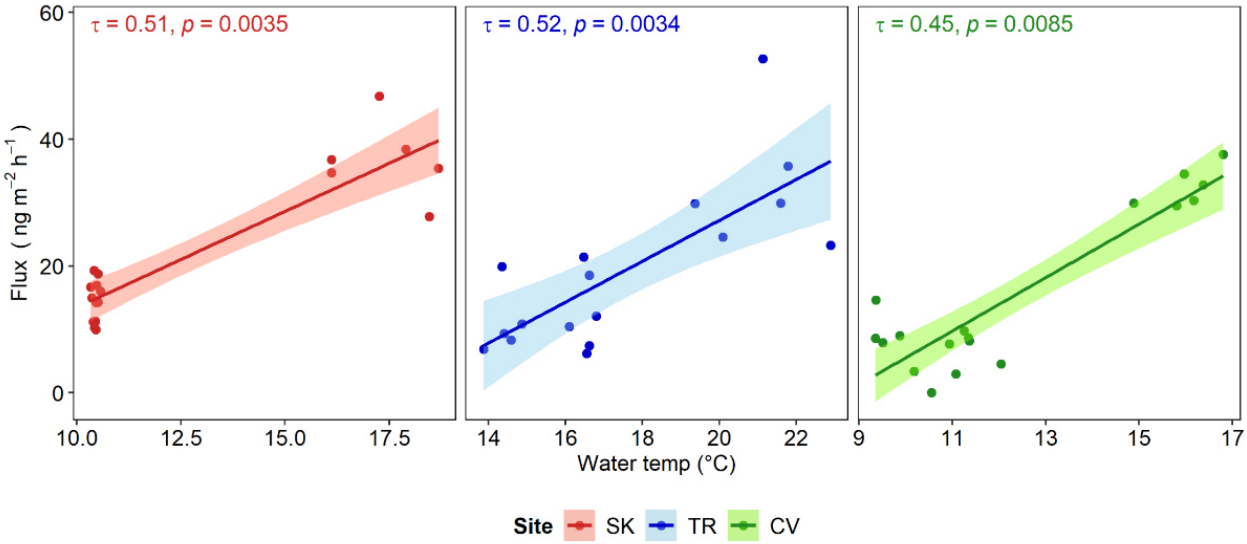

Figure 5. Correlation between water temperature and gaseous Hg fluxes for the selected sampling sites. Kendall's rank correlation coefficients (τ) and 95% confidence intervals are reported.

Dark abiotic reduction is mainly a consequence of Hg^{2+} interactions with DOM in the absence of light, particularly with humic substances [113]. The *Mer*-mediated bacterial reduction is catalyzed by Hg^{2+} reductase (Mer A) present in the Hg-resistant bacteria, and is mostly active in oxic environments [114]; the presence of these bacteria was previously reported for the contaminated sediments of the Aussa River [115], nearby our study area. Dark biotic reduction is linked to microbially mediated processes occurring in the dark, including the production and excretion of reducing compounds [116,117], cellular response to oxidative stress [118], DOM mineralisation [119], and unspecific reduction processes [120]. A further contribution to the DGM pool from demethylation reactions could not be excluded; mostly oxidative MeHg demethylation, mediated by sulphate-reducing bacteria producing Hg^{2+}, actively occurs in surface sediments of the Marano and Grado Lagoon, along with some reductive demethylation in oxic conditions producing Hg^0 [121]. Moreover, a pronounced Hg reduction potential in the water column of the nearby Gulf of Trieste, subject to relevant past Hg inputs [53], was demonstrated and assigned most likely to photochemical processes in summer and to phytoplankton (diatoms) and phytoplankton-associated bacterial taxa in autumn [122]. Among them, *Rhodobacteraceaea* and *Gammaproteobacteria* contain known Hg reducers. A recent study by Liang et al. demonstrated that Hg reduction mediated by phytoplankton and algal cell exudates can occur either under sunlit or dark conditions [123].

These processes, together with lower DGM diffusivity in saltwater than in freshwater [38], could explain the higher concentrations detected at the bottom water than in the surface water at the same time during summer at TR; in spring, the salt wedge did not occur, and this phenomenon was less evident (Table S4). In addition, DGM vertical diffusion could also be limited by losses through oxidation under low light conditions [124,125], complexation by chlorides [126], and enhanced flocculation at the salt and freshwater mix zone [55]. The progressive depletion of surface DGM during the sampling periods coupled with increasing evasion fluxes (Figure 2b,e,h) could further suggest limited supplies from

deep layers, as observed in other stratified lakes [102]. Further experimental studies are needed to confirm these hypotheses.

Differently from TR, the mining-impacted site of SK, located about 60 km downstream the Hg source, was characterised by lower atmospheric GEM concentrations, which were slightly higher than that of the natural background reported for the Northern Hemisphere (1.5–1.8 ng m^{-3}, [127]); this likely caused the surface water to be supersaturated in DGM with respect to the atmosphere over the study period, supporting the observed higher emissions [34]. In conditions of DGM supersaturation, indeed, the rate of gas exchange depends more on the transfer velocity through the interface rather than the occurring gradient concentration [37,38], thus the fluxes can also be influenced by wind speed, water current, turbulence, and turbidity [128]. In conditions of relatively high turbulence, the measures conducted with flux chambers can also be significantly affected [98]. The chamber design adopted in this study limits the influence of these parameters on the flux measured [66] and, in addition, all measures in this study were conducted under relatively calm conditions. However, a possible influence of water movement was detected at site SK, which, differently from TR, was located in a reservoir where the current is actively regulated by an artificial dam. Here, relatively higher DGM concentrations and gaseous Hg evasion occurred when an increase in water flow in the reservoir was observed. Water turbulence could promote both gaseous exchange at the WAI [129] and the DGM supply to the surface layer [67,102]. However, a possible contribution to DGM concentrations at SK related to transport of Hg forms from upstream, a process still ongoing along the Isonzo River both in dissolved form or bound to particulate or organic matter [84], cannot be ignored.

Cavazzo Lake is the only site where DGM concentration and gaseous Hg evasion always follow the incoming UV irradiation relatively well during the sampling period. This could support the hypothesis that Hg present in the area originates from the atmosphere, and it can be readily re-emitted to the atmosphere after deposition. Such recently deposed Hg^{2+} is more available for photoreactions [130] and quickly subject to reduction processes [5,131].

5. Conclusions

The formation of DGM and its subsequent volatilisation to the atmosphere are a notable pathway of the Hg biogeochemical cycle, promoting its removal from aquatic environments and thus reducing the pool available for methylation and bioaccumulation. In this context, the estimate of gaseous Hg exchange at the WAI provides useful information on the potential impact of Hg in the environment. In this work, relevant gaseous Hg evasion fluxes were measured in freshwater environments suffering from chlor-alkali industry (TR) and mining (SK) Hg contamination. This was particularly evident in summer when the fluxes were higher than those commonly observed in pristine environments, especially at SK, and suggests that these processes, enhanced by photo-reduction and water temperature, affect the environment even decades after the input of "fresh" Hg. The presence of comparable gaseous Hg fluxes at the pristine site CV suggests that this area should be further investigated for different aspects (i.e., atmospheric depositions, long-term atmospheric measurements, and sediment quality). Other questionable evidence arises at TR, where in spite of the significant contamination, evasion seems to be more affected by atmosphere and water column physico-chemical characteristics. At this site, measurements of benthic fluxes could elucidate the role of sediments as a sink or secondary source of Hg for the water column. In conclusion, the evaluation of gaseous Hg evasion during the nocturnal period would be helpful in reaching a better estimate of Hg budget in these environments, whereas more repeated measurements in each season would likely improve the definition of the pattern of gaseous Hg release during the day.

Supplementary Materials: The following supporting information can be downloaded at: https://www.mdpi.com/article/10.3390/ijerph19138149/s1, Table S1: summary of data collected during sampling at Solkan reservoir; Table S2: summary of data collected during sampling at Torviscosa dockyard; Table S3: summary of data collected during sampling at Cavazzo Lake; Figure S1: diurnal variation in THg_D concentrations at the selected sites; Figure S2: correlation between incident UV radiation and DGM concentrations; Table S4: parameters in surface and bottom water at TR site in summer and spring.

Author Contributions: Conceptualization and methodology, F.F., A.A. and S.C.; validation, F.F., S.C. and J.F.; formal analysis, F.F. and A.A.; investigation, F.F., A.A., S.C., N.B. and K.K.; resources, S.C., J.F. and K.K.; data curation, F.F.; writing—original draft preparation, F.F., A.A., S.C. and J.F.; visualization, F.F.; supervision, S.C. and J.F.; project administration, S.C. All authors have read and agreed to the published version of the manuscript.

Funding: This research received no external funding.

Institutional Review Board Statement: Not applicable.

Informed Consent Statement: Not applicable.

Data Availability Statement: The data presented in this study are available on request from the corresponding author. Meteorological data was obtained from OSMER-ARPA FVG and ARSO and are available upon request at http://www.meteo.fvg.it/ (accessed on 1 March 2022).

Acknowledgments: The authors are grateful to the mayor of Torviscosa (UD) Roberto Fasan and to Domenico Perosa who have allowed the access to the restricted area of Torviscosa dockyard and supported the sampling operations. OSMER-ARPA FVG and ARSO are acknowledged for providing meteorological wind data. A special thanks to thank Marco Burello, Gabriele Faoro, Valeria Zappella, and Samuel Princi for their valuable support in sampling operations. Karry Close is warmly acknowledged for proofreading the manuscript. The four anonymous reviewers are warmly acknowledged for their reviews and useful suggestions, which improved the earlier version of the manuscript.

Conflicts of Interest: The authors declare no conflict of interest.

References

1. Ariya, P.A.; Amyot, M.; Dastoor, A.; Deeds, D.; Feinberg, A.; Kos, G.; Poulain, A.; Ryjkov, A.; Semeniuk, K.; Subir, M.; et al. Mercury Physicochemical and Biogeochemical Transformation in the Atmosphere and at Atmospheric Interfaces: A Review and Future Directions. *Chem. Rev.* **2015**, *115*, 3760–3802. [CrossRef] [PubMed]
2. Amos, H.M.; Jacob, D.J.; Holmes, C.D.; Fisher, J.A.; Wang, Q.; Yantosca, R.M.; Corbitt, E.S.; Galarneau, E.; Rutter, A.P.; Gustin, M.S.; et al. Gas-Particle Partitioning of Atmospheric Hg (II) and Its Effect on Global Mercury Deposition. *Atmos. Chem. Phys.* **2012**, *12*, 591–603. [CrossRef]
3. Schroeder, W.H.; Munthe, J. Atmospheric Mercury—An Overview. *Atmos. Environ.* **1998**, *32*, 809–822. [CrossRef]
4. Fitzgerald, W.F.; Engstrom, D.R.; Mason, R.P.; Nater, E.A. The Case for Atmospheric Mercury Contamination in Remote Areas. *Environ. Sci. Technol.* **1998**, *32*, 1–7. [CrossRef]
5. Hines, N.A.; Brezonik, P.L. Mercury Inputs and Outputs at a Small Lake in Northern Minnesota. *Biogeochemistry* **2007**, *84*, 265–284. [CrossRef]
6. Brigham, M.E.; Wentz, D.A.; Aiken, G.R.; Krabbenhoft, D.P. Mercury Cycling in Stream Ecosystems. 1. Water Column Chemistry and Transport. *Environ. Sci. Technol.* **2009**, *43*, 2720–2725. [CrossRef]
7. Chen, J.; Hintelmann, H.; Zheng, W.; Feng, X.; Cai, H.; Wang, Z.; Yuan, S.; Wang, Z. Isotopic Evidence for Distinct Sources of Mercury in Lake Waters and Sediments. *Chem. Geol.* **2016**, *426*, 33–44. [CrossRef]
8. Kocman, D.; Wilson, S.J.; Amos, H.M.; Telmer, K.H.; Steenhuisen, F.; Sunderland, E.M.; Mason, R.P.; Outridge, P.; Horvat, M. Toward an Assessment of the Global Inventory of Present-Day Mercury Releases to Freshwater Environments. *Int. J. Environ. Res. Public Health* **2017**, *14*, 138. [CrossRef] [PubMed]
9. Ullrich, S.M.; Tanton, T.W.; Abdrashitova, S.A. Mercury in the Aquatic Environment: A Review of Factors Affecting Methylation. *Crit. Rev. Environ. Sci. Technol.* **2001**, *31*, 241–293. [CrossRef]
10. Fitzgerald, W.F.; Lamborg, C.H.; Hammerschmidt, C.R. Marine Biogeochemical Cycling of Mercury. *Chem. Rev.* **2007**, *107*, 641–662. [CrossRef] [PubMed]
11. Strode, S.A.; Jaeglé, L.; Selin, N.E.; Jacob, D.J.; Park, R.J.; Yantosca, R.M.; Mason, R.P.; Slemr, F. Air-Sea Exchange in the Global Mercury Cycle. *Glob. Biogeochem. Cycles* **2007**, *21*, 1–12. [CrossRef]

12. Poulain, A.J.; Orihel, D.M.; Amyot, M.; Paterson, M.J.; Hintelmann, H.; Southworth, G.R. Relationship between the Loading Rate of Inorganic Mercury to Aquatic Ecosystems and Dissolved Gaseous Mercury Production and Evasion. *Chemosphere* **2006**, *65*, 2199–2207. [CrossRef] [PubMed]
13. Amos, H.M.; Jacob, D.J.; Streets, D.G.; Sunderland, E.M. Legacy Impacts of All-Time Anthropogenic Emissions on the Global Mercury Cycle. *Glob. Biogeochem. Cycles* **2013**, *27*, 410–421. [CrossRef]
14. Morel, F.M.M.; Kraepiel, A.M.L.; Amyot, M. The Chemical Cycle and Bioaccumulation of Mercury. *Annu. Rev. Ecol. Syst.* **1998**, *29*, 543–566. [CrossRef]
15. Fitzgerald, W.F.; Clarkson, T.W. Mercury and Monomethylmercury: Present and Future Concerns. *Environ. Health Perspect.* **1991**, *96*, 159–166. [CrossRef] [PubMed]
16. Rice, K.M.; Walker, E.M.; Wu, M.; Gillette, C.; Blough, E.R. Environmental Mercury and Its Toxic Effects. *J. Prev. Med. Public Health* **2014**, *47*, 74–83. [CrossRef]
17. O'Driscoll, N.J.; Beauchamp, S.; Siciliano, S.D.; Rencz, A.N.; Lean, D.R.S. Continuous Analysis of Dissolved Gaseous Mercury (DGM) and Mercury Flux in Two Freshwater Lakes in Kejimkujik Park, Nova Scotia: Evaluating Mercury Flux Models with Quantitative Data. *Environ. Sci. Technol.* **2003**, *37*, 2226–2235. [CrossRef] [PubMed]
18. Muresan, B.; Cossa, D.; Richard, S.; Burban, B. Mercury Speciation and Exchanges at the Air-Water Interface of a Tropical Artificial Reservoir, French Guiana. *Sci. Total Environ.* **2007**, *385*, 132–145. [CrossRef] [PubMed]
19. Fu, X.; Feng, X.; Guo, Y.; Meng, B.; Yin, R.; Yao, H. Distribution and Production of Reactive Mercury and Dissolved Gaseous Mercury in Surface Waters and Water/Air Mercury Flux in Reservoirs on Wujiang River, Southwest China. *J. Geophys. Res. Atmos.* **2013**, *118*, 3905–3917. [CrossRef]
20. Poulain, A.J.; Amyot, M.; Findlay, D.; Telor, S.; Barkay, T.; Hintelmann, H. Biological and Photochemical Production of Dissolved Gaseous Mercury in a Boreal Lake. *Limnol. Oceanogr.* **2004**, *49*, 2265–2275. [CrossRef]
21. Ahn, M.C.; Kim, B.; Holsen, T.M.; Yi, S.M.; Han, Y.J. Factors Influencing Concentrations of Dissolved Gaseous Mercury (DGM) and Total Mercury (TM) in an Artificial Reservoir. *Environ. Pollut.* **2010**, *158*, 347–355. [CrossRef] [PubMed]
22. Lepak, R.F.; Tate, M.T.; Ogorek, J.M.; DeWild, J.F.; Peterson, B.D.; Hurley, J.P.; Krabbenhoft, D.P. Aqueous Elemental Mercury Production versus Mercury Inventories in the Lake Michigan Airshed: Deciphering the Spatial and Diel Controls of Mercury Gradients in Air and Water. *ACS EST Water* **2021**, *1*, 719–727. [CrossRef]
23. Amyot, M.; Gill, G.A.; Morel, F.M.M. Production and Loss of Dissolved Gaseous Mercury in Coastal Seawater. *Environ. Sci. Technol.* **1997**, *31*, 3606–3611. [CrossRef]
24. Oh, S.; Kim, M.K.; Lee, Y.M.; Zoh, K.D. Effect of Abiotic and Biotic Factors on the Photo-Induced Production of Dissolved Gaseous Mercury. *Water Air Soil Pollut.* **2011**, *220*, 353–363. [CrossRef]
25. Bonzongo, J.C.J.; Donkor, A.K. Increasing UV-B Radiation at the Earth's Surface and Potential Effects on Aqueous Mercury Cycling and Toxicity. *Chemosphere* **2003**, *52*, 1263–1273. [CrossRef]
26. Amyot, M.; Mierle, G.; Lean, D.; Mcqueen, D.J. Effect of Solar Radiation on the Formation of Dissolved Gaseous Mercury in Temperate Lakes. *Geochim. Cosmochim. Acta* **1997**, *61*, 975–987. [CrossRef]
27. Haverstock, S.; Sizmur, T.; Murimboh, J.; O'Driscoll, N.J. Modeling the Photo-Oxidation of Dissolved Organic Matter by Ultraviolet Radiation in Freshwater Lakes: Implications for Mercury Bioavailability. *Chemosphere* **2012**, *88*, 1220–1226. [CrossRef] [PubMed]
28. Luo, H.; Cheng, Q.; Pan, X. Photochemical Behaviors of Mercury (Hg) Species in Aquatic Systems: A Systematic Review on Reaction Process, Mechanism, and Influencing Factor. *Sci. Total Environ.* **2020**, *720*, 137540. [CrossRef] [PubMed]
29. Jeremiason, J.D.; Portner, J.C.; Aiken, G.R.; Hiranaka, A.J.; Dvorak, M.T.; Tran, K.T.; Latch, D.E. Photoreduction of Hg(II) and Photodemethylation of Methylmercury: The Key Role of Thiol Sites on Dissolved Organic Matter. *Environ. Sci. Process. Impacts* **2015**, *17*, 1892–1903. [CrossRef] [PubMed]
30. Ravichandran, M. Interactions between Mercury and Dissolved Organic Matter—A Review. *Chemosphere* **2004**, *55*, 319–331. [CrossRef] [PubMed]
31. O'Driscoll, N.J.; Vost, E.; Mann, E.; Klapstein, S.; Tordon, R.; Lukeman, M. Mercury Photoreduction and Photooxidation in Lakes: Effects of Filtration and Dissolved Organic Carbon Concentration. *J. Environ. Sci.* **2018**, *68*, 151–159. [CrossRef] [PubMed]
32. Whalin, L.; Kim, E.H.; Mason, R. Factors Influencing the Oxidation, Reduction, Methylation and Demethylation of Mercury Species in Coastal Waters. *Mar. Chem.* **2007**, *107*, 278–294. [CrossRef]
33. He, F.; Zhao, W.; Liang, L.; Gu, B. Photochemical Oxidation of Dissolved Elemental Mercury by Carbonate Radicals in Water. *Environ. Sci. Technol. Lett.* **2014**, *1*, 499–503. [CrossRef]
34. Vette, A.F.; Landis, M.S.; Keeler, G.J. Deposition and Emission of Gaseous Mercury to and from Lake Michigan during the Lake Michigan Mass Balance Study (July 1994–October 1995). *Environ. Sci. Technol.* **2002**, *36*, 4525–4532. [CrossRef] [PubMed]
35. Southworth, G.; Lindberg, S.; Hintelmann, H.; Amyot, M.; Poulain, A.; Bogle, M.A.; Peterson, M.; Rudd, J.; Harris, R.; Sandilands, K.; et al. Evasion of Added Isotopic Mercury from a Northern Temperate Lake. *Environ. Toxicol. Chem.* **2007**, *26*, 53–60. [CrossRef] [PubMed]
36. Lindberg, S.I.S.; Meyers, T.P. Evasion of Mercury Vapor from the Surface of a Recently Limed Acid Lake Forest in Sweden. *Water Air Soil Pollut.* **1995**, *85*, 725–730. [CrossRef]
37. Poissant, L.; Amyot, M.; Pilote, M.; Lean, D. Mercury Water—Air Exchange over the Upper St. Lawrence River and Lake Ontario. *Environ. Sci. Technol.* **2000**, *34*, 3069–3078. [CrossRef]

38. Kuss, J.; Holzmann, J.; Ludwig, R. An Elemental Mercury Diffusion Coefficient for Natural Waters Determined by Molecular Dynamics Simulation. *Environ. Sci. Technol.* **2009**, *43*, 3183–3186. [CrossRef]
39. Obrist, D.; Kirk, J.L.; Zhang, L.; Sunderland, E.M.; Jiskra, M.; Selin, N.E. A Review of Global Environmental Mercury Processes in Response to Human and Natural Perturbations: Changes of Emissions, Climate, and Land Use. *Ambio* **2018**, *47*, 116–140. [CrossRef]
40. Selin, H.; Keane, S.E.; Wang, S.; Selin, N.E.; Davis, K.; Bally, D. Linking Science and Policy to Support the Implementation of the Minamata Convention on Mercury. *Ambio* **2018**, *47*, 198–215. [CrossRef]
41. Stefani, C.; Fellin, M.G.; Zattin, M.; Zuffa, G.G.; Dalmonte, C.; Mancin, N.; Zanferrari, A. Provenance and Paleogeographic Evolution in a Multi-Source Foreland: The Cenozoic Venetian-Friulian Basin (NE Italy). *J. Sediment. Res.* **2007**, *77*, 867–887. [CrossRef]
42. Fontana, A.; Mozzi, P.; Bondesan, A. Alluvial Megafans in the Venetian-Friulian Plain (North-Eastern Italy): Evidence of Sedimentary and Erosive Phases during Late Pleistocene and Holocene. *Quat. Int.* **2008**, *189*, 71–90. [CrossRef]
43. Covelli, S.; Acquavita, A.; Piani, R.; Predonzani, S.; De Vittor, C. Recent Contamination of Mercury in an Estuarine Environment (Marano Lagoon, Northern Adriatic, Italy). *Estuar. Coast. Shelf Sci.* **2009**, *82*, 273–284. [CrossRef]
44. Regione Autonoma Friuli Venezia Giulia. Piano Regionale di Tutela Delle Acque. 2012. Available online: https://www.regione.fvg.it/rafvg/cms/RAFVG/ambiente-territorio/pianificazione-gestione-territorio/FOGLIA20/ (accessed on 6 May 2022).
45. Ramieri, E.; Barbanti, A.; Picone, M.; Menchini, G.; Bressan, E.; Dal Forno, E. Integrated Plan for the Sustainable Management of the Lagoon of Marano and Grado. *Littoral* **2011**, 05008. [CrossRef]
46. Piani, R.; Covelli, S.; Biester, H. Mercury Contamination in Marano Lagoon (Northern Adriatic Sea, Italy): Source Identification by Analyses of Hg Phases. *Appl. Geochem.* **2005**, *20*, 1546–1559. [CrossRef]
47. Acquavita, A.; Biasiol, S.; Lizzi, D.; Mattassi, G.; Pasquon, M.; Skert, N.; Marchiol, L. Gaseous Elemental Mercury Level and Distribution in a Heavily Contaminated Site: The Ex-Chlor Alkali Plant in Torviscosa (Northern Italy). *Water Air Soil Pollut.* **2017**, *228*, 62. [CrossRef]
48. Cozzi, S.; Falconi, C.; Comici, C.; Čermelj, B.; Kovac, N.; Turk, V.; Giani, M. Recent Evolution of River Discharges in the Gulf of Trieste and Their Potential Response to Climate Changes and Anthropogenic Pressure. *Estuar. Coast. Shelf Sci.* **2012**, *115*, 14–24. [CrossRef]
49. Comici, C.; Bussani, A. Analysis of the River Isonzo Discharge (1998–2005). *Boll. Geofis. Teor. Appl.* **2007**, *48*, 435–454.
50. Hines, M.E.; Faganeli, J.; Adatto, I.; Horvat, M. Microbial Mercury Transformations in Marine, Estuarine and Freshwater Sediment Downstream of the Idrija Mercury Mine, Slovenia. *Appl. Geochem.* **2006**, *21*, 1924–1939. [CrossRef]
51. Smolar-Žvanut, N.; Mikoš, M. The Impact of Flow Regulation by Hydropower Dams on the Periphyton Community in the Soča River, Slovenia. *Hydrol. Sci. J.* **2014**, *59*, 1032–1045. [CrossRef]
52. Siché, I.; Arnaud-Fassetta, G. Anthropogenic Activities since the End of the Little Ice Age: A Critical Factor Driving Fuvial Changes on the Isonzo River (Italy, Slovenia). *Mediterranee* **2014**, *122*, 183–199. [CrossRef]
53. Covelli, S.; Faganeli, J.; Horvat, M.; Brambati, A. Mercury Contamination of Coastal Sediments as the Result of Long-Term Cinnabar Mining Activity (Gulf of Trieste, Northern Adriatic Sea). *Appl. Geochem.* **2001**, *16*, 541–558. [CrossRef]
54. Gosar, M.; Pirc, S.; Bidovec, M. Mercury in the Idrijca River Sediments as a Reflection of Mining and Smelting Activities of the Idrija Mercury Mine. *J. Geochem. Explor.* **1997**, *58*, 125–131. [CrossRef]
55. Covelli, S.; Piani, R.; Kotnik, J.; Horvat, M.; Faganeli, J.; Brambati, A. Behaviour of Hg Species in a Microtidal Deltaic System: The Isonzo River Mouth (Northern Adriatic Sea). *Sci. Total Environ.* **2006**, *368*, 210–223. [CrossRef] [PubMed]
56. Kocman, D.; Kanduč, T.; Ogrinc, N.; Horvat, M. Distribution and Partitioning of Mercury in a River Catchment Impacted by Former Mercury Mining Activity. *Biogeochemistry* **2011**, *104*, 183–201. [CrossRef]
57. Covelli, S.; Piani, R.; Acquavita, A.; Predonzani, S.; Faganeli, J. Transport and Dispersion of Particulate Hg Associated with a River Plume in Coastal Northern Adriatic Environments. *Mar. Pollut. Bull.* **2007**, *55*, 436–450. [CrossRef] [PubMed]
58. Baptista-Salazar, C.; Biester, H. The Role of Hydrological Conditions for Riverine Hg Species Transport in the Idrija Mining Area. *Environ. Pollut.* **2019**, *247*, 716–724. [CrossRef]
59. Baptista-Salazar, C.; Richard, J.H.; Horf, M.; Rejc, M.; Gosar, M.; Biester, H. Grain-Size Dependence of Mercury Speciation in River Suspended Matter, Sediments and Soils in a Mercury Mining Area at Varying Hydrological Conditions. *Appl. Geochem.* **2017**, *81*, 132–142. [CrossRef]
60. Majerová, L.; Bábek, O.; Navrátil, T.; Nováková, T.; Štojdl, J.; Elznicová, J.; Hron, K.; Matys Grygar, T. Dam Reservoirs as an Efficient Trap for Historical Pollution: The Passage of Hg and Pb through the Ohře River, Czech Republic. *Environ. Earth Sci.* **2018**, *77*, 574. [CrossRef]
61. Colizza, E.; Fanzutti, G.P.; Melis, R.; Polano, S.; Pugliese, N.; Andreetto, G.; Bavdaz, R.; Bitsikas, H.; Cabras, C.; Carta, A.; et al. Primi Risultati Sui Sedimenti e Sulle Ostracofaune Del Lago Di Cavazzo o Dei Tre Comuni (Udine). In Proceedings of the Atti Tavola Rotonda "Ecologia e Paleontologia", Gradisca d'Isonzo, Italy, 12 December 1988; pp. 51–80.
62. Polonia, A.; Albertazzi, S.; Bellucci, L.G.; Bonetti, C.; Bonetti, J.; Giorgetti, G.; Giuliani, S.; Correa, M.L.; Mayr, C.; Peruzza, L.; et al. Decoding a Complex Record of Anthropogenic and Natural Impacts in the Lake of Cavazzo Sediments, NE Italy. *Sci. Total Environ.* **2021**, *787*, 147659. [CrossRef]
63. Marinelli, O. Studi Sul Lago Di Cavazzo. *Boll. Soc. Geogr. It.* **1894**, *43*, 174–214.

64. Venturini, C.; Discenza, K. Stratigrafia e Paleo-Idrografia Del Friuli Centrale (Prealpi Carniche) Miocene Superiore-Pliocene Inferiore. *Gortania Udine* **2010**, *30*, 31–52.
65. Pironio, P.; Dri, G.; Rabassi, V. Condizioni Fisiche Del Lago Di Cavazzo o Dei Tre Comuni: Un Patrimonio Da Salvare e Valorizzare. In Proceedings of the Convegno Tecnico Scientifico, Alesso di Trasaghis, Italy, 12–13 September 1987.
66. Bagnato, E.; Sproveri, M.; Barra, M.; Bitetto, M.; Bonsignore, M.; Calabrese, S.; Di Stefano, V.; Oliveri, E.; Parello, F.; Mazzola, S. The Sea-Air Exchange of Mercury (Hg) in the Marine Boundary Layer of the Augusta Basin (Southern Italy): Concentrations and Evasion Flux. *Chemosphere* **2013**, *93*, 2024–2032. [CrossRef] [PubMed]
67. Floreani, F.; Acquavita, A.; Petranich, E.; Covelli, S. Diurnal Fluxes of Gaseous Elemental Mercury from the Water-Air Interface in Coastal Environments of the Northern Adriatic Sea. *Sci. Total Environ.* **2019**, *668*, 925–935. [CrossRef] [PubMed]
68. Kalinchuk, V.V.; Lopatnikov, E.A.; Astakhov, A.S.; Ivanov, M.V.; Hu, L. Distribution of Atmospheric Gaseous Elemental Mercury (Hg(0)) from the Sea of Japan to the Arctic, and Hg(0) Evasion Fluxes in the Eastern Arctic Seas: Results from a Joint Russian-Chinese Cruise in Fall 2018. *Sci. Total Environ.* **2021**, *753*, 142003. [CrossRef] [PubMed]
69. Sholupov, S.E.; Ganeyev, A.A. Zeeman Atomic Absorption Spectrometry Using High Frequency Modulated Light Polarization. *Spectrochim. Acta Part B At. Spectrosc.* **1995**, *50*, 1227–1236. [CrossRef]
70. Engle, M.A.; Gustin, M.S.; Goff, F.; Counce, D.A.; Janik, C.J.; Bergfeld, D.; Rytuba, J.J. Atmospheric Mercury Emissions from Substrates and Fumaroles Associated with Three Hydrothermal Systems in the Western United States. *J. Geophys. Res. Atmos.* **2006**, *111*. [CrossRef]
71. Eckley, C.S.; Gustin, M.; Lin, C.J.; Li, X.; Miller, M.B. The Influence of Dynamic Chamber Design and Operating Parameters on Calculated Surface-to-Air Mercury Fluxes. *Atmos. Environ.* **2010**, *44*, 194–203. [CrossRef]
72. Carpi, A.; Lindberg, S.E. Application of a Teflon® Dynamic Flux Chamber for Quantifying Soil Mercury Flux: Tests and Results over Background Soil. *Atmos. Environ.* **1998**, *32*, 873–882. [CrossRef]
73. *EPA/600/R-96/084*; U. S. Environmental Protection Agency Office of Environmental Information Guidance for Data Quality Assessment: Practical Methods for Data Analysis EPA QA/G-9 QA00 UPDATE. U. S. Environmental Protection Agency Office: Washington, DC, USA, 2000.
74. Sugimura, Y.; Suzuki, Y. A High-Temperature Catalytic Oxidation Method for the Determination of Non-Volatile Dissolved Organic Carbon in Seawater by Direct Injection of a Liquid Sample. *Mar. Chem.* **1988**, *24*, 105–131. [CrossRef]
75. O'Driscoll, N.J.; Covelli, S.; Petranich, E.; Floreani, F.; Klapstein, S.; Acquavita, A. Dissolved Gaseous Mercury Production at a Marine Aquaculture Site in the Mercury-Contaminated Marano and Grado Lagoon, Italy. *Bull. Environ. Contam. Toxicol.* **2019**, *103*, 218–224. [CrossRef] [PubMed]
76. Andersson, M.E.; Gårdfeldt, K.; Wängberg, I.; Strömberg, D. Determination of Henry's Law Constant for Elemental Mercury. *Chemosphere* **2008**, *73*, 587–592. [CrossRef] [PubMed]
77. *RCoreTeam R: A Language and Environment for Statistical Computing*; R Foundation for Statistical Computing: Vienna, Austria, 2022; Available online: https://www.r-project.org/ (accessed on 21 April 2022).
78. Wickham, H. *Ggplot2: Elegant Graphics for Data Analysis*; Springer: New York, NY, USA, 2016; ISBN 978-3-319-24277-4.
79. Shapiro, S.; Wilk, M.B. An Analysis of Variance Test for Normality (Complete Samples). In *Biometrika*; Oxford University Press: Oxford, UK, 1965; Volume 52, pp. 591–611. Available online: http://www.jstor.org/stable/2333709 (accessed on 1 March 2022).
80. Zar, J.H. *Biostatistical Analysis*; Prentice Hall: Upper Saddle River, NJ, USA, 1996; ISBN 0130845426 9780130845429.
81. Dunn, O.J. Multiple Comparisons Using Rank Sums. *Technometrics* **1964**, *6*, 241–252. [CrossRef]
82. Ogle, D.H.; Doll, J.C.; Wheeler, P.; Dinno, A. *FSA: Fisheries Stock Analysis Package*, Version 0.9.3. 2022. Available online: https://github.com/fishR-Core-Team/FSA (accessed on 1 March 2022).
83. OSMER-ARPA FVG, "OMNIA" database. Available online: http://www.meteo.fvg.it/ (accessed on 16 June 2022).
84. Bratkič, A.; Ogrinc, N.; Kotnik, J.; Faganeli, J.; Žagar, D.; Yano, S.; Tada, A.; Horvat, M. Mercury Speciation Driven by Seasonal Changes in a Contaminated Estuarine Environment. *Environ. Res.* **2013**, *125*, 171–178. [CrossRef] [PubMed]
85. Park, J.S.; Oh, S.; Shin, M.Y.; Kim, M.K.; Yi, S.M.; Zoh, K.D. Seasonal Variation in Dissolved Gaseous Mercury and Total Mercury Concentrations in Juam Reservoir, Korea. *Environ. Pollut.* **2008**, *154*, 12–20. [CrossRef]
86. Guédron, S.; Amouroux, D.; Sabatier, P.; Desplanque, C.; Develle, A.L.; Barre, J.; Feng, C.; Guiter, F.; Arnaud, F.; Reyss, J.L.; et al. A Hundred Year Record of Industrial and Urban Development in French Alps Combining Hg Accumulation Rates and Isotope Composition in Sediment Archives from Lake Luitel. *Chem. Geol.* **2016**, *431*, 10–19. [CrossRef]
87. Roberts, S.; Kirk, J.L.; Wiklund, J.A.; Muir, D.C.G.; Yang, F.; Gleason, A.; Lawson, G. Mercury and Metal(Loid) Deposition to Remote Nova Scotia Lakes from Both Local and Distant Sources. *Sci. Total Environ.* **2019**, *675*, 192–202. [CrossRef]
88. Feng, X.; Wang, S.; Qiu, G.; He, T.; Li, G.; Li, Z.; Shang, L. Total Gaseous Mercury Exchange between Water and Air during Cloudy Weather Conditions over Hongfeng Reservoir, Guizhou, China. *J. Geophys. Res. Atmos.* **2008**, *113*, D15309. [CrossRef]
89. Dill, C.; Kuiken, T.; Zhang, H.; Ensor, M. Diurnal Variation of Dissolved Gaseous Mercury (DGM) Levels in a Southern Reservoir Lake (Tennessee, USA) in Relation to Solar Radiation. *Sci. Total Environ.* **2006**, *357*, 176–193. [CrossRef]
90. O'Driscoll, N.J.; Poissant, L.; Canário, J.; Ridal, J.; Lean, D.R.S. Continuous Analysis of Dissolved Gaseous Mercury and Mercury Volatilization in the Upper St. Lawrence River: Exploring Temporal Relationships and UV Attenuation. *Environ. Sci. Technol.* **2007**, *41*, 5342–5348. [CrossRef]
91. Selvendiran, P.; Driscoll, C.T.; Montesdeoca, M.R.; Choi, H.D.; Holsen, T.M. Mercury Dynamics and Transport in Two Adirondack Lakes. *Limnol. Oceanogr.* **2009**, *54*, 413–427. [CrossRef]

92. Carulli, G.B. Note Illustrative Carta Geologica del Friuli Venezia Giulia 1:150.000. 2006. Available online: https://www.regione.fvg.it/rafvg/cms/RAFVG/ambiente-territorio/geologia/FOGLIA01/ (accessed on 1 March 2022).
93. Dell'Oste, G.; Gemo, G.; Tacus, N.; Dell'Oste, D.; Tacus, S. *Il Carbone Di Creta d'Oro. Storia Della Miniera Di Cludinico*; Forum Editrice: Udine, Italy, 2012.
94. Ponton, M. Dolomie Bituminose Nella Dolomia Principale: La Miniera Del Rio Resartico (Prealpi Giulie—Italia). *Gortania Geol. Paleontol. Paletnologia* **2016**, *38*, 9–37.
95. Auguścik-Górajek, J.; Nieć, M. The Variability of Mercury Content in Bituminous Coal Seams in the Coal Basins in Poland. *Resources* **2020**, *9*, 127. [CrossRef]
96. Yudovich, Y.E.; Ketris, M.P. Mercury in Coal: A Review. Part 1. Geochemistry. *Int. J. Coal Geol.* **2005**, *62*, 107–134. [CrossRef]
97. Boudala, F.S.; Folkins, I.; Beauchamp, S.; Tordon, R.; Neima, J.; Johnson, B. Mercury Flux Measurements over Air and Water in Kejimkujik National Park, Nova Scotia. *Water Air Soil Pollut.* **2000**, *122*, 183–202. [CrossRef]
98. Feng, X.; Yan, H.; Wang, S.; Qiu, G.; Tang, S.; Shang, L.; Dai, Q.; Hou, Y. Seasonal Variation of Gaseous Mercury Exchange Rate between Air and Water Surface over Baihua Reservoir, Guizhou, China. *Atmos. Environ.* **2004**, *38*, 4721–4732. [CrossRef]
99. Crocker, W.C.; Zhang, H. Seasonal and Diurnal Variation of Air/Water Exchange of Gaseous Mercury in a Southern Reservoir Lake (Cane Creek Lake, Tennessee, USA). *Water* **2020**, *12*, 2102. [CrossRef]
100. Kotnik, J.; Horvat, M.; Fajon, V.; Logar, M. Mercury in Small Freshwater Lakes: A Case Study: Lake Velenje, Slovenia. *Water Air Soil Pollut.* **2002**, *134*, 319–339. [CrossRef]
101. Fu, X.; Feng, X.; Wan, Q.; Meng, B.; Yan, H.; Guo, Y. Probing Hg Evasion from Surface Waters of Two Chinese Hyper/Meso-Eutrophic Reservoirs. *Sci. Total Environ.* **2010**, *408*, 5887–5896. [CrossRef] [PubMed]
102. Wollenberg, J.L.; Peters, S.C. Mercury Emission from a Temperate Lake during Autumn Turnover. *Sci. Total Environ.* **2009**, *407*, 2909–2918. [CrossRef] [PubMed]
103. Gårdfeldt, K.; Feng, X.; Sommar, J.; Lindqvist, O. Total Gaseous Mercury Exchange between Air and Water at River and Sea Surfaces in Swedish Coastal Regions. *Atmos. Environ.* **2001**, *35*, 3027–3038. [CrossRef]
104. Lindberg, S.E.; Zhang, H. Air/Water Exchange of Mercury in the Everglades II: Measuring and Modeling Evasion of Mercury from Surface Waters in the Everglades Nutrient Removal Project. *Sci. Total Environ.* **2000**, *259*, 135–143. [CrossRef]
105. Ferrara, R.; Mazzolai, B.; Lanzillotta, E.; Nucaro, E.; Pirrone, N. Temporal Trends in Gaseous Mercury Evasion from the Mediterranean Seawaters. *Sci. Total Environ.* **2000**, *259*, 183–190. [CrossRef]
106. Tseng, C.M.; Lamborg, C.; Fitzgerald, W.F.; Engstrom, D.R. Cycling of Dissolved Elemental Mercury in Arctic Alaskan Lakes. *Geochim. Cosmochim. Acta* **2004**, *68*, 1173–1184. [CrossRef]
107. Zhang, H.; Dill, C. Apparent Rates of Production and Loss of Dissolved Gaseous Mercury (DGM) in a Southern Reservoir Lake (Tennessee, USA). *Sci. Total Environ.* **2008**, *392*, 233–241. [CrossRef] [PubMed]
108. Peters, S.C.; Wollenberg, J.L.; Morris, D.P.; Porter, J.A. Mercury Emission to the Atmosphere from Experimental Manipulation of DOC and UVR in Mesoscale Field Chambers in a Freshwater Lake. *Environ. Sci. Technol.* **2007**, *41*, 7356–7362. [CrossRef] [PubMed]
109. Sanemasa, I. The Solubility of Elemental Mercury Vapor in Water. *Bull. Chem. Soc. Jpn.* **1975**, *48*, 1795–1798. [CrossRef]
110. Cizdziel, J.V.; Zhang, Y.; Nallamothu, D.; Brewer, J.S.; Gao, Z. Air/Surface Exchange of Gaseous Elemental Mercury at Different Landscapes in Mississippi, USA. *Atmosphere* **2019**, *10*, 538. [CrossRef]
111. Wang, C.; Wang, Z.; Zhang, X. Characteristics of the Air–sea Exchange of Gaseous Mercury and Deposition Flux of Atmospheric Mercury at an Island near the Boundary of the Bohai Sea and Yellow Sea. *Atmos. Environ.* **2020**, *232*, 117547. [CrossRef]
112. Floreani, F.; Barago, N.; Acquavita, A.; Covelli, S.; Skert, N.; Higueras, P. Spatial Distribution and Biomonitoring of Atmospheric Mercury Concentrations over a Contaminated Coastal Lagoon (Northern Adriatic, Italy). *Atmosphere* **2020**, *11*, 1280. [CrossRef]
113. Vudamala, K.; Chakraborty, P.; Sailaja, B.B.V. An Insight into Mercury Reduction Process by Humic Substances in Aqueous Medium under Dark Condition. *Environ. Sci. Pollut. Res.* **2017**, *24*, 14499–14507. [CrossRef] [PubMed]
114. Barkay, T.; Miller, S.M.; Summers, A.O. Bacterial Mercury Resistance from Atoms to Ecosystems. *FEMS Microbiol. Rev.* **2003**, *27*, 355–384. [CrossRef]
115. Baldi, F.; Marchetto, D.; Gallo, M.; Fani, R.; Maida, I.; Covelli, S.; Fajon, V.; Zizek, S.; Hines, M.; Horvat, M. Chlor-Alkali Plant Contamination of Aussa River Sediments Induced a Large Hg-Resistant Bacterial Community. *Estuar. Coast. Shelf Sci.* **2012**, *113*, 96–104. [CrossRef]
116. Lanzillotta, E.; Ceccarini, C.; Ferrara, R.; Dini, F.; Frontini, F.P.; Banchetti, R. Importance of the Biogenic Organic Matter in Photo-Formation of Dissolved Gaseous Mercury in a Culture of the Marine Diatom *Chaetoceros* sp. *Sci. Total Environ.* **2004**, *318*, 211–221. [CrossRef]
117. Grégoire, D.S.; Poulain, A.J. A Physiological Role for HgII during Phototrophic Growth. *Nat. Geosci.* **2016**, *9*, 121–125. [CrossRef]
118. Barkay, T.; Wagner-Döbler, I.B.T.-A. *Microbial Transformations of Mercury: Potentials, Challenges, and Achievements in Controlling Mercury Toxicity in the Environment*; Academic Press: Cambridge, MA, USA, 2005; Volume 57, pp. 1–52, ISBN 0065-2164.
119. Lin, C.-C.; Yee, N.; Barkay, T. Microbial Transformations in the Mercury Cycle. In *Environmental Chemistry and Toxicology of Mercury*; Liu, G., Cai, Y., O'Driscoll, N.J., Eds.; John Wiley and Sons: Hoboken, NJ, USA, 2012; pp. 155–192. ISBN 978-047057872-8.
120. Fantozzi, L.; Ferrara, R.; Frontini, F.P.; Dini, F. Dissolved Gaseous Mercury Production in the Dark: Evidence for the Fundamental Role of Bacteria in Different Types of Mediterranean Water Bodies. *Sci. Total Environ.* **2009**, *407*, 917–924. [CrossRef]

121. Hines, M.E.; Poitras, E.N.; Covelli, S.; Faganeli, J.; Emili, A.; Žižek, S.; Horvat, M. Mercury Methylation and Demethylation in Hg-Contaminated Lagoon Sediments (Marano and Grado Lagoon, Italy). *Estuar. Coast. Shelf Sci.* **2012**, *113*, 85–95. [CrossRef]
122. Bratkič, A.; Tinta, T.; Koron, N.; Guevara, S.R.; Begu, E.; Barkay, T.; Horvat, M.; Falnoga, I.; Faganeli, J. Mercury Transformations in a Coastal Water Column (Gulf of Trieste, Northern Adriatic Sea). *Mar. Chem.* **2018**, *200*, 57–67. [CrossRef]
123. Liang, X.; Zhu, N.; Johs, A.; Chen, H.; Pelletier, D.A.; Zhang, L.; Yin, X.; Gao, Y.; Zhao, J.; Gu, B. Mercury Reduction, Uptake, and Species Transformation by Freshwater Alga Chlorella Vulgaris under Sunlit and Dark Conditions. *Environ. Sci. Technol.* **2022**, *56*, 4961–4969. [CrossRef] [PubMed]
124. Garcia, E.; Poulain, A.J.; Amyot, M.; Ariya, P.A. Diel Variations in Photoinduced Oxidation of Hg0 in Freshwater. *Chemosphere* **2005**, *59*, 977–981. [CrossRef] [PubMed]
125. Lalonde, J.D.; Amyot, M.; Kraepiel, A.M.L.; Morel, F.M.M. Photooxidation of Hg(0) in Artificial and Natural Waters. *Environ. Sci. Technol.* **2001**, *35*, 1367–1372. [CrossRef] [PubMed]
126. Ramalhosa, E.; Pereira, E.; Vale, C.; Válega, M.; Monterroso, P.; Duarte, A.C. Mercury Distribution in Douro Estuary (Portugal). *Mar. Pollut. Bull.* **2005**, *50*, 1218–1222. [CrossRef] [PubMed]
127. Valente, R.J.; Shea, C.; Lynn Humes, K.; Tanner, R.L. Atmospheric Mercury in the Great Smoky Mountains Compared to Regional and Global Levels. *Atmos. Environ.* **2007**, *41*, 1861–1873. [CrossRef]
128. Sharif, A.; Tessier, E.; Bouchet, S.; Monperrus, M.; Pinaly, H.; Amouroux, D. Comparison of Different Air-Water Gas Exchange Models to Determine Gaseous Mercury Evasion from Different European Coastal Lagoons and Estuaries. *Water Air Soil Pollut.* **2013**, *224*, 1606. [CrossRef]
129. Schmidt, R.; Schneider, B. The Effect of Surface Films on the Air-Sea Gas Exchange in the Baltic Sea. *Mar. Chem.* **2011**, *126*, 56–62. [CrossRef]
130. Luo, H.W.; Yin, X.; Jubb, A.M.; Chen, H.; Lu, X.; Zhang, W.; Lin, H.; Yu, H.Q.; Liang, L.; Sheng, G.P.; et al. Photochemical Reactions between Mercury (Hg) and Dissolved Organic Matter Decrease Hg Bioavailability and Methylation. *Environ. Pollut.* **2017**, *220*, 1359–1365. [CrossRef]
131. Amyot, M.; Southworth, G.; Lindberg, S.E.; Hintelmann, H.; Lalonde, J.D.; Ogrinc, N.; Poulain, A.J.; Sandilands, K.A. Formation and Evasion of Dissolved Gaseous Mercury in Large Enclosures Amended with $^{200}HgCl_2$. *Atmos. Environ.* **2004**, *38*, 4279–4289. [CrossRef]

Supplementary material

Table S1: values of meteorological parameters, DOC, total dissolved and dissolved gaseous Hg concentration, gaseous Hg fluxes, and atmospheric GEM levels in the different seasonal samplings at the Solkan reservoir (SK). Wind data provided as hourly averages by Slovenian Environmental Agency (ARSO) through database OMNIA (http://www.meteo.fvg.it/).

	Summer		Autumn		Spring	
	Mean ± SD	Min - Max	Mean ± SD	Min - Max	Mean ± SD	Min - Max
Air temperature (°C)	30.3 ± 2.6	27.2 - 34.5	18.8 ± 3.6	12.8 - 22.4	22.5 ± 3.2	16.5 - 24.8
UV radiation (W m^{-2})	41.8 ± 6.4	27.6 - 49.9	22.6 ± 7.0	5.6 - 29.8	34.3 ± 12.1	13.8 - 53.5
Wind speed (m s^{-1})	2.0 ± 0.8	0.9 – 3.3	2.0 ± 1.1	0.4 – 3.7	1.9 ± 1.1	0.6 – 3.1
Water temperature (°C)	17.42 ± 1.13	16.11 - 18.68	10.49 ± 0.06	10.46 - 10.57	10.41 ± 0.06	10.33 - 10.48
DOC (mg L^{-1})	1.1 ± 0.3	0.8 - 1.4	1.2 ± 0.2	1.1 - 1.4	0.9 ± 0.3	0.7 - 1.5
THg (ng L^{-1})	19.98 ± 7.53	14.31 - 32.22	6.39 ± 0.67	5.51 - 7.37	4.69 ± 2.86	2.27 - 9.96
DGM (pg L^{-1})	421.2 ± 167.0	197.5 - 696.1	112.6 ± 18.0	95.9 - 142.2	163.8 ± 36.8	121.0 - 218.1
% DGM/THg_D	2.4 ± 1.4	0.8 - 4.9	1.8 ± 0.4	1.4 - 2.4	4.2 ± 1.6	1.8 - 6.5
Gaseous Hg flux (ng m^{-2} h^{-1})	36.65 ± 6.15	34.96 - 46.77	14.07 ± 3.19	9.96 - 18.74	14.91 ± 3.51	10.24 - 19.31
Atmospheric GEM (ng m^{-3})	2.77 ± 0.98	< 2 - 5.28	2.19 ± 2.13	< 2 - 6.48	4.61 ± 4.09	< 2 - 10.62

Table S2: values of meteorological parameters, DOC, total dissolved and dissolved gaseous Hg concentration, gaseous Hg fluxes, and atmospheric GEM levels in the different seasonal samplings at the Torviscosa dockyard (TR). Wind data provided as hourly averages by Weather Forecast Regional Observatory of Friuli Venezia Giulia region (OSMER-ARPA FVG) through database OMNIA (http://www.meteo.fvg.it/).

	Summer		Autumn		Spring	
	Mean ± SD	Min - Max	Mean ± SD	Min - Max	Mean ± SD	Min - Max
Air temperature (°C)	31.8 ± 1.5	29.7 - 33.6	16.8 ± 2.1	13.3 - 18.5	23.3 ± 1.2	21.7 - 24.5
UV radiation (W m^{-2})	43.3 ± 7.2	23.0 - 51.7	19.1 ± 5.1	10.3 - 28.6	44.1 ± 6.8	27.2 - 55.2
Wind speed (m s^{-1})	1.7 ± 0.7	0.4 – 2.7	1.0 ± 0.7	0.6 – 2.5	2.9 ± 0.4	1.7 – 3.8
Water temperature (°C)	21.15 ± 1.26	19.37 - 22.90	14.33 ± 0.40	13.86 - 14.87	16.53 ± 0.23	16.11 - 16.80
DOC (mg L^{-1})	1.5 ± 0.7	0.8 - 2.5	1.0 ± 0.3	0.6 - 1.3	0.8 ± 0.3	0.5 - 1.2
THg (ng L^{-1})	9.43 ± 1.22	7.96 - 10.80	1.93 ± 0.37	1.61 -2.65	5.72 ± 2.57	1.89 - 9.12
DGM (pg L^{-1})	143.9 ± 38.5	109.8 - 195.6	79.1 ± 25.5	58.1 - 122.6	153.2 ± 58.9	103.6 - 259.7
% DGM/THg_D	1.6 ± 0.4	1.1 - 2.0	4.3 ± 1.7	2.2 - 6.7	3.3 ± 1.9	1.5 - 5.5
Gaseous Hg flux (ng m^{-2} h^{-1})	32.68 ± 10.78	23.27 - 52.71	11.07 ± 5.16	6.91 - 15.47	12.68 ± 6.08	9.55 - 35.24
Atmospheric GEM (ng m^{-3})	1.92 ± 2.10	< 2 - 4.61	71.09 ± 98.43	< 2 - 543.61	48.73 ± 77.91	3.38 - 344.08

Table S3: values of meteorological parameters, DOC, total dissolved and dissolved gaseous Hg concentration, gaseous Hg fluxes, and atmospheric GEM levels in the different seasonal samplings at Cavazzo Lake (CV). Wind data provided as hourly averages by Weather Forecast Regional Observatory of Friuli Venezia Giulia region (OSMER-ARPA FVG) through database OMNIA (http://www.meteo.fvg.it/).

	Summer		Autumn		Spring	
	Mean ± SD	Min - Max	Mean ± SD	Min - Max	Mean ± SD	Min - Max
Air temperature (°C)	30.4 ± 2.5	25.9 - 32.9	15.7 ± 2.6	12.5 -19.7	17.9 ± 1.7	15.8 - 20.8
UV radiation (W m^{-2})	42.4 ± 7.7	19.3 - 52.2	20.7 ± 7.4	5.3 - 28.2	19.7 ± 9.0	4.9 - 44.5
Wind speed (m s^{-1})	1.9 ± 1.2	0.1 – 3.5	2.1 ± 1.1	1.0 – 3.5	4.6 ± 1.5	2.5 – 6.9
Water temperature (°C)	16.00 ± 0.65	14.88 - 16.80	11.08 ± 0.31	10.55 - 11.36	10.05 ± 1.03	9.35 - 10.18
DOC (mg L^{-1})	1.0 ± 0.2	0.7 - 1.3	1.5 ± 0.7	1.0 - 2.8	1.5 ± 0.5	1.0 - 2.5
THg (ng L^{-1})	9.62 ± 5.34	3.93 - 16.46	3.88 ± 0.57	3.44 - 4.90	2.69 ± 3.03	< 0.63 - 8.49
DGM (pg L^{-1})	152.7 ± 28.9	114.1 - 194.0	59.6 ± 4.0	55.8 - 66.4	80.7 ± 14.5	62.7 - 93.5
% DGM/THg_D	2.3 ± 1.5	0.8 - 4.4	1.6 ± 0.3	1.1 - 1.9	3.2 ± 1.9	0.7 - 5.1
Gaseous Hg flux (ng m^{-2} h^{-1})	32.45 ± 3.17	29.48 - 37.59	6.22 ± 3.84	0 - 9.79	8.02 ± 3.96	3.41 - 14.63
Atmospheric GEM (ng m^{-3})	1.30 ± 1.00	< 2 - 3.85	1.25 ± 0.62	< 2 - 4.81	3.61 ± 2.67	< 2 - 16.07

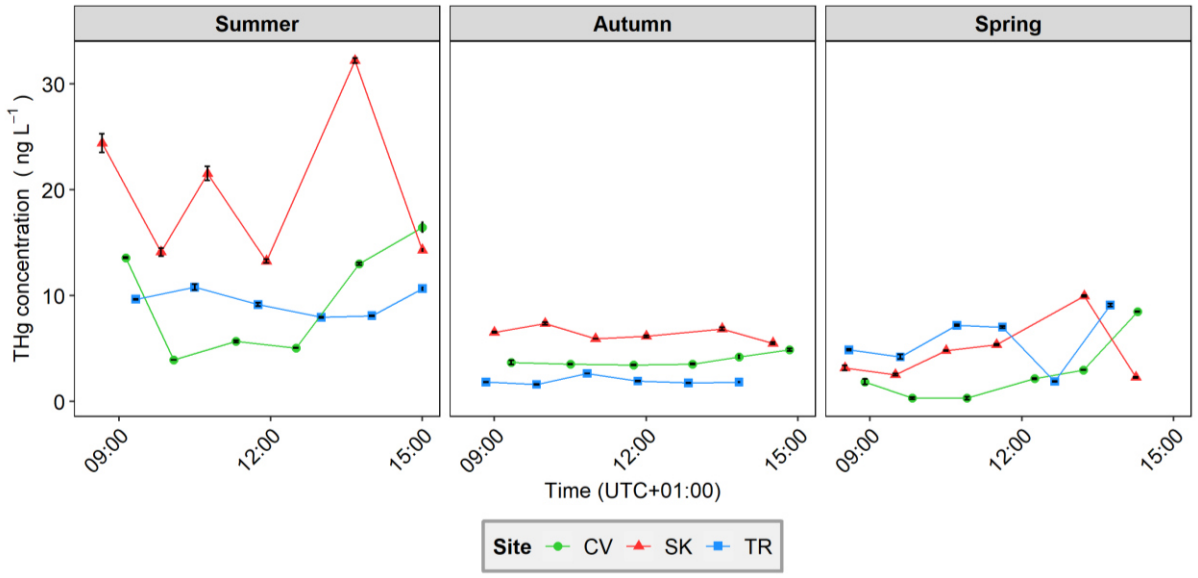

Figure S1: diurnal variation of THg_D concentrations in the different seasons at the various selected sites.

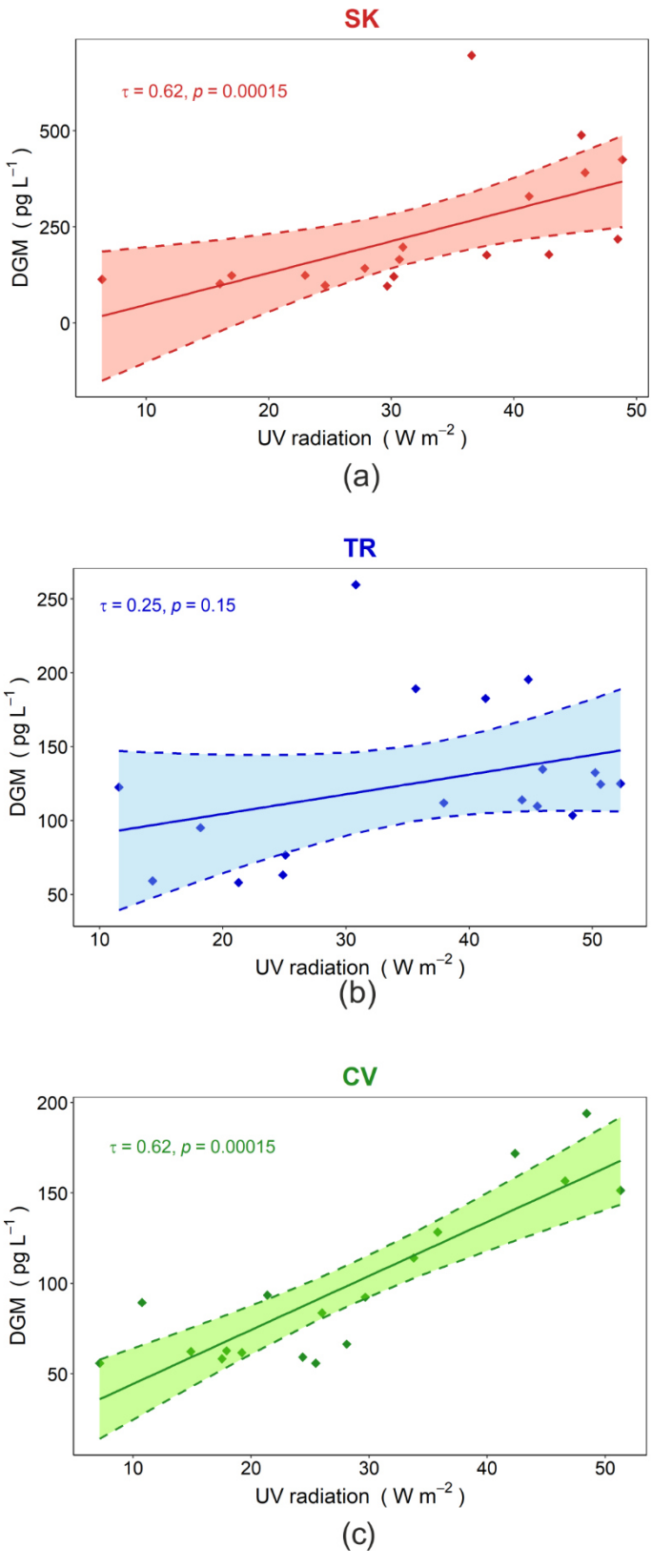

Figure S2: DGM concentrations versus incident UV radiation during samplings at the three selected sites (a): Solkan Reservoir, (b): Torviscosa dockyard, (c): Lake of Cavazzo. Kendall's rank correlation coefficients (τ) and 95% confidence intervals are reported.

Table S4: parameters in surface and bottom water at TR site in summer and spring

	Surface water	Bottom water
28/07/2020-T5 (15:00)		
Temperature (°C)	22.90	21.23
Salinity (PSU)	0.34	12.26
DOC (mg L^{-1})	1.0	7.9
THg (ng L^{-1})	10.66	8.26
DGM (pg L^{-1})	111.9	190.1
10/05/2021-T2 (10:43)		
Temperature (°C)	16.48	17.92
Salinity (PSU)	0.32	0.34
DOC (mg L^{-1})	7.9	1.7
THg (ng L^{-1})	7.20	1.65
DGM (pg L^{-1})	113.9	123.4

3.4 Article III: Hg^0 fluxes at soil-air interface in terrestrial environments

Gaseous mercury evasion from bare and grass-covered soils contaminated by mining and ore roasting (Isonzo River alluvial plain, Northeastern Italy)

Federico Floreani[a,b]*, Valeria Zappella[a], Jadran Faganeli[c], Stefano Covelli[a]

[a]*Department of Mathematics & Geosciences, University of Trieste, Via E. Weiss 2, Trieste, Italy.*

[b]*Department of Life Sciences, University of Trieste, Via L. Giorgieri 5, Trieste, Italy*

[c]*Marine Biology Station, National Institute of Biology, Fornace 41, Piran, Slovenia*

Graphical abstract

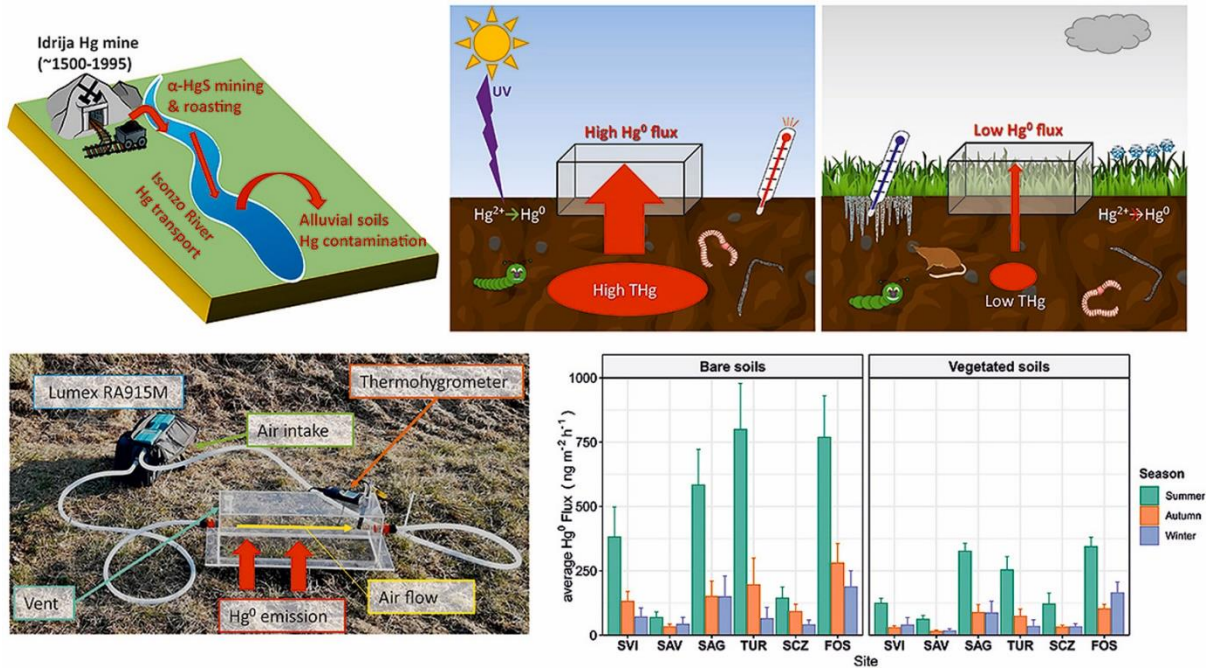

Highlights

- Field study of mercury evasion from soils contaminated by historic cinnabar mining.
- Highest mercury releases in summer driven by UV radiation and temperatures.
- Fluxes variability function of soil mercury and organic matter content.
- Slow activation of mercury evasion from cinnabar in winter under low temperatures.
- Living native grass vegetation cover significantly limits mercury volatilisation.

Environmental Pollution 318 (2023) 120921

Contents lists available at ScienceDirect

Environmental Pollution

journal homepage: www.elsevier.com/locate/envpol

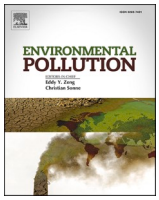

Gaseous mercury evasion from bare and grass-covered soils contaminated by mining and ore roasting (Isonzo River alluvial plain, Northeastern Italy)☆

Federico Floreani [a,b,*], Valeria Zappella [a], Jadran Faganeli [c], Stefano Covelli [a]

[a] Department of Mathematics and Geosciences, University of Trieste, Via E. Weiss 2, Trieste, Italy
[b] Department of Life Sciences, University of Trieste, Via L. Giorgieri 5, Trieste, Italy
[c] Marine Biology Station, National Institute of Biology, Fornace 41, Piran, Slovenia

ARTICLE INFO

Keywords:
Soil contamination
Hg mining
Gaseous Hg fluxes
Flux chamber
Vegetation
Cinnabar

ABSTRACT

High amounts of mercury (Hg) can be released into the atmosphere from soil surfaces of legacy contaminated areas as gaseous elemental mercury (Hg^0). The alluvial plain of the Isonzo River (NE Italy) suffered widespread Hg contamination due to the re-distribution of Hg-enriched material discharged by historical cinnabar mining at the Idrija mine (Slovenia), but an assessment of Hg^0 releases from the soils of this area is still lacking. In this work, Hg^0 fluxes at the soil-air interface were evaluated using a non-steady state flux chamber coupled with a real-time Hg^0 analyser at 6 sites within the Isonzo River plain. Measurements were performed in summer, autumn, and winter both on bare and grass-covered soil plots at regular time intervals during the diurnal period. Moreover, topsoils were analysed for organic matter content and Hg total concentration and speciation. Overall, Hg^0 fluxes tracked the incident UV radiation during the sampling periods with daily averages significantly higher in summer (62.4 ± 14.5–800.2 ± 178.8 ng m^{-2} h^{-1}) than autumn (15.2 ± 4.7–280.8 ± 75.6 ng m^{-2} h^{-1}) and winter (16.9 ± 7.9–187.8 ± 62.7 ng m^{-2} h^{-1}) due to higher irradiation and temperature, which favoured Hg reduction reactions. In summer and autumn significant correlations were observed between Hg^0 fluxes and soil Hg content (78–95% cinnabar), whereas this relationship was not observed in winter likely due to relatively low emissions found in morning measurements in all sites coupled with low temperatures. Finally, vegetation cover effectively reduced Hg^0 releases in summer (~9–68%) and autumn (~41–78%), whereas the difference between fluxes from vegetated and bare soils was not evident during winter dormancy due to scarce soil shading. These results suggest the opportunity of more extended spatial monitoring of Hg^0 fluxes particularly in the croplands covering most of the Isonzo River alluvial plain and where bare soils are frequently disturbed by agricultural practices and directly exposed to radiation.

1. Introduction

Mercury (Hg) is a widespread pollutant of global concern that poses serious threats to ecosystems and human health, mostly due to the neurotoxic effects of its methylated form (Boening, 2000; Clarkson and Magos, 2006). A peculiarity of this metal is the high volatility of its elemental form, often referred to as "gaseous elemental mercury" (hereafter Hg^0), which can be emitted to the atmosphere from both natural and anthropogenic sources (Pirrone et al., 2010). Once emitted, Hg^0 can persist in the atmosphere for more than 1 year (Saiz-Lopez et al., 2018) and thus be subject to long-range atmospheric transport before being removed through dry and wet depositions (Berg et al., 2008; Horowitz et al., 2017), even reaching remote areas (Kurz et al., 2019). Moreover, deposited Hg can be re-emitted back into the atmosphere from natural terrestrial and aquatic surfaces, thus the multiple surface-atmosphere exchanges can further expand its spread and residence time in the environment, a phenomenon previously referred to as "hopping effect" (Agnan et al., 2016; Jiskra et al., 2015; Lei et al., 2021).

Hg^0 exchanges at the soil-air interface represent a key aspect of the biogeochemical cycle of this element, with relevant Hg^0 emissions often reported for areas characterised by Hg-enriched substrates due to local geology and/or anthropogenic activities. These sites may constitute a

☆ This paper has been recommended for acceptance by Prof. Dr.Jörg Rinklebe.

* Corresponding author. Department of Mathematics and Geosciences University of Trieste Via E. Weiss 2, 34128, Trieste, Italy.
E-mail address: federico.floreani@phd.units.it (F. Floreani).

https://doi.org/10.1016/j.envpol.2022.120921
Received 18 October 2022; Received in revised form 30 November 2022; Accepted 20 December 2022
Available online 21 December 2022

relevant secondary source of atmospheric Hg (Gustin et al., 2003; Kocman et al., 2013) where the magnitude of Hg^0 fluxes is primarily influenced by the total Hg (THg) concentrations in the substrate (Agnan et al., 2016). Generally, most Hg found in soil is present in oxidised forms (Hg^{2+}) (Anderson, 1979; Palmieri et al., 2006; Terzano et al., 2010; Beckers and Rinklebe, 2017) that must be reduced to the volatile form Hg^0 before being emitted (Carpi and Lindberg, 1998). The reduction of Hg^{2+} in soils can occur through abiotic pathways such as photoreduction, mostly mediated by UV radiation (Moore and Carpi, 2005), or reduction facilitated by interaction with functional groups of OM (Gabriel and Williamson, 2004) or iron-bearing minerals (Debure et al., 2020), but also Hg^{2+} reduction mediated by microbial activity can contribute to Hg^0 formation (Fritsche et al., 2008) as a detoxification pathway of mostly microorganisms containing the *mer* operon in their genome, activated by exposure to Hg (Mathema et al., 2011). On the other hand, Hg^0 adsorption on soil surfaces, favoured by its high affinity for reduced sulphur groups of organic matter (OM) as well as for iron and manganese minerals, can limit its vertical mobility through the soil (Schuster, 1991; Skyllberg and Drott, 2010; Yuan et al., 2019). As a result, Hg^0 volatilisation depends both on the rate of reduction reactions and on the sorption-desorption equilibrium between the soil matrix and pore space air (Carmona et al., 2013; Pannu et al., 2014), which in turn are influenced by several factors, e.g. incident solar radiation (Wang et al., 2005), soil and air temperature (Shi et al., 2020), precipitation and soil moisture (MacSween and Edwards, 2021), soil cover by vegetation and litter (Ma et al., 2018), soil disturbance (Sommar et al., 2016). These factors act in both contaminated and background areas (Miller et al., 2011), but their relative importance seems to be extremely site-specific (Agnan et al., 2016). Additionally, Hg speciation in soils deeply impacts its availability for reduction and subsequent volatilisation, as emissions are generally more rapid and intense where mobile and soluble forms of Hg are prevalent compared to sites dominated by insoluble forms such as cinnabar (α-HgS) (García-Sánchez et al., 2006; Kocman and Horvat, 2010; Llanos et al., 2011).

Anthropogenic inputs related to mining, coal combustion, and various industrial processes significantly affected the biogeochemical cycle of Hg and the amounts of the element circulating in the environment (Streets et al., 2019). The implementation of the Minamata Convention, aimed at phasing-out primary Hg mining and its use in precious metal extraction and industrial processes (Selin et al., 2018), is expected to reduce Hg emissions related to human activities. However, sites subject to past severe Hg pollution are able to emit high amounts of Hg^0 into the atmosphere even years after the primary source of contamination is no longer active, as evidenced by high Hg^0 fluxes recorded in areas contaminated by past mining (Dalziel and Tordon, 2014; Fantozzi et al., 2013; Kotnik et al., 2005) or industrial activities (Eckley et al., 2015; Osterwalder et al., 2019; Zhu et al., 2018). Understanding the fate of Hg in these areas is crucial to assess the potential exposure of the local population and wildlife to this metal and to evaluate possible mitigation and remediation strategies (Selin et al., 2018; Zhu et al., 2018).

The alluvial plain of the Isonzo River (NE Italy) is characterised by widespread Hg contamination as a consequence of historical Hg mining which took place at Idrija (Slovenia) from the 16th century until 1995 (Kotnik et al., 2005). Throughout ~500 years of exploitation, approximately 35,000 tons of Hg were lost in the surrounding environment (Dizdarevič, 2001) through atmospheric leaks and direct dumping of roasting residues on banks and riverbed sediments of the local Idrijca River, a tributary of the Isonzo River (Gosar et al., 1997; Žibret and Gosar, 2006), resulting in extended contamination of all environmental compartments (Bavec and Gosar, 2016 and references therein). Leaching and erosion of contaminated soils and sediments, mostly during rain events, favour the mobilization and transport of Hg to the Isonzo River and then finally to the northern Adriatic Sea (Baptista-Salazar et al., 2017; Pavoni et al., 2021). Due to flooding events, Hg has been re-distributed over the entire alluvial plain of the Isonzo River, resulting in high concentrations in soils (up to 76 mg kg^{-1}) which progressively decrease as the distance from the river increases (Acquavita et al., 2022; Cerovac et al., 2018; Piani et al., 2013). Few studies have highlighted the occurrence of Hg^0 atmospheric concentrations which are slightly higher than the natural background, mostly in the coastal sector of the southernmost part of the plain (Barago et al., 2020; Floreani et al., 2020), but a direct evaluation of potential Hg^0 releases at the soil-air interface is still lacking. The main aims of this study were to evaluate the Hg^0 emissions in selected sites along the plain characterised by a different degree of substrate contamination and to relate the results to soil Hg concentration and speciation and OM content in order to understand how differences in these parameters may influence the mobility of Hg at the soil-air interface. Hg^0 fluxes were measured in field by means of a manually operated non-steady state flux chamber coupled with a real-time portable Hg^0 analyser. This technique allows for a simple, rapid, and relatively cost-effective evaluation of Hg^0 evasion from the soil surface. Measurements were performed during the diurnal period in different seasons in order to verify the existence of any variability related to environmental parameters such as UV radiation and temperature. In addition, at each site Hg^0 emissions were measured over plots of bare and grass-covered soils in order to examine the potential influence of native vegetation cover.

2. Materials and methods

2.1. Study area

At the extreme eastern edge of the Friulian plain (Friuli Venezia Giulia Region, NE Italy), the Isonzo River alluvial plain is formed by quaternary sediments deposited during the Last Glacial Maximum by the Isonzo and Torre Rivers (Fontana et al., 2008) and is divided into two different geomorphological sectors (High and Low plain) by an East-West oriented Resurgence Belt (Cucchi et al., 2008; Treu et al., 2017). The southernmost coastal area of the plain adjacent to the mouth of the Isonzo River derives from hydraulic reclamation works carried out in past centuries to obtain cultivable areas from former lagoon and wetlands (Da Lio and Tosi, 2018; Marocco, 1989). Intense agriculture of prevalently maize and soybean occurs throughout the plain with the scarce presence of permanent meadows and a general increase in urbanisation and industrial settlements moving southwards (Acquavita et al., 2022; Contin et al., 2012; Salata et al., 2019). According to Rivas-Martínez et al. (2011), the bioclimate of the study area is classifiable as temperate oceanic, with relatively mild temperatures throughout the year and frequent precipitation. The annual mean rainfall in the area ranges between ~1000 and ~1400 mm moving from the coastal area to the High plain and the mean annual temperature is around 14 °C, with lowest values in January (~4.3 °C) and highest in July (~23.8 °C) (reference period: 1991–2021, data from ARPA FVG-Regional Agency for Environmental Protection of Friuli Venezia Giulia, through OSMER and GRN-Regional Meteorological Observatory and Natural Risk Management, respectively, https://www.meteo.fvg.it/). Local anemometry is determined by the breeze regime and synoptic winds from north-eastern direction, with episodic gusts of strong Bora winds (Giaiotti et al., 2003).

For this study, we focused on 6 sites along the plain (Fig. 1) near the present course of the Isonzo River located between 40 and 70 km downstream the confluence with the Idrijca River. The sites were selected on the basis of existing information about Hg concentrations in soils (Acquavita et al., 2022): 3 were located in the High plain, in the municipalities of Savogna d'Isonzo (SVI and SAV) and Sagrado (SAG), and the remaining in the Low plain near the villages of Turriaco (TUR), San Canzian d'Isonzo (SCZ) and Fossalon di Grado (FOS). The soils of the latter two sites are classifiable as Gleyic Fluvic Cambisols according to the World Reference Base for Soil Resources (WRB, https://www.isric.org/explore/wrb), whereas those of the other 4 sites belong to the group of Calcaric Fluvic Cambisols. Measurements of Hg^0 fluxes were

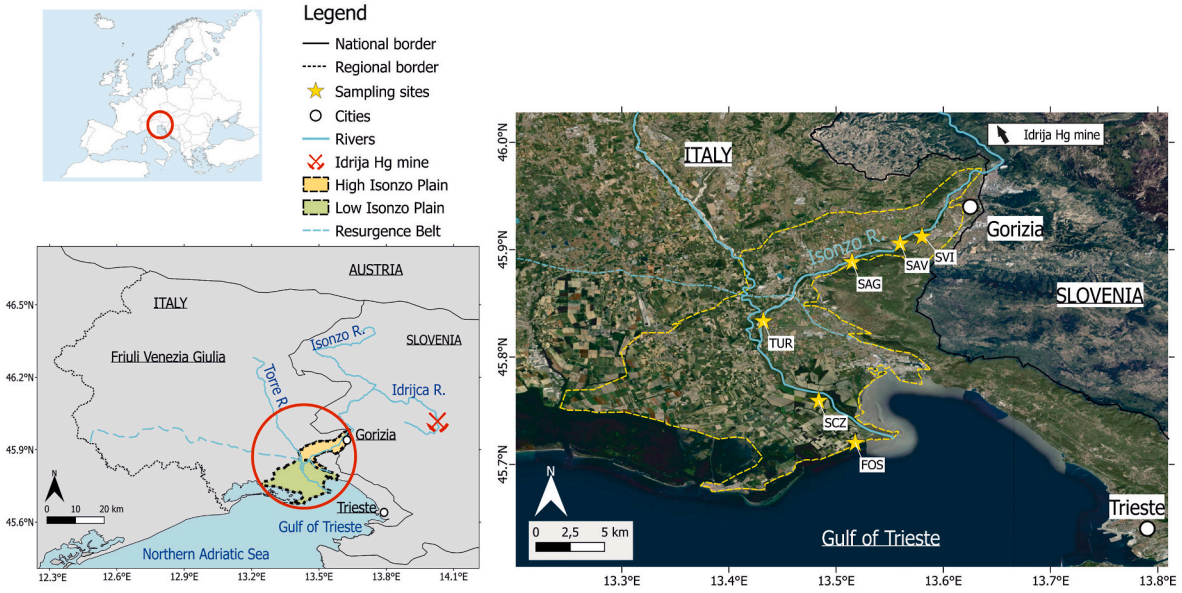

Fig. 1. Study area and location of sampling sites.

taken in meadows consisting of low lying non-woody vegetation. The sites referred to as SCZ and FOS were located near farmland soils with the occurrence of species such as *Setaria pumila*, *Cynodon dactylon*, *Artemisia vulgaris*, *Amaranthus retroflexus*. Conversely, sampling points at SVI, SAV, SAG, and TUR were located in permanent meadows along the course of the Isonzo River, which represent preserved natural environments with an important connectivity function in the ecological network in the context of regional landscape planning of the Friuli Venezia Giulia region (Sigura et al., 2017) and consequently protected as areas of relevant environmental interest (A.R.I.A.; Regional Law n. 42/1996). Common wild vegetation is dominated by *Poaceae*, including species as *Arrhenatherum elatius*, *Festuca arundinacea*, *Poa pratensis*, *Dactylis glomerata*.

2.2. Soil sampling and analysis

After Hg^0 flux measurements, topsoil samples (~0–2 cm) from each plot directly under the chamber were collected, sieved in the field at <2 cm to remove coarser particles, stored in clean polyethylene bags and taken to the laboratory, where an aliquot was immediately weighed for gravimetric determination of the moisture percentage. Plant residues of both aboveground (stems and leaves) and belowground biomass (roots) were carefully separated from the soil samples in the laboratory before analysis. Grain-size was determined only on samples collected in summer according to ISO 13320:2020 using a laser granulometer (Mastersizer 2000; Malvern Instruments Ltd., Worcestershire, UK). An aliquot (20 g) of fresh soil was used after a 24 h H_2O_2 (10%) treatment to reduce the bonding effect of the OM to the particles, followed by wet sieving at <2 mm and analytical determination on 2-mL aliquots.

For other determinations, a second aliquot of all soil samples was air-dried, gently disaggregated into a ceramic mortar, and sieved to 2 mm. Soil pH was measured with a glass electrode after equilibrating 5 g of soil with 12.5 mL of ultrapure water for 2 h according to Italian Decree 13/09/99. Organic matter content was determined as loss on ignition (LOI) at 550 °C (Heiri et al., 2001). Total Hg (THg) concentrations in soils were determined using a DMA-80 Direct Mercury Analyser (Milestone, Sorisole, Italy) atomic absorption spectrophotometer according to US-EPA Method 7374 (U.S. EPA, 1998). The limit of detection (LOD) was approximately 0.005 ng of Hg. A certified material (PACS-3 Marine Sediment Certified Reference Material, NRCC, Canada; Hg = 2.98 ± 0.36 mg kg^{-1}) was regularly analysed to verify the accuracy of the method and the obtained results showed acceptable recoveries (95–106%). The speciation of Hg in soil was evaluated following the thermo-desorption procedure described by Petranich et al. (2022). Briefly, approximately 80 mg of sample were progressively heated (0.5 °C s^{-1}) in a quartz boat from ambient temperature to ~700 °C in a furnace (Pyro-915+) coupled with a portable real-time gaseous Hg analyser (Lumex RA-915 M, Lumex Instruments, St. Petersburg, Russia) based on the atomic adsorption spectrophotometry technique with Zeeman background correction (Sholupov et al., 2004). A complete description of the thermoscanning unit was reported by Mashyanov et al. (2017). Temperature was continuously monitored through a type K thermocouple and the occurring Hg forms were identified by comparing their desorption temperatures with those of standard Hg compounds. The relative amounts of the different "thermospecies" were then determined by integrating the area under each desorption peak (Biester and Scholz, 1997) using the RAPID software (ver. 1.00.585) which controls the Lumex instrumentation.

2.3. Soil-air Hg^0 flux measurements

Hg^0 fluxes at the soil-air interface were evaluated during one diurnal period for each selected site in summer (July–September 2021), autumn (October–November 2021), and winter (January 2022). Hg^0 fluxes were not measured during spring, but considering that weather conditions and vegetation development in our study area in this season are not very much dissimilar to those encountered in autumn, it may be assumed that fluxes during these two periods are comparable. At each location, fluxes were measured in two adjacent sampling points, i.e. from soils characterised by the presence of native herbaceous vegetation cover and bare soil plots where grass was manually removed before sampling. Sampling points were chosen as close as possible to those previously used for the characterisation of Hg contamination of the Isonzo River plain (Acquavita et al., 2022). Flux measurements were performed by means of a Plexiglas non-steady state (NSS) flux chamber (60 × 20 × 25 cm) coupled with the Lumex analyser, which allows for the direct determination of Hg concentrations in the air in a wide dynamic range (2–30,000 ng m^{-3}). Operatively, the chamber was placed on the ground with edges inserted 1 cm into the soil fitting on a pre-installed stainless-steel frame. In order to achieve an optimal seal and minimise the intrusion of external air, soil was gently packed around the outer walls (Gillis and Miller, 2000). The Hg analyser was connected to the chamber in a closed

circuit through two Teflon tubes attached to 2 cm holes on the opposite short sides of the chamber. During the chamber deployment, air was recirculated through the system thanks to the Lumex internal pump at a constant flow rate of at least 10 L min^{-1}, creating a continuous gas movement over the soil surface (During et al., 2009). Due to the relatively high dimensions of the chamber, the use of a high air flow rate is required to provide a good level of mixing inside the chamber, necessary to obtain measurements of Hg^0 concentrations representative of the air in the chamber headspace (Maier et al., 2022). However, a high flow rate can potentially lead to bias in flux estimation due to pressure gradients between the outside and the inside of the chamber, particularly in highly permeable soils (Camarda et al., 2009; Davidson et al., 2002). To minimise the occurrence of pressure gradients between the outside and inside of the chamber and the disturbance on natural gas exchange processes at the soil-air interface related to the occurrence of advective fluxes between soil and air, two vents were placed on the upper wall of the chamber (Hutchinson and Livingston, 2001). However, these artefacts related to high flow rate are generally greater for open dynamic flux chambers (DFC) than for closed recirculation chambers due to the higher connection with ambient air (Camarda et al., 2009; Cotel et al., 2015). Concentrations of Hg^0 were continuously (every 1s) recorded for 5 min, as recommended for NSS chamber measurements using online real-time analysers (Maier et al., 2022), before removing the chamber. This short sampling time allowed for a reduction of the influence of the chamber on environmental parameters near the soil surface, such as temperature (Fantozzi et al., 2013; Rochette and Hutchinson, 2005), compared to DFC technique, more frequently adopted for Hg^0 soil emission measurement (Sommar et al., 2020). Thus, it was possible to take more distinct measurements from the selected points in a short time interval using the same Hg^0 analyser. Our chamber has a design similar to the DFCs used in other studies (e.g. Carpi and Lindberg, 1998; Sizmur et al., 2017) and coupled with a Lumex analyser (Fantozzi et al., 2013; García-Sánchez et al., 2006; Wang et al., 2006; Zhu et al., 2011) and our unpublished tests performed using both configurations (NSS and DFC) and the same air flow rate, comparable to those adopted in the cited studies, revealed a good agreement between fluxes measured with the two techniques ($r = 0.97$, $p < 0.001$, $n = 30$), with no systematic over- or underestimation of the flux calculated for the NSS technique compared to the well-established DFC configuration.

During each sampling day, Hg^0 fluxes were measured at regular time intervals of 1 h through 6/7 distinct set of measurements, each consisting of two consecutive replicate flux measurements conducted alternatively from bare and vegetated soil plots. The Hg^0 flux from soil (F) was then calculated from the increase of concentration inside the chamber during the enclosure (dC/dt) according to equation (1) (Bagnato et al., 2014; Kyllönen et al., 2012):

$$F = \frac{V}{A}\frac{dC}{dt} \quad (1)$$

where V is the internal volume of the chamber and A is the soil surface area covered by the chamber. As the increase of Hg^0 concentration inside the chamber can be assumed to be approximately linear for short chamber deployment times (Di Francesco et al., 1998; Kandel et al., 2016), the time derivative of Eq. (1) was quantified through the slope of Hg^0 concentration vs. time curve (Bagnato et al., 2014; Chiodini et al., 1998; Cotel et al., 2015; Davidson et al., 2002) and results were rejected if a good linear regression ($r^2 > 0.8$) could not be achieved (Kyllönen et al., 2012). Chamber blanks were determined daily by placing the chamber on a clean polycarbonate surface and the average value (1.6 ± 1.0 ng m^{-2} h^{-1}, $n = 18$) was subtracted to fluxes calculated from field measurements.

In parallel with soil-air Hg^0 fluxes, incident UV radiation between 250 and 400 nm were monitored in the field using a SU-420 sensor (Apogee Instruments, Logan, USA) mounted 2 m above ground near the sampling points. Data were logged every 1 min as the average value of readings taken every 1s. In addition, air temperature and relative humidity were measured using a portable thermohygrometer (HI9565, Hanna Instruments, Padova, Italy) which was also used to monitor the variation of these parameters inside the chamber headspace during the entire period of measurement (5 min) by inserting the probe in the chamber through a hole in the upper wall. Soil temperature was determined at a depth of 2 cm near sampling points using a thermal probe.

2.4. Statistical analyses

Statistical analyses were performed using R software ver. 4.1.3 (R Foundation, Vienna, Austria) and package *ggplot2* for data visualisation (Wickham et al., 2016). After checking data normality and homogeneity of variances with the Shapiro-Wilk and Bartlett tests, respectively, the statistical significance of differences between data groups was tested by means of Kruskal-Wallis (K–W) coupled with Dunn's post-hoc test. Pearson and Kendall correlation coefficients were used to assess the relationships between variables in the case of normal and non-normal data distribution.

3. Results and discussion

3.1. Physico-chemical characteristics of soils

General physico-chemical characteristics of investigated soils are summarised in Table 1. Overall, all the topsoils were characterised by a moderate alkaline pH (average = 8.09 ± 0.10), with no significant differences between samples collected at the same site in different seasons. In terms of grain size, silt was the predominant fraction at SAG (50.7 ± 0.9%) followed by sand (45.8 ± 1.1%) and clay (3.5 ± 0.2%), whereas the soils from all other sites showed a greater abundance of the sandy component (55.8 ± 4.5%) than the silty (40.9 ± 4.3%) and clayey (3.3 ± 0.9%) ones: according to United States Department of Agriculture (USDA) textural classification (USDA, 1987), these soils can be defined as *Sandy loam*, whereas samples from SAG fall in the class of *Silty loam* (Fig. S1).

The organic matter content was quite variable between sites, with the highest average value found at SCZ (17.51 ± 3.26%) and the lowest obtained for soils of FOS (2.92 ± 0.33%) in the reclaimed coastal area. The soils of the other sites were characterised by similar OM contents ranging on average between 8.30 ± 1.69% (SAG) and 10.76 ± 1.31%

Table 1
Overview of the main physico-chemical parameters of soil of the investigated study sites. Except for grain-size, data reported are the average (±std) values of all collected samples in the three different seasons.

	SVI	SAV	SAG	TUR	SCZ	FOS
pH	8.12 ± 0.06	8.17 ± 0.08	8.15 ± 0.08	8.14 ± 0.06	8.01 ± 0.05	7.96 ± 0.08
Sand (%)	53.8 ± 3.5	57.6 ± 6.2	45.8 ± 1.1	53.7 ± 2.8	55.0 ± 3.4	58.7 ± 5.4
Silt (%)	43.0 ± 3.0	40.0 ± 5.6	50.7 ± 0.9	43.6 ± 2.6	41.2 ± 2.7	36.9 ± 4.7
Clay (%)	3.1 ± 0.5	2.5 ± 0.6	3.5 ± 0.2	2.7 ± 0.2	3.8 ± 0.7	4.4 ± 0.8
LOI (%)	10.32 ± 1.00	10.76 ± 1.31	8.30 ± 1.69	8.93 ± 0.92	17.51 ± 3.26	2.92 ± 0.33
THg (mg kg^{-1})	16.58 ± 2.07	2.22 ± 0.50	17.22 ± 1.91	25.33 ± 4.12	8.01 ± 0.52	16.30 ± 3.66
α-HgS (%)	85 ± 2	94 ± 2	91 ± 2	94 ± 2	78 ± 1	90 ± 3
No-α-HgS (%)	15 ± 2	6 ± 2	9 ± 2	6 ± 2	22 ± 1	10 ± 3

(SAV), with little variability between samples collected in different seasons (Fig. S2+Table 1). Moreover, no significant differences were found between OM contents in topsoils from bare and vegetated plots for flux measurement.

3.2. Meteorological parameters

Field measurements for the determination of Hg^0 fluxes at the soil-air interface were performed under sunny weather conditions at almost all sites, except for sampling conducted at FOS in summer and autumn characterised by a more extended cloud cover and an irregular pattern of UV radiation during field operations. The highest UV irradiation was recorded during summer, with daily averages ranging from 29.7 (FOS) to 40.8 W m^{-2} (TUR), while minimum values were encountered in winter, when all single radiation measures were below 20 W m^{-2} (see Tables S1–S3). Air temperatures showed the same seasonal trend, ranging from 22.7 to 33.6 °C in summer, from 11.7 to 20.1 °C in autumn, and from −2.0 to 11.6 °C in winter with higher values typically recorded in the central part of the day and the minimum in the morning. Soil temperatures were similar and slightly higher than air in summer (27–34.5 °C) and on average colder in winter (−1.5-7 °C). In autumn relatively high values were recorded at TUR and SCZ, sampled in October (14–26 °C), whereas at other sites, sampled in November, soil temperatures were always below 15 °C (see Tables S1–S3). Generally, lower soil temperatures were found for vegetated than bare soil plots, particularly in summer due to the greater vegetation height and density which caused increased shading of vegetated soil and resulted in generally higher values of soil moisture (Fig. S3).

3.3. Total Hg concentration and Hg speciation in soils

The THg concentrations in the topsoils were quite variable. The average values considering all soil samples collected in the different seasons ranged from a minimum of 2.22 ± 0.50 mg kg^{-1} at SAV to a maximum of 25.33 ± 4.12 mg kg^{-1} at TUR. Intermediate and similar THg concentrations were found at SAG (17.21 ± 1.91 mg kg^{-1}), SVI (16.58 ± 2.07 mg kg^{-1}) and FOS (16.30 ± 3.66 mg kg^{-1}), whereas a slightly lower value was determined for SCZ (8.01 ± 0.52 mg kg^{-1}) (Table 1). These concentrations fall in the range previously reported for the entire area of the plain (<0.06–41.0 mg kg^{-1} from Acquavita et al., 2022), all exceeding the threshold level of 1 mg kg^{-1} established by Italian Decree 152/2006 for soils intended for public, private and residential use. Total Hg concentrations found in this study are one order of magnitude lower than those observed for soils of the Idrija Hg mining district (Bavec and Gosar, 2016; Teršič et al., 2011), undoubtedly due to the relevant distance from the source of contamination (Ottesen et al., 2013). However, no regular spatial pattern was found considering the selected sampling points along the Isonzo plain, suggesting that the observed concentrations could be dependent on irregular re-distribution of Hg-contaminated material by flooding events (Acquavita et al., 2022; Colica et al., 2019). In each site, no significant variations in terms of soil THg content were observed between bare and vegetated plots where Hg^0 flux measurements were performed (Fig. S4), and also the variability between samples collected from the same plot in different seasons was relatively limited and attributable to soil heterogeneity and to the uneven distribution of contaminated material even on a small spatial scale (Gilli et al., 2018; Rinklebe et al., 2009).

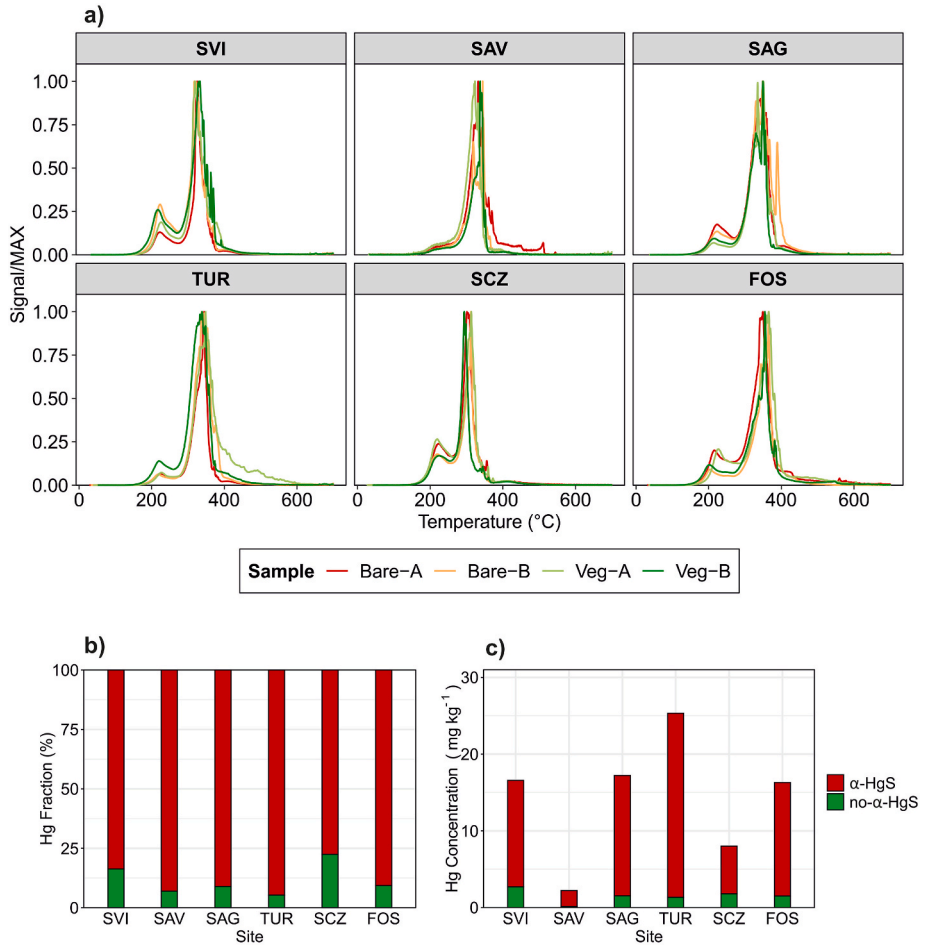

Fig. 2. a) termoscanning curves obtained from soil samples b) average percentage abundance of α-HgS and no-α-HgS fraction calculated from peak integration c) average concentrations of Hg extracted in the α-HgS and no-α-HgS fraction.

The thermal desorption profiles of all topsoil samples showed curves characterised by the presence of a double peak, with a first release between 200 °C and 230 °C and a second, more pronounced peak at temperatures ranging between ~300 °C and 365 °C (Fig. 2). According to the curves of standard materials reported by Petranich et al. (2022), the desorption temperature range of this second peak fits well with that of red cinnabar (α-HgS) from Idrija. This Hg form is considered the less mobile and bioavailable in soils (Gai et al., 2016; Pelcová et al., 2021) and its occurrence in our study area is likely the result of erosion and transport of α-HgS containing material from bottom sediments and riverbanks of the Idrijca River, where mining residues were directly discharged (Žibret and Gosar, 2006). Due to the incomplete decomposition during roasting process, these residues can still contain a certain amount of α-HgS (Esbrí et al., 2010; Yin et al., 2013). On the other hand, the first peak (200–230 °C) can be representative of the release of Hg from various non-cinnabar (no-α-HgS) forms which are potentially more mobile: similar desorption temperatures are indeed reported in the literature, e.g. for Hg bound to OM or to iron oxyhydroxides, and $HgCl_2$, but also for metacinnabar (β-HgS) (Biester et al., 2000; Coufalík et al., 2012; Petranich et al., 2022; Reis et al., 2015a; Rumayor et al., 2017). The occurrence of β-HgS as a by-product of ore roasting processes has been previously reported in mining residues discharged at Idrija (Biester et al., 2000; Teršič et al., 2011), whereas Hg bound to OM is present in notable amounts in the fine fraction of Idrija soils as a result of atmospheric depositions and is available for leaching and erosion during rain events (Baptista-Salazar et al., 2017). Based on the integration of peak areas, the contribution of this no-α-HgS fraction ranged from 5 to 22% of THg and is significantly correlated ($r = 0.67$, $p < 0.05$) to OM content, thus suggesting a contribution of the OM-bound Hg fraction, whereas Hg adsorption by iron oxyhydroxides can be considered less relevant in presence of relatively high concentrations of OM (Beckers and Rinklebe, 2017). The relative abundances of the α-HgS fraction (78–95%) are in good agreement with those of the non-mobile fraction determined by Acquavita et al. (2022) for the soils of the Isonzo River alluvial plain using a chemical sequential extraction procedure.

3.4. Hg^0 fluxes at the soil-air interface

Significantly ($p < 0.05$, K–W) higher Hg^0 fluxes were found for both bare and vegetated soils during the summer season compared to autumn and winter (Fig. 3). The greatest average fluxes for bare and vegetated soils were found at site TUR (800.2 ± 178.8 ng m^{-2} h^{-1}) and FOS (344.6 ± 36.2 ng m^{-2} h^{-1}) respectively, whereas the minimum values for both soil cover types in this season corresponded to site SAV (68.8 ± 21.6 and 62.4 ± 14.5 ng m^{-2} h^{-1}, respectively). This last site also provided the lowest average fluxes during autumn, respectively equal to 32.8 ± 10.1 and 15.2 ± 4.5 ng m^{-2} h^{-1} for bare and vegetated soils, whereas the highest values were found at FOS (280.9 ± 75.6 ng m^{-2} h^{-1} for bare soils and 102.6 ± 17.6 ng m^{-2} h^{-1} for vegetated soils). Finally, Hg^0 fluxes observed in winter varied from 187.8 ± 62.7 ng m^{-2} h^{-1} (FOS) to 40.0 ± 18.6 ng m^{-2} h^{-1} (SCZ) for bare soils and from 164.5 ± 36.1 ng m^{-2} h^{-1} (FOS) to 16.9 ± 7.9 ng m^{-2} h^{-1} (SAV) for vegetated soils. These values were the lowest of all the sampling campaigns for all bare soils with the exception of SAV, whereas they were slightly higher than the autumn averages from vegetated soils at SVI, SAV, SCZ, and FOS. However, differences between the average fluxes in autumn and winter were generally not significant ($p > 0.05$, K-M) except for emissions from bare soils at SVI, TUR and SCZ and from vegetated soil at FOS.

During some winter measurements, a peculiar trend for Hg^0 concentrations inside the chamber characterised by an abrupt change in the slope of the increasing curve after ~2 min of sampling was observed. This evidence concerned measurements taken in the morning hours over vegetated plots at SVI, SAV, TUR, and SCZ, when temperatures near or below 0 °C were observed coupled with a notable presence of frost on surfaces which can retain oxidised forms of Hg (Sherman et al., 2012), contributing to wet depositions (Converse et al., 2014). However, the majority of adsorbed Hg can be readily subject to photoreduction to Hg^0 and re-volatilisation (Ferrari et al., 2008), particularly when frost/ice is melting (Douglas and Blum, 2019). In our case, the chamber positioning may have caused a heating of the inside space due to high insolation, and a subsequent increase in frost melting and evaporation that may have led to the higher release of Hg^0 (Marsik et al., 2005), possibly influencing the build-up of the internal concentration. Consequently, for the calculation of Hg^0 emission from soil, only the first ~120 s after the initial period of ~20–30s (when the signal was affected by the disturbance caused by placing the chamber on the ground (Davidson et al., 2002)) were considered (Fig. S5).

The magnitude of Hg^0 releases observed in our study area impacted by the dispersion of Hg-enriched material derived from the Idrija Hg mine is in the range recently reported by Agnan et al. (2016) in a global database of Hg fluxes for mining sites, further confirming the importance of this activity in promoting high soil emissions. Moreover, values in the same order of magnitude of those presented in this study were previously reported for soils from Idrija (Kocman and Horvat, 2010; Kotnik et al., 2005) and for other sites impacted by various anthropogenic activities such as chlor-alkali plants, PVC production (Osterwalder et al., 2019; Zhu et al., 2018), metal smelters (Eckley et al., 2015), or coal combustion (Li et al., 2018). However, comparison with the literature should be interpreted with caution due to the different experimental setup adopted. Considering studies based on non-steady state systems, very low values have been reported for a boreal background forest in Finland (-1–3.5 ng m^{-2} h^{-1}, Kyllönen et al., 2012), whereas values similar to our study have been found for contaminated floodplains of the Elbe River in Germany (8.6–850 ng m^{-2} h^{-1}, Rinklebe et al., 2010; During et al., 2009). The NSS chamber approach is more frequently adopted in volcanic and geothermal areas using both

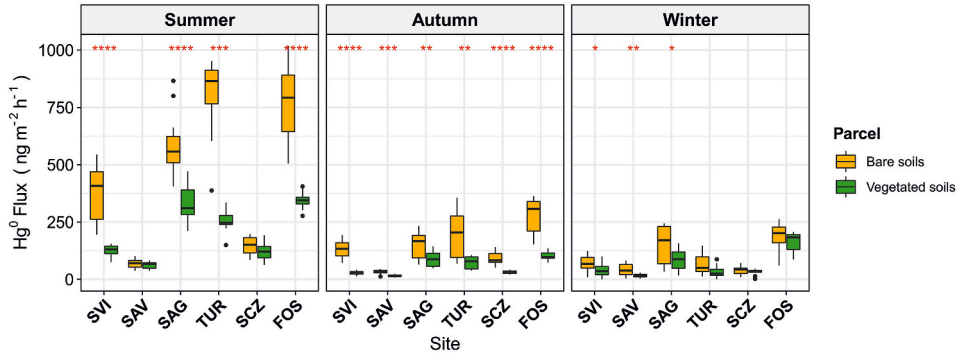

Fig. 3. Comparison among Hg^0 fluxes at soil-air interface from bare and vegetated soil plots in the various seasons; red asterisks indicate the statistically significant differences according to Kruskal-Wallis test (*$p < 0.05$; **$p < 0.01$; ***$p < 0.001$; ****$p < 0.0001$). (For interpretation of the references to colour in this figure legend, the reader is referred to the Web version of this article.)

dynamic systems with air recirculation inside the chamber (Bagnato et al., 2014; Sun et al., 2020a) and static systems without air movement in the inside space and periodic collection of gaseous samples for Hg^0 concentration analysis (Cabassi et al., 2021; Tassi et al., 2016). Regardless of the experimental setup adopted, Hg^0 emissions in these environments can reach values up to thousands or tens of thousands of ng m^{-2} h^{-1}.

3.4.1. Effects of UV radiation and soil and air temperatures

The above described seasonal variation of Hg^0 emissions from soils, with the highest values found during the warm season and the lowest in winter, has frequently been reported in various field studies (Eckley et al., 2015; Lei et al., 2021; Ma et al., 2018; Rinklebe et al., 2010; Shi et al., 2020; Wang et al., 2006). This seasonal pattern is usually related to temporal variations of parameters such as incident solar radiation and soil and air temperatures, which can synergistically regulate the release of Hg^0 at the soil-air interface (Ci et al., 2016; Ma et al., 2018). Solar radiation, particularly in the UV wavelength range, is effective in promoting the formation of Hg^0 through the photoreduction of Hg^{2+} in surface soils (Choi and Holsen, 2009a; Moore and Carpi, 2005), whereas high temperatures facilitate the desorption of bound Hg from organic and mineral surfaces due to increased vapour pressure and thermal motion (Carmona et al., 2013; Sigler and Lee, 2006) and lead to the expansion of gases, favouring the evaporation processes (Schlüter, 2000). Furthermore, increasing temperature can enhance reaction rates and microbial activity, resulting in a greater abiotic and biotic formation of Hg^0 (Pannu et al., 2014; Schlüter, 2000). Considering all the data collected in this study, Hg^0 fluxes from both bare and vegetated soils were significantly ($p < 0.001$) correlated with both average UV radiation calculated during the time of the single flux measurements and air and soil temperature measurements (Table 2), confirming the key role of these parameters in controlling the gaseous exchange of Hg at the soil-air interface (Beckers and Rinklebe, 2017). Negative relationships were generally found between Hg^0 fluxes and the relative humidity of the air (RH), likely due to the correlations existing between this variable and both incident radiation and air temperature, similar to that observed in other studies (Tao et al., 2017; Wang et al., 2006).

The relationship between Hg^0 fluxes and UV radiation was often stronger than those found between fluxes and both soil and air temperatures and may have been more relevant in controlling Hg^0 releases during our field measurements than thermal effects. This is consistent with results previously reported in other studies (Agnan et al., 2016; García-Sánchez et al., 2006; Liu et al., 2014; Wallschläger et al., 1999; Wang et al., 2005) and likely confirms that radiation, despite contributing to soil heating and subsequently to the thermal enhancement of Hg^0 fluxes, can also have an effect on Hg^0 evasion independent from that related to soil temperature (Bahlmann et al., 2006). Further research is needed to evaluate the possible contributions of Hg^0 formation and volatilisation related to biotic reduction mediated by Hg-resistant microorganisms, frequently isolated from Hg-contaminated soils (Mahbub et al., 2016) and also present in the Idrija Hg mine area (Bourdineaud et al., 2020; Campos-Guillén et al., 2014; Hines et al., 2000). The relatively scarce bioavailability of the α-HgS fraction predominant in our soils could have limited this contribution, but recent studies suggested that under particular conditions (i.e. after complexation) this form can also be taken up and transformed by microorganisms (O'Connor et al., 2019; Zhang et al., 2012).

The strong dependence of Hg^0 fluxes on UV radiation is also confirmed considering the variation of both parameters during the measurement periods over each individual day (Fig. 4 and Figs. S6–S10). Hg^0 fluxes generally increase in the morning up to a peak in the central part of the day and then decline in the afternoon, following the pattern of incident UV radiation, as already observed in several studies in various environments (Kyllönen et al., 2012; Shi et al., 2020; Zhu et al., 2018). The Hg^0 emission drop in the afternoon was particularly rapid at TUR (Fig. S9), where sampling points were shaded by surrounding trees. Conversely, soil temperatures showed a smaller fluctuation during the monitoring period, remaining almost constant during afternoon measurements in summer and showing slight decreases in autumn and winter. Moreover, during summer sampling at FOS the sun was intermittently hidden by clouds, resulting in an irregular variation of UV radiation and a corresponding trend of Hg^0 fluxes, whereas soil temperatures did not show notable variations (Fig. 4). These rapid changes of fluxes in response to changes in the UV radiation could reinforce the hypothesis that Hg^0 emissions at our study sites are more influenced by irradiation than soil temperatures (García-Sánchez et al., 2006; Zhu et al., 2011) and that the soil portion more involved in gaseous exchanges is restricted to a shallow surface layer more affected by incident radiation variations (Eckley et al., 2015; Sigler and Lee, 2006; Zhou et al., 2021). However, higher temperatures could explain the generally higher Hg^0 fluxes recorded in the afternoon than in the morning (excluding TUR) despite the comparable incident UV radiation levels.

Table 2
Kendall rank correlation coefficients (τ) among Hg^0 fluxes and environmental parameters values recorded in all seasons at the different sampling sites. The significance level is also reported (***$p < 0.001$; **$p < 0.01$; *$p < 0.05$).

	T soil (°C)	UV (W m^{-2})	T air (°C)	air RH (%)
Bare soils				
SVI	0.72***	0.75***	0.76***	-0.54***
SAV	0.43***	0.55***	0.46***	-0.32**
SAG	0.53***	0.74***	0.61***	-0.73***
TUR	0.80***	0.82***	0.78***	-0.34**
SCZ	0.69***	0.78***	0.76***	0.41***
FOS	0.76***	0.65***	0.79***	-0.10
Vegetated soil				
SVI	0.42***	0.69***	0.45***	-0.59***
SAV	0.53***	0.61***	0.60***	-0.16
SAG	0.51***	0.74***	0.57***	-0.65***
TUR	0.80***	0.78***	0.79***	-0.37**
SCZ	0.46***	0.60***	0.49***	0.32**
FOS	0.39***	0.62***	0.37***	-0.16

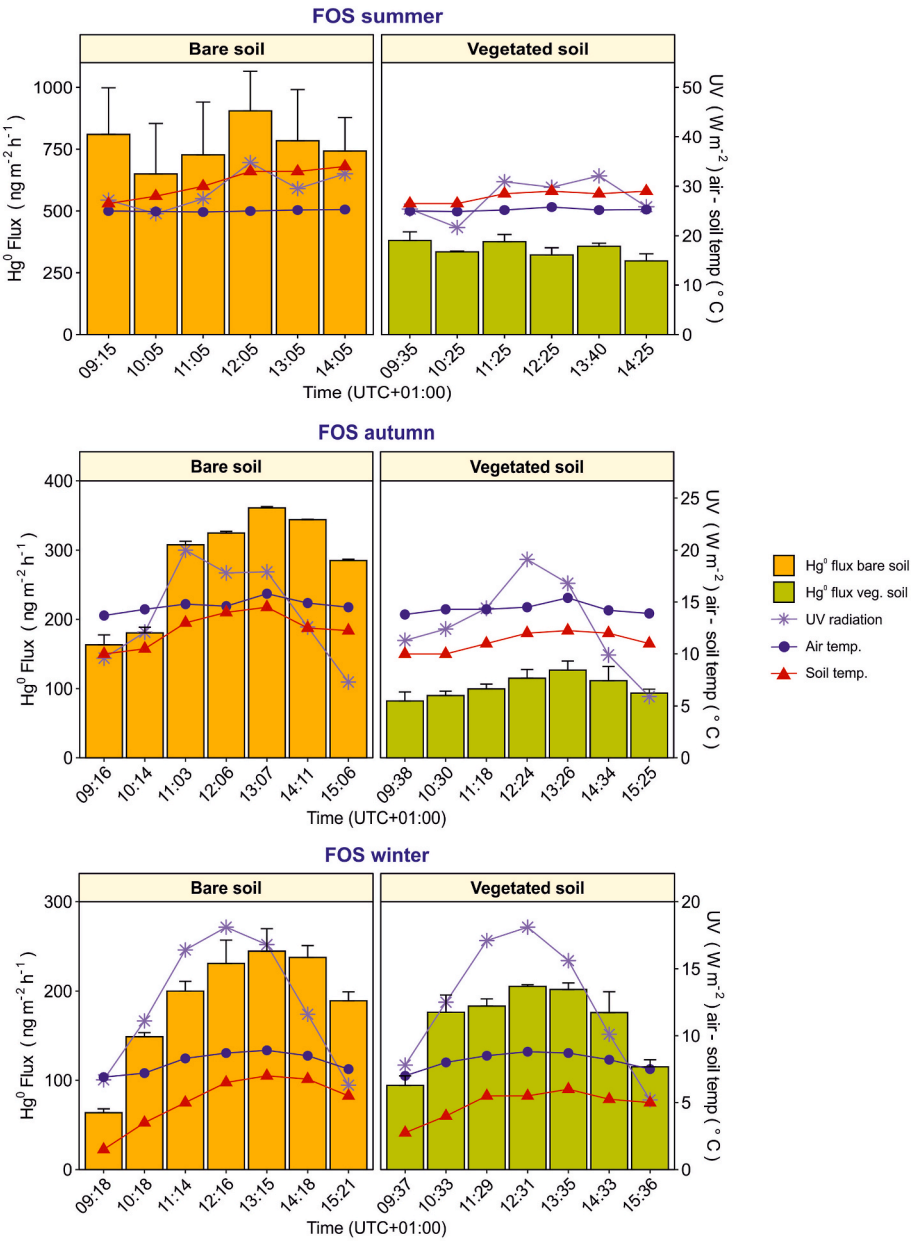

Fig. 4. Example of diurnal variation of Hg^0 fluxes from bare and vegetated soil at site FOS in the various seasons (results from other sites are reported in supplementary material).

This effect was more evident for bare soils and could also be related to progressive soil drying observed in the field, as water evaporation can enhance Hg transport to the surface and its subsequent release (Briggs and Gustin, 2013). A better agreement between patterns of Hg^0 fluxes and soil temperatures was generally observed in autumn and winter than in summer coupled with relatively higher soil moisture, possibly confirming that thermal effects on Hg emissions are more relevant in wet rather than dry soils (Park et al., 2014; Zhou et al., 2017). This is likely related to an increase desorption of bound Hg at a relatively high soil water contents due to the competition of more polar water molecules for binding sites and decreasing binding energy (Briggs and Gustin, 2013; Park et al., 2014). Moreover, increasing water content could also stimulate microbial processes leading to Hg desorption from surfaces (Pannu et al., 2014). Desorbed Hg^{2+} is more available for reduction to Hg^0, a reaction further enhanced at a relatively high soil moisture through the decreasing of soil redox potential (Schlüter, 2000), but this effect has been observed only for relatively high soil water contents (>30% Zhou et al., 2017; MacSween and Edwards, 2021) as most of those observed in our study in autumn and winter (Fig. S3). Temperature increase under such conditions can further enhance the rate of these reactions and favour the transport of both Hg^{2+} and Hg^0 to the soil surface together with water evaporation and the subsequent release of Hg^0 to the atmosphere (Briggs and Gustin, 2013; O'Connor et al., 2019).

Despite low temperatures, Hg^0 fluxes recorded in winter were generally comparable to those found in autumn, particularly in the case of vegetated soil plots likely due to changes in vegetation cover (see Section 3.4.2). During winter, the soil was generally covered by frost in the morning and then gradually thawed. In the first measurements conducted under conditions of low irradiation and temperatures, Hg^0 emissions were generally low, close to the chamber blank, and then sharply increased during the rest of the day. While soil thaws during the day, the contraction of the frozen liquid fraction of the soil matrix can connect the interstitial pore spaces, favouring the movement of Hg^0 potentially stored in soil pore air to the surface (Ci et al., 2018)

particularly at relatively high soil water content (Corbett-Hains et al., 2012) such as those observed in this study in winter, explaining the observed patterns of Hg^0 fluxes. Furthermore, in a recent laboratory study, Walters et al. (2016) observed increasing Hg^0 emission from soils thawing at a constant temperature of around 0 °C and related this increase to the energy transfer to the system rather than changes in temperature. The results of our study appear to be in agreement with this hypothesis, as winter measurements were characterised by relatively high insolation and small changes in soil temperatures during the morning. This effect could explain the occurrence of positive fluxes in winter with soil temperatures near 0 °C, but these low values still limited absolute Hg^0 emission, considering that Hg^0 winter fluxes at SCZ, SVI, and TUR from bare soil plots were significantly ($p < 0.05$, K–W) lower than those recorded in autumn.

3.4.2. *Effects of grass-vegetation cover*

In general, Hg^0 fluxes from grass-vegetated soils were lower than those calculated for bare soils at the same site: considering the daily averages, the vegetation cover caused a reduction of Hg^0 releases compared to bare soil plots of 9.3–68.2% in summer, 41.4–78.0% in autumn, and 12.4–60.0% in winter (Fig. 5). The presence of vegetation influences the environmental variables at the soil-air interface through affecting air mixing, reducing solar radiation that reaches the surface and consequently influencing soil temperature and moisture (Gustin et al., 2004). Through these effects, the presence of vegetation often limits the formation and volatilisation of Hg^0 from soils compared to non-vegetated areas (Agnan et al., 2016; Choi and Holsen, 2009b; Zhang et al., 2021). Lower Hg^0 fluxes from grass-covered as compared to bare soils have been previously reported for areas directly impacted by Hg mining activity (Fantozzi et al., 2013) or waste disposal (Tao et al., 2017), confirming the role of vegetation in reducing the impact of substrate pollution on the local atmosphere (Yan et al., 2019), but also for background zones (Fu et al., 2008; Sun et al., 2020b). However, it should be stressed that Hg^0 fluxes from soils characterised by the presence of vegetation are still regulated by the combined influence of radiation and temperature (Ma et al., 2018; Osterwalder et al., 2019), as also confirmed by the similar trends of emission, UV radiation, and soil temperatures recorded in this study (Fig. 4 and Figs. S6–S10).

Another important aspect that should be considered is the vegetation growth stage, which can seriously control the Hg^0 releases at the soil-air interface (Gao et al., 2020), as typically the reduction of Hg^0 fluxes is higher during active growth and peak vegetation periods and decreases during senescence (Eckley et al., 2021; Sun et al., 2020b). The results obtained in this study are in good agreement with this hypothesis. During summer, Hg^0 fluxes from vegetated soils were significantly ($p < 0.05$, K–W, Fig. 3) lower than from bare soils at sites SVI, SAG, TUR, and FOS, where vegetation was well developed ensuring effective shading and limiting photoreduction and energy reaching the soil surface (Gao et al., 2019). Conversely, measurements at SAV and SCZ were conducted after mowing and removing grass and consequently the shading effect was limited, as confirmed by values of soil temperatures comparable to those found for bare soils. Hence, Hg^0 fluxes, enhanced by higher radiation reaching the surface, were lower but comparable to those found for bare soils, as commonly observed after harvest in agricultural soils (Sommar et al., 2016; Zhu et al., 2011). In autumn, despite a lower vegetation growth, Hg^0 emissions from vegetated plots were found to be significantly lower than those from bare soils at all sites (Fig. 3), suggesting that the physical structure of plants may still have limited the gaseous exchange through reducing light penetration, in agreement with the results of a previous study conducted in pristine meadows (Converse et al., 2010). Finally, in winter Hg^0 fluxes from vegetated soils were comparable and in some cases (SVI, SAV, SCZ, FOS) slightly higher than those found in autumn despite the lower temperatures, likely due to the presence of dry plant stubble which allowed for an increase in light that could reach the soil surface and consequently the formation of Hg^0, as already noted in other studies (Converse et al., 2010; Sun et al., 2020b). Interestingly, Hg^0 fluxes recorded from vegetated soils at site FOS in winter were significantly ($p < 0.05$, K–W) higher than those observed in autumn at the same site, likely due to the combination of scarce vegetation cover during winter and relatively high UV irradiation, as measurements in autumn were conducted under partial cloud cover. Winter conditions with dormant vegetation likely represent soil fluxes with minimal vegetation effects, with emissions that can be comparable to those from bare soils (Stamenkovic et al., 2008), as generally occurred in this study (Fig. 3). Moreover, in some morning measurements during winter slightly higher Hg^0 fluxes from vegetated than bare soils were detected (Fig. 4, S6-S8, S10), pointing to the extremely high uncertainty of the estimation of average Hg^0 flux reduction from vegetated soil plots in winter (Fig. 5): consequently, despite average daily Hg^0 fluxes from vegetated soils in winter being lower than those from bare soils, it is possible to assume that these differences are only marginally related to the presence of vegetation during this season (During et al., 2009). These results confirm that favouring the growth of vegetation on contaminated substrates could represent a simple and inexpensive remediation strategy to reduce Hg^0 releases into the atmosphere, mostly at sites where the local climate allows for the presence of dense natural vegetation during the hottest months of the year, when the highest emissions are expected. However, the efficacy of this strategy should be evaluated considering the local characteristics of each site, as the occurrence of periods with low vegetation development corresponding to high irradiation and temperature could significantly affect the reduction of Hg^0 emissions from soils by vegetation due to lack of soil cover, as observed at SAV and SCZ during summer in this study. For example, this situation could be caused by droughts events, the frequency of which is expected to increase due to global warming: this aspect should be considered when assessing the possible use of this mitigation strategy for Hg-contaminated sites (Zhao and Running, 2010; Jiskra et al., 2018).

On ecosystem level, living plants could also limit the amount of Hg

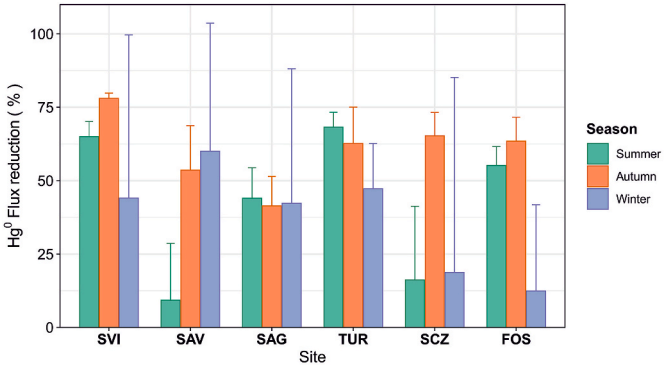

Fig. 5. Estimation of daily average Hg^0 fluxes reduction from grass-vegetated soil plots compared to bare soil plots in the different sites and seasons.

released to the atmosphere through stomatal uptake of Hg^0 emitted by the soil (Eckley et al., 2016) or cuticolar adsorption (Stamenkovic and Gustin, 2009). These processes are thought to be more effective at high atmospheric Hg concentrations and, more importantly, are reversible, as Hg present in the leaf interior or on the surface can be re-emitted to the atmosphere when ambient conditions change (Fu et al., 2008; Naharro et al., 2020). The experimental setup adopted in this study does not allow for the discrimination of the relative contribution of these processes to Hg^0 releases, but the impact of foliar Hg uptake may be considered negligible compared to shading effects, particularly in grassland ecosystems characterised by low leaf areas (Converse et al., 2010; Gao et al., 2020; Sun et al., 2020b).

As fluxes from bare and vegetated soils were measured on contiguous but different plots, it cannot be excluded that the differences in Hg^0 fluxes may be also related to upper soil horizon characteristics (e.g. porosity, THg concentration), which could be highly variable even over short distances (During et al., 2009; Rinklebe et al., 2009). Considering, however, that vegetated plots showed consistently lower fluxes than bare soils, even when characterised by slightly higher THg contents, it can be assumed that the influence of vegetation (in summer and autumn seasons) is greater than that of soil characteristics. Conversely, the variable Hg content in soils heavily influenced the variability of Hg^0 fluxes between the different sites, as discussed in the next section.

3.4.3. *Effects of soil Hg and organic matter content*

The availability of Hg in surface soils represents one of the most important parameters controlling the magnitude of Hg^0 fluxes into the atmosphere, particularly in Hg-enriched areas (Agnan et al., 2016; Osterwalder et al., 2019), and the results of this study are in good agreement with this evidence. The average Hg^0 fluxes from bare soils were indeed significantly correlated with THg concentrations in topsoils both in summer ($r = 0.95$, $p < 0.01$) and autumn ($r = 0.77$, $p < 0.05$), whereas no relation was found in winter (Fig. 6) likely due to the low emissions recorded at all sites during the mornings. Generally, the differences between average Hg^0 fluxes at different sites in summer and autumn may be explained by the different THg concentrations in soils, whereas in winter the Hg^0 releases were more homogenous. For example, Hg^0 fluxes from both bare and vegetated soils at the most impacted site (TUR) in winter, limited by both low temperatures and tree shading in the afternoon, were not statistically different from those of SAV and SCZ, characterised by the lowest Hg content in the substrate.

Moreover, average Hg^0 fluxes in summer and autumn were also significantly correlated with the concentration of α-HgS (Fig. 6), representing the largely predominant Hg fraction in the selected soils. These

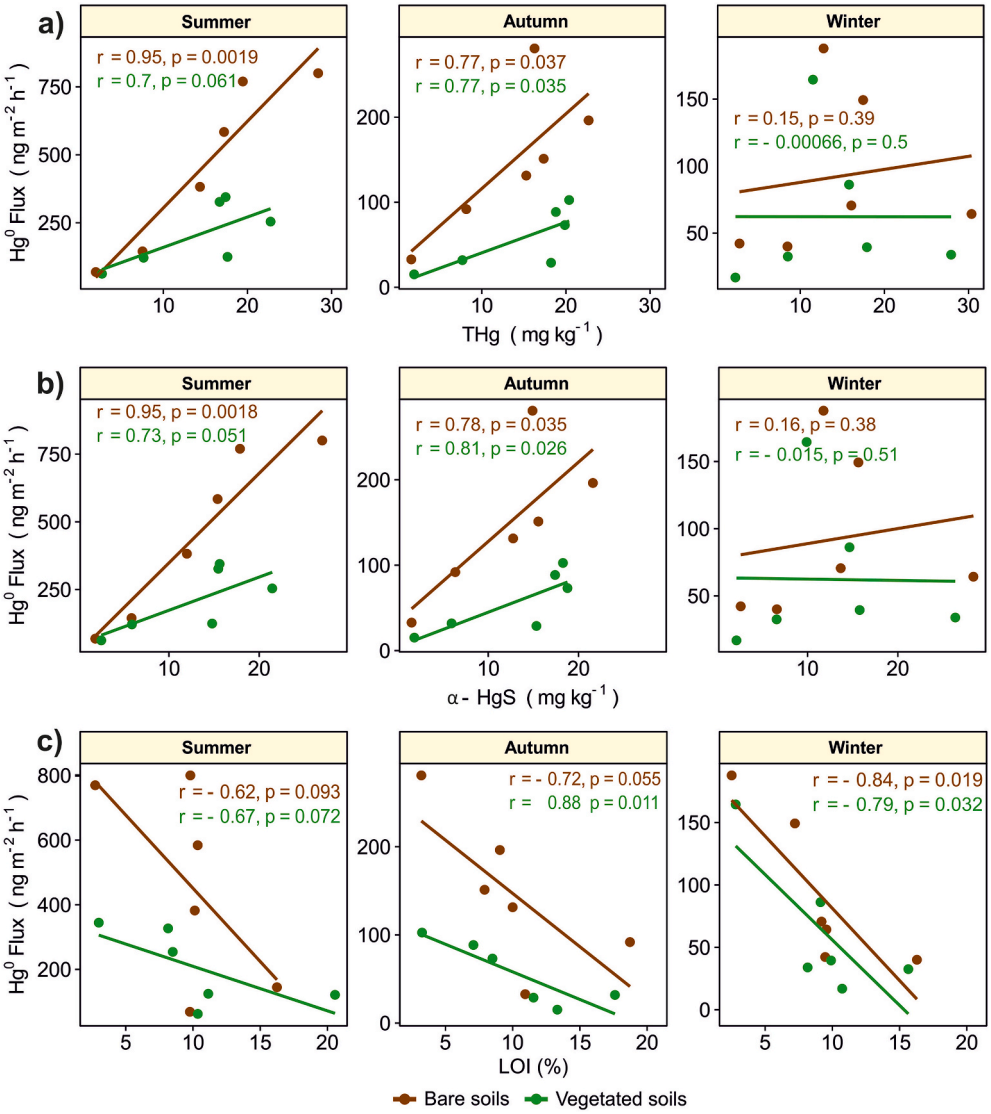

Fig. 6. Correlation between average Hg^0 fluxes from bare and vegetated soils at the experimental sites with a) average soil total Hg concentration b) average soil α-HgS concentration c) average soil OM content (as LOI).

results confirm that despite the low mobility of α-HgS in the environment (Gai et al., 2016), this form can significantly contribute to the releases of Hg^0 from soils likely thanks to the energy provided by irradiation.

The relatively high activation energy required to initiate volatilisation from α-HgS compared to other Hg forms (Gustin et al., 2002; Schlüter, 2000) may also explain the low Hg^0 fluxes recorded during morning measurements in winter coupled with low temperatures. Emissions recorded in these conditions are likely attributable to the no-α-HgS fraction, present in comparable amounts at all the sites. Indeed, Hg forms occurring in this fraction are generally more mobile than α-HgS and could generate a more rapid increase in Hg^0 volatilisation in response to light or thermal excitation (Gustin et al., 2002; Kocman and Horvat, 2010; Llanos et al., 2011). Moreover, a greater contribution of α-HgS to Hg^0 formation and volatilisation could also represent the reason why the highest average fluxes during the winter season corresponded to measurements at SAG and FOS sites, characterised by the highest values of both UV radiation and temperatures (Table S3).

Considering the average Hg^0 fluxes from vegetated soil plots, weaker relationships between soil Hg content and Hg^0 releases were observed especially in summer (Fig. 6), confirming the importance of vegetation for Hg^0 emission abatement. A striking example is represented by comparable emissions recorded from vegetated soil at SVI and SCZ in summer despite the difference in THg (17.63 and 7.65 mg kg^{-1}, respectively): as aforementioned, emissions at SCZ may have been enhanced by vegetation cutting, whereas a thriving grass cover limited the emission at SVI (Zhang et al., 2021).

Additionally, Hg^0 fluxes at FOS were generally higher than expected in all seasons and greater than those recorded, for example, at TUR and SAG despite the lower average Hg content in soil and the cloud cover during field sampling in summer. A possible explanation may be found in the different OM content in soils, lower at FOS than at all other sites. Organic matter has a strong affinity for Hg^0 and can therefore effectively adsorb it in the soil pore space, limiting its vertical diffusion and subsequent release into the atmosphere (Fu et al., 2012; Obrist et al., 2014; Yuan et al., 2019). Moreover, the formation of strong covalent bonds between Hg^{2+} and functional groups of OM, particularly those containing reduced sulphur (Reis et al., 2015b), could also influence the amount of Hg available for reduction to Hg^0 and consequently limit gaseous releases (Gao et al., 2020; Yang et al., 2007). The results obtained in this study are in agreement with this hypothesis, as confirmed by the negative relationships generally observed between average values of LOI and Hg^0 fluxes (Fig. 6), confirming that a low content of OM in soil may be conducive for Hg evasion (Llanos et al., 2011). However, further research is needed to assess if this effect could be at least partially ascribed to changes in the type of OM in the soil (not determined in this study), which can also significantly affect Hg mobility (Sysalová et al., 2017).

4. Conclusions

The results of the field measurements presented in this work represent the first direct evidence of Hg^0 releases from the contaminated soils of the Isonzo River alluvial plain, impacted by Hg due to historical extraction activity from the Idrija mining district. Despite the distance from the contamination source, the obtained values were comparable to those reported worldwide for sites impacted by mining, confirming that past supplies of Hg-enriched material still enhance gaseous releases even more than 25 years after the closure of the mine. Overall, Hg^0 emissions were significantly higher during the summer than autumn and winter, which conversely showed comparable values, due to higher incident UV radiation and temperatures that likely promoted the formation of volatile Hg^0.

Mercury content in the soil, mostly occurring as α-HgS, played an important role in influencing the magnitude of Hg^0 fluxes in the different sites, particularly during summer and autumn, whereas emissions in winter were more homogeneous, likely due to a low contribution of α-HgS to volatilisation under low temperature conditions. Moreover, soil organic matter content likely influenced the evasion of Hg^0 to the atmosphere through the adsorption of Hg, too.

Actively growing native grass-vegetation significantly limited Hg^0 emissions during summer and autumn compared to that from bare soils due to soil shading, whereas in winter this effect was not observed due to the presence of only dormant vegetation, ineffectively covering the soil surface. Considering that a remediation of the plain is unlikely due to the spread of contamination over many kilometres, the preservation of the "natural" situation with grass vegetation cover represents a valuable option to limit the amount of Hg^0 releases and thus the impact of substrate Hg-contamination on the local atmosphere and further spatial spreading through atmospheric transport. However, further research is needed to examine the contribution of plants to Hg^0 exchanges in this area.

Having ascertained the existence of relevant diurnal Hg^0 emissions from the selected contaminated soils, further long-term continuous monitoring is needed to better define the diurnal trend of Hg^0 emissions, also taking into consideration the processes occurring during the nocturnal period and evaluating the possible contribution related to dry and wet atmospheric deposition. Furthermore, considering the good response of the accumulation chamber technique to changes in environmental conditions, particularly of incident radiation, and the rapidity of measures (5 min each), this approach could allow for a high number of distinct measures over a short time in different points. Increasing the number of sampling points per area may then allow for a better evaluation of the variability of Hg^0 fluxes on a small spatial scale, and to accurately assess the diffuse emissions of Hg^0 from a selected area. This approach needs also to be tested with regard to risk assessment procedures in contaminated sites, in order to evaluate the potential exposure of local inhabitants to Hg through inhalation after evaporation from soil surfaces. Moreover, it would be desirable to measure Hg^0 fluxes at the soil-air interface in other environments e.g. the croplands that cover a large part of the Isonzo River alluvial plain, where agricultural activities such as ploughing and harvesting cause a marked disturbance of soils and the exposure of bare soil surfaces to direct incident radiation, potentially leading to strong Hg emissions into the atmosphere.

Credit author statement

Federico Floreani: Conceptualization, Methodology, Investigation, Data curation, Formal analysis, Writing – original draft, Writing – review & editing, Visualisation. Valeria Zappella: Investigation, Data curation, Visualisation. Jadran Faganeli: Conceptualization, Validation. Stefano Covelli: Conceptualization, Methodology, Resources, Writing – original draft, Writing – review & editing, Project administration, Supervision.

Funding

This research did not receive any specific grant from funding agencies in the public, commercial, or not-for-profit sectors.

Declaration of competing interest

The authors declare that they have no known competing financial interests or personal relationships that could have appeared to influence the work reported in this paper.

Data availability

Data will be made available on request.

Acknowledgements

This work is part of the Ph.D. thesis written by Federico Floreani at the University of Trieste; the Ph.D. fellowship was founded by PO FRIULI VENEZIA GIULIA-FONDO SOCIALE EUROPEO 2014/2020. The authors are very grateful to Dr. Alessandro Acquavita for his useful suggestions and his support in identifying sampling points. A special thanks to Federico Vito Zotta for his valuable support in sampling operations. Karry Close is warmly acknowledged for proofreading the manuscript. The two anonymous reviewers are warmly acknowledged for their thorough reviews and useful suggestions which improved the earlier version of the manuscript.

Appendix A. Supplementary data

Supplementary data to this article can be found online at https://doi.org/10.1016/j.envpol.2022.120921.

References

Acquavita, A., Brandolin, D., Cattaruzza, C., Felluga, A., Maddaleni, P., Meloni, C., Pasquon, M., Predonzani, S., Poli, L., Skert, N., Zanello, A., 2022. Mercury distribution and speciation in historically contaminated soils of the Isonzo River Plain (NE Italy). J. Soils Sediments 22, 79–92. https://doi.org/10.1007/s11368-021-03038-2.

Agnan, Y., Le Dantec, T., Moore, C.W., Edwards, G.C., Obrist, D., 2016. New constraints on terrestrial surface-atmosphere fluxes of gaseous elemental mercury using a global database. Environ. Sci. Technol. 50, 507–524. https://doi.org/10.1021/acs.est.5b04013.

Anderson, A., 1979. Mercury in Soils. In: Nriagu, J.O. (Ed.), The Biogeochemistry of Mercury in the Environment. Elsevier/North Holland, Amsterdam, pp. 79–112.

ARPA FVG-OSMER e GRN, 2021. Database "OMNIA". Available online: http://www.meteo.fvg.it/. (Accessed 27 September 2022).

Bagnato, E., Barra, M., Cardellini, C., Chiodini, G., Parello, F., Sprovieri, M., 2014. First combined flux chamber survey of mercury and CO2 emissions from soil diffuse degassing at Solfatara of Pozzuoli crater, Campi Flegrei (Italy): mapping and quantification of gas release. J. Volcanol. Geoth. Res. 289, 26–40. https://doi.org/10.1016/j.jvolgeores.2014.10.017.

Bahlmann, E., Ebinghaus, R., Ruck, W., 2006. Development and application of a laboratory flux measurement system (LFMS) for the investigation of the kinetics of mercury emissions from soils. J. Environ. Manag. 81, 114–125. https://doi.org/10.1016/j.jenvman.2005.09.022.

Baptista-Salazar, C., Richard, J.H., Horf, M., Rejc, M., Gosar, M., Biester, H., 2017. Grain-size dependence of mercury speciation in river suspended matter, sediments and soils in a mercury mining area at varying hydrological conditions. Appl. Geochem. 81, 132–142. https://doi.org/10.1016/j.apgeochem.2017.04.006.

Barago, N., Floreani, F., Acquavita, A., Esbrí, J.M., Covelli, S., Higueras, P., 2020. Spatial and temporal trends of gaseous elemental mercury over a highly impacted coastal environment (Northern Adriatic, Italy). Atmosphere (Basel) 11, 935. https://doi.org/10.3390/atmos11090935.

Bavec, Š., Gosar, M., 2016. Speciation, mobility and bioaccessibility of Hg in the polluted urban soil of Idrija (Slovenia). Geoderma 273, 115–130. https://doi.org/10.1016/j.geoderma.2016.03.015.

Beckers, F., Rinklebe, J., 2017. Cycling of mercury in the environment: sources, fate, and human health implications: a review. Crit. Rev. Environ. Sci. 47, 693–794. https://doi.org/10.1080/10643389.2017.1326277.

Berg, T., Aspmo, K., Steinnes, E., 2008. Transport of Hg from Atmospheric mercury depletion events to the mainland of Norway and its possible influence on Hg deposition. Geophys. Res. Lett. 35, L09802 https://doi.org/10.1029/2008GL033586.

Biester, H., Gosar, M., Covelli, S., 2000. Mercury speciation in sediments affected by dumped mining residues in the drainage area of the Idrija mercury mine, Slovenia. Environ. Sci. Technol. 34, 3330–3336. https://doi.org/10.1021/es991334v.

Biester, H., Scholz, C., 1997. Determination of mercury binding forms in contaminated soils: mercury pyrolysis versus sequential extractions. Environ. Sci. Technol. 31, 233–239. https://doi.org/10.1021/es960369h.

Boening, D.W., 2000. Ecological effects, transport, and fate of mercury: a general review. Chemosphere 40, 1335–1351. https://doi.org/10.1016/S0045-6535(99)00283-0.

Bourdineaud, J.P., Durn, G., Režun, B., Manceau, A., Hrenović, J., 2020. The chemical species of mercury accumulated by Pseudomonas idrijaensis, a bacterium from a rock of the Idrija mercury mine, Slovenia. Chemosphere 248, 126002. https://doi.org/10.1016/j.chemosphere.2020.126002.

Briggs, C., Gustin, M.S., 2013. Building upon the conceptual model for soil mercury flux: evidence of a link between moisture evaporation and Hg evasion. Water, Air, Soil Pollut. 224, 1744. https://doi.org/10.1007/s11270-013-1744-5.

Cabassi, J., Venturi, S., Di Bennardo, F., Nisi, B., Tassi, F., Magi, F., Ricci, A., Picchi, G., Vaselli, O., 2021. Flux measurements of gaseous elemental mercury (GEM) from the geothermal area of "Le Biancane" natural park (Monterotondo Marittimo, Grosseto, Italy): biogeochemical processes controlling GEM emission. J. Geochem. Explor. 228, 106824 https://doi.org/10.1016/j.gexplo.2021.106824.

Camarda, M., Gurrieri, S., Valenza, M., 2009. Effects of soil permeability and recirculation flux on soil CO_2 flux measurements performed using a closed dynamic accumulation chamber. Chem. Geol. 265, 387–393. https://doi.org/10.1016/j.chemgeo.2009.05.002.

Campos-Guillén, J., Pérez, J.C., Medina, J.A.C., Vera, C.M., Rosas, L.M.S., Gutiérrez, C.L., Salinas, I.G., Hernández Ramírez, M.R., Alonso, G.S., Hernández, A.C., Gutiérrez, C. S., Gómez, S.R., Martínez, X.P., Hidalgo, E., álvarez, Gosar, M., Dizdarevič, T., 2014. Draft genome sequence of the mercury-resistant bacterium Acinetobacter idrijaensis strain MII, isolated from a mine-impacted area, Idrija, Slovenia. Genome Announc. 2 https://doi.org/10.1128/genomeA.01177-14.

Carmona, M., Llanos, W., Higueras, P., Kocman, D., 2013. Mercury emissions in equilibrium: a novel approach for the quantification of mercury emissions from contaminated soils. Anal. Methods 5, 2793–2801. https://doi.org/10.1039/c3ay25700b.

Carpi, A., Lindberg, S.E., 1998. Application of a Teflon® dynamic flux chamber for quantifying soil mercury flux: tests and results over background soil. Atmos. Environ. 32, 873–882. https://doi.org/10.1016/S1352-2310(97)00133-7.

Cerovac, A., Covelli, S., Emili, A., Pavoni, E., Petranich, E., Gregorič, A., Urbanc, J., Zavagno, E., Zini, L., 2018. Mercury in the unconfined aquifer of the Isonzo/SoČa River alluvial plain downstream from the Idrija mining area. Chemosphere 195, 749–761. https://doi.org/10.1016/j.chemosphere.2017.12.105.

Chiodini, G., Cioni, R., Guidi, M., Raco, B., Marini, L., 1998. Soil CO2 flux measurements in volcanic and geothermal areas. Appl. Geochem. 13, 543–552. https://doi.org/10.1016/S0883-2927(97)00076-0.

Choi, H.D., Holsen, T.M., 2009a. Gaseous mercury emissions from unsterilized and sterilized soils: the effect of temperature and UV radiation. Environ. Pollut. 157, 1673–1678. https://doi.org/10.1016/j.envpol.2008.12.014.

Choi, H.D., Holsen, T.M., 2009b. Gaseous mercury fluxes from the forest floor of the Adirondacks. Environ. Pollut. 157, 592–600. https://doi.org/10.1016/j.envpol.2008.08.020.

Ci, Z., Peng, F., Xue, X., Zhang, X., 2018. Temperature sensitivity of gaseous elemental mercury in the active layer of the Qinghai-Tibet Plateau permafrost. Environ. Pollut. 238, 508–515. https://doi.org/10.1016/j.envpol.2018.02.085.

Ci, Z., Peng, F., Xue, X., Zhang, X., 2016. Air-surface exchange of gaseous mercury over permafrost soil: an investigation at a high-altitude (4700 m.a.s.l.) and remote site in the central Qinghai-Tibet Plateau. Atmos. Chem. Phys. 16, 14741–14754. https://doi.org/10.5194/acp-16-14741-2016.

Clarkson, T.W., Magos, L., 2006. The toxicology of mercury and its chemical compounds. Crit. Rev. Toxicol. 36, 609–662. https://doi.org/10.1080/10408440600845619.

Colica, A., Benvenuti, M., Chiarantini, L., Costagliola, P., Lattanzi, P., Rimondi, V., Rinaldi, M., 2019. From point source to diffuse source of contaminants: the example of mercury dispersion in the Paglia River (Central Italy). Catena 172, 488–500. https://doi.org/10.1016/j.catena.2018.08.043.

Contin, M., Rizzardini, C.B., Catalano, L., De Nobili, M., 2012. Contamination by mercury affects methane oxidation capacity of aerobic arable soils. Geoderma 189–190, 250–256. https://doi.org/10.1016/j.geoderma.2012.06.031.

Converse, A.D., Riscassi, A.L., Scanlon, T.M., 2014. Seasonal contribution of dewfall to mercury deposition determined using a micrometeorological technique and dew chemistry. J. Geophys. Res. 119, 284–292. https://doi.org/10.1002/2013JD020491.

Converse, A.D., Riscassi, A.L., Scanlon, T.M., 2010. Seasonal variability in gaseous mercury fluxes measured in a high-elevation meadow. Atmos. Environ. 44, 2176–2185. https://doi.org/10.1016/j.atmosenv.2010.03.024.

Corbett-Hains, H., Walters, N.E., Van Heyst, B.J., 2012. Evaluating the effects of sub-zero temperature cycling on mercury flux from soils. Atmos. Environ. 63, 102–108. https://doi.org/10.1016/j.atmosenv.2012.09.047.

Cotel, S., Schäfer, G., Traverse, S., Marzougui-Jaafar, S., Gay, G., Razakarisoa, O., 2015. Evaluation of VOC fluxes at the soil-air interface using different flux chambers and a quasi-analytical approach. Water, Air, Soil Pollut. 226, 356. https://doi.org/10.1007/s11270-015-2596-y.

Coufalík, P., Krásenský, P., Dosbaba, M., Komárek, J., 2012. Sequential extraction and thermal desorption of mercury from contaminated soil and tailings from Mongolia. Cent. Eur. J. Chem. 10, 1565–1573. https://doi.org/10.2478/s11532-012-0074-6.

Cucchi, F., Franceschini, G., Zini, L., 2008. Hydrogeochemical investigations and groundwater provinces of the Friuli Venezia Giulia Plain aquifers, northeastern Italy. Environ. Geol. 55, 985–999. https://doi.org/10.1007/s00254-007-1048-4.

Da Lio, C., Tosi, L., 2018. Land subsidence in the Friuli Venezia Giulia coastal plain, Italy: 1992–2010 results from SAR-based interferometry. Sci. Total Environ. 633, 752–764. https://doi.org/10.1016/j.scitotenv.2018.03.244.

Dalziel, J., Tordon, R., 2014. Gaseous mercury flux measurements from two mine tailing sites in the Seal Harbour area of Nova Scotia. Geochem. Explor. Environ. Anal. 14, 17–24. https://doi.org/10.1144/geochem2011-112.

Davidson, E.A., Savage, K., Verchot, L.V., Navarro, R., 2002. Minimizing artifacts and biases in chamber-based measurements of soil respiration. Agric. For. Meteorol. 113, 21–37. https://doi.org/10.1016/S0168-1923(02)00100-4.

Debure, M., Grangeon, S., Robinet, J.C., Madé, B., Fernández, A.M., Lerouge, C., 2020. Influence of soil redox state on mercury sorption and reduction capacity. Sci. Total Environ. 707, 136069 https://doi.org/10.1016/j.scitotenv.2019.136069.

Di Francesco, F., Ferrara, R., Mazzolai, B., 1998. Two ways of using a chamber for mercury flux measurement - a simple mathematical approach. Sci. Total Environ. 213, 33–41. https://doi.org/10.1016/S0048-9697(98)00068-0.

Dizdarevič, T., 2001. The influence of mercury production in Idrija mine on the environment in the Idrija region and over a broad area. RMZ Mater. Geoenviron 48, 56–64.

Douglas, T.A., Blum, J.D., 2019. Mercury isotopes reveal atmospheric gaseous mercury deposition directly to the arctic coastal snowpack. Environ. Sci. Technol. Lett. 6, 235–242. https://doi.org/10.1021/acs.estlett.9b00131.

During, A., Rinklebe, J., Böhme, F., Wennrich, R., Stärk, H.J., Mothes, S., Du Laing, G., Schulz, E., Neue, H.U., 2009. Mercury volatilization from three floodplain soils at the Central Elbe River, Germany. Soil Sediment Contam. 18, 429–444. https://doi.org/10.1080/15320380902962395.

Eckley, C.S., Blanchard, P., McLennan, D., Mintz, R., Sekela, M., 2015. Soil-air mercury flux near a large industrial emission source before and after closure (flin flon, manitoba, Canada). Environ. Sci. Technol. 49, 9750–9757. https://doi.org/10.1021/acs.est.5b01995.

Eckley, C.S., Eagles-Smith, C., Tate, M.T., Krabbenhoft, D.P., 2021. Surface-air mercury fluxes and a watershed mass balance in forested and harvested catchments. Environ. Pollut. 277, 116869 https://doi.org/10.1016/j.envpol.2021.116869.

Eckley, C.S., Tate, M.T., Lin, C.J., Gustin, M., Dent, S., Eagles-Smith, C., Lutz, M.A., Wickland, K.P., Wang, B., Gray, J.E., Edwards, G.C., Krabbenhoft, D.P., Smith, D.B., 2016. Surface-air mercury fluxes across Western North America: a synthesis of spatial trends and controlling variables. Sci. Total Environ. 568, 651–665. https://doi.org/10.1016/j.scitotenv.2016.02.121.

Esbrí, J.M., Bernaus, A., Ávila, M., Kocman, D., García-Noguero, E.M., Guerrero, B., Gaona, X., Álvarez, R., Perez-Gonzalez, G., Valiente, M., Higueras, P., Horvat, M., Loredo, J., 2010. XANES speciation of mercury in three mining districts - almadén, Asturias (Spain), Idria (Slovenia). J. Synchrotron Radiat. 17, 179–186. https://doi.org/10.1107/S0909049510001925.

Fantozzi, L., Ferrara, R., Dini, F., Tamburello, L., Pirrone, N., Sprovieri, F., 2013. Study on the reduction of atmospheric mercury emissions from mine waste enriched soils through native grass cover in the Mt. Amiata region of Italy. Environ. Res. 125, 69–74. https://doi.org/10.1016/j.envres.2013.02.004.

Ferrari, C.P., Padova, C., Faïn, X., Gauchard, P.A., Dommergue, A., Aspmo, K., Berg, T., Cairns, W., Barbante, C., Cescon, P., Kaleschke, L., Richter, A., Wittrock, F., Boutron, C., 2008. Atmospheric mercury depletion event study in Ny-Alesund (Svalbard) in spring 2005. Deposition and transformation of Hg in surface snow during springtime. Sci. Total Environ. 397, 167–177. https://doi.org/10.1016/j.scitotenv.2008.01.064.

Floreani, F., Barago, N., Acquavita, A., Covelli, S., Skert, N., Higueras, P., 2020. Spatial distribution and biomonitoring of atmospheric mercury concentrations over a contaminated coastal lagoon (Northern Adriatic, Italy). Atmosphere (Basel) 11, 1280. https://doi.org/10.3390/atmos11121280.

Fontana, A., Mozzi, P., Bondesan, A., 2008. Alluvial megafans in the Venetian-Friulian plain (north-eastern Italy): evidence of sedimentary and erosive phases during late pleistocene and holocene. Quat. Int. 189, 71–90. https://doi.org/10.1016/j.quaint.2007.08.044.

Fritsche, J., Obrist, D., Alewell, C., 2008. Evidence of microbial control of Hg0 emissions from uncontaminated terrestrial soils. J. Plant Nutr. Soil Sci. 171, 200–209. https://doi.org/10.1002/jpln.200625211.

Fu, X., Feng, X., Wang, S., 2008. Exchange fluxes of Hg between surfaces and atmosphere in the eastern flank of Mount Gongga, Sichuan province, southwestern China. J. Geophys. Res. Atmos. 113, D20306 https://doi.org/10.1029/2008JD009814.

Fu, X., Feng, X., Zhang, H., Yu, B., Chen, L., 2012. Mercury emissions from natural surfaces highly impacted by human activities in Guangzhou province, South China. Atmos. Environ. 54, 185–193. https://doi.org/10.1016/j.atmosenv.2012.02.008.

Gabriel, M.C., Williamson, D.G., 2004. Principal biogeochemical factors affecting the speciation and transport of mercury through the terrestrial environment. Environ. Geochem. Health 26, 421–434. https://doi.org/10.1007/s10653-004-1308-0.

Gai, K., Hoelen, T.P., Hsu-Kim, H., Lowry, G.V., 2016. Mobility of four common mercury species in model and natural unsaturated soils. Environ. Sci. Technol. 50, 3342–3351. https://doi.org/10.1021/acs.est.5b04247.

Gao, Y., Wang, Z., Wang, C., Zhang, X., 2019. The soil displacement measurement of mercury emission flux of the sewage irrigation farmlands in Northern China. Ecosys. Health Sustain. 5, 169–180. https://doi.org/10.1080/20964129.2019.1647117.

Gao, Y., Wang, Z., Zhang, X., Wang, C., 2020. Observation and estimation of mercury exchange fluxes from soil under different crop cultivars and planting densities in North China Plain. Environ. Pollut. 259, 113833 https://doi.org/10.1016/j.envpol.2019.113833.

García-Sánchez, A., Contreras, F., Adams, M., Santos, F., 2006. Atmospheric mercury emissions from polluted gold mining areas (Venezuela). Environ. Geochem. Health 28, 529–540. https://doi.org/10.1007/s10653-006-9049-x.

Giaiotti, D., Nordio, S., Stel, F., 2003. The climatology of hail in the plain of Friuli Venezia Giulia. Atmos. Res. 67–68, 247–259. https://doi.org/10.1016/S0169-8095(03)00084-X.

Gilli, R.S., Karlen, C., Weber, M., Rüegg, J., Barmettler, K., Biester, H., Boivin, P., Kretzschmar, R., 2018. Speciation and mobility of mercury in soils contaminated by legacy emissions from a chemical factory in the rhône valley in canton of valais, Switzerland. Soil Syst 2, 44. https://doi.org/10.3390/soilsystems2030044.

Gillis, A., Miller, D.R., 2000. Some potential errors in the measurement of mercury gas exchange at the soil surface using a dynamic flux chamber. Sci. Total Environ. 260, 181–189. https://doi.org/10.1016/S0048-9697(00)00562-3.

Gosar, M., Pirc, S., Bidovec, M., 1997. Mercury in the Idrijca River sediments as a reflection of mining and smelting activities of the Idrija mercury mine. J. Geochem. Explor. 58, 125–131. https://doi.org/10.1016/S0375-6742(96)00064-7.

Gustin, M.S., Biester, H., Kim, C.S., 2002. Investigation of the light-enhanced emission of mercury from naturally enriched substrates. Atmos. Environ. 36, 3241–3254. https://doi.org/10.1016/S1352-2310(02)00329-1.

Gustin, M.S., Coolbaugh, M.F., Engle, M.A., Fitzgerald, B.C., Keislar, R.E., Lindberg, S.E., Nacht, D.M., Quashnick, J., Rytuba, J.J., Sladek, C., Zhang, H., Zehner, R.E., 2003. Atmospheric mercury emissions from mine wastes and surrounding geologically enriched terrains. Environ. Geol. 43, 339–351. https://doi.org/10.1007/s00254-002-0630-z.

Gustin, M.S., Ericksen, J.A., Schorran, D.E., Johnson, D.W., Lindberg, S.E., Coleman, J.S., 2004. Application of controlled mesocosms for understanding mercury air-soil-plant exchange. Environ. Sci. Technol. 38, 6044–6050. https://doi.org/10.1021/es0487933.

Heiri, O., Lotter, A.F., Lemcke, G., 2001. Loss on ignition as a method for estimating organic and carbonate content in sediments: reproducibility and comparability of results. J. Paleolimnol. 25, 101–110. https://doi.org/10.1023/A:1008119611481.

Hines, M.E., Horvat, M., Faganeli, J., Bonzongo, J.C.J., Barkay, T., Major, E.B., Scott, K.J., Bailey, E.A., Warwick, J.J., Lyons, W.B., 2000. Mercury biogeochemistry in the idrija river, Slovenia, from above the mine into the gulf of trieste. Environ. Res. 83, 129–139. https://doi.org/10.1006/enrs.2000.4052.

Horowitz, H.M., Jacob, D.J., Zhang, Y., Dibble, T.S., Slemr, F., Amos, H.M., Schmidt, J.A., Corbitt, E.S., Marais, E.A., Sunderland, E.M., 2017. A new mechanism for atmospheric mercury redox chemistry: implications for the global mercury budget. Atmos. Chem. Phys. 17, 6353–6371. https://doi.org/10.5194/acp-17-6353-2017.

Hutchinson, G.L., Livingston, G.P., 2001. Vents and seals in non-steady-state chambers used for measuring gas exchange between soil and the atmosphere. Eur. J. Soil Sci. 52, 675–682. https://doi.org/10.1046/j.1365-2389.2001.00415.x.

ISO 13320:2020, 2020. Particle Size Analysis - Laser Diffraction Methods, second ed. 01, Geneva.

Jiskra, M., Sonke, J.E., Obrist, D., Bieser, J., Ebinghaus, R., Myhre, C.L., Pfaffhuber, K.A., Wängberg, I., Kyllönen, K., Worthy, D., Martin, L.G., Labuschagne, C., Mkololo, T., Ramonet, M., Magand, O., Dommergue, A., 2018. A vegetation control on seasonal variations in global atmospheric mercury concentrations. Nat. Geosci. 11, 244–250. https://doi.org/10.1038/s41561-018-0078-8.

Jiskra, M., Wiederhold, J.G., Skyllberg, U., Kronberg, R.M., Hajdas, I., Kretzschmar, R., 2015. Mercury deposition and Re-emission pathways in boreal forest soils investigated with Hg isotope signatures. Environ. Sci. Technol. 49, 7188–7196. https://doi.org/10.1021/acs.est.5b00742.

Kandel, T.P., Lærke, P.E., Elsgaard, L., 2016. Effect of chamber enclosure time on soil respiration flux: a comparison of linear and non-linear flux calculation methods. Atmos. Environ. 141, 245–254. https://doi.org/10.1016/j.atmosenv.2016.06.062.

Kocman, D., Horvat, M., 2010. A laboratory based experimental study of mercury emission from contaminated soils in the River Idrijca catchment. Atmos. Chem. Phys. 10, 1417–1426. https://doi.org/10.5194/acp-10-1417-2010.

Kocman, D., Horvat, M., Pirrone, N., Cinnirella, S., 2013. Contribution of contaminated sites to the global mercury budget. Environ. Res. 125, 160–170. https://doi.org/10.1016/j.envres.2012.12.011.

Kotnik, J., Horvat, M., Dizdarevič, T., 2005. Current and past mercury distribution in air over the Idrija Hg mine region, Slovenia. Atmos. Environ. 39, 7570–7579. https://doi.org/10.1016/j.atmosenv.2005.06.061.

Kurz, A.Y., Blum, J.D., Washburn, S.J., Baskaran, M., 2019. Changes in the mercury isotopic composition of sediments from a remote alpine lake in Wyoming. USA. Sci. Total Environ. 669, 973–982. https://doi.org/10.1016/j.scitotenv.2019.03.165.

Kyllönen, K., Hakola, H., Hellén, H., Korhonen, M., Verta, M., 2012. Atmospheric mercury fluxes in a southern boreal forest and wetland. Water, Air, Soil Pollut. 223, 1171–1182. https://doi.org/10.1007/s11270-011-0935-1.

Lei, D., Xiaohui, S., Yao, L., Baoyu, D., Qiong, W., Kaiyun, L., Jiawei, Z., Qingru, W., Shuxiao, W., 2021. Soil-atmosphere exchange of gaseous elemental mercury in three subtropical forests with different substrate Hg concentrations. Atmos. Environ. 244, 117869 https://doi.org/10.1016/j.atmosenv.2020.117869.

Li, C., Liang, H., Liang, M., Chen, Y., Zhou, Y., 2018. Mercury emissions flux from various land uses in old mining area, Inner Mongolia, China. J. Geochem. Explor. 192, 132–141. https://doi.org/10.1016/j.gexplo.2018.06.011.

Liu, F., Cheng, H., Yang, K., Zhao, C., Liu, Y., Peng, M., Li, K., 2014. Characteristics and influencing factors of mercury exchange flux between soil and air in Guangzhou City. J. Geochem. Explor. 139, 115–121. https://doi.org/10.1016/j.gexplo.2013.09.005.

Llanos, W., Kocman, D., Higueras, P., Horvat, M., 2011. Mercury emission and dispersion models from soils contaminated by cinnabar mining and metallurgy. J. Environ. Monit. 13, 3460–3468. https://doi.org/10.1039/c1em10694e.

Ma, M., Sun, T., Du, H., Wang, D., 2018. A two-year study on mercury fluxes from the soil under different vegetation cover in a subtropical region, South China. Atmosphere (Basel) 9, 30. https://doi.org/10.3390/atmos9010030.

MacSween, K., Edwards, G.C., 2021. The role of precipitation and soil moisture in enhancing mercury air-surface exchange at a background site in south-eastern Australia. Atmos. Environ. 255, 118445 https://doi.org/10.1016/j.atmosenv.2021.118445.

Mahbub, K.R., Krishnan, K., Megharaj, M., Naidu, R., 2016. Bioremediation potential of a highly mercury resistant bacterial strain Sphingobium SA2 isolated from contaminated soil. Chemosphere 144, 330–337. https://doi.org/10.1016/j.chemosphere.2015.08.061.

Maier, M., Weber, T.K.D., Fiedler, J., Fuß, R., Glatzel, S., Huth, V., Jordan, S., Jurasinski, G., Kutzbach, L., Schäfer, K., Weymann, D., Hagemann, U., 2022. Introduction of a guideline for measurements of greenhouse gas fluxes from soils using non-steady-state chambers. J. Plant Nutr. Soil Sci. 185, 447–461. https://doi.org/10.1002/jpln.202200199.

Marocco, R., 1989. Lineamenti geomorfologici della costa e dei fondali del Golfo di Trieste e considerazioni sulla loro evoluzione Tardo-Quaternaria. Int. J. Speleol. 18, 87–110. https://doi.org/10.5038/1827-806x.18.3.2.

Marsik, F.J., Keeler, G.J., Lindberg, S.E., Zhang, H., 2005. Air-surface exchange of gaseous mercury over a mixed sawgrass-cattail stand within the Florida Everglades. Environ. Sci. Technol. 39, 4739–4746. https://doi.org/10.1021/es0404015.

Mashyanov, N.R., Pogarev, S.E., Panova, E.G., Panichev, N., Ryzhov, V., 2017. Determination of mercury thermospecies in coal. Fuel 203, 973–980. https://doi.org/10.1016/j.fuel.2017.03.085.

Mathema, V.B., Thakuri, B.C., Sillanpää, M., 2011. Bacterial mer operon-mediated detoxification of mercurial compounds: a short review. Arch. Microbiol. 193, 837–844. https://doi.org/10.1007/s00203-011-0751-4.

Miller, M.B., Gustin, M.S., Eckley, C.S., 2011. Measurement and scaling of air-surface mercury exchange from substrates in the vicinity of two Nevada gold mines. Sci. Total Environ. 409, 3879–3886. https://doi.org/10.1016/j.scitotenv.2011.05.040.

Moore, C., Carpi, A., 2005. Mechanisms of the emission of mercury from soil: role of UV radiation. J. Geophys. Res. Atmos. 110, D24302 https://doi.org/10.1029/2004JD005567.

Naharro, R., Esbrí, J.M., Amorós, J.A., Higueras, P.L., 2020. Experimental assessment of the daily exchange of atmospheric mercury in Epipremnum aureum. Environ. Geochem. Health 42, 3185–3198. https://doi.org/10.1007/s10653-020-00557-8.

O'Connor, D., Hou, D., Ok, Y.S., Mulder, J., Duan, L., Wu, Q., Wang, S., Tack, F.M.G., Rinklebe, J., 2019. Mercury speciation, transformation, and transportation in soils, atmospheric flux, and implications for risk management: a critical review. Environ. Int. 126, 747–761. https://doi.org/10.1016/j.envint.2019.03.019.

Obrist, D., Pokharel, A.K., Moore, C., 2014. Vertical profile measurements of soil air suggest immobilization of gaseous elemental mercury in mineral soil. Environ. Sci. Technol. 48, 2242–2252. https://doi.org/10.1021/es4048297.

Osterwalder, S., Huang, J.H., Shetaya, W.H., Agnan, Y., Frossard, A., Frey, B., Alewell, C., Kretzschmar, R., Biester, H., Obrist, D., 2019. Mercury emission from industrially contaminated soils in relation to chemical, microbial, and meteorological factors. Environ. Pollut. 250, 944–952. https://doi.org/10.1016/j.envpol.2019.03.093.

Ottesen, R.T., Birke, M., Finne, T.E., Gosar, M., Locutura, J., Reimann, C., Tarvainen, T., Albanese, S., Andersson, M., Arnoldussen, A., Batista, M.J., Bel-lan, A., Cicchella, D., Demetriades, A., Dinelli, E., De Vivo, B., De Vos, W., Duris, M., Dusza, A., Eggen, O. A., Eklund, M., Ernstsen, V., Filzmoser, P., Flight, D., Fuchs, M., Fugedi, U., Gilucis, A., Gregorauskiene, V., Gulan, A., Halamić, J., Haslinger, E., Hayoz, P., Hoffmann, R., Hoogewerff, J., Hrvatovic, H., Husnjak, S., Johnson, C.C., Jordan, G., Kaste, L., Keilert, B., Kivisilla, J., Klos, V., Krone, F., Kwecko, P., Kuti, L., Ladenberger, A., Lima, A., Lucivjansky, D.P., Mackovych, D., Malyuk, B.I., Maquil, R., McDonnell, P., Meuli, R.G., Miosic, N., Mol, G., Négrel, P., O'Connor, P., Pasieczna, A., Petersell, W., Poňavič, M., Pramuka, S., Prazeres, C., Rauch, U., Reitner, H., Sadeghi, M., Salpeteur, I., Samardzic, N., Schedl, A., Scheib, A., Schoeters, I., Sefcik, P., Skopljak, F., Slaninka, I., Šorša, A., Stafilov, T., Sellersjö, E., Trendavilov, V., Valera, P., Verougstraete, V., Vidojević, D., Zomeni, Z., 2013. Mercury in European agricultural and grazing land soils. Appl. Geochem. 33, 1–12. https://doi.org/10.1016/j.apgeochem.2012.12.013.

Palmieri, H.E.L., Nalini, H.A., Leonel, L.V., Windmöller, C.C., Santos, R.C., de Brito, W., 2006. Quantification and speciation of mercury in soils from the tripuí ecological station, minas gerais, Brazil. Sci. Total Environ. 368, 69–78. https://doi.org/10.1016/j.scitotenv.2005.09.085.

Pannu, R., Siciliano, S.D., O'Driscoll, N.J., 2014. Quantifying the effects of soil temperature, moisture and sterilization on elemental mercury formation in boreal soils. Environ. Pollut. 193, 138–146. https://doi.org/10.1016/j.envpol.2014.06.023.

Park, S.Y., Holsen, T.M., Kim, P.R., Han, Y.J., 2014. Laboratory investigation of factors affecting mercury emissions from soils. Environ. Earth Sci. 72, 2711–2721. https://doi.org/10.1007/s12665-014-3177-x.

Pavoni, E., Petranich, E., Signore, S., Fontolan, G., Covelli, S., 2021. The legacy of the idrija mine twenty-five years after closing: is mercury in the water column of the gulf of trieste still an environmental issue? Int. J. Environ. Res. Publ. Health 18, 10192. https://doi.org/10.3390/ijerph181910192.

Pelcová, P., Ridošková, A., Hrachovinová, J., Grmela, J., 2021. Evaluation of mercury bioavailability to vegetables in the vicinity of cinnabar mine. Environ. Pollut. 283, 117092 https://doi.org/10.1016/j.envpol.2021.117092.

Petranich, E., Predonzani, S., Acquavita, A., Mashyanov, N., Covelli, S., 2022. Applied Geochemistry Rapid thermoscanning technique for direct analysis of mercury species in contaminated sediments : from pure compounds to real sample application. Appl. Geochem. 143, 105393 https://doi.org/10.1016/j.apgeochem.2022.105393.

Piani, A., Acquavita, A., Catalano, L., Contin, M., Mattassi, G., De Nobili, M., 2013. Effects of long term Hg contamination on soil mercury speciation and soil biological activities. E3S Web Conf. 1, 1–4. https://doi.org/10.1051/e3sconf/20130108001.

Pirrone, N., Cinnirella, S., Feng, X., Finkelman, R.B., Friedli, H.R., Leaner, J., Mason, R., Mukherjee, A.B., Stracher, G.B., Streets, D.G., Telmer, K., 2010. Global mercury emissions to the atmosphere from anthropogenic and natural sources. Atmos. Chem. Phys. 10, 5951–5964. https://doi.org/10.5194/acp-10-5951-2010.

Reis, A.T., Coelho, J.P., Rucandio, I., Davidson, C.M., Duarte, A.C., Pereira, E., 2015a. Thermo-desorption: a valid tool for mercury speciation in soils and sediments? Geoderma 237, 98–104. https://doi.org/10.1016/j.geoderma.2014.08.019.

Reis, A.T., Lopes, C.B., Davidson, C.M., Duarte, A.C., Pereira, E., 2015b. Extraction of available and labile fractions of mercury from contaminated soils: the role of operational parameters. Geoderma 259–260, 213–223. https://doi.org/10.1016/j.geoderma.2015.06.004.

Rinklebe, J., During, A., Overesch, M., Du Laing, G., Wennrich, R., Stärk, H.J., Mothes, S., 2010. Dynamics of mercury fluxes and their controlling factors in large Hg-polluted floodplain areas. Environ. Pollut. 158, 308–318. https://doi.org/10.1016/j.envpol.2009.07.001.

Rinklebe, J., During, A., Overesch, M., Wennrich, R., Stärk, H.J., Mothes, S., Neue, H.U., 2009. Optimization of a simple field method to determine mercury volatilization from soils-Examples of 13 sites in floodplain ecosystems at the Elbe River (Germany). Ecol. Eng. 35, 319–328. https://doi.org/10.1016/j.ecoleng.2008.04.019.

Rivas-Martínez, S., Rivas-Sáenz, S., Penas-Merino, A., 2011. Worldwide bioclimatic classification system. Glob. Geobot. 1, 1–638. https://doi.org/10.1127/0340-269X/2006.

Rochette, P., Hutchinson, G.L., 2005. Measurement of Soil Respiration in Situ: Chamber Techniques. In: Micrometeorology in Agricultural Systems. John Wiley & Sons, Ltd, pp. 247–286. https://doi.org/10.2134/agronmonogr47.c12.

Rumayor, M., Gallego, J.R., Rodríguez-Valdés, E., Díaz-Somoano, M., 2017. An assessment of the environmental fate of mercury species in highly polluted brownfields by means of thermal desorption. J. Hazard Mater. 325, 1–7. https://doi.org/10.1016/j.jhazmat.2016.11.068.

Saiz-Lopez, A., Sitkiewicz, S.P., Roca-Sanjuán, D., Oliva-Enrich, J.M., Dávalos, J.Z., Notario, R., Jiskra, M., Xu, Y., Wang, F., Thackray, C.P., Sunderland, E.M., Jacob, D. J., Travnikov, O., Cuevas, C.A., Acuña, A.U., Rivero, D., Plane, J.M.C., Kinnison, D. E., Sonke, J.E., 2018. Photoreduction of gaseous oxidized mercury changes global atmospheric mercury speciation, transport and deposition. Nat. Commun. 9, 4796. https://doi.org/10.1038/s41467-018-07075-3.

Salata, S., Peccol, E., Borsato, O., 2019. A Framework to evaluate land take control policy efficiency in friuli Venezia Giulia, Italy. Sustain. Times 11, 6406. https://doi.org/10.3390/su11226406.

Schlüter, K., 2000. Review: evaporation of mercury from soils. An integration and synthesis of current knowledge. Environ. Geol. 39, 249–271. https://doi.org/10.1007/s002540050005.

Schuster, E., 1991. The behavior of mercury in the soil with special emphasis on complexation and adsorption processes - a review of the literature. Water, Air, Soil Pollut. 56, 667–680. https://doi.org/10.1007/BF00342308.

Selin, H., Keane, S.E., Wang, S., Selin, N.E., Davis, K., Bally, D., 2018. Linking science and policy to support the implementation of the Minamata Convention on Mercury. Ambio 47, 198–215. https://doi.org/10.1007/s13280-017-1003-x.

Sherman, L.S., Blum, J.D., Douglas, T.A., Steffen, A., 2012. Frost flowers growing in the Arctic ocean-atmosphere-sea ice-snow interface: 2. Mercury exchange between the atmosphere, snow, and frost flowers. J. Geophys. Res. Atmos. 117, D00R10. https://doi.org/10.1029/2011JD016186.

Shi, T., Gong, Y., Ma, J., Wu, H., Yang, S., Ju, T., Qu, Y., Liu, L., 2020. Soil-air exchange of mercury from agricultural fields in Zhejiang, East China: seasonal variations, influence factors, and models of fluxes. Chemosphere 249, 126063. https://doi.org/10.1016/j.chemosphere.2020.126063.

Sholupov, S., Pogarev, S., Ryzhov, V., 2004. Zeeman atomic absorption spectrometer RA-915 + for direct determination of mercury in air and complex matrix samples, 85, 473–485. https://doi.org/10.1016/j.fuproc.2003.11.003.

Sigler, J.M., Lee, X., 2006. Gaseous mercury in background forest soil in the northeastern United States. J. Geophys. Res. Biogeosciences 111, G02007. https://doi.org/10.1029/2005JG000106.

Sigura, M., Boscutti, F., Buccheri, M., Dorigo, L., Glerean, P., Lapini, L., 2017. La REL dei paeasaggi di pianura, di area Montana e urbanizzati. Piano Paesaggistico regionale del Friuli-Venezia Giulia (Parte Strategica) E1-allegato alla scheda di RER. Reg. Friuli -Venezia Giulia 84. http://www.regione.fvg.it/rafvg/cms/RAFVG/ambiente-territorio/pianificazione-gestione-territorio/FOGLIA21/#id9.

Sizmur, T., McArthur, G., Risk, D., Tordon, R., O'Driscoll, N.J., 2017. Gaseous mercury flux from salt marshes is mediated by solar radiation and temperature. Atmos. Environ. 153, 117–125. https://doi.org/10.1016/j.atmosenv.2017.01.024.

Skyllberg, U., Drott, A., 2010. Competition between disordered iron sulfide and natural organic matter associated thiols for mercury(II) - an EXAFS study. Environ. Sci. Technol. 44, 1254–1259. https://doi.org/10.1021/es902091w.

Sommar, J., Osterwalder, S., Zhu, W., 2020. Recent advances in understanding and measurement of Hg in the environment: surface-atmosphere exchange of gaseous elemental mercury (Hg0). Sci. Total Environ. 721, 137648 https://doi.org/10.1016/j.scitotenv.2020.137648.

Sommar, J., Zhu, W., Shang, L., Lin, C.J., Feng, X., 2016. Seasonal variations in metallic mercury (Hg0) vapor exchange over biannual wheat-corn rotation cropland in the North China Plain. Biogeosciences 13, 2029–2049. https://doi.org/10.5194/bg-13-2029-2016.

Stamenkovic, J., Gustin, M.S., 2009. Nonstomatal versus stomatal uptake of atmospheric mercury. Environ. Sci. Technol. 43, 1367–1372. https://doi.org/10.1021/es801583a.

Stamenkovic, J., Gustin, M.S., Arnone, J.A., Johnson, D.W., Larsen, J.D., Verburg, P.S.J., 2008. Atmospheric mercury exchange with a tallgrass prairie ecosystem housed in mesocosms. Sci. Total Environ. 406, 227–238. https://doi.org/10.1016/j.scitotenv.2008.07.047.

Streets, D.G., Horowitz, H.M., Lu, Z., Levin, L., Thackray, C.P., Sunderland, E.M., 2019. Five hundred years of anthropogenic mercury: spatial and temporal release profiles. Environ. Res. Lett. 14, 084004 https://doi.org/10.1088/1748-9326/ab281f.

Sun, Y., Guo, Z., Du, J., Zhao, W., 2020a. Diffuse emission and transport of gaseous elemental mercury (GEM) in the Mapamyum geothermal system, Western Tibet (China). J. Volcanol. Geoth. Res. 397, 106825 https://doi.org/10.1016/j.jvolgeores.2020.106825.

Sun, S., Ma, M., He, X., Obrist, D., Zhang, Q., Yin, X., Sun, T., Huang, J., Guo, J., Kang, S., Qin, D., 2020b. Vegetation mediated mercury flux and atmospheric mercury in the alpine permafrost region of the central Tibetan plateau. Environ. Sci. Technol. 54, 6043–6052. https://doi.org/10.1021/acs.est.9b06636.

Sysalová, J., Kučera, J., Drtinová, B., Červenka, R., Zvěřina, O., Komárek, J., Kameník, J., 2017. Mercury species in formerly contaminated soils and released soil gases. Sci. Total Environ. 584 (585), 1032–1039. https://doi.org/10.1016/j.scitotenv.2017.01.157.

Tao, Z., Liu, Y., Zhou, M., Chai, X., 2017. Exchange pattern of gaseous elemental mercury in landfill: mercury deposition under vegetation coverage and interactive effects of multiple meteorological conditions. Environ. Sci. Pollut. Res. 24, 26586–26593. https://doi.org/10.1007/s11356-017-0275-9.

Tassi, F., Cabassi, J., Calabrese, S., Nisi, B., Venturi, S., Capecchiacci, F., Giannini, L., Vaselli, O., 2016. Diffuse soil gas emissions of gaseous elemental mercury (GEM)

from hydrothermal-volcanic systems: an innovative approach by using the static closed-chamber method. Appl. Geochem. 66, 234–241. https://doi.org/10.1016/j.apgeochem.2016.01.002.

Teršič, T., Gosar, M., Biester, H., 2011. Distribution and speciation of mercury in soil in the area of an ancient mercury ore roasting site, Frbejžene trate (Idrija area, Slovenia). J. Geochem. Explor. 110, 136–145. https://doi.org/10.1016/j.gexplo.2011.05.002.

Terzano, R., Santoro, A., Spagnuolo, M., Vekemans, B., Medici, L., Janssens, K., Göttlicher, J., Denecke, M.A., Mangold, S., Ruggiero, P., 2010. Solving mercury (Hg) speciation in soil samples by synchrotron X-ray microspectroscopic techniques. Environ. Pollut. 158, 2702–2709. https://doi.org/10.1016/j.envpol.2010.04.016.

Treu, F., Zini, L., Zavagno, E., Biolchi, S., Boccali, C., Gregorič, A., Napolitanoc, R., Urbancd, J., Zuecco, G., Cucchi, F., 2017. Intrinsic vulnerability of the Isonzo/Soča high plain aquifer (NE Italy - W Slovenia). J. Maps 13, 799–810. https://doi.org/10.1080/17445647.2017.1384935.

U.S. EPA, 1998. Method 7473 (SW-846): Mercury in Solids and Solutions by Thermal Decomposition, Amalgamation, and Atomic Absorption Spectrophotometry. Revision 0, Washington, DC.

USDA, 1987. USDA Textural Soil Classification. Soil Mech. Lev. I Modul. 3. USDA Textural Soil Classif.

Wallschläger, D., Turner, R.R., London, J., Ebinghaus, R., Kock, H.H., Sommar, J., Xiao, Z., 1999. Factors affecting the measurement of mercury emissions from soils with flux chambers. J. Geophys. Res. Atmos. 104, 21859–21871. https://doi.org/10.1029/1999JD900314.

Walters, N.E., Glassford, S.M., Van Heyst, B.J., 2016. Mercury flux from naturally enriched bare soils during simulated cold weather cycling. Atmos. Environ. 129, 134–141. https://doi.org/10.1016/j.atmosenv.2016.01.029.

Wang, D., He, L., Shi, X., Wei, S., Feng, X., 2006. Release flux of mercury from different environmental surfaces in Chongqing, China. Chemosphere 64, 1845–1854. https://doi.org/10.1016/j.chemosphere.2006.01.054.

Wang, S., Feng, X., Qiu, G., Wei, Z., Xiao, T., 2005. Mercury emission to atmosphere from Lanmuchang Hg-Tl mining area, Southwestern Guizhou, China. Atmos. Environ. 39, 7459–7473. https://doi.org/10.1016/j.atmosenv.2005.06.062.

Wickham, H., Chang, W., Henry, L., Pendersen, T.L., Takahashi, K., Wilke, C., Woo, K., Yutani, H., Dunnington, D., 2016. ggplot2: Elegant Graphics for Data Analysis. Springer-Verlag, New York.

Yan, J., Wang, C., Wang, Z., Yang, S., Li, P., 2019. Mercury concentration and speciation in mine wastes in Tongren mercury mining area, southwest China and environmental effects. Appl. Geochem. 106, 112–119. https://doi.org/10.1016/j.apgeochem.2019.05.008.

Yang, Y.K., Zhang, C., Shi, X.J., Lin, T., Wang, D.Y., 2007. Effect of organic matter and pH on mercury release from soils. J. Environ. Sci. 19, 1349–1354. https://doi.org/10.1016/S1001-0742(07)60220-4.

Yin, R., Feng, X., Wang, J., Li, P., Liu, J., Zhang, Y., Chen, J., Zheng, L., Hu, T., 2013. Mercury speciation and mercury isotope fractionation during ore roasting process and their implication to source identification of downstream sediment in the Wanshan mercury mining area, SW China. Chem. Geol. 336, 72–79. https://doi.org/10.1016/j.chemgeo.2012.04.030.

Yuan, W., Wang, X., Lin, C.J., Sommar, J., Lu, Z., Feng, X., 2019. Process factors driving dynamic exchange of elemental mercury vapor over soil in broadleaf forest ecosystems. Atmos. Environ. 219, 117047 https://doi.org/10.1016/j.atmosenv.2019.117047.

Zhang, G., Zhou, X., Li, Xu, Wang, L., Li, Xiangyun, Luo, Z., Zhang, Y., Yang, Z., Hu, R., Tang, Z., Wang, D., Wang, Z., 2021. Gaseous elemental mercury exchange fluxes over air-soil interfaces in the degraded grasslands of northeastern China. Biology 10, 917. https://doi.org/10.3390/biology10090917.

Zhang, T., Kim, B., Levard, C., Reinsch, B.C., Lowry, G.V., Deshusses, M.A., Hsu-Kim, H., 2012. Methylation of mercury by bacteria exposed to dissolved, nanoparticulate, and microparticulate mercuric sulfides. Environ. Sci. Technol. 46, 6950–6958. https://doi.org/10.1021/es203181m.

Zhao, M., Running, S.W., 2010. Drought-induced reduction in global terrestrial net primary production from 2000 through 2009. Science 329, 940–943. https://doi.org/10.1126/science.1192666.

Zhou, J., Wang, Z., Zhang, X., Driscoll, C.T., 2021. Measurement of the vertical distribution of gaseous elemental mercury concentration in soil pore air of subtropical and temperate forests. Environ. Sci. Technol. 55, 2132–2142. https://doi.org/10.1021/acs.est.0c05204.

Zhou, J., Wang, Z., Zhang, X., Sun, T., 2017. Investigation of factors affecting mercury emission from subtropical forest soil: a field controlled study in southwestern China. J. Geochem. Explor. 176, 128–135. https://doi.org/10.1016/j.gexplo.2015.10.007.

Zhu, J., Wang, D., Liu, X., Zhang, Y., 2011. Mercury fluxes from air/surface interfaces in paddy field and dry land. Appl. Geochem. 26, 249–255. https://doi.org/10.1016/j.apgeochem.2010.11.025.

Zhu, W., Li, Z., Li, P., Yu, B., Lin, C.J., Sommar, J., Feng, X., 2018. Re-emission of legacy mercury from soil adjacent to closed point sources of Hg emission. Environ. Pollut. 242, 718–727. https://doi.org/10.1016/j.envpol.2018.07.002.

Žibret, G., Gosar, M., 2006. Calculation of the mercury accumulation in the Idrijca River alluvial plain sediments. Sci. Total Environ. 368, 291–297. https://doi.org/10.1016/j.scitotenv.2005.09.086.

Supplementary material

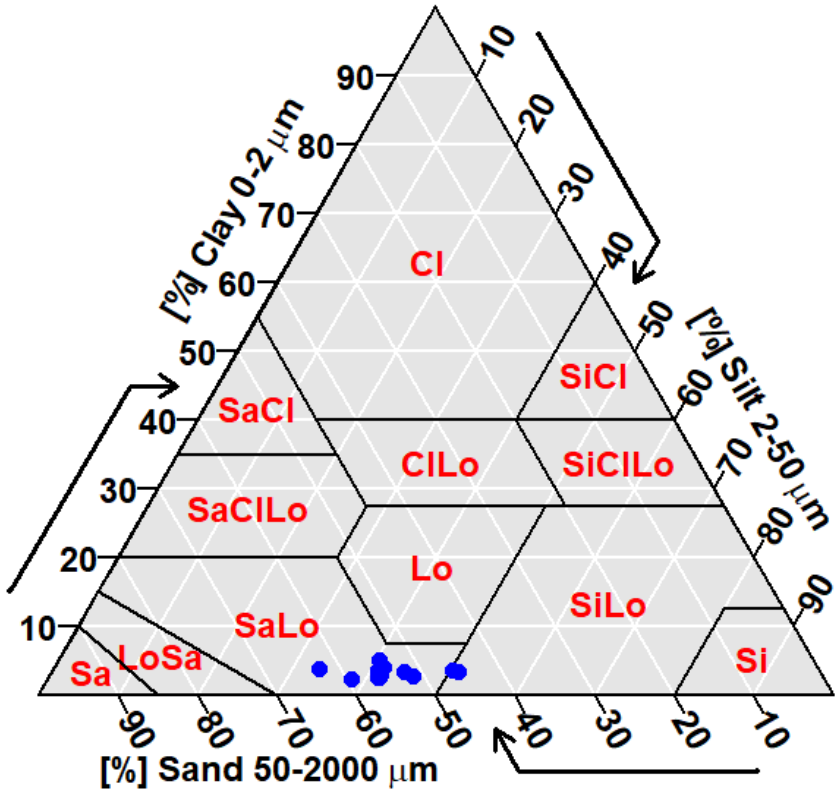

Fig. S1: Grain-Size classification of selected soils according to USDA classification.

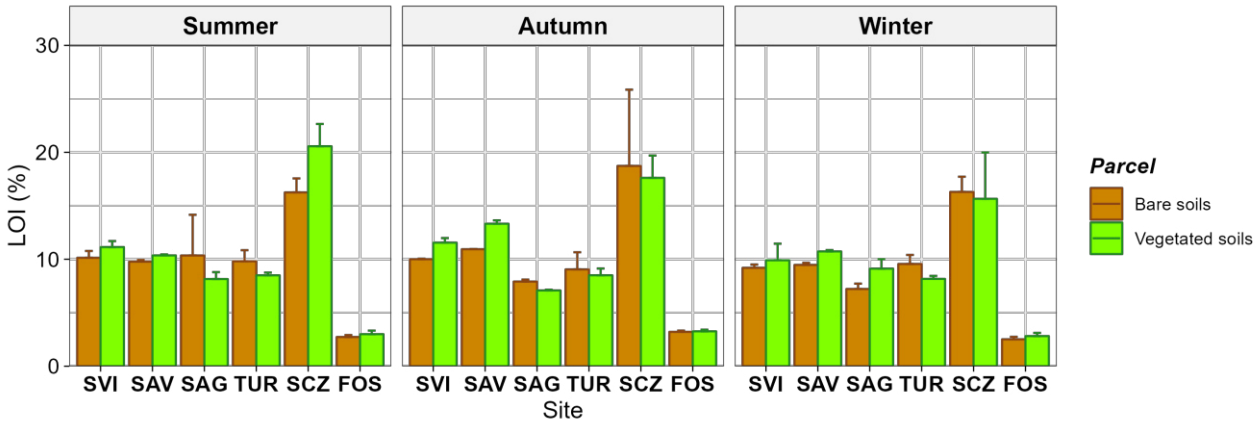

Fig. S2: Organic matter content (expressed as LOI) of soil samples collected at the various sites in the different seasons.

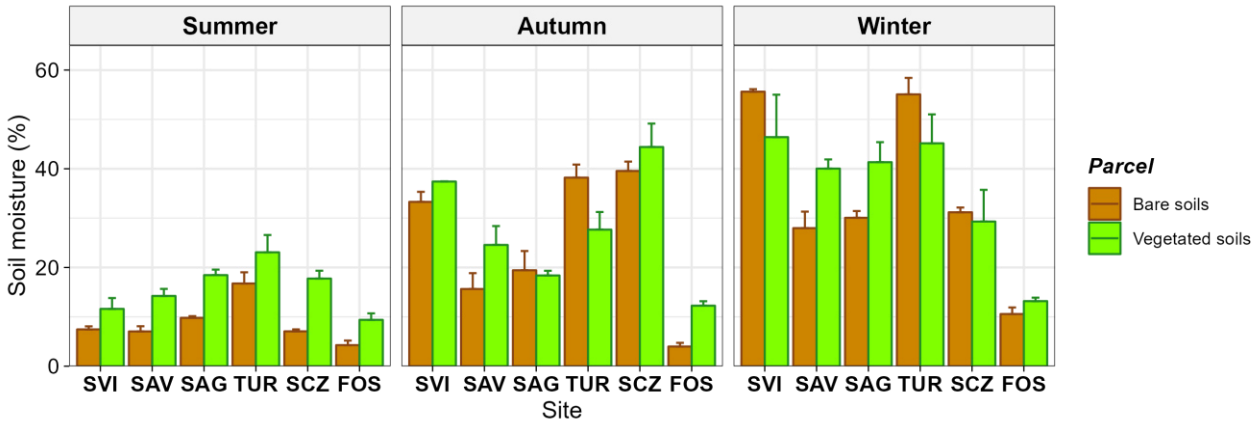

Fig. S3: Soil moisture content determined gravimetrically of samples collected at the various sites in the different seasons.

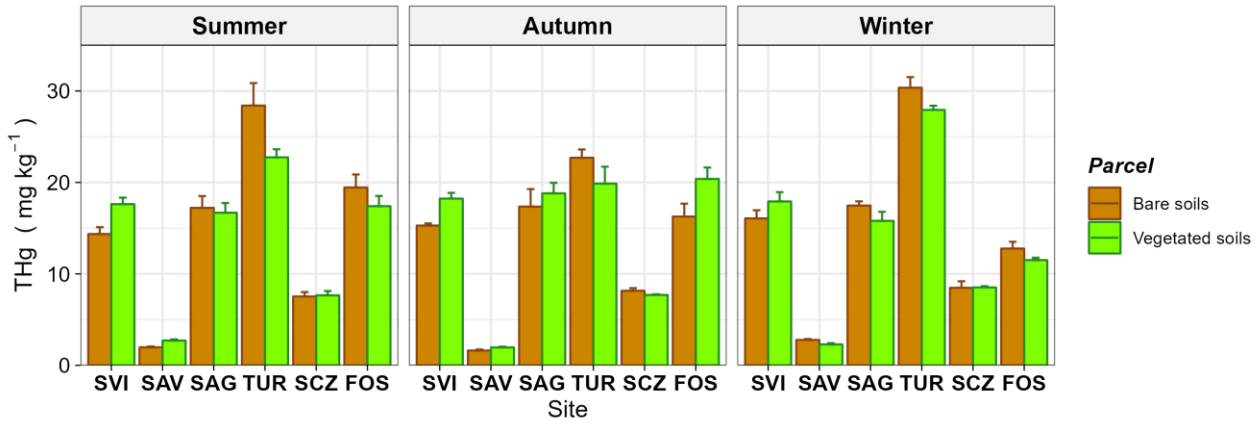

Fig. S4: total Hg concentration (THg) of soil samples collected at the various sites in the different seasons.

Table S1: Overview of average THg content and α-HgS relative abundance in bare and vegetated soil plots at each measurement site, statistical summary of Hg^0 fluxes, overview of average soil physico-chemical properties and daily averages of meteorological parameters for summer season.

Site	Soil cover	Soil THg (mg kg^{-1}) Mean ± SD	α-HgS (%) Mean ± SD	Hg^0 flux (ng m^{-2} h^{-1}) Mean ± SD	Hg^0 flux (ng m^{-2} h^{-1}) Range	Soil temp. (°C) Mean ± SD	UV rad (W m^{-2})[a] Mean ± SD	Air temp. (°C)[a] Mean ± SD	LOI (%) Mean ± SD	Soil moist. (%) Mean ± SD
SVI	Bare soil	14.36±1.19	83±3	382.2±115.9	195.2-544.0	25.8±3.5	35.3±5.6	28.0±2.0	10.13±0.64	7.45±0.62
SVI	Grassland	17.63±0.45	84±3	133.7±18.7	75.1-156.3	24.7±3.3	35.7±5.3	28.0±2.0	11.14±0.56	11.61±2.20
SAV	Bare soil	1.98±0.11	93±1	68.8±21.6	37.1-101.5	27.6±3.6	33.8±8.5	25.7±1.8	9.77±0.17	7.04±1.05
SAV	Grassland	2.69±0.58	93±1	62.4±14.5	37.6-81.7	26.3±3.0	33.8±7.7	25.5±1.3	10.36±0.10	14.23±1.43
SAG	Bare soil	17.22±0.17	89±2	584.1±138.25	405.6-866.2	28.6±3.6	40.0±6.0	28.2±1.5	10.35±3.81	9.79±0.35
SAG	Grassland	16.69±0.24	93±2	326.8±74.8	211.5-471.2	26.2±2.2	40.8±5.0	28.1±1.3	8.15±0.65	18.45±1.12
TUR	Bare soil	28.40±2.78	95±2	800.2±178.8	387.5-952.4	33.0±2.7	39.9±10.3	31.6±0.7	9.80±1.04	16.76±2.27
TUR	Grassland	22.75±0.73	94±4	254.2±51.1	149.7-335.5	31.6±2.2	40.1±11.0	31.1±0.9	8.49±0.26	23.07±3.51
SCZ	Bare soil	7.53±0.20	78±1	144.8±42.5	85.7-197.8	32.2±2.2	40.1±5.7	32.8±0.9	16.25±1.31	7.06±0.40
SCZ	Grassland	7.66±0.77	77±2	121.3±42.6	63.2-192.3	32.9±1.6	40.7±5.3	33.0±0.3	20.56±2.09	17.75±1.59
FOS	Bare soil	19.45±3.04	92±3	769.7±160.6	505.5-1018.4	30.8±3.0	29.3±4.5	25.0±0.2	2.73±0.18	4.27±0.92
FOS	Grassland	17.41±0.47	90±2	344.6±36.2	276.9-405.3	28.0±1.2	27.6±4.1	25.2±0.3	2.99±0.33	9.38±1.31

[a] average values of UV radiation and air temperature recorded during measurements on respectively bare and vegetated soil plots.

Table S2: Overview of average THg content and α-HgS relative abundance in bare and vegetated soil plots at each measurement site, statistical summary of Hg^0 fluxes, overview of average soil physico-chemical properties and daily averages of meteorological parameters for autumn season.

Site	Soil cover	Soil THg ($mg\ kg^{-1}$)	α-HgS (%)	Hg^0 flux ($ng\ m^{-2}\ h^{-1}$)		Soil temp. (°C)	UV rad ($W\ m^{-2}$)[a]	Air temp. (°C)[a]	LOI (%)	Soil moist. (%)
		Mean ± SD	Mean ± SD	Mean ± SD	Range	Mean ± SD	Mean ± SD	Mean ± SD	Mean ± SD	Mean ± SD
SVI	Bare soil	15.28±0.51	86±1	131.3±38.4	72.6-193.3	12.1±2.3	11.7±4.1	17.3±2.6	10.00±0.05	33.29±2.04
SVI	Grassland	18.23±2.06	86±2	28.8±8.2	14.0-41.6	12.0±1.8	11.2±4.3	17.6±2.3	11.55±0.43	37.41±0.03
SAV	Bare soil	1.62±0.02	95±1	32.8±10.1	12.2-44.7	13.2±2.5	17.1±4.0	17.1±2.3	10.93±0.02	15.64±3.21
SAV	Grassland	1.96±0.06	97±2	15.2±4.7	8.1-23.7	12.8±1.5	17.1±4.5	17.3±1.9	13.32±0.32	24.57±3.83
SAG	Bare soil	17.36±4.57	91±1	151.2±59.2	64.6-233.0	12.1±2.4	14.9±5.5	15.7±2.2	7.91±0.19	19.43±3.90
SAG	Grassland	18.81±2.88	90±1	88.5±30.6	48.0-144.0	11.5±1.9	14.7±6.0	15.8±2.1	7.08±0.07	18.38±0.95
TUR	Bare soil	22.70±1.56	94±2	196.2±103.4	69.1-355.9	21.5±3.7	19.5±8.6	15.8±1.5	9.05±1.61	38.20±2.65
TUR	Grassland	19.87±1.35	93±1	73.1±28.4	38.7-106.0	20.0±4.3	19.3±8.8	15.8±1.8	8.50±0.64	27.67±3.57
SCZ	Bare soil	8.16±0.53	78±2	91.9±28.7	51.2-140.7	20.2±2.3	23.3±4.9	18.0±0.7	18.72±7.13	39.55±1.90
SCZ	Grassland	7.70±0.18	78±2	31.9±7.1	21.6-42.3	21.0±1.7	22.9±5.6	17.9±0.9	17.61±2.09	44.41±4.75
FOS	Bare soil	16.27±0.30	92±3	280.8±75.6	153.1-362.3	12.4±1.6	13.9±4.6	14.7±0.6	3.21±0.12	3.98±0.75
FOS	Grassland	20.38±1.78	91±3	102.6±17.6	73.0-136.0	11.2±1.2	12.8±4.3	14.3±0.5	3.26±0.16	12.25±0.91

[a] average values of UV radiation and air temperature recorded during measurements on respectively bare and vegetated soil plots.

Table S3: Overview of average THg content and α-HgS relative abundance in bare and vegetated soil plots at each measurement site, statistical summary of Hg^0 fluxes, overview of average soil physico-chemical properties and daily averages of meteorological parameters for winter season.

Site	Soil cover	Soil THg ($mg\ kg^{-1}$)	α-HgS (%)	Hg^0 flux ($ng\ m^{-2}\ h^{-1}$)		Soil temp. (°C)	UV rad ($W\ m^{-2}$)[a]	Air temp. (°C)[a]	LOI (%)	Soil moist. (%)
		Mean ± SD	Mean ± SD	Mean ± SD	Range	Mean ± SD	Mean ± SD	Mean ± SD	Mean ± SD	Mean ± SD
SVI	Bare soil	16.07±0.30	85±4	70.6±35.2	9.3-123.6	0.7±1.0	9.9±3.3	7.4±4.8	9.19±0.31	55.62±0.51
SVI	Grassland	17.92±3.98	88±1	39.5±28.8	< 1.6-99.6	0.6±1.0	10.0±3.4	7.9±4.3	9.90±1.55	46.41±8.60
SAV	Bare soil	2.78±0.08	94±1	42.2±26.9	4.0-81.3	2.3±1.4	11.0±4.0	7.7±1.3	9.47±0.20	27.97±3.35
SAV	Grassland	2.29±0.57	95±1	16.9±7.9	3.4-28.8	2.4±1.0	11.1±4.0	7.8±1.1	10.73±0.13	40.04±1.86
SAG	Bare soil	17.47±0.90	90±3	149.3±80.7	33.8-244.3	3.1±1.8	11.6±3.7	7.2±2.7	7.21±0.51	30.06±1.37
SAG	Grassland	15.80±0.30	93±2	86.2±45.7	17.3-156.9	2.2±1.4	11.8±3.9	7.4±2.5	9.12±0.89	41.33±4.06
TUR	Bare soil	30.36±1.96	93±2	64.3±43.5	12.9-147.5	0.2±0.7	10.4±3.5	7.3±2.1	9.56±0.85	55.07±3.34
TUR	Grassland	27.93±0.69	94±2	33.9±25.8	< 1.6-106.0	0.6±1.0	10.6±3.7	7.7±2.0	8.16±0.28	45.16±5.86
SCZ	Bare soil	8.48±0.18	78±1	40.0±18.6	9.8-71.8	1.5±1.7	9.9±3.6	7.8±1.6	16.29±1.43	31.18±0.96
SCZ	Grassland	8.52±0.26	79±1	32.5±12.1	2.2-46.3	2.1±1.4	10.1±4.0	8.1±1.4	15.65±4.33	29.31±6.42
FOS	Bare soil	12.77±2.43	92±1	187.8±62.7	60.6-262.4	5.1±2.0	12.4±4.7	8.0±0.6	2.51±0.23	10.57±1.33
FOS	Grassland	11.51±1.62	86±2	164.5±42.3	86.8-206.9	4.8±1.1	12.4±4.7	8.1±0.6	2.81±0.30	13.18±0.70

[a] average values of UV radiation and air temperature recorded during measurements on respectively bare and vegetated soil plots.

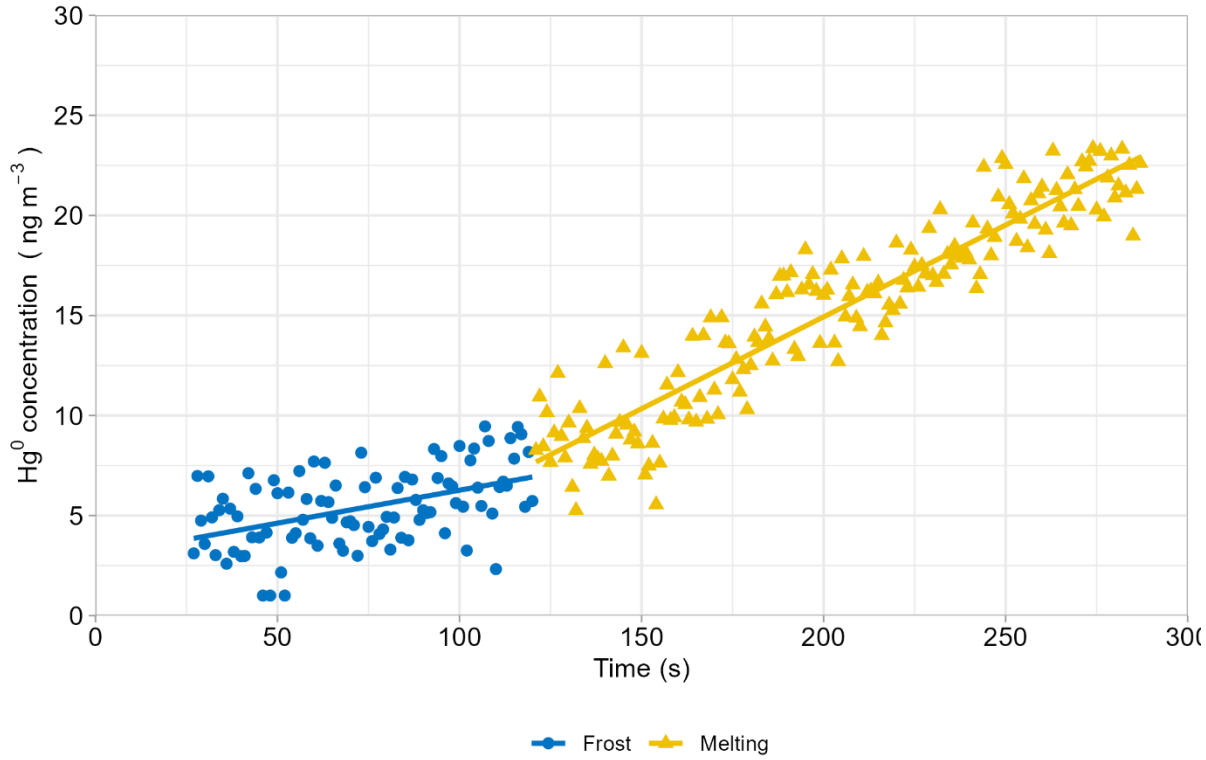

Fig S5: Hg^0 concentration increase inside the chamber during a flux measurement in winter with the abrupt change of slope likely due to frost melting. For flux calculation only the first part of the curve (in blue) was considered.

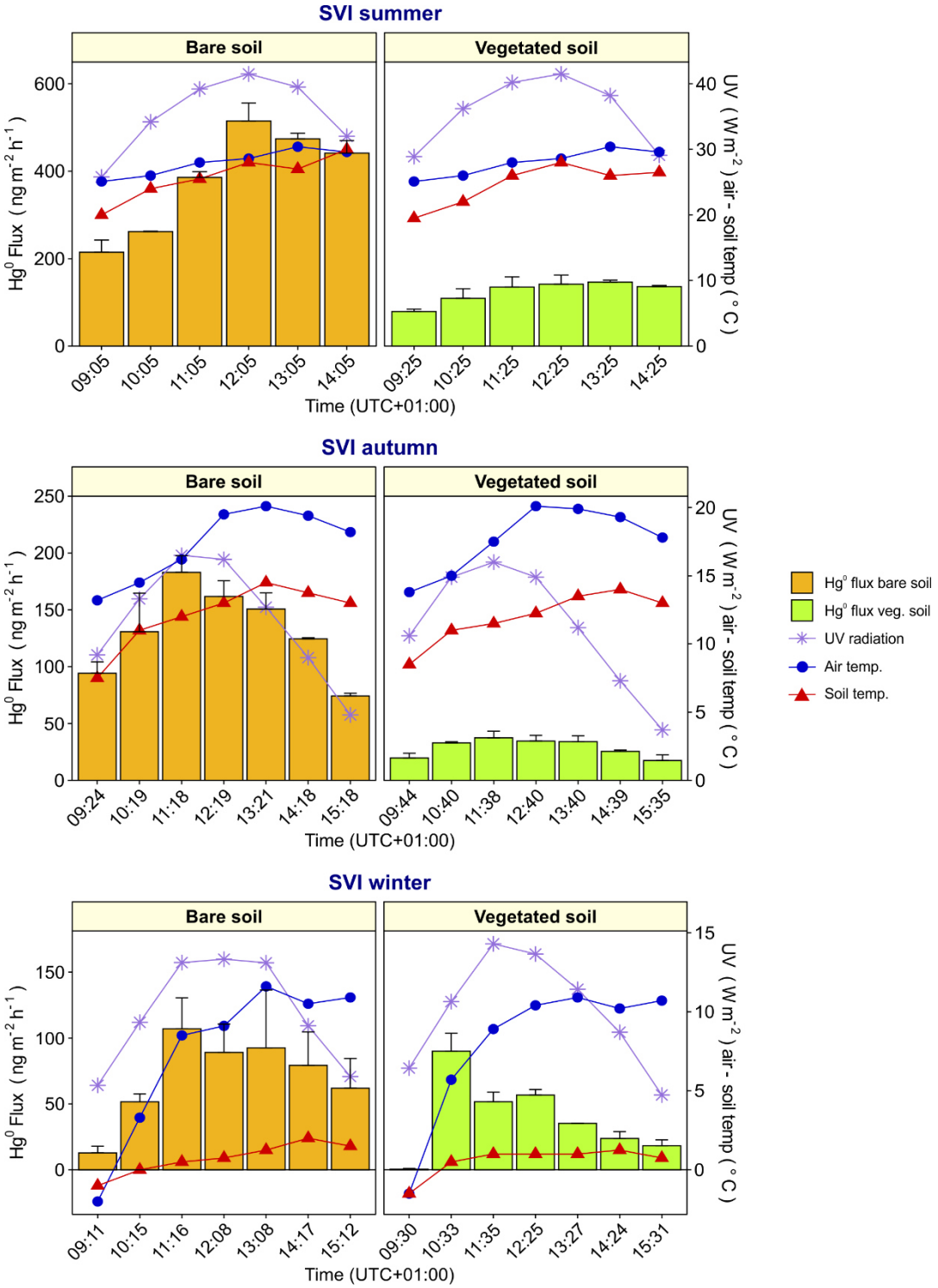

Fig. S6: diurnal variation of Hg^0 fluxes from bare and vegetated soil at site SVI in the various seasons.

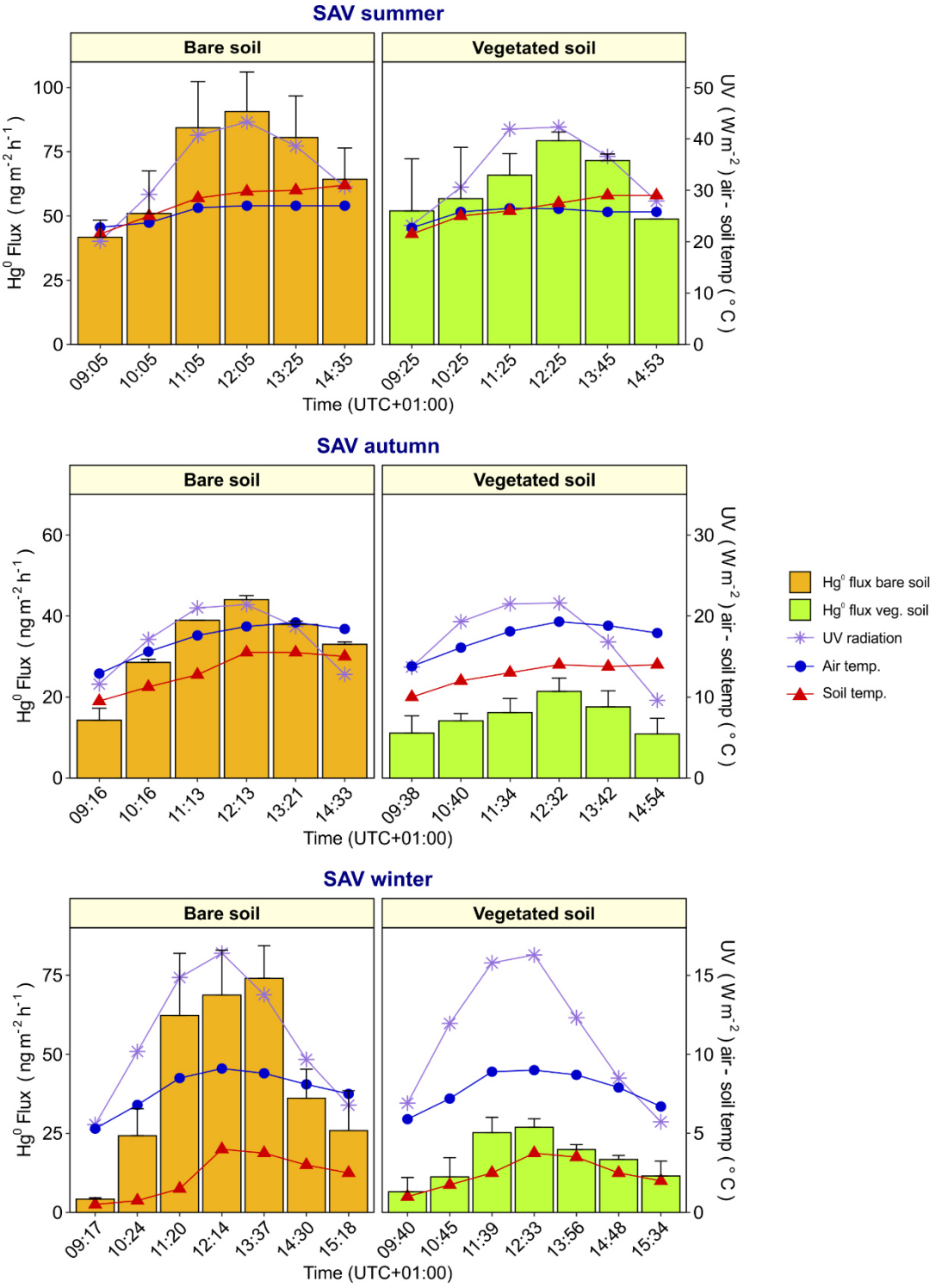

Fig. S7: diurnal variation of Hg^0 fluxes from bare and vegetated soil at site SAV in the various seasons.

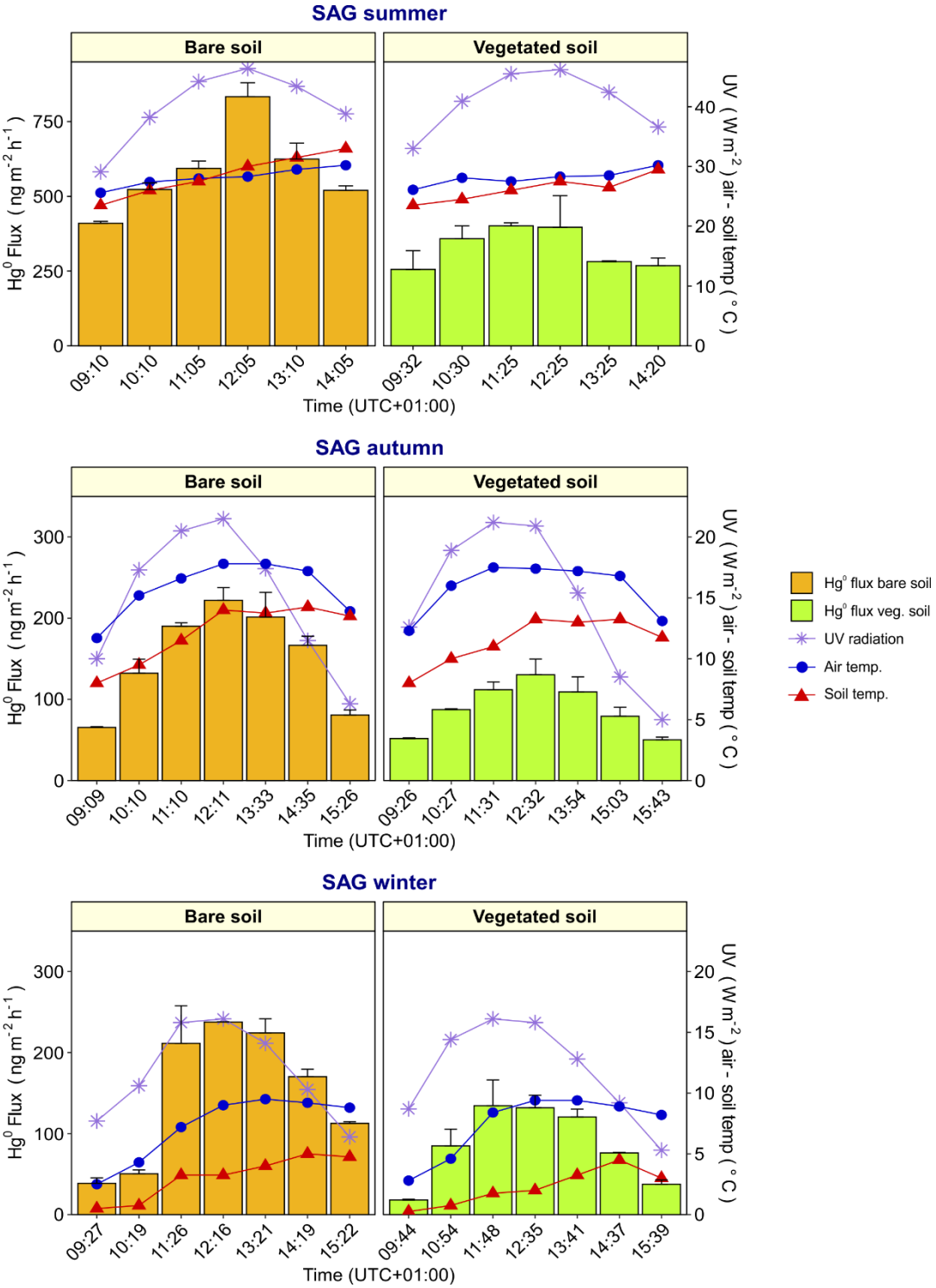

Fig. S8: diurnal variation of Hg^0 fluxes from bare and vegetated soil at site SAG in the various seasons.

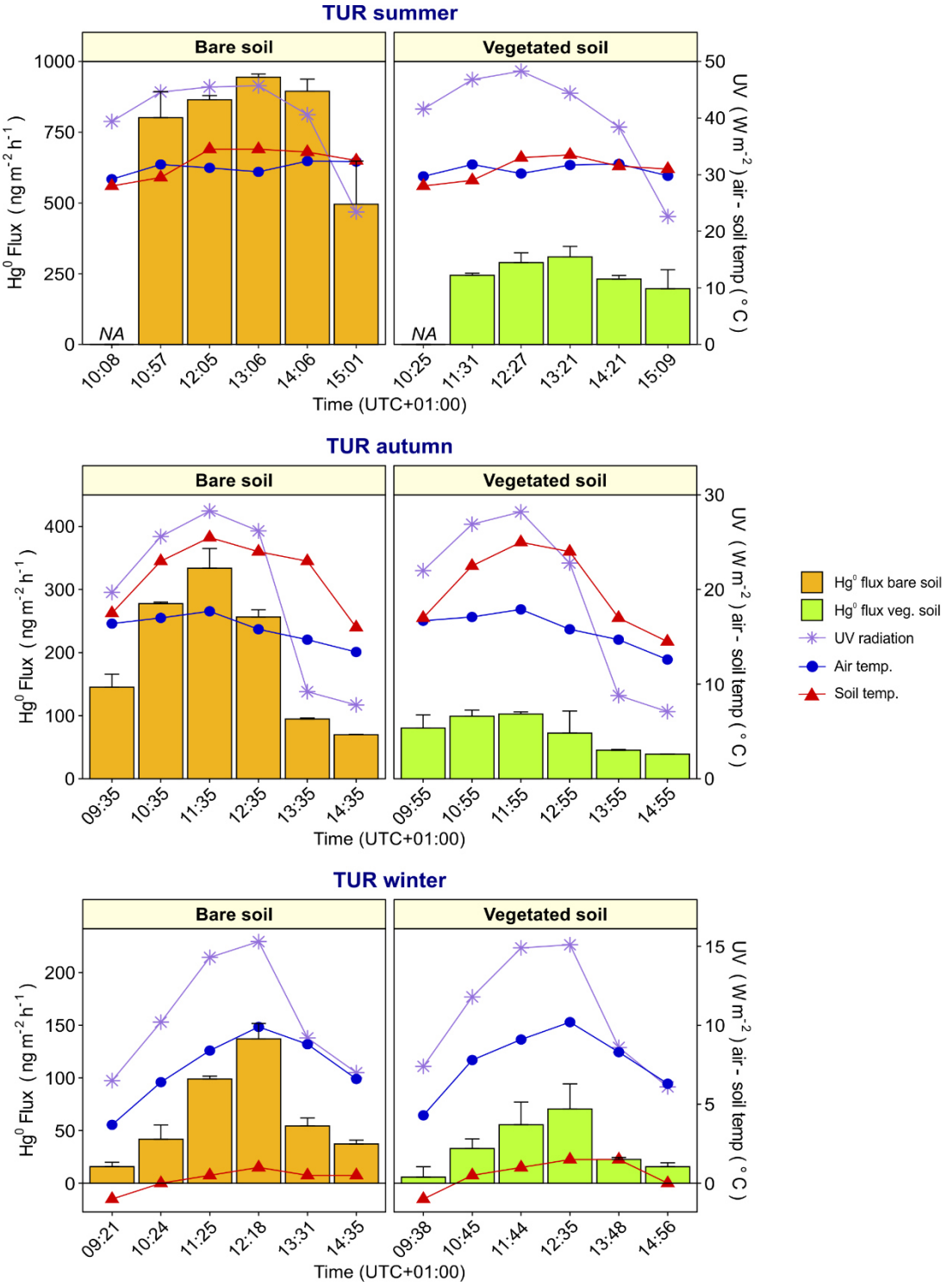

Fig. S9: diurnal variation of Hg^0 fluxes from bare and vegetated soil at site TUR in the various seasons.

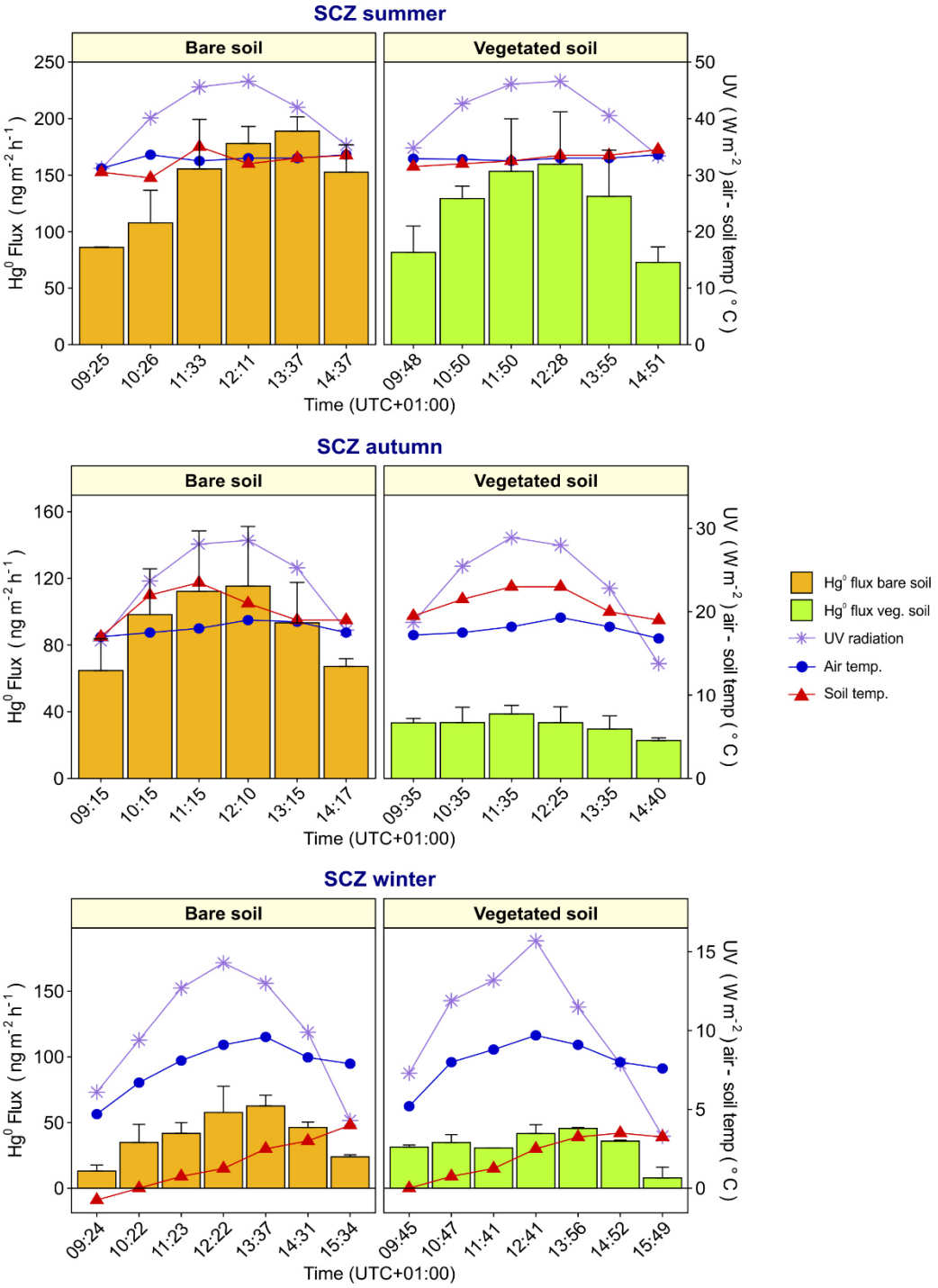

Fig. S10: diurnal variation of Hg^0 fluxes from bare and vegetated soil at site SCZ in the various seasons.

3.5 Atmospheric Hg concentrations

3.5.1 Introduction

As a complement to the flux measurements at water-air and soil-air interfaces described in the previous chapters, the values of Hg^0 concentrations in the atmosphere measured during the sampling days are briefly reported here. Considering that this chapter focuses only on Hg^0 concentrations in the gaseous phase in the atmosphere, hereafter this form will be referred to by the acronym commonly used to indicate its presence in this compartment: GEM (Gaseous Elemental Mercury).

Even though the collected data are too little to study the dynamics of GEM dispersion in the atmosphere, the main aims of these data acquisitions were 1) to roughly examine the amount of this chemical specie in the air during the flux measurements and 2) to understand if the releases from the studied contaminated surfaces can influence the GEM concentrations in the local atmosphere and lead to the attainment or exceeding of values potentially dangerous to health as a result of exposure through inhalation.

According to the World Health Organisation (WHO), the Lowest Observed Adverse Effect Level (LOAEL) for total Hg vapour is around 15,000-30,000 ng m^{-3}, but applying an uncertainty factor of 20 due to the variable sensitive of higher risk population and to the extrapolation from LOAEL to NOAEL (No Observed Adverse Effect Level) the estimated guideline for total Hg concentration in air to avoid negative outcomes is estimated at 1000 ng m^{-3} (WHO, 2000). Moreover, as reported in Oyarzun et al. (2007), minimum risk levels for chronic exposure are set to 200 ng m^{-3} by US Occupational Safety and Health Administration (OSHA) and to 300 ng m^{-3} by US Environmental Protection Agency (EPA). In Italy, only the Tuscany regional authorities established a guideline value for Hg concentrations in outdoor air above contaminated sites, which should not exceed 300 ng m^{-3} after remediation procedure (Vaselli et al., 2013).

In addition, mostly at background sites where Hg content in the substrate is relatively low, the occurrence of high atmospheric GEM concentrations as a result of atmospheric transport from source areas can limit the evasion of this metal to the atmosphere through diffusion (Agnan et al., 2016; Yu et al., 2018). This potentially results in net Hg deposition both in aquatic (Castelle et al., 2009; Fu et al., 2013; Wang et al., 2020) and terrestrial ecosystems (Eckley et al., 2021; Ericksen et al., 2005), particularly when environmental conditions are not favourable to Hg evasion, e.g. under conditions of low solar radiation or temperatures (Ci et al., 2016). Also in contaminated areas, the occurrence of extremely high atmospheric GEM concentrations can

limit the evasion from contaminated surfaces, mostly in environments downwind strong point sources of GEM (Eckley et al., 2015; Miller et al., 2011): depending on Hg content in the substrate, if GEM level is above a so-called “compensation point”, net depositions can be observed (Agnan et al., 2016).

3.5.2 Methods

Measurements of atmospheric GEM concentrations were performed using the same portable Hg^0 analyser Lumex RA915-M described in the previous chapters. This instrument meets the requirements of UE standard method EN 15852:2010 for the determination of total gaseous mercury in ambient air (Higueras et al., 2014). In order to assess the potential exposure to GEM of local inhabitants through inhalation, air was sampled through a Teflon tube connected to the inlet port of the Lumex at ~1.5 m height directly over the point where flux measurements with the chambers were performed. Measurements lasted for 10-20 minutes and GEM concentrations were continuously (every 1 sec) recorded. For data processing, all values below the limit of detection (LOD) of the Lumex (2 ng m^{-3}) were set to 1/2 of the LOD according to the medium bound approach (US EPA, 2000).

During the monitoring of Hg^0 fluxes over the entire 24h period in the coastal environments of Val Noghera fish farm (VN) and Bay of Piran (PR), measurements were carried out in different periods of the day: namely, at the beginning of the sampling period in the first day of measurement (around midday), in the evening after the sunset, before sunrise and in the middle of the morning of the second sampling day as indicated in table 1.

Conversely, during diurnal sampling at freshwater and terrestrial environments only two continuous measurements were performed at each monitored site at the beginning and at the end of sampling days because during the rest of the time the only analyser available had to be used for flux measurements with the chamber or for the determination of DGM concentration in surface water.

Table 1: temporal distribution of GEM measurements taken during 24h sampling periods at the selected coastal sites and corresponding meteorological conditions.

Site-Season	Measure	Time (UTC+01:00)	UV (W m^{-2})	Wind speed (m s^{-1})	Temperature (°C)	Air humidity (%)
Val Noghera						
Summer	A	12:00	50.7	3.7	30.3	39.6
	B	20:00	0	2.8	22.1	66.6
	C	04:45	0.2	1.6	19.5	83.2
	D	10:00	19.3	4.5	27.9	52.3
Autumn	A	12:00	20.5	1.1	21.5	54.2
	B	18:15	0	0.3	11.0	90.3
	C	06:30	0	1.3	8.4	82.0
	D	10:00	13.7	3.1	20.7	44.7
Spring	A	11:40	50.1	2.3	24.4	54.8
	B	19:30	0.1	1.2	19.8	77.4
	C	04:45	0	0.8	15.5	89.1
	D	10:00	43.9	1.4	23.6	61.5
Piran						
Summer	A	11:45	46.5	2.7	22.9	46.2
	B	20:00	0	2.5	20.6	67.5
	C	05:00	0.3	2.9	15.8	94.0
	D	10:30	39.7	2.0	24.1	62.1
Autumn	A	11:45	12.5	1.6	16.7	51.2
	B	18:45	0	3.5	10.5	68.7
	C	05:45	0	3.7	7.7	86.6
	D	10:15	9.9	1.5	15.5	61.3
Spring	A	12:00	52.0	2.7	27.9	49.9
	B	20:00	0	2.5	17.6	88.8
	C	04:45	0	3.4	18.3	84.5
	D	10:00	38.5	1.4	23.4	57.9

3.5.3 Results: GEM concentrations during 24h monitoring at coastal sites

Generally, higher GEM concentrations were observed at the fish farm site (VN), located inside the impacted environment of the Marano and Grado Lagoon, than at the more pristine site of the Bay of Piran (PR), whereas no relevant variations were detected among the different seasons. The summary statistics of the GEM concentrations recorded during continuous 24h sampling activity is reported in table 2.

Table 2: summary statistics of GEM concentrations observed during 24h sampling at coastal sites.

Site - Season	Mean±sd ($ng\ m^{-3}$)	Median ($ng\ m^{-3}$)	Min-Max ($ng\ m^{-3}$)	N data
Val Noghera				
Summer	4.34 ± 3.20	3.35	< 2 – 15.68	2388
Autumn	2.40 ± 1.35	2.40	< 2 – 7.47	1944
Spring	4.25 ± 2.03	3.99	< 2 – 14.35	2248
Total	*3.77 ± 2.58*	*3.22*	*< 2 – 15.68*	*6580*
Bay of Piran				
Summer	1.57 ± 0.90	< 2	< 2 – 5.64	2309
Autumn	2.01 ± 1.15	< 2	< 2 – 6.64	2268
Spring	1.99 ± 1.14	2.01	< 2 – 6.62	2401
Total	*1.83 ± 1.07*	*< 2*	*< 2 – 6.64*	*6978*

Overall, these values are comparable or, especially at VN, slightly higher than the average GEM concentrations previously reported for the Marano and Grado Lagoon (2.53±0.73 $ng\ m^{-3}$, Floreani et al., 2020) and for the coastal area of the Gulf of Trieste (2.70±1.50 $ng\ m^{-3}$, Barago et al., 2020). Moreover, average GEM concentrations recorded at PR are also of the same order of magnitude of the natural atmospheric background of 1.7-1.8 $ng\ m^{-3}$ estimated for the whole Mediterranean area (Wängberg et al., 2008).

Considering the comparable Hg^0 fluxes at the water-air interface recorded in these two sites (Chapter 3.2), the relatively higher concentrations observed at VN can suggest that atmospheric levels of GEM strongly depends not only on the evasion from the local substrate but also on mixing processes that can occur in the atmosphere in function of local meteorological conditions (Esbrí et al., 2020). The transport of air masses from upwind areas characterised by strong point Hg sources (e.g. mining facilities or industrial areas) can constitute an additional supply of GEM, whereas air masses coming from uncontaminated areas can favour a dilution of emissions from local contaminated surfaces and limit the increase of atmospheric concentrations of this element (Ci et al., 2011; Kalinchuk et al., 2022). This effect can be particularly important in coastal areas like those investigated in this study and where air

circulation is deeply impacted by the sea/land breeze regime caused by the differential heating of water and terrestrial surfaces. The resulting varying wind directions and speeds during the day may consequently strongly affect the atmospheric transport and dispersion of GEM as observed in several studies (Lan et al., 2014; Malcolm et al., 2003; Nie et al., 2020).
The atmospheric dilution with clean air can potentially explain the relatively low GEM concentrations found at PR, whereas GEM levels observed at VN may potentially have been influenced also by the transport of this contaminant emitted from surrounding contaminated areas. Indeed, a recent study (Floreani et al., 2020) based on both direct measurements of GEM in air and determination of Hg bioaccumulated in lichens following atmospheric depositions found that the distribution of GEM over the Marano and Grado Lagoon can be significantly affected by supplies from both the Isonzo River plain and the Torviscosa chlor-alkali plant (CAP) other than local emissions from water and sediment surfaces. Moreover, a potential contribution of enhanced GEM oxidation in the marine boundary layer thanks to the presence of oxidant species such as halogens (Griggs et al., 2020; Holmes et al., 2009; Malcolm et al., 2003; Mao et al., 2008) in limiting the increase of this chemical species in air cannot be excluded. However, still large uncertainties exists on Hg redox dynamics and pathways in the atmosphere and on the importance of the associated oxidation and reduction processes (Gabay et al., 2020; Si and Ariya, 2018).

Considering the single measurements performed in different times of the day, generally, no relevant differences in terms of GEM concentrations were recorded between night and day periods (Fig. 1). A particular situation was encountered during measurements conducted in summer at VN, where the highest GEM values were recorded before sunrise (mean±sd = 8.84±1.89 ng m^{-3}) while the next measurement taken in the morning provided the lowest value for this site (mean±sd = 1.24±0.57 ng m^{-3}). Although the data collected in this study are too sparse to establish a robust diurnal trend of atmospheric GEM concentrations, the occurrence of higher values during nights can be explained by the lower wind speeds resulting in a thinner mixing layer. Under these conditions there is a reduced dilution of GEM emitted from local contaminated surfaces, which can therefore lead to an increase in its concentrations in the atmosphere as observed in several studies (Esbrí et al., 2020; Han et al., 2014; Hong et al., 2016; Liu et al., 2007). The built-up of GEM concentrations in air during night in summer at the fish farm may have been supported by the relatively high and constant evasion fluxes at the water-air interface even in absence of solar radiation described above (Chapter 3.2). A similar situation has been previously observed in a coastal area of the southern part of the Isonzo River

alluvial plain, a few kilometres east of the Marano and Grado Lagoon during continuous atmospheric GEM measurements (Barago et al., 2020): in this study, peaks of GEM concentrations up to 48.46 ng m^{-3} were observed at sunset and during night, corresponding to temperature decrease and breeze drops which resulted in temporary atmospheric stable conditions that limited air mixing. After the sunrise, the thickness of the mixing layer can increase in parallel with the rise of wind and temperatures thus favouring, particularly during summer, the dilution of GEM in the atmosphere and resulting in lower values (Esbrí et al., 2020; Griggs et al., 2020; Lan et al., 2014) as observed in this study.

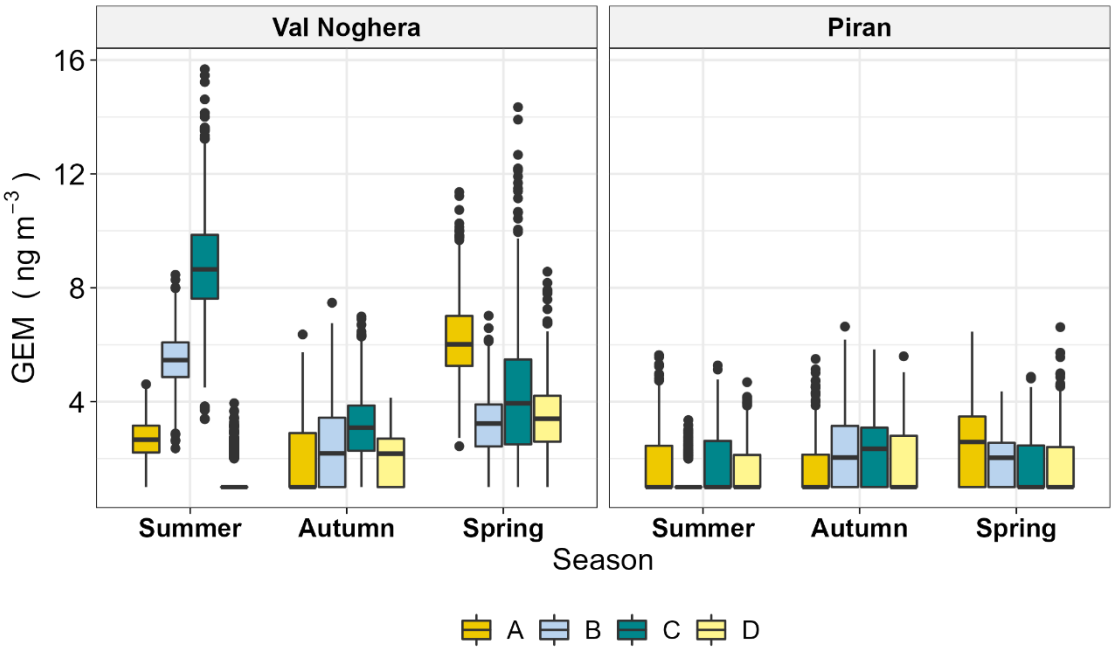

Figure 1: distribution of GEM concentrations recorded during 24h sampling activity at coastal sites of Val Noghera fish farm and Bay of Piran. Measures were taken A: around midday, B: after sunset, C: before sunrise, D: during morning.

This situation was not so evident in the other sites, probably because our measurements were not performed exactly when static atmospheric conditions occurred and might not have intercept the possible occurrence of peaks of GEM. However, it must be specified that wind speeds were not measured direct in field during this study but obtained from the nearest weather monitoring stations (Fossalon of OSMER-ARPA FVG for VN and Portoroz of ARSO Slovenia for PR) and thus may not be representative of exact wind conditions at the sampling points.

3.5.4 Results: GEM concentrations during diurnal sampling at freshwater sites

The data about GEM concentrations measured at the beginning and at the end of sampling periods for Hg^0 fluxes at the water-air interface at the Solkan Reservoir (SK), Torviscosa Dockyard (TR), and Cavazzo Lake (CV) were briefly discussed above (Chapter 3.3) and summarised hereafter. The basic univariate statistics of all GEM data collected during these sampling days is reported in table 3. Unfortunately, due to a technical issue with the instrumentation GEM data for morning measurements at TR were not recorded.

Table 3: summary statistics of GEM concentrations observed during diurnal sampling at freshwater sites. For summer measurements at TR, the morning measure is missing due to a technical issue.

Site - Season	Mean±sd (ng m^{-3})	Median (ng m^{-3})	Min-Max (ng m^{-3})	N data
Solkan				
Summer	2.77±0.98	2.60	< 2 – 5.28	1340
Autumn	2.19±2.13	2.18	< 2 – 6.48	1700
Spring	4.61±4.09	4.31	< 2 – 10.62	1384
Total	*3.24±1.89*	*3.06*	*< 2 - 10.62*	*4424*
Torviscosa				
Summer*	1.92±0.95	2.10	< 2 – 4.61	849
Autumn	71.46±110.90	10.83	< 2 – 543.61	1424
Spring	68.72±88.96	12.64	3.57 – 344.08	1383
Total	*54.28±92.80*	*7.94*	*< 2 – 543.61*	*3656*
Cavazzo				
Summer	1.30±0.61	< 2	< 2 – 3.85	1654
Autumn	1.25±0.62	< 2	< 2 – 4.81	1413
Spring	3.41±2.67	2.89	< 2 – 16.07	1413
Total	*2.01±1.92*	*< 2*	*< 2 – 16.07*	*4480*

Similarly to what was observed at coastal environments, GEM concentrations detected at CV and SK were relatively low with average values in the same order of magnitude or slightly higher than the natural atmospheric background of the Northern Hemisphere (1.5-1.7 ng m^{-3}, Sprovieri et al., 2010). Considering the relatively high Hg^0 fluxes at the water-air interface recorded at these environments particularly during summer, higher than those commonly reported for pristine freshwater ecosystems (Chapter 3.3), these findings may further confirm the importance of atmospheric dilution of GEM. In these sites, the highest GEM concentrations were observed during spring sampling campaign, in accordance with a common reported seasonal trend of atmospheric GEM in continental areas characterised by late winter to spring maximum values and late summer to autumn minimum values. This seasonal variation can be

related to a reduced height of boundary mixing layer during winter and spring periods or enhanced GEM oxidation during summer (Mao et al., 2016).

In addition, potential supplies of GEM derived from anthropogenic emissions cannot be ruled out as two industrial complexes are located within 10 km of the Cavazzo Lake (Polonia et al., 2021) whereas near Solkan Reservoir at about the same distance there is a cement plant that a recent study identified as a point source for GEM dispersion in the atmosphere (Vijayakumaran Nair et al., 2022). However, to confirm this hypothesis more continuous monitoring of atmospheric GEM levels during different times of the year is needed.

Conversely, measurements performed at Torviscosa (TR) showed the occurrence of high atmospheric GEM concentrations during autumn and spring which, as stated above, probably strongly affected Hg^0 evasion at the water-air interface. As can be seen through the boxplot representation reported in figure 2, these elevated values occurred mainly during measures taken in the morning. Data collected during these measurements were also characterised by a high variability, ranging between < 2 and 543.61 ng m^{-3} and 6.61 and 344.08 ng m^{-3} in autumn and spring, respectively. Conversely, relatively lower GEM concentrations were observed during monitoring performed in the afternoon, ranging between < 2 and 278.51 ng m^{-3} in autumn, 3.57 and 27.08 ng m^{-3} in spring and < 2 and 4.61 ng m^{-3} in summer, respectively.

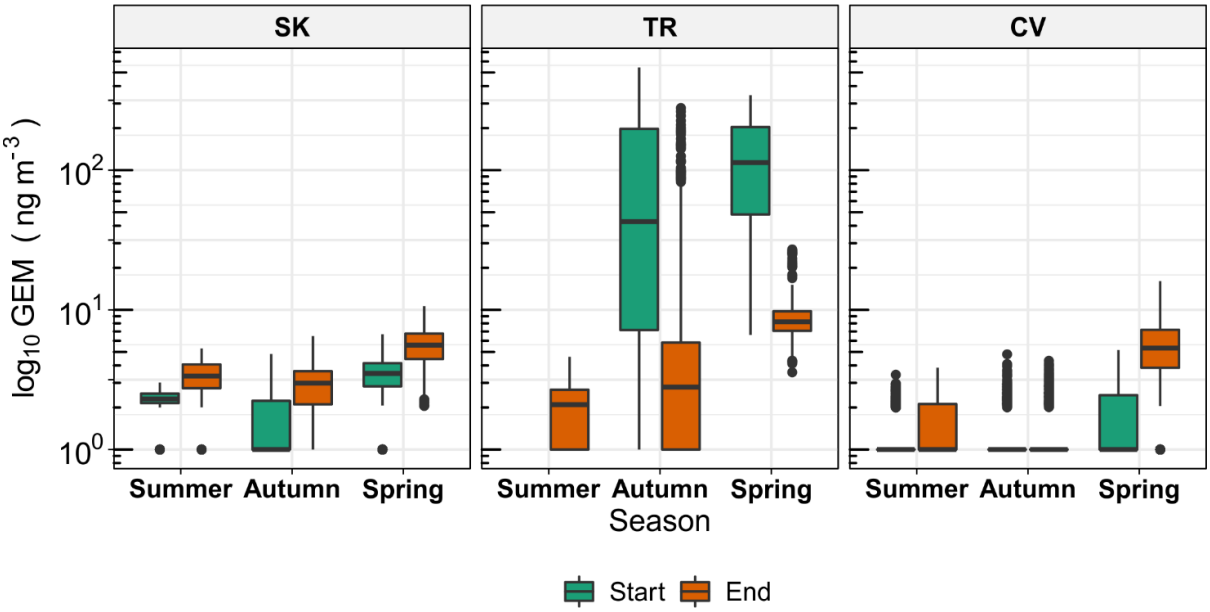

Figure 2: distribution of GEM concentrations recorded during diurnal sampling activity at freshwater sites (SK: Solkan Reservoir, TR: Torviscosa Dockyard, CV: Cavazzo Lake). Measures were taken at the beginning and at the end of sampling period for Hg^0 fluxes determination.

The occurrence of these high GEM concentrations may be related to the dispersion from the area of the former local CAP, where levels up to over 5000 ng m^{-3} have been observed previously near the old plant's buildings (Acquavita et al., 2017). Our sampling site was located less than 500 m from this area. During morning measures, wind came from the direction of the plant, favouring the transport of emitted GEM to our monitoring site. This is in agreement with the observations reported in various studies conducted in the surroundings of closed CAPs, thus confirming that due to the strong contamination of former industrial facilities related to Hg releases occurring in the Hg cell process of chlor-alkali production, these plants can still represent a relevant point source of GEM for downwind environments (Esbrí et al., 2018; Fantozzi et al., 2021; Huremović et al., 2017; Zhu et al., 2018).

GEM concentrations observed during our short measurements were, however, significantly lower than those observed in close proximity of former plant buildings (Acquavita et al., 2017): this can be related to the strong atmospheric dilution of GEM levels moving away from point sources, usually occurring in few hundreds of meters (Esbrí et al., 2020; Higueras et al., 2014). Moreover, average and median GEM concentrations observed at Torviscosa (Tab. 3) were below the above cited reference levels for exposure to Hg vapours. Yet, a more continuous and wider monitoring of GEM levels is needed for a comprehensive assess the potential exposure of workers of local industrial complex.

3.5.4 Results: GEM concentrations during diurnal sampling at terrestrial sites

Atmospheric GEM concentrations at the selected sites for the determination of Hg^0 fluxes at the soil-air interface along the Isonzo River plain were checked by means of 10-minutes continuous measurements at the beginning and at the end of each sampling day in every season. The summary statistic of GEM levels recorded during these measurements is reported in table 4.

On average, the observed GEM concentrations are in the range previously reported for the Isonzo River alluvial plain (1.12-21.4 ng m^{-3}, Acquavita et al., 2022) and far below the threshold values for inhalation exposure. However, these concentrations are slightly higher than the natural atmospheric background of the Northern Hemisphere, likely due to the contribution of the relatively high emissions at the soil-air interface recorded in this study. Indeed, the lowest GEM concentrations were recorded at site SAV (2.46±1.47 ng m^{-3}), characterised by both the lowest THg content in the topsoil (2.22±0.50 mg kg^{-1}) and Hg^0 fluxes (from 15.2±4.5 ng m^{-2} h^{-1} in autumn to 68.8±21.6 ng m^{-2} h^{-1} in summer), whereas the highest

GEM level was observed at FOS (6.75±4.30 ng m^{-3}) where, generally, also the highest fluxes at soil-air interface were observed for both vegetated and bare soils.

Table 4: summary statistic of GEM concentrations observed during diurnal sampling at terrestrial sites.

Site - Season	Mean±sd (ng m^{-3})	Median (ng m^{-3})	Min-Max (ng m^{-3})	N data
SVI				
Summer	3.10±1.30	3.09	< 2 – 7.32	1093
Autumn	3.20±1.55	3.20	< 2 – 8.67	1377
Winter	3.98±2.27	3.83	< 2 – 20.37	1150
Total	*3.43±1.81*	*3.33*	*< 2 – 20.37*	*3394*
SAV				
Summer	2.58±1.53	2.52	< 2 – 7.22	1151
Autumn	2.20±1.21	2.23	< 2 – 6.77	1152
Winter	2.57±1.58	2.43	< 2 – 7.71	1150
Total	*2.46±1.47*	*2.38*	*< 2 – 7.71*	*3679*
SAG				
Summer	6.36±3.09	5.89	< 2 – 19.90	1150
Autumn	5.06±2.30	4.91	< 2 – 12.13	1152
Winter	4.21±2.48	3.91	< 2 – 12.61	1150
Total	*5.21±2.79*	*4.93*	*< 2 – 19.90*	*3452*
TUR				
Summer	7.29±3.13	6.64	< 2 – 16.73	863
Autumn	3.56±2.06	3.33	< 2 – 10.50	1095
Winter	6.56±2.92	6.16	< 2 – 16.74	1150
Total	*5.71±3.16*	*5.26*	*< 2 – 16.74*	*3108*
SCZ				
Summer	5.90±2.04	5.43	< 2 – 14.34	1150
Autumn	3.58±1.74	3.46	< 2 – 10.40	1099
Winter	5.98±2.71	5.84	< 2 – 15.37	1151
Total	*5.18±2.47*	*4.89*	*< 2 – 15.37*	*3400*
FOS				
Summer	8.61±4.63	7.52	< 2 – 27.21	1093
Autumn	2.90±1.42	2.97	< 2 – 7.64	1092
Winter	8.72±3.14	8.25	< 2 – 19.77	1095
Total	*6.75±4.30*	*5.88*	*< 2 – 27.21*	*3280*

The observed GEM levels are significantly lower than those commonly reported in literature for Hg mining areas where concentrations of hundreds to thousands of ng m^{-3} can be reached (Ao et al., 2017; Higueras et al., 2013; Kocman et al., 2011; Li et al., 2012; Vaselli et al., 2013). However, these high peaks of GEM concentrations are usually restricted to a distance of a few hundred meters from point sources such as ventilation shafts of Hg mines, former metallurgical facilities where Hg ore was processed or areas where waste materials still containing a certain amount of cinnabar were dumped (Esbrí et al., 2020). The absence of this anomalous peaks during our measurements can further support the hypothesis that GEM in this area derives from diffuse emissions from contaminated soils rather than from dispersion from a strong point source.

Generally, comparable GEM concentrations were recorded during measurements taken in the morning and in the afternoon in all seasons and sites (Fig. 3). Only in winter, concentrations observed in the afternoon measurements were generally slightly higher than those recorded in the morning, likely due to the fact that measures were performed in the late afternoon when atmospheric mixing could be reduced but soils are still able to emit a certain amount of Hg^0 as observed at other polluted or urban sites (Esbrí et al., 2016; Liu et al., 2007; Mao et al., 2016; Zhang et al., 2013). This is also in agreement with the diurnal trend of GEM previously observed in the coastal area of the Isonzo River alluvial plain described above (Barago et al., 2020).

High and comparable GEM concentrations were observed in summer and winter sampling, whereas measurements conducted in autumn showed the lowest values at all sites. The relatively low GEM observed in autumn could be related to the reduced emissions from contaminated soil surfaces coupled with an expected good atmospheric mixing favoured by solar radiation and temperatures still relatively high. On the contrary, in winter, although emissions from soils were lower but comparable to those occurred in autumn, the lower air temperatures can have caused a reduction in vertical mixing in the atmosphere, resulting in lower dilution of emitted GEM. A reduced GEM scavenging through oxidation can also have contributed to high winter GEM levels (Mao et al., 2016, 2008). However, a further contribution to high GEM levels in winter related to emissions derived from the combustion of biomass for energy production or domestic heating, generally higher during this season, cannot be ruled out (Cheng et al., 2014; Ci et al., 2011; Civerolo et al., 2014; Kim et al., 2005; Weigelt et al., 2015). Finally, in summer, high GEM concentrations were generally observed in sites characterised by higher Hg^0 release from soil surfaces (TUR, FOS, and SAG), likely

confirming that these contaminated soils can represent a secondary source of Hg for the local atmosphere (Agnan et al., 2016; Wang et al., 2005).

Relatively high GEM levels were observed also at SCZ, located in the southern part of the plain, despite the low emissions recorded with the flux chamber: considering the widespread Hg contamination of this area (Acquavita et al., 2022), it is not possible to exclude that this relatively high levels are related to emissions from surrounding farmlands heavily disturbed by agricultural practices (Sommar et al., 2016), but further research is needed to confirm this hypothesis. Moreover, the relatively low GEM concentrations generally observed at SVI, located within a more pristine area characterised by permanent meadows and scarce anthropogenic disturbance, can further support this observation.

The general increasing trend in GEM concentrations observed moving southwards, from site SVI to site FOS (Fig. 3), can also be related to the increased urbanization and industrialization present in the southern part of the Isonzo River alluvial plain (Acquavita et al., 2022; Mistaro et al., 2018), potentially leading to an higher contribution of anthropogenic sources located in the surrounding area of our sampling sites to the observed GEM concentrations.

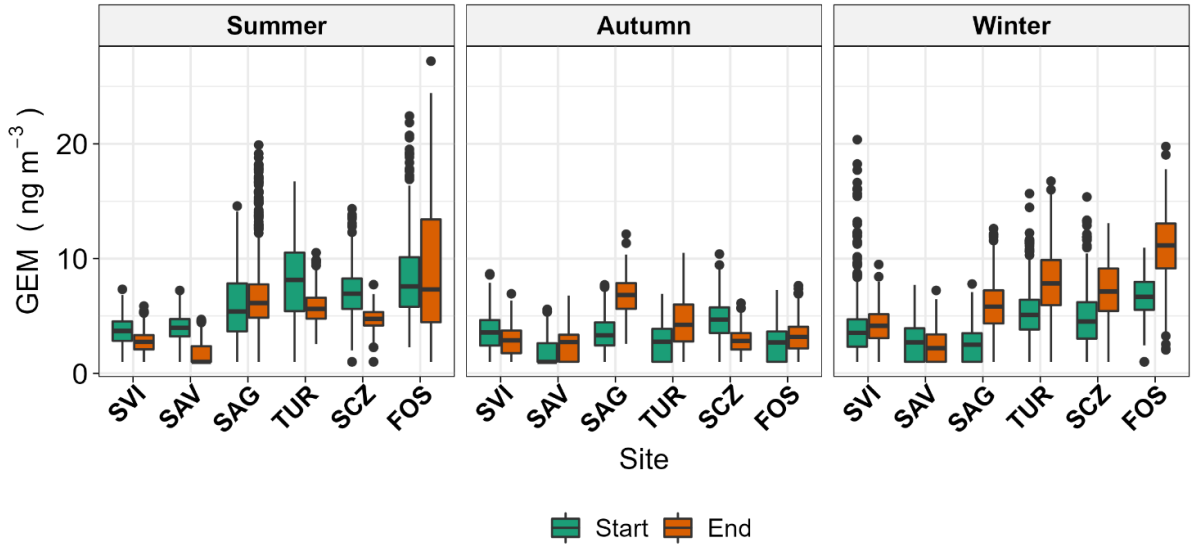

Figure 3: distribution of GEM concentrations recorded during diurnal sampling activity at selected terrestrial sites. Measures were taken at the beginning and at the end of sampling period for gaseous Hg flux determinations.

References

Acquavita, A., Biasiol, S., Lizzi, D., Mattassi, G., Pasquon, M., Skert, N., Marchiol, L., 2017. Gaseous Elemental Mercury Level and Distribution in a Heavily Contaminated Site: the Ex-chlor Alkali Plant in Torviscosa (Northern Italy). Water. Air. Soil Pollut. 228. https://doi.org/10.1007/s11270-016-3234-z

Acquavita, A., Brandolin, D., Cattaruzza, C., Felluga, A., Maddaleni, P., Meloni, C., Pasquon, M., Predonzani, S., Poli, L., Skert, N., Zanello, A., 2022. Mercury distribution and speciation in historically contaminated soils of the Isonzo River Plain (NE Italy). J. Soils Sediments 22, 79–92. https://doi.org/10.1007/s11368-021-03038-2

Agnan, Y., Le Dantec, T., Moore, C.W., Edwards, G.C., Obrist, D., 2016. New Constraints on Terrestrial Surface-Atmosphere Fluxes of Gaseous Elemental Mercury Using a Global Database. Environ. Sci. Technol. 50, 507–524. https://doi.org/10.1021/acs.est.5b04013

Ao, M., Meng, B., Sapkota, A., Wu, Y., Qian, X., Qiu, G., Zhong, S., Shang, L., 2017. The influence of atmospheric Hg on Hg contaminations in rice and paddy soil in the Xunyang Hg mining district, China. Acta Geochim. 36, 181–189. https://doi.org/10.1007/s11631-017-0142-x

Barago, N., Floreani, F., Acquavita, A., Esbrí, J.M., Covelli, S., Higueras, P., 2020. Spatial and temporal trends of gaseous elemental mercury over a highly impacted coastal environment (Northern Adriatic, Italy). Atmosphere (Basel). 11, 935. https://doi.org/10.3390/atmos11090935

Castelle, S., Schäfer, J., Blanc, G., Dabrin, A., Lanceleur, L., Masson, M., 2009. Gaseous mercury at the air-water interface of a highly turbid estuary (Gironde Estuary, France). Mar. Chem. 117, 42–51. https://doi.org/10.1016/j.marchem.2009.01.005

Cheng, I., Zhang, L., Mao, H., Blanchard, P., Tordon, R., Dalziel, J., 2014. Seasonal and diurnal patterns of speciated atmospheric mercury at a coastal-rural and a coastal-urban site. Atmos. Environ. 82, 193–205. https://doi.org/10.1016/j.atmosenv.2013.10.016

Ci, Z., Peng, F., Xue, X., Zhang, X., 2016. Air-surface exchange of gaseous mercury over permafrost soil: An investigation at a high-altitude (4700 m.a.s.l.) and remote site in the central Qinghai-Tibet Plateau. Atmos. Chem. Phys. 16, 14741–14754. https://doi.org/10.5194/acp-16-14741-2016

Ci, Z., Zhang, X., Wang, Z., Niu, Z., 2011. Atmospheric gaseous elemental mercury (GEM) over a coastal/rural site downwind of East China: Temporal variation and long-range transport. Atmos. Environ. 45, 2480–2487. https://doi.org/10.1016/j.atmosenv.2011.02.043

Civerolo, K.L., Rattigan, O. V., Dirk Felton, H., Hirscli, M.J., DeSantis, S., 2014. Mercury wet deposition and speeiated air concentrations from two urban sites in New York state: Temporal patterns and regional context. Aerosol Air Qual. Res. 14, 1822–1837. https://doi.org/10.4209/aaqr.2014.03.0052

Eckley, C.S., Blanchard, P., McLennan, D., Mintz, R., Sekela, M., 2015. Soil-Air Mercury Flux near a Large Industrial Emission Source before and after Closure (Flin Flon, Manitoba, Canada). Environ. Sci. Technol. 49, 9750–9757. https://doi.org/10.1021/acs.est.5b01995

Eckley, C.S., Eagles-Smith, C., Tate, M.T., Krabbenhoft, D.P., 2021. Surface-air mercury fluxes and a watershed mass balance in forested and harvested catchments. Environ. Pollut. 277, 116869. https://doi.org/10.1016/j.envpol.2021.116869

Ericksen, J.A., Gustin, M.S., Lindberg, S.E., Olund, S.D., Krabbenhoft, D.P., 2005. Assessing the potential for re-emission of mercury deposited in precipitation from arid soils using a stable isotope. Environ. Sci. Technol. 39, 8001–8007. https://doi.org/10.1021/es0505651

Esbrí, J.M., Cacovean, H., Higueras, P., 2018. Usage Proposal of a common urban decorative tree (Salix alba L.) to monitor the dispersion of gaseous mercury: A case study from Turda (Romania). Chemosphere 193, 74–81. https://doi.org/10.1016/j.chemosphere.2017.11.007

Esbrí, J.M., L. Higueras, P., Martínez-Coronado, A., Naharro, R., 2020. 4D dispersion of total gaseous mercury derived from a mining source: Identification of criteria to assess risks related to high concentrations of atmospheric mercury. Atmos. Chem. Phys. 20, 12995–13010. https://doi.org/10.5194/acp-20-12995-2020

Esbrí, J.M., Martínez-Coronado, A., Higueras, P.L., 2016. Temporal variations in gaseous elemental mercury concentrations at a contaminated site: Main factors affecting nocturnal maxima in daily cycles. Atmos. Environ. 125, 8–14. https://doi.org/10.1016/j.atmosenv.2015.10.064

Fantozzi, L., Guerrieri, N., Manca, G., Orrù, A., Marziali, L., 2021. An integrated investigation of atmospheric gaseous elemental mercury transport and dispersion around a chlor-alkali plant in the ossola valley (Italian central alps). Toxics 9, 172. https://doi.org/10.3390/toxics9070172

Floreani, F., Barago, N., Acquavita, A., Covelli, S., Skert, N., Higueras, P., 2020. Spatial distribution and biomonitoring of atmospheric mercury concentrations over a contaminated coastal lagoon (Northern Adriatic, Italy). Atmosphere (Basel). 11, 1280. https://doi.org/10.3390/atmos11121280

Fu, X., Feng, X., Guo, Y., Meng, B., Yin, R., Yao, H., 2013. Distribution and production of reactive mercury and dissolved gaseous mercury in surface waters and water/air mercury flux in reservoirs on Wujiang River, Southwest China. J. Geophys. Res. Atmos. 118, 3905–3917. https://doi.org/10.1002/jgrd.50384

Gabay, M., Raveh-Rubin, S., Peleg, M., Fredj, E., Tas, E., 2020. Is oxidation of atmospheric mercury controlled by different mechanisms in the polluted continental boundary layer vs. remote marine boundary layer? Environ. Res. Lett. 15, 064026. https://doi.org/10.1088/1748-9326/ab7b26

Griggs, T., Liu, L., Talbot, R.W., Torres, A., Lan, X., 2020. Comparison of atmospheric mercury speciation at a coastal and an urban site in Southeastern Texas, USA. Atmosphere (Basel). 11. https://doi.org/10.3390/ATMOS11010073

Han, Y.J., Kim, J.E., Kim, P.R., Kim, W.J., Yi, S.M., Seo, Y.S., Kim, S.H., 2014. General trends of atmospheric mercury concentrations in urban and rural areas in Korea and characteristics of high-concentration events. Atmos. Environ. 94, 754–764. https://doi.org/10.1016/j.atmosenv.2014.06.002

Higueras, P., María Esbrí, J., Oyarzun, R., Llanos, W., Martínez-Coronado, A., Lillo, J., Angel López-Berdonces, M., Maria García-Noguero, E., 2013. Industrial and natural sources of gaseous elemental mercury in the Almadén district (Spain): An updated report on this issue after the ceasing of mining and metallurgical activities in 2003 and major land reclamation works. Environ. Res. 125, 197–208. https://doi.org/10.1016/j.envres.2012.10.011

Higueras, P., Oyarzun, R., Kotnik, J., Esbrí, J.M., Martínez-Coronado, A., Horvat, M., López-Berdonces, M.A., Llanos, W., Vaselli, O., Nisi, B., Mashyanov, N., Ryzov, V., Spiric, Z., Panichev, N., McCrindle, R., Feng, X., Fu, X., Lillo, J., Loredo, J., García, M.E., Alfonso, P., Villegas, K., Palacios, S., Oyarzún, J., Maturana, H., Contreras, F., Adams, M., Ribeiro-Guevara, S., Niecenski, L.F., Giammanco, S., Huremović, J., 2014. A compilation of field surveys on gaseous elemental mercury (GEM) from contrasting environmental settings in Europe, South America, South Africa and China: Separating fads from facts. Environ. Geochem. Health 36, 713–734. https://doi.org/10.1007/s10653-013-9591-2

Holmes, C.D., Jacob, D.J., Mason, R.P., Jaffe, D.A., 2009. Sources and deposition of reactive gaseous mercury in the marine atmosphere. Atmos. Environ. 43, 2278–2285. https://doi.org/10.1016/j.atmosenv.2009.01.051

Hong, Q., Xie, Z., Liu, C., Wang, F., Xie, P., Kang, H., Xu, J., Wang, J., Wu, F., He, P., Mou, F., Fan, S., Dong, Y., Zhan, H., Yu, X., Chi, X., Liu, J., 2016. Speciated atmospheric mercury on haze and non-haze days in an inland city in China. Atmos. Chem. Phys. 16, 13807–13821. https://doi.org/10.5194/acp-16-13807-2016

Huremović, J., Horvat, M., Kotnik, J., Kocman, D., Žižek, S., Ribeiro Guevara, S., Muhić-Šarac, T., Memić, M., 2017. Characterization of Mercury Contamination Surrounding a Chloralkali Production Facility in Tuzla, Bosnia and Herzegovina. Anal. Lett. 50, 1049–1064. https://doi.org/10.1080/00032719.2016.1205595

Kalinchuk, V., Yatsuk, A., Marchesini, L.B., Lopatnikov, E., Nesterova, O., Valentini, R., Aksentov, K., 2022. The first simultaneous and continuous underway measurements of atmospheric gaseous elemental mercury, carbon dioxide and methane in the marine boundary layer: Results of cruise study in the Sea of Japan in May 2018. Atmos. Pollut. Res. 13, 101458. https://doi.org/10.1016/j.apr.2022.101458

Kim, K.H., Ebinghaus, R., Schroeder, W.H., Blanchard, P., Kock, H.H., Steffen, A., Froude, F.A., Kim, M.Y., Hong, S., Kim, J.H., 2005. Atmospheric mercury concentrations from several observatory sites in the Northern Hemisphere. J. Atmos. Chem. 50, 1–24. https://doi.org/10.1007/s10874-005-9222-0

Kocman, D., Vreča, P., Fajon, V., Horvat, M., 2011. Atmospheric distribution and deposition of mercury in the Idrija Hg mine region, Slovenia. Environ. Res. 111, 1–9. https://doi.org/10.1016/j.envres.2010.10.012

Lan, X., Talbot, R., Laine, P., Lefer, B., Flynn, J., Torres, A., 2014. Seasonal and diurnal variations of total gaseous mercury in Urban Houston, TX, USA. Atmosphere (Basel). 5, 399–419. https://doi.org/10.3390/atmos5020399

Li, P., Feng, X., Qiu, G., Shang, L., Wang, S., 2012. Mercury pollution in Wuchuan mercury mining area, Guizhou, Southwestern China: The impacts from large scale and artisanal mercury mining. Environ. Int. 42, 59–66. https://doi.org/10.1016/j.envint.2011.04.008

Liu, B., Keeler, G.J., Dvonch, J.T., Barres, J.A., Lynam, M.M., Marsik, F.J., Morgan, J.T., 2007. Temporal variability of mercury speciation in urban air. Atmos. Environ. 41, 1911–1923. https://doi.org/10.1016/j.atmosenv.2006.10.063

Malcolm, E.G., Keeler, G.J., Landis, M.S., 2003. The effects of the coastal environment on the atmospheric mercury cycle. J. Geophys. Res. 108, 1–10. https://doi.org/10.1029/2002JD003084

Mao, H., Cheng, I., Zhang, L., 2016. Current understanding of the driving mechanisms for spatiotemporal variations of atmospheric speciated mercury: A review. Atmos. Chem. Phys. 16, 12897–12924. https://doi.org/10.5194/acp-16-12897-2016

Mao, H., Talbot, R.W., Sigler, J.M., Sive, B.C., Hegarty, J.D., 2008. Seasonal and diurnal variations of Hg◦ over New England. Atmos. Chem. Phys. 8, 1403–1421. https://doi.org/10.5194/acp-8-1403-2008

Miller, M.B., Gustin, M.S., Eckley, C.S., 2011. Measurement and scaling of air-surface mercury exchange from substrates in the vicinity of two Nevada gold mines. Sci. Total Environ. 409, 3879–3886. https://doi.org/10.1016/j.scitotenv.2011.05.040

Mistaro, A., Felluga, A., Moimas, F., Abatangelo, A., Asquini, T., Bruno, R., Celic, L., Guidarelli, M., Pastrello, A., Bertocchi, A.S., 2018. Chemical characterization of atmospheric particulate matter in Friuli Venezia Giulia (NE Italy) by exploratory data analysis with multisite and multivariate approach. Environ. Sci. Pollut. Res. 25, 28808–28828. https://doi.org/10.1007/s11356-018-1883-8

Nie, X., Mao, H., Li, P., Li, T., Zhou, J., Wu, Y., Yang, M., Zhen, J., Wang, X., Wang, Y., 2020. Total gaseous mercury in a coastal city (Qingdao , China): Influence of sea-land breeze and regional transport. Atmos.

Environ. 235, 1–11.

Oyarzun, R., Higueras, P., Esbrí, J.M., Pizarro, J., 2007. Mercury in air and plant specimens in herbaria: A pilot study at the MAF Herbarium in Madrid (Spain). Sci. Total Environ. 387, 346–352. https://doi.org/10.1016/j.scitotenv.2007.05.034

Polonia, A., Albertazzi, S., Bellucci, L.G., Bonetti, C., Bonetti, J., Giorgetti, G., Giuliani, S., Correa, M.L., Mayr, C., Peruzza, L., Stanghellini, G., Gasperini, L., 2021. Decoding a complex record of anthropogenic and natural impacts in the Lake of Cavazzo sediments, NE Italy. Sci. Total Environ. 787, 147659. https://doi.org/10.1016/j.scitotenv.2021.147659

Si, L., Ariya, P.A., 2018. Recent advances in atmospheric chemistry of mercury. Atmosphere (Basel). 9, 76. https://doi.org/10.3390/atmos9020076

Sommar, J., Zhu, W., Shang, L., Lin, C.J., Feng, X., 2016. Seasonal variations in metallic mercury (Hg0) vapor exchange over biannual wheat-corn rotation cropland in the North China Plain. Biogeosciences 13, 2029–2049. https://doi.org/10.5194/bg-13-2029-2016

Sprovieri, F., Pirrone, N., Ebinghaus, R., Kock, H., Dommergue, A., 2010. A review of worldwide atmospheric mercury measurements. Atmos. Chem. Phys. 10, 8245–8265. https://doi.org/10.5194/acp-10-8245-2010

USEPA, 2000. U.S. Environmental Protection Agency Office of Environmental Information. Guidance for Data Quality Assessment: Practical Methods for Data Analysis EPA QA/G-9 QA00 UPDATE; EPA/600/R-96/084; U.S. Environmental Protection Agency Office: San Francisco, CA, U.

Vaselli, O., Higueras, P., Nisi, B., María Esbrí, J., Cabassi, J., Martínez-Coronado, A., Tassi, F., Rappuoli, D., 2013. Distribution of gaseous Hg in the Mercury mining district of Mt. Amiata (Central Italy): A geochemical survey prior the reclamation project. Environ. Res. 125, 179–187. https://doi.org/10.1016/j.envres.2012.12.010

Vijayakumaran Nair, S., Kotnik, J., Gačnik, J., Živković, I., Koenig, A.M., Mlakar, T.L., Horvat, M., 2022. Dispersion of airborne mercury species emitted from the cement plant. Environ. Pollut. 312. https://doi.org/10.1016/j.envpol.2022.120057

Wang, C., Wang, Z., Zhang, X., 2020. Characteristics of the air–sea exchange of gaseous mercury and deposition flux of atmospheric mercury at an island near the boundary of the Bohai Sea and Yellow Sea. Atmos. Environ. 232, 117547. https://doi.org/10.1016/j.atmosenv.2020.117547

Wang, S., Feng, X., Qiu, G., Wei, Z., Xiao, T., 2005. Mercury emission to atmosphere from Lanmuchang Hg-Tl mining area, Southwestern Guizhou, China. Atmos. Environ. 39, 7459–7473. https://doi.org/10.1016/j.atmosenv.2005.06.062

Wängberg, I., Munthe, J., Amouroux, D., Andersson, M.E., Fajon, V., Ferrara, R., Gårdfeldt, K., Horvat, M., Mamane, Y., Melamed, E., Monperrus, M., Ogrinc, N., Yossef, O., Pirrone, N., Sommar, J., Sprovieri, F., 2008. Atmospheric mercury at mediterranean coastal stations. Environ. Fluid Mech. 8, 101–116. https://doi.org/10.1007/s10652-007-9047-2

Weigelt, A., Ebinghaus, R., Manning, A.J., Derwent, R.G., Simmonds, P.G., Spain, T.G., Jennings, S.G., Slemr, F., 2015. Analysis and interpretation of 18 years of mercury observations since 1996 at Mace Head, Ireland. Atmos. Environ. 100, 85–93. https://doi.org/10.1016/j.atmosenv.2014.10.050

WHO, 2000. Air quality guidelines for Europe, 2nd ed. ed, WHO Regional Publications, European Series; 91. World Health Organization. Regional Office for Europe, Copenhagen PP - Copenhagen.

Yu, Q., Luo, Y., Wang, S., Wang, Z., Hao, J., Duan, L., 2018. Gaseous elemental mercury (GEM) fluxes over canopy of two typical subtropical forests in south China. Atmos. Chem. Phys. 18, 495–509. https://doi.org/10.5194/acp-18-495-2018

Zhang, L., Wang, S.X., Wang, L., Hao, J.M., 2013. Atmospheric mercury concentration and chemical speciation at a rural site in Beijing, China: Implications of mercury emission sources. Atmos. Chem. Phys. 13, 10505–10516. https://doi.org/10.5194/acp-13-10505-2013

Zhu, W., Li, Z., Li, P., Yu, B., Lin, C.J., Sommar, J., Feng, X., 2018. Re-emission of legacy mercury from soil adjacent to closed point sources of Hg emission. Environ. Pollut. 242, 718–727. https://doi.org/10.1016/j.envpol.2018.07.002

4 Conclusions

In this work, the Hg^0 exchanges at the interface between natural surfaces (soil and water) and the atmosphere were evaluated in field by means of the flux chamber technique coupled with a real-time Hg^0 analyser. This approach was applied in different environmental contexts strongly impacted by past anthropogenic activities, namely the historical cinnabar (α-HgS) mining at the Idrija mine (Slovenia) and the discharges of the chlor-alkali plant located in Torviscosa (Italy) where Hg was used as catalyst in the electrolytic cells.

Measurements of Hg^0 fluxes at the water-air interface were conducted in both coastal marine and freshwater environments subject to different Hg supplies and hydrodynamic conditions. In the first case, the research activity was focused on two sites of the Northern Adriatic Sea area, a fish farm of the Marano and Grado Lagoon (Val Noghera, VN) as a confined heavily impacted environment and the Bay of Piran (Slovenia, PR) selected as an open marine environment less subject to Hg contamination from the Isonzo River, the main source of Hg in this area. Fluxes of Hg^0 were monitored over the entire day-night cycle in different seasons to deepen the knowledge on the dynamics of this process under different UV irradiation conditions. In the second case, the study was focused on freshwater sites subject to Hg supplies from different sources: the Solkan Reservoir (Slovenia, SK) along the Isonzo River for Hg contamination related to mining, the Torviscosa Dockyard (TR) inside the local chemical complex for contamination from industrial activity, and the Cavazzo Lake (Italy, CV) as a pristine site with unknown Hg sources. Measurements were performed during the diurnal period in different seasons to understand the influence of different contamination sources on magnitude and temporal variability of Hg^0 fluxes.
In addition, Hg^0 fluxes at the soil-air interface were evaluated in 6 selected sites (from north to south: SVI, SAV, SAG, TUR, SCZ, FOS) along the highly impacted alluvial plain of the Isonzo River and characterised, based on existing data, by a different total Hg concentration in soil. In this case, measurements were performed during the diurnal period in permanent meadows both on soils covered by native grass vegetation and bare soil plots previously prepared.

Generally, Hg^0 fluxes observed in the terrestrial environment were significantly higher than those recorded for the aquatic compartments. This is likely due to a greater availability of Hg in the surface layer involved in gaseous exchanges with the atmosphere, in the order of ppt and ppm in aquatic and terrestrial contexts respectively. Average daily Hg^0 fluxes at the water-air

interface ranged between 6.22±3.84 ng m^{-2} h^{-1} (site CV, in autumn) and 36.65±6.15 ng m^{-2} h^{-1} (site SK, in summer) in freshwater environments and between 11.32±9.85 and 36.58±25.15 ng m^{-2} h^{-1} (site PR in autumn and summer, respectively) in coastal marine environments. Conversely, average daily Hg^0 fluxes at the soil-air interface from bare soil plots ranged between 32.8±10.1 ng m^{-2} h^{-1} (site SAV, in autumn) and 800.2±178.8 ng m^{-2} h^{-1} (site TUR, in summer), whereas emissions from vegetated plots ranged between 15.2±4.5 ng m^{-2} h^{-1} (site SAV, in autumn) and 344.6±36.2 ng m^{-2} h^{-1} (site FOS, in summer).
In both contexts, observed Hg^0 fluxes resulted higher than those commonly reported in literature for pristine aquatic and terrestrial environments and comparable to those recorded in other areas strongly impacted by mining or industrial activities. These findings confirm that even decades after the closure of the main contamination sources (the Idrija Hg mine in 1996 and the installation of appropriate filtration systems at the Torviscosa CAP in 1984) the studied environments can still represent a secondary source of Hg for the atmosphere.

Interestingly, during the 24 hours experiments in coastal marine environments, Hg^0 evasion into the atmosphere was observed also during night, indicating a constant super-saturation of the surface water. This situation may be explained by continuous supplies of Hg^0 during night likely related to dark reduction processes at VN or to transport from other zones thanks to sea currents at PR. These findings confirm that gaseous exchanges represent an important aspect of biogeochemical cycle of Hg in these contaminated environments and suggest that Hg^0 fluxes during the complete day-night cycle should be evaluated in the future also in freshwater sites in order to reach a more comprehensive estimate of the Hg budget in these environments.
Both in aquatic and terrestrial environments, the highest releases of Hg^0 were observed during the summer season because of high UV irradiation and temperatures, which can catalyse both the abiotic (photochemical) reduction of Hg^{2+} and biotic reduction reactions related to microbial activity, leading to the formation of volatile Hg^0. Moreover, higher temperatures can increase the desorption of Hg from soil surfaces and its movement through the soil pores due to increased thermal motion. In aquatic environments, Hg^0 solubility decreases with increasing temperature, thus favouring its release into the atmosphere. However, it must be stressed that the highest DGM concentrations (the volatile Hg fraction in water, which is almost totally formed by Hg^0 near the water-air interface) were generally observed in spring due to the relative high UV irradiation and photoreduction rates. In contrast, Hg^0 fluxes in spring were lower than those observed in summer likely due to lower temperatures and consequently a lower transfer velocity of produced volatile Hg^0 to the atmosphere.

The limitation of Hg^0 fluxes due to low temperatures was evident also in terrestrial environments. In this case, emissions recorded at the various sites were significantly positively correlated to Hg concentrations in the substrate in summer and autumn but not in winter, likely due to extremely low fluxes recorded in all sites in this season in the morning, independently from Hg concentration. This effect could be explained by a low contribution of the predominant α-HgS fraction in soil to gaseous releases, as this form of Hg is characterised by a relatively high activation energy for volatilisation and low winter temperatures limited the energy available for this reaction. No correlation was found between Hg^0 fluxes and the amount of Hg occurring in the no-α-HgS fraction in soils, which however can include several Hg forms not easily discriminated by pyrolysis due to overlapping of desorption peaks and likely characterised by different mobility and availability for reduction.

Focusing on aquatic environments, the results obtained in this study indicated that hydrodynamic conditions have a strong influence on the magnitude of Hg^0 releases at the water-air interface. Particularly in the coastal marine environment, at PR site, the relatively high peaks of emission were recorded in parallel with an increase in wave motion observed in field which likely favoured the gaseous exchanges; moreover, the water movement may have contributed to the replenishment of Hg in surface water layer. A similar situation probably occurred also at the reservoir (SK site), due to supplies of Hg from upstream related to the current flow, actively regulated by the artificial dam downstream. In fact, at this site, increases in Hg^0 evasion were observed in parallel with increases in water movement observed in field. Unfortunately, water current was not measured and no public data are available to support this observation. Conversely, static water column conditions may have strongly limited Hg^0 evasion, as confirmed by relatively low fluxes calculated for the confined fish farm environment (VN) and the Torviscosa Dockyard (TR), where only limited water exchanges with nearby open aquatic environments occurred. In the first case, this limitation was particularly evident in spring, when to extremely high DGM concentrations did not correspond high Hg^0 evasion. The high DGM concentrations observed at VN could also be related to the relative high DOM amounts observed in this site, which can have both favoured the photo-induced formation of Hg^0 acting as photosensitiser but also have limited gaseous exchanges through Hg^0 adsorption. However, these assumptions should be tested by means of specific analysis of DOM quality at this and other investigated sites.

In the industrially impacted site, characterised by a greater water depth (~2.5 m), the thermoaline stratification observed in field due to the occurrence of a “saltwedge” through the

nearby Aussa River likely limited the vertical diffusion of Hg from contaminated sediments to the surface water layer. This consideration was confirmed by higher DGM concentrations observed in deep water column than at the surface. As a consequence, the evasion to the atmosphere was also limited. Moreover, the abundance of oxidants (e.g. chlorides, bromides) in saltwater of these two sites could have favoured a higher loss of Hg^0 through oxidation to Hg^{2+} rather than volatilisation to the atmosphere.

These restrictions to volatilisation may reduce the potential of gaseous exchanges in limiting Hg burden in aquatic environments despite the observed emissions. Indeed, considering the DGM concentrations recorded, significantly higher Hg^0 emissions can be expected under more dynamic conditions, especially at VN. This hypothesis can be reinforced by the relatively high fluxes observed at PR site under more dynamic conditions despite the low DGM concentrations. As a result, static water conditions may increase the residence time of Hg in the water column and, consequently, its availability for methylation and accumulation in the food webs. Future research should be devoted to assessing this aspect by monitoring Hg^0 fluxes under different hydrodynamic conditions, particularly at the fish farm environment where a greater water exchange can be artificially induced through an active control of sluice gates which ensure the connection with the open lagoon environment. This activity would help in accurately estimating the impact of past Hg supplies on local ecosystems and how fast they can recover from this historic anthropogenic contamination.

Moreover, considering the shallow water depth at the fish farm, it cannot be excluded that benthic releases of Hg from contaminated sediments deeply impact also the magnitude of Hg^0 fluxes by influencing the amount of Hg in the water column available for reduction and volatilisation. An interesting extension of the research might be represented by the evaluation of the direct volatilisation of Hg^0 from the highly contaminated sediments of the Marano and Grado Lagoon, e.g. tidal flats and saltmarshes, assessing the possible effect of submersion-emersion cycles on the magnitude of Hg^0 fluxes to the atmosphere. In addition, measurements of benthic fluxes at the sediment-water interface at TR would be helpful to elucidate if these sediments represent a sink or a secondary source of Hg for the water column and to completely assess the fate of this metal in this environment.

The evasion of Hg^0 at TR could have been also limited by the high GEM concentrations (up to over 500 ng m^{-3}) in the local atmosphere related to emissions from the nearby former CAP buildings, still extremely contaminated. This was evident particularly during morning periods as a result of favourable wind direction. The occurrence of high atmospheric levels of Hg may

have represented an additional source of Hg for surface water thanks to dry atmospheric depositions. This aspect should be monitored in the future through long-term continuous monitoring of Hg^0 fluxes combined with a parallel assessment of atmospheric deposition. Moreover, extending this combined monitoring over the entire area considered in this work could also be useful to fully understand the dynamics of Hg^0 exchanges and to calculate a more accurate budget of supplies and losses of this metal in the water column.
Last but not least, relatively high Hg^0 fluxes (and Hg concentrations in water) were surprisingly found at the pristine environment of Cavazzo (CV), comparable to those observed in the other aquatic environments. This evidence suggests that this area should be investigated for different aspects (i.e. atmospheric depositions, sediment quality) in order to understand if the source of Hg in the lake can be related to supplies from the atmosphere or from geological settings in the lake catchment.

Considering terrestrial environments, our results confirmed that the presence of grass vegetation on soil surfaces can significantly reduce (9.3-78.0%) the Hg^0 emissions to the atmosphere compared to bare soil surfaces likely due to soil shading. This effect was particularly evident when vegetation was well developed, i.e. in summer and autumn. Conversely in winter, due to the presence of only dry plant stubble, the difference between the two treatments was not so evident and likely ascribable to small-scale spatial variability between the investigated plots. However, removing the herbaceous cover resulted in immediate increase in Hg^0 fluxes to levels comparable to those of bare soils, as confirmed by similar fluxes observed from both treatments in summer at SAV and SCZ, sampled short after mowing. These results suggest that favouring the development of natural grass vegetation during the warm season, more favourable to high Hg^0 emissions, can represent a simple and cost-effective strategy to limit the impact of substrate contamination on the local atmosphere through fluxes at soil-air interface.
Moreover, increasing amounts of soil OM likely limited Hg^0 evasion by favouring adsorption of Hg^0 on its surfaces, as confirmed by the relative high emissions recorded at FOS coupled with low OM concentrations in soil. The role of OM concentration and speciation should be further investigated in the future, for example to understand if soil amendment with specific organic ligands can further limit Hg mobility and release to the atmosphere even in this environment where this metal occurs mostly as scarcely mobile α-HgS.
To scale up emission estimates from the impacted area of the Isonzo River alluvial plain and accurately assess the amount of Hg released to the atmosphere, larger data sets are required.

Therefore, the spatial cover of the measures should be extended considering: 1) different types of environments such as forests or arable lands frequently disturbed by agricultural practices and directly exposed to solar radiation; 2) the temporal variability of the processes under different environmental conditions in terms of solar radiation (e.g. evaluating fluxes during night period and under different cloud cover conditions) and temperatures; 3) the possible role of precipitation and subsequent variations of soil humidity.

Moreover, measurements of Hg^0 fluxes in forest ecosystems present in the study area or in its surroundings may be coupled with assessment of atmospheric deposition of Hg to assess their possible role as sinks for atmospheric Hg. Indeed, other than limiting evasion through soil shading, forests can sequestrate and retain relevant amounts of Hg^0 thanks to cuticular or stomatal absorption and subsequent transfer to the soil through litterfall and throughfall. However, the role of plants in gaseous exchanges of Hg in these areas may be investigated with *ad hoc* experiments (e.g. estimation of gaseous exchanges from whole plants by means of flux bags). Moreover, the research could be broadened by extending the measure of Hg^0 fluxes at soil-air interface in areas impacted by different Hg sources (e.g. industrial discharges and/or atmospheric depositions) and characterised by a different Hg speciation in soils. This may help to test the performance of the adopted experimental setup also in areas where α-HgS is not the dominant form of Hg.

The research activity conducted for this work confirmed that the flux chamber approach used for the estimation of Hg^0 fluxes is particularly sensitive to changes of environmental conditions. This can be confirmed for example by the good agreement observed between fluxes and irregular incoming UV radiation under partially cloudy conditions observed during sampling at CV in spring and FOS in summer and autumn. Considering the relative rapidity of measures, the simple functioning of the systems and the low economic costs for the execution of measurements, the experimental approaches used in this work could be considered in the future for a possible implementation in the risk assessment procedure: the possibility of carrying out a relatively large number of direct measurements of Hg^0 emissions from natural surfaces at contaminated sites distributed both in space and time would make possible to more comprehensively assess the actual emission of this contaminant into the atmosphere. Furthermore, to achieve a more exhaustive assessment of the risk associated with a potential exposure to this contaminant through inhalation by possible frequenters of the areas, also atmospheric dispersion of emitted Hg^0 should be carefully evaluated through long-term continuous air monitoring. These measurements could also allow the assessment of possible supplies of Hg^0 from other unknown areas and/or sources through atmospheric transport.

Acknowledgements

I would like to thank all the people who in various ways contributed to the realization of this work.

Thanks to my supervisors Prof. Stefano Covelli and Prof. Jadran Faganeli for making this research possible and for their support and availability, indispensable suggestions, and trust shown to me throughout my doctoral journey, as well as for teaching me their passion and dedication to research. Special thanks to Prof. Covelli also for his culinary skills in the Val Noghera barbecues during sampling and to Prof. Faganeli for providing fantastic accommodation at the Marine Biology Station during the "Piran nights".

Thanks to Dr. Alessandro Acquavita for providing valuable information for planning this research, for his useful advice and for his expertise both scientific and eno-gastronomic.

Thanks to all members of the Mercurilab research group: Nicolò Barago, for sharing the journey and for the "refreshing" trips to Cave del Predil and beyond, Dr. Elisa Petranich and Dr. Elena Pavoni, for their teachings and advice and for making me understand how to get into the soul of the instruments.

Thanks to Claudio Furlanut, Marco Cambi, and the entire staff of the Val Noghera fish farm for their kind hospitality and willingness to allow us to reach and stay overnight in the fish farm.

Thanks to Daniele Karlicek, Cristiano Landucci, Mauro Bussi and Gualtiero Tujach for their useful help in finding and preparing material for external sampling and for grain-size analysis.

Thanks to Dr. Katja Klun of Marine Biology Station in Pirano for providing DOC analysis. Additional thank to the Marine Biology Station for accommodation during sampling activity.

Thanks to Karry Close for her availability and for proof-reading part of this text, as well as for her encouragement during the last days before submission of this work.

Thanks to Mara Mauri of *Regione Friuli Venezia Giulia, servizio disciplina gestione rifiuti e siti inquinati* for providing information about existing gaseous mercury fluxes measures in the Low Isonzo plain.

Thanks to the former mayor of Torviscosa Roberto Fasan, to Dr. Domenico Perosa of Caffaro Industrie and to Dr. Franco Sturzi for making possible and allowing access to the restricted area of Torviscosa Dockyard and for support during sampling operations.

Thanks to all the students whose theses or simply help during sampling facilitated the realization of this work: Marco Burello, Valeria Zappella, Federico Vito Zotta, Gabriele Faoro, Samuel Princi.

Thanks to Operational Programme 2014/2020 of the European Social Found (ESF) of the Friuli Venezia Giulia Region (code FP2012684801) for funding this PhD fellowship.

Last but not least, thanks to my parents and all my family for their unconditional support before and throughout this period and non-interference with my choices, as well as for always giving me a safe place to return to in times of trouble. There are no words to express all my gratitude.